UC San Diego

UC San Diego Electronic Theses and Dissertations

Title

Utilization of Bioorthogonal Chemistry for Live-Cell Labeling of Glycoconjugates and the Liposomal-Based Engineering of Dynamic Artificial Cellular Models

Permalink

https://escholarship.org/uc/item/5v86s9x9

Author

Cole, Christian

Publication Date

2016

Peer reviewed|Thesis/dissertation

eScholarship.org Powered by the California Digital Library
University of California

UNIVERSITY OF CALIFORNIA, SAN DIEGO

Utilization of Bioorthogonal Chemistry for Live-Cell Labeling of Glycoconjugates and the Liposomal-Based Engineering of Dynamic Artificial Cellular Models

A Dissertation submitted in partial satisfaction of the

requirements for the degree

Doctor of Philosophy

in

Chemistry

by

Christian M. Cole

Committee in charge:

Professor Neal K. Devaraj, Chair
Professor Michael Galperin
Professor Gourisankar Ghosh
Professor Jeff M. Hasty
Professor Elizabeth A. Komives

2016

Copyright
Christian M. Cole, 2016
All rights reserved

The Dissertation of Christian M. Cole is approved, and it is acceptable in quality and form for publication on microfilm and electronically:

_____

_____

_____

_____

_____
Chair

University of California, San Diego

2016

Dedication

This work is dedicated to the
loving memory of my grandparents

Roy Schram – 1992 *Margret Schram -2010*

Gilbert Cole – 2001 *Christina Cole -2016*

You will never be forgotten

Epigraph

There are no facts, only interpretations and relatives.

~Friedrich Nietzsche

Table of Contents

List of Abbreviations

AcOH	acetic acid
ADP	adenosine diphosphate
BME	2-mercaptoethanol
BODIPY	boron-dipyrromethene
BSA	bovine serum albumin
°C	degree Celsius
CcO	cytochrome c oxidase
CuAAC	copper(I)-catalyzed azide-alkyne cycloaddition
cmc	critical micelle concentration
Da	dalton
DAPI	4', 6-diamidino-2-phenylindole
DCM	dichloromethane
DDM	N-dodecyl-beta-maltoside
DIC	N,N'-diisopropylcarbodiimide
DMEM	dulbecco's-modified Eagle medium
DMF	N,N-dimethylformamide
DMSO	dimethyl sulfoxide
DOPC	1,2-dioleoyl-sn-glycero-3-phosphocholine
DTT	dithiothreitol
EDTA	ethylenediaminetetraacetic acid
Et	ethyl

FITC	fluorescein isothiocyanate
FP	fluorescent protein
FRET	förster resonance energy transfer
GalN	galactosamine
GFP	green fluorescent protein
GlcN	glucosamine
GUV	giant unilamellar vesicle
HEPES	4-(2-hydroxyethyl)-1-piperazineethanesulfonic acid
HPLC	high-performance liquid chromatography
IPTG	isopropyl β-D-1-thiogalactopyranoside
LacI	lac repressor
LUV	large unilamellar vesicle
ManNAc	N-acetylmannosamine
MESNA	2-mercaptoethanesulfonic acid
NCL	native chemical ligation
NHS	N-hydroxysuccinimide
NMR	nuclear magnetic resonance spectroscopy
OD	optical density
OptiMEM	opti minimum essential medium
PBS	phosphate buffer saline
PC	phosphatidylcholine
PDMS	polydimethylsiloxane
PEG	poly(ethylene glycol)

pH	negative log of hydrogen ion concentration
Ph	phenyl
PMSF	phenylmethane sulfonyl fluoride
POPC	1-palmitoyl-2-oleoyl-sn-glycero-3-phosphocholine
py	pyridine
RFP	red fluorescent protein
RNase	ribonuclease
rt	room temperature
SUV	small unilamellar vesicle
TCEP	tris(2-carboxyethyl)phosphine
TEM	transmission electron microscopy
TFA	trifluoroacetic acid
THF	tetrahydrofuran
TLC	thin-layer chromatography
Tx-DHPE	Texas red 1,2-dihexadecanoyl-sn-glycerol-3-phosphoethanolamine
TX-TL	transcription – translation expression systems

List of Figures

List of Schemes

List of Graphs

Acknowledgements

As I take this opportunity to reflect, there are many people I would like to acknowledge. I would like to start with those I did not know, but recognize as instrumental to my own personal journey. I thank the generations before me, as their many sacrifices and hard work undoubtedly provided me the opportunities and tools that ultimately allowed me to achieve both personal and academic success.

I would like to thank three amazing physicians, Dr. Gringeri, Dr. Bach and the late Dr. Steven Burke. Without their dedication, tenacity and care for their patients, my journey may have never started. In the face of lawsuits, malpractice suits, and slander, thank you for not being detoured.

I would like to thank my undergraduate advisor Professor Jebrell Glover for welcoming me into his lab and taking the time to personal train me in the practice of doing "good science". Jebrell was a remarkable mentor and fostered my curiosity and love of science. It was from his guidance I found myself at UCSD, thank you Jebrell for your continued support.

Shortly after arriving to San Diego I had the privilege of working for Professor Patricia Jennings an excellent biophysical researcher. I would like to thank her for being a 3rd mother to me during my time at UCSD. Her encouragement and stories provided an uplifting reminder not to stress, but to carry on. I would like to extend my thanks to the Jennings' Lab; in particular I would like to thank Kendra, Sulyman, Dominique, Melinda and Maria. They were great mentors and friend's way back when I was a neonate in biochemistry. I had many great and eclectic conversations with them

(although sometimes we ended up discussing raccoons…) and I feel this experience would have felt twice as long without their friendship.

I would like to thank the members of my thesis committee, professor Jeff Hasty and professor Elizabeth Komives. Professor Jeff Hasty's research inspired many of my own projects early on. After collaborating with him I admire the research atmosphere that he fosters. I would like to thank professor Elizabeth Komives for being my 2nd mother at UCSD. She was not only an amazing mentor and researcher, but also an exceptional advisor who cared about my success and the success of my fellow graduate students. Thank you for always making yourself available and approachable.

A very special thanks goes to professor Neal Devaraj, my advisor and scientific role model. We started at UCSD at the same time embarking on our separate journeys; I am forever fortunate our paths crossed. My gratitude goes out to Neal for allowing me the freedom to develop into an independent scientist. He pushed me when I needed to be motivated and talked to me candidly when my efforts fell short. Thank you for believing in me and thank you for always asking, "what's next?" I would like to thank the members of the Devaraj lab. I would like to thank Professor Jun Yang and Professor HaoXing Wu. Both of them were incredible synthetic chemists that made me appreciate and admire organic chemistry. Thank you for your invaluable help in synthesizing many of the compounds that contributed to my work. I would like to thank Jolita Seckute for being an outstanding mentor, colleague and friend. I thank you for not only assisting me on my initial projects, but also being a wonderful friend outside of lab. I really enjoyed those initial years of the three of us exploring San Diego. I would like to thank my friend and colleague Michael Hardy. Before rotations I remember waving to one of my

classmates standing outside Mayer Hall wearing toe-shoes … I remember feeling "we end up in the same lab" and that is exactly what happened. Michael and I were the first graduate students in Neal's lab and we will remain friends for life. Me gustaría extender un gran agradecimiento a Roberto Brea. Roberto Brea ha sido un compañero maravilloso y un gran amigo. Roberto hizo que muchos de los compuestos que han contribuido a mi éxito, así como a enseñarme cómo hacerlas. El laboratorio Devaraj nunca fue el mismo después de Roberto se unió; gracias por unirse al laboratorio, gracias por ser mi amigo, espero permanecer siempre en contacto con usted. Deseo agradecer a todos los nuevos miembros del laboratorio de Devaraj. Thank you to Andrew Rudd for being a friend and fellow colleague. I greatly enjoyed our conversations and always appreciated your assistance in lab. Thanks to Brandon, Eric, Ahanjit, Kayla, Seth, Henrike and Fabian, I couldn't ask for a better group of individuals.

I would like to thank my girlfriend, Jessica Cifelli. She has been a friend, colleague, and a light of inspiration. I cherish her support and the strength she has given me. Looking forward to the many adventures to come.

I especially want to thank my family; Michael Cole, Diana Cole, Todd Cole, Jade Cole and the late Cotton Babies. My family has been everything to me. Over the years they always have been there for me, sending their love and offering me boundless support and wisdom. I am forever grateful to all of you. Thanks for being in my life; I could not have done this without you.

Notes about the chapters:

Chapter two, in full, is a reprint (with co-author permission) of the material as it appears in the publication; J. Yang, J. Seckute, **C. M. Cole**, N. K. Devaraj. "Live-Cell Imaging of Cyclopropene Tags with Fluorogenic Tetrazine Cycloadditions," *Angew. Chem. Int. Ed.*, 2012, 51(30), 7476-7479. My contribution to this chapter was in the preparation of one of the precursors to compound 6. Additionally, I spectroscopically monitored the reaction between compound 5 and compound 6 and took all the live-cell images. I thank Jun Yang, Jolita Seckute, and Neal Devaraj for their invaluable contributions to this chapter: Jun Yang synthesized and characterized all the compounds presented in this chapter; Jolita Seckute monitored the kinetics between compound 3 and the methylcyclopropene derivatives. In addition, she prepared the majority of the manuscript; and I would like to thank Neal Devaraj for directing the research and in the preparation of the manuscript.

Chapter three, in full, is a reprint (with co-author permission) of the material as it appears in the publication; **Christian M. Cole**, Dr. Jun Yang, Dr. Jolita Šečkutė and Prof. Neal K. Devaraj "Fluorescent Live-Cell Imaging of Metabolically Incorporated Unnatural Cyclopropene-Mannosamine Derivatives" *ChemBioChem*, 2013, 14(2), 205-208. I would like to thank Jun Yang, Jolita Seckute, and Neal Devaraj for their invaluable contributions to this chapter: Jun Yang synthesized and characterized all the compounds presented in this chapter; Jolita Seckute measured the fluorogenic response of tetrazine-Alexa Fluor 488 and its derivatives. I would like to thank Neal Devaraj for directing the research and for preparing the majority of the manuscript. The author of the dissertation is the primary author of this manuscript.

Chapter four, in full, is a reprint (with co-author permission) of the material as it appears in the publication; Sampreeti Chowdhuri, **Christian M. Cole** and Prof. Neal K. Devaraj "Encapsulation of Living Cells within Giant Phospholipid Liposomes Formed by the Inverse-Emulsion Technique" *ChemBioChem*, 2016, 17(10), 886-889. I would like to thank Sampreeti Chowdhuri for her invaluable contributions to this chapter: Sampreeti Chowdhuri prepared the encapsulated E. coli samples and carried out the CFU viability assay. I would like to thank Neal Devaraj for funding the research. The author of the dissertation is co-primary author of this manuscript and directed the research.

Chapter five is unpublished work. I would like to thank Roberto Brea, Hoaxing Wu, Robert Cooper, Shi Xinying and Neal Devaraj for their invaluable contributions to this chapter: Roberto Brea synthesized and characterized all the NCL compounds presented in this chapter; Hoaxing Wu synthesized and characterized all the CuAAC compounds; Shi Xinying purified ClpXP protein, eGFP superfolder-ssrA protein, and prepared the S30 lysate and reaction mix; Robert Cooper provided the CueR plasmid and the LacI plasmid. I would like to thank Neal Devaraj for help funding the research.

Chapter six, in full, is a reprint (with co-author permission) of the material as it appears in the publication; Dr. Roberto J. Brea, **Christian M. Cole**, Prof. Neal K. Devaraj "In Situ Vesicle Formation by Native Chemical Ligation" *Angew. Chem. Int. Ed.*, 2014, 53(51), 14102-14105. I would like to thank Roberto Brea and Neal Devaraj for their invaluable contributions to this chapter: Roberto Brea synthesized and characterized the majority of compounds presented in this chapter and characterized all the phospholipid analogues; I would like to thank Neal Devaraj for directing the

research. I purified eGFP, assisted in the synthesis of **19, 21** and helped with all microscopy.

Chapter seven, in part, is a reprint (with co-author permission) of the material as it appears in the publication; **Cole C.M.**, Brea R.J., Kim Y.H., Hardy M.D., Yang J., Devaraj N.K. "Spontaneous Reconstitution of Functional Transmembrane Proteins During Bioorthogonal Phospholipid Membrane Synthesis" *Angew. Chem. Int. Ed.*, 2015, 54(43), 12738-12742. I would like to thank Roberto Brea, Young Hun Kim, Michael Hardy, Hoaxing Wu, Jerry Yang and Neal Devaraj for their invaluable contributions to this chapter: Roberto Brea assisted in the synthesis of the NCL compounds; Young Hun Kim preformed the electrophysiology experiments; Michael Hardy assisted in the purification of compound **16** and **17**; Hoaxing Wu did the original CuAAC synthesis; I would like to thank Jerry Yang and Neal Devaraj for directing the research. The author of the dissertation is the primary author of this manuscript.

For the "Future Directions" in chapter seven, I would like to thank my collaborator Brent Lyda for his invaluable contributions for preforming the binding assays of A2a and for providing aliquots of the purified A2a protein. I would also like to thank Roger Sunahara for his insight and consultation and Roberto Brea for helping synthesize **26**.

Vita

Education

2004	B.S. Biochemistry, Lehigh University, Bethlehem, PA
2013	M.S. Chemistry & Biochemistry, University of California, San Diego, La Jolla, CA
2016	Ph.D. in Chemistry, University of California, San Diego, La Jolla, CA

Research Experience

2012-2015	UCSD Molecular Biophysics Training Program
2012-2013	Med-into-Grad Initiative HHMI
2009-2011	Research Assistant, UCSD Chemistry Dept.
2008	Summer Lab Assistant, Lehigh University, Chemistry Dept.

Publications

"Encapsulation of Living Cells within Giant Phospholipid Liposomes Formed by the Inverse Emulsion Technique", Sampreeti Chowdhuri · Christian M Cole · Neal K Devaraj, ChemBioChem, *in press* (2016)

"Site-specific covalent labeling of RNA by enzymatic transglycosylation", Seth C Alexander · Kayla N Busby · Christian M Cole · Cun Yu Zhou · Neal K Devaraj, Journal of the American Chemical Society 137 (40): 12756–12759 (2015)

"Spontaneous Reconstitution of Functional Transmembrane Proteins During Bioorthogonal Phospholipid Membrane Synthesis", Christian M. Cole · Roberto J. Brea · Young Hun Kim · Michael D. Hardy · Jerry Yang · Neal K. Devaraj, Angewandte Chemie International Edition 54 (43): 12738–12742 (2015)

"Self-reproducing catalyst drives repeated phospholipid synthesis and membrane growth", Michael D Hardy · Jun Yang · Jangir Selimkhanov · Christian M Cole · Lev S

Tsimring · Neal K Devaraj, Proceedings of the National Academy of Sciences 112(27):8187-8192 (2015)

"Bioorthogonal Tetrazine-Mediated Transfer Reactions Facilitate Reaction Turnover in Nucleic Acid-Templated Detection of MicroRNA", Haoxing Wu · Brandon T Cisneros · Christian M Cole · Neal K Devaraj, Journal of the American Chemical Society 136(52): 7942–17945 (2014)

"In Situ Vesicle Formation by Native Chemical Ligation", Roberto J. Brea · Christian M. Cole · Neal K. Devaraj, Angewandte Chemie International Edition 53(51): 14102–14105 (2014)

"Fluorescent Live-Cell Imaging of Metabolically Incorporated Unnatural Cyclopropene-Mannosamine Derivatives", Christian M Cole · Jun Yang · Jolita Sečkutė · Neal K Devaraj ChemBioChem14(2): 205-208 (2013)

"Live-Cell Imaging of Cyclopropene Tags with Fluorogenic Tetrazine Cycloadditions", Jun Yang · Jolita Šečkutė · Christian M Cole · Neal K Devaraj, Angewandte Chemie International Edition 51(30): 7476-7479 (2012)

Fellowship and Awards

2012-2015	San Diego Fellowship
2015	Poster Award for MBTG Seminar Retreat
2012	Recipient of the SDCSB seed grant
2012	Winner of The SDCSB Pre- & Post-Doc Challenge

Presentations

2015	Lipid Metabolism and Human Metabolic Disorders: CSH Asia Conference
2010	24th Annual Symposium of the Protein Society

Outreach

2010-2015	Laboratory mentorships

2013, 2015 Hands On Lab

2012, 2014 Young Scholar Program

Abstract of the Dissertation

Utilization of Bioorthogonal Chemistry for Live-Cell Labeling of Glycoconjugates and the Liposomal-Based Engineering of Dynamic Artificial Cellular Models

By

Christian Michael Cole

Doctor of Philosophy in Chemistry

University of California, San Diego, 2016

Professor Neal K. Devaraj, Chair

This dissertation will first explore the use of methylcyclopropene as an activated dienophile in the [4 + 2] inverse Diels–Alder cycloaddition with a tetrazine coupling partner for applications in bioimaging. Recently, bioorthogonal chemistries to label and track biomolecules in their native environment has received considerable interest from biochemists and chemical biologists. The tetrazine ligation is one such example, exhibiting robust kinetics and is mutually exclusive to other bioorthogonal reactions

making it feasible to carryout multiple-color labeling experiments. However, the classical coupling partners of tetrazine are bulky dienophiles, like norbornene and *trans*-cyclooctene. This potentially limits live-cell applications requiring sterically small labeling probes. In contrast, methylcyclopropene is the smallest cyclic alkene and as a tetrazine coupling partner it provides minimal steric impact that is often desired in intracellular investigations. In addition to the fast kinetics (k 13 $M^{-1}s^{-1}$), fluorophore conjugated tetrazines can also exhibit a fluorogenic "turn-on" upon cycloaddition with methylcyclopropene, making them well suited for live-cell imaging probes.

In the second investigation, this dissertation will explore two fundamental features of a phospholipid bilayer; their ability to encapsulate macromolecules and reconstitute transmembrane proteins. Phospholipid liposomes are akin to micron-sized flasks that can function as a delivery system and/or a bioreactor. In both of these applications high encapsulation efficiency is greatly desired or even necessary, but there are few liposomal methodologies that can achieve this. In order to integrate genetic circuits in liposomes we employed the inverted emulsion technique to make giant unilamellar vesicles that can be visualized by light microscopy. In addition, this method achieves greater than 90% encapsulation efficiency for polar macromolecules. Building off this technique we show it is possible to encapsulate live bacteria and yeast at high densities, which was previously only possible via microfluidics.

An alternative methodology of encapsulation can be accomplished with synthetic lipids that are composed of two clickable precursors, comprising of an alkyl chain and a lysophospholipid. Initial we demonstrated how this could work between an oleoyl azide and an alkyne lysophospholipid to form a triazole phospholipid, but due to

the low solubility of the azide oil in aqueous solutions we pioneered vesicle formation by native chemical ligation (NCL). In this system both precursors are water soluble allowing for higher encapsulation efficiency and similarly to the Cu(I)-catalyzed azide–alkyne cycloaddition, the NCL system can also spontaneously reconstitute active transmembrane proteins during membrane growth.

~ CHAPTER 1 ~

1 Introduction

1.1 Past to Present: Chemical Biology

Chemical biology is an interfacial scientific discipline that bridges the gap between biochemistry, organic chemistry, and pharmacology. In the past twenty years chemical biology has witnessed unprecedented growth and incredible innovation, furthering our understanding of complex biological systems. Undoubtedly, the practice of chemical biology has a rich history going back to the late eighteenth century with the accidental synthesis of urea[1] by Friedrich Wohler. However, the term "chemical biology" has no discernible origin, although it can be traced back to Caltech in the early 1920s by Thomas Morgan and Warren Weaver[2,3]. The "new-biology" program of this era was *molecular biology* and *physico-chemical biology*, inspired by variations of the *Institut de Biologie Physico-Chimique* (IBPC) program offered in France around the same time period. In the mid-1950s, through the vision of Thomas Morgan and Warren Weaver, the Laboratory of Chemical Biology at the California Institute of Technology was opened (Figure 1.1)[4] and is perhaps the earliest known example of "chemical biology" being adapted in the United States.

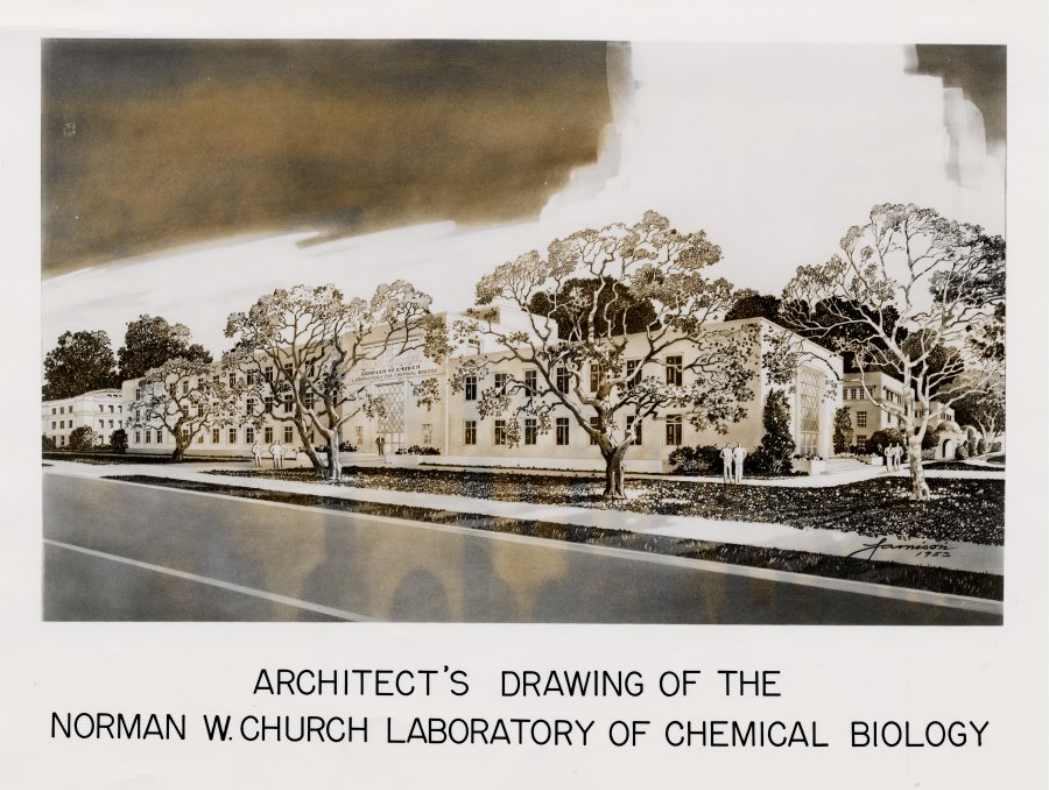

Figure 1.1 Architect's drawing of the Norman W. Church Laboratory of Chemical Biology at the California Institute of Technology in 1955

Historically the toolbox of a chemical biologist is with little exception that of chemistry, with applications focusing on the life sciences. This is a cogent notion considering the ultimate currency of biology is molecules and the compounds they form.[5] By the early-twentieth century chemistry had reached a degree of maturity and chemists had enormous success in their abilities to synthesize almost any desired compound and apply it to biological systems.[6] To better evaluate biology; additional quantitative tools were adapted from the habits and practices of chemists. The seminal

work of Francois Jacob, Jacques Monod, and colleagues is an example of the synergy between chemistry and biology in this era. Monod was testing substrates and inducers of the yet to be determined *lac* operon to provide a working model of gene regulation. These studies were made possible by the synthetic compound o-nitrophenyl-β-galactoside (ONPG). Colorless ONPG is hydrolyzed by β-galactosidase resulting in the yellowish compound o-nitrophenol.[7] In hand with a quantitative and sensitive assay for β-galactosidase Monod and colleagues identified numerous regulators of gene expression, including UV light and externally supplied lactose.[8] This would subsequently lead to the synthesis and use of isopropyl-β-D-thiogalactoside (IPTG) for bacterial inductions, an influential discovery still widely employed today. However, the overlap of chemistry and biology was still in its infancy largely due to the lack of structural knowledge obscuring the chemical workings of biology.[9] Consequently, many of the initial applications of chemical biology lacked rational design and instead focused on the administration of synthetic compounds on biological systems, thereby empirically deducing the compounds function.

Going into the early twenty-first century a major theme in chemical biology is the progression and development of many new chemical tools that were rationally designed to probe biological systems.[6] The classical example of biomolecular tagging is ectopically expressed fluorescent proteins (FP), however this approach is not well suited for non-protein base biomolecules; such as nucleic acids, glycans, lipids, small-molecule metabolites, and post-translational modifications in living systems. [10] These limitations were ameliorated by adorning "chemical handles" on biomolecules, which contain unique functional groups capable of the chemoselective bioconjugation to

chemical probes. A notable example came out of the Cravatt lab showcasing a library of fluorescent probes conjugated to specific substrates, which provided the activity units of a protein resulting from an acrylamide gel. This is in contrast to the typical coomassie dye employed, which only stains protein irrespective of their functional state[11]. This work highlights another every growing central facet of chemical biology, which is the bioconjugation of fluorescent molecules to specific targets.[12]

1.2 Bioorthogonal Chemistry

During the pioneering studies on metabolic engineering of cell surfaces by Carolyn Bertozzi, there was a strong interest in coupling agents that were chemoselective even in the biological milieu of a cell. While ligation reactions were available they often relied on functional groups that were susceptible to nucleophilic attack, most notable are the maleimides, N-hydroxysuccinimides and hydrazones. The need for better selectivity became apparent and lead Saxon and Bertozzi to the Staudinger reaction. The original Staudinger reaction was reported by Staudinger and Meyer in 1919, demonstrating that azides could react with triaryl phosphanes to form iminophosphoranes[13] (Scheme 1.1). There are several key intermediate steps, and it is

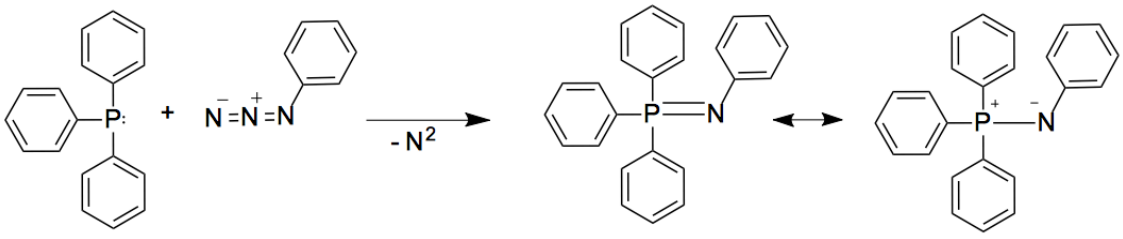

Scheme 1.1 Staudinger reaction: phosphane and an azide forms an iminophosphorane.

important to fully appreciate that the reaction proceeds without the formation of radicals or nitrenes, which would make them chemically promiscuous. Upon formation of the iminophosphorane the resonance form engenders the highly nucleophilic nitrogen capable of reacting with neighboring electrophiles.[14] Bertozzi rationally designed the phosphane with an electrophile attached on one of the phenyl rings, effectively trapping the nucleophilic aza-ylide, thus establishing a new form of ligation reaction (Scheme 1.2). This extremely powerful technique offered both, chemoselectivity and covalent chemistry to be used for the purposes of labeling and tracking biomolecules in living systems.

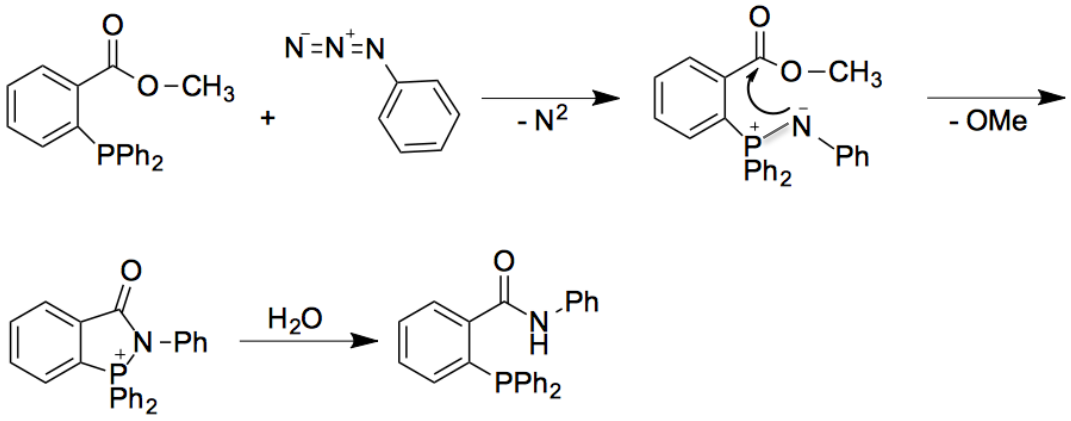

Scheme 1.2 Modified Staudinger reaction: the aza-ylide attacks the carbonyl thereby displacing a methoxy group and forming a stable amide bond after hydrolysis.

The modification of the Staudinger reaction ushered in a new conception of chemistry termed bioorthogonal chemistry. To be considered bioorthogonal chemistry as originally coined by Carolyn Bertozzi it had to fulfill two requirements: 1) Biologically and chemically Inert; to prevent the formation of undesired side reactions

in living cells, which includes a plethora of functional groups necessary to sustain life. 2) Fast kinetics; under physiological conditions it is often preferred to use low concentration of a compound to prevent toxicity, but still provide adequate temporal resolution compatible with living systems.[15]

Bioorthogonal chemistries have since proven to be powerful tools for the chemical biologist. In the past decade alone there has been well over a thousand bioorthogonal papers published, amassing over twenty thousand citations (Figure 1.4). Remarkably, the success of this field rests primarily on a handful of coupling reactions, notably including the modified–staudinger ligation[16], copper-catalyzed azide–alkyne cycloaddition[17], strain promoted azide–alkyne cycloaddition[18], photoinduced tetrazole-alkene cycloaddition[19], strain-promoted alkyne-nitrone cycloaddition[20], palladium-mediated cross-coupling reactions[21], ruthenium-catalyzed reactions[22] and the tetrazine ligation.[23]

Nevertheless, the applications of these techniques are exceedingly versatile. They have been employed to study glycans, proteins, lipids, nucleic acids and found

Graph 1.1 a) Journal entries published in the past decade on the concept of bioorthogonal chemistry as displayed by *web of science's* portal. b) Citations in past decade on the papers recorded in the previous graph

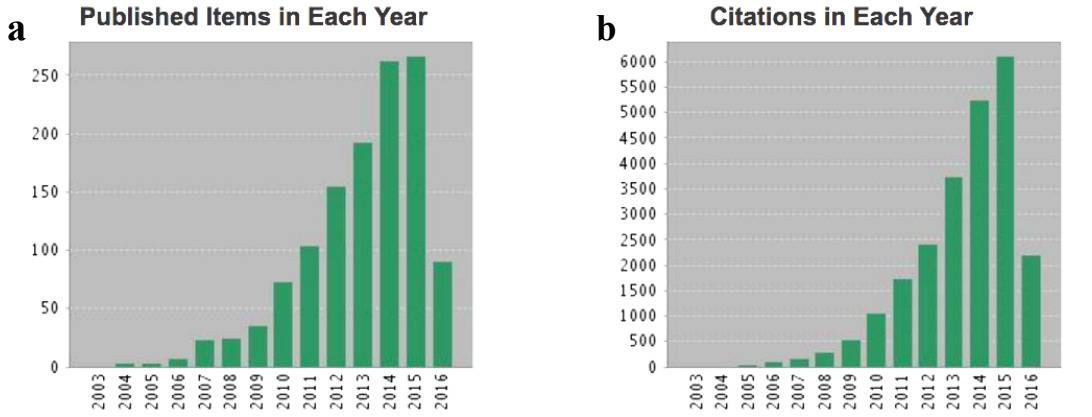

several applications outside of the life sciences. Depending on the intended application there are considerations for each technique (i.e. the copper catalyzed azide-alkyne reaction requires copper, which can be cytotoxic and proteotoxic; the rate constants of the modified-staudinger reaction is sluggish making live cell investigations challenging). A benefit of bioorthogonal chemistry is that many of the above approaches are mutually exclusive and employ bioorthogonal pairs that can have applications in multi-labeling experiments. In the first part of this thesis we will explore the use of a mutually exclusive tetrazine ligation in tandem with a strain-promoted azide-alkyne cycloaddition reaction in a duel-labeling experiment of SK-BR-3 cells.

1.3 Tetrazine Ligation

The tetrazine ligation originated with the pioneering work done by Ruhemann [24,25,26] towards the end of the nineteenth century, he synthesized the core-ring of the s-tetrazine, also known as the 1,2,4,5-tetrazines from hydrazine and potash. Later, Carboni and Lindsey[27] shows that tetrazines can react with unsaturated compounds releasing nitrogen gas in the process. This was further expounded upon by Sauer in the 1990s[28], whereby he characterized the kinetics of tetrazine and dienophile pairs. Still it will take another decade before a water-stable tetrazine derivative is used for bioconjugation[23]. Tetrazines substituted with electron withdrawing groups are often attributed to have extremely fast kinetics without a catalyst and proceed in high yield in organic solvents, water, and even cell lysate[23] making them ideal for live-cell bioorthogonal applications. To put the kinetics of tetrazine into perspective; the

majority of the commonly used bioorthogonal ligations have a second order rate constant of ($k_2 < 1$ $M^{-1}sec^{-1}$)[18,29,30]. Assuming a second-order rate constant between the labeling agent and coupling partner to be a customary concentration of one micromolar, then it would take over eleven days for fifty-percent of the coupling reaction to be completed. Thus, in live cells these methodologies suffer from slow kinetics, requiring long reaction times or excessive concentration of either the labeling agent or coupling agent.[31] The 1,2,4,5-tetrazines proceeds through a [4 + 2] Diels-Alder cycloaddition with *trans*-cyclooctene resulting in a dihydropyridazine product forming a irreversible ligation at k_2 ~2000 $M^{-1}sec^{-1}$ [23]. More recently Hilderbrand and colleagues have shown a k_2 of ~30000 $M^{-1}sec^{-1}$ between a 1,2,4,5-Tetrazin-3-yl-benzoic Acid and *trans*-cyclooctene.[32] These extremely fast rates make the tetrazine ligation applicable for a wide range of biological inquiry.

The derivatives of the s-tetrazines, substituted commonly with phenyl groups, are relatively large molecules (>300 da). However, in order to achieve the rapid rates of the tetrazine ligation it is also necessary to employ sterically large dienophiles such as *trans*-cyclooctene, cyclooctyne, and norbornene. Of course, this is a conflict with the growing trend to use bioorthogonal probes as "chemical handles" in the study of the cell's metabolic pathways. These pathways can be highly sensitive to the size and chemical properties of the handle.[33] Consequently, the use of smaller dienophiles would alleviate these potential limitations and provide an additional tool for the tetrazine ligation. In the subsequent chapters we will discuss the feasibility of using cyclopropene as a dienophile in the [4 + 2] Diels-Alder cycloaddition with tetrazine.

~ CHAPTER 2 ~

2 Live-Cell Imaging of Cyclopropene Tags with Fluorogenic Tetrazine Cycloadditions

2.1 Introduction

There is growing interest in the use of inverse Diels–Alder tetrazine cycloadditions as rapid, catalyst-free bioorthogonal reactions.[23,31,34] Fluorogenic tetrazines that increase in fluorescence after reactions with dienophiles are particularly useful for live-cell imaging applications.[35] Fluorogenic tetrazines have recently been used for live-cell imaging of small molecules, biomolecules tagged enzymatically with dienophiles, and proteins modified by reactive unnatural amino acids.[35,36] Although fluorogenic tetrazine probes hold great potential for intracellular imaging of small molecules, previous approaches are limited by requiring a large strained dienophile, such as trans-cyclooctene, cyclooctyne, or norbornene.[35,37–40] This methodology is in contrast to Staudinger ligations or strain-promoted azide–cycloalkyne cycloadditions that utilize a small azide functional group.[16,29] This requirement has limited the use of tetrazine reactions in methods that require tags with minimal steric impact or nominal effect on the partition ratio.[31] The development of smaller dienophile partners capable of reacting rapidly with tetrazines would therefore represent a major advance. However, it has been unclear whether small dienophiles could be developed that react rapidly with tetrazines while maintaining their stability. Herein, we demonstrate the applicability of methylcyclopropene tags as dienophiles for reaction with fluorogenic

tetrazines. Through systematic synthetic modifications we have optimized the stability, size, and reactivity of the cyclopropene scaffold. We have developed methylcyclopropene derivatives that react rapidly with tetrazines while retaining their aqueous stability and small size. These cyclopropene handles elicit fluorescent responses from quenched tetrazine dyes and are suitable for cellular imaging applications, which we demonstrate by imaging cyclopropene phospholipids distributed in live human breast cancer cells. The use of cyclopropenes offers a possible approach to smaller dienophile partners for tetrazine cycloadditions. It has long been known that cyclopropenes react rapidly with tetrazines to form stable

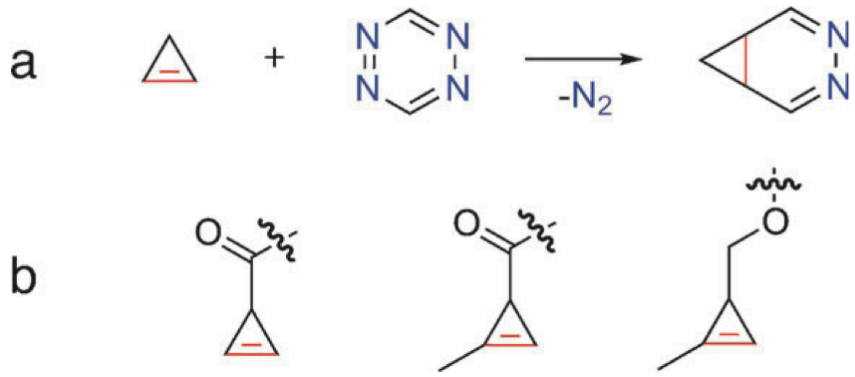

Scheme 2.1 a) Inverse Diels–Alder reaction of cyclopropene with tetrazine results in loss of nitrogen gas and formation of a diazanorcaradiene. b) Examples of substituted cyclopropene handles that may be suitable dienophiles for tetrazine cycloaddition.

diazanorcaradienes (Scheme 2.1a).[41–44] In seminal work, Sauer and co-workers demonstrated that unsubstituted cyclopropene reacts with dimethyl 1,2,4,5- tetrazine-

3,6-dicarboxylate extremely rapidly, measuring a rate constant of 448 m^{-1} s^{-1} in dioxane at 20°C.[28] However, unsubstituted cyclopropene is highly unstable, dimerizing and polymerizing readily at room temperature.[45,46] Our challenge was to create a stable cyclopropene handle while maintaining rapid tetrazine reactivity and small size. The stability of cyclopropenes can be dramatically increased by substitution and we envisioned several substituted cyclopropenes that could be suitable for cycloaddition with tetrazines (Scheme 2.1b).[45,47,48] Sauer and co-workers demonstrated that substitutions do not necessarily diminish the reactivity of cyclopropenes with tetrazine. In fact, the reaction of 3-methylcycloprop-1-ene with tetrazine proceeded with a slightly higher rate constant than the unsubstituted cyclopropene. However, 3,3-dimethylcycloprop-1-ene reacted with the same tetrazine approximately 5766-times slower, illustrating the importance of balancing stability with reactivity.[28]

2.2 Designing Cyclopropenes: Balancing Stability and Reactiveness

Based on studies from Sauer and co-workers, we initially synthesized carboxamide derivatives of cycloprop-2-enecarboxylic acid without substitution of the double bond. These dienophiles reacted very rapidly with monoaryl tetrazines, but the substituted cyclopropenes proved to be highly unstable and could not be stored overnight at 20°C without degradation. Recently, Fox and co-workers have elegantly demonstrated that N-acyloxazolidinone derivatives of cycloprop-2-enecarboxylic acid are unusually stable and therefore valuable cyclopropene synthons.[49] Unfortunately, these modifications require a significant increase in the size of the reactive moiety and

would defeat the purpose of using a small cyclopropene tag. The addition of a methyl substituent on the alkene offers an alternative method to improve stability with a less-dramatic steric impact.[48] Protected methylcyclopropene **1** was generated by rhodium-catalyzed cyclopropenation and used to synthesize 2-methylcycloprop-2-enecarboxamide (**2**).[50] The synthesis of **2** required four steps from commercially available starting materials and was completed in 21 % overall yield (Scheme 2.1a). As expected, the addition of a methyl group dramatically improved cyclopropene stability, and **2** could be stored for extended periods of time at −20°C without degradation. However, these derivatives reacted sluggishly with benzyl alcohol tetrazine (**3**; Scheme 2.1b)[51] By monitoring the disappearance of the characteristic tetrazine absorption band at 520 nm, we measured a second-order rate constant of 0.137 ±0.004$M^{-1}s^{-1}$ at 37°C in a solution of water/ DMSO (12% DMSO by volume; Figure 2.1). Although this rate constant is comparable to previous bioorthogonal labeling strategies,[29] it is much slower than the reaction of other strained alkenes with tetrazine, such as *trans*-cyclooctene and even norbornene.[23] Faster kinetics would improve coupling yields, particularly for applications where it is not possible to flood the target with a large excess of reactant, for example in live-cell intracellular labeling or in vivo.

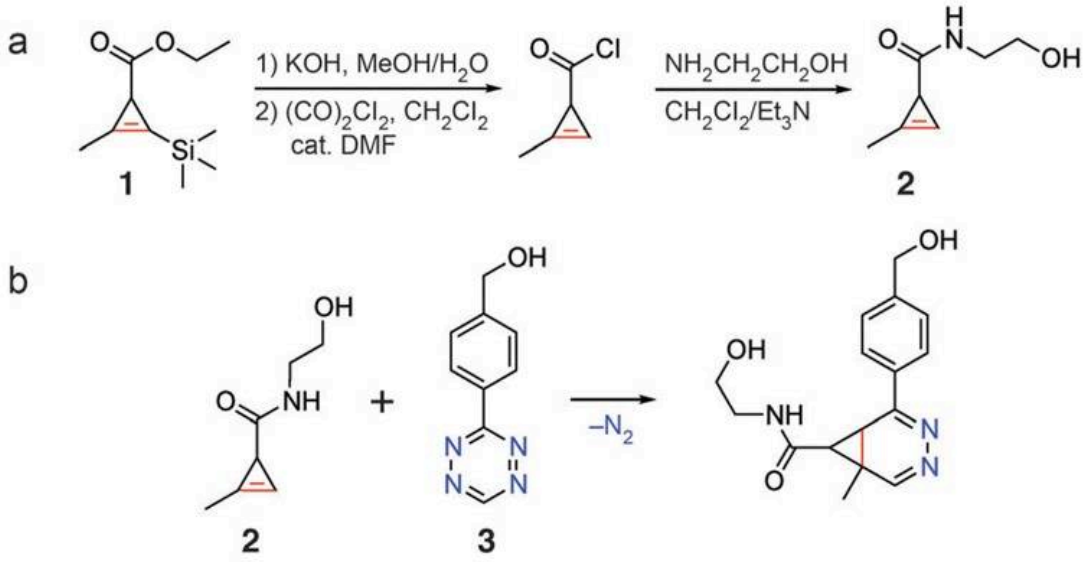

Scheme 2.2 a) Synthesis of 2-methylcycloprop-2-enecarboxamide (**2**). DMF =dimethylformamide. b) Reaction of **2** with monoaryl tetrazine **3** leads to formation of diazanorcaradiene isomers (only one regioisomer is depicted).

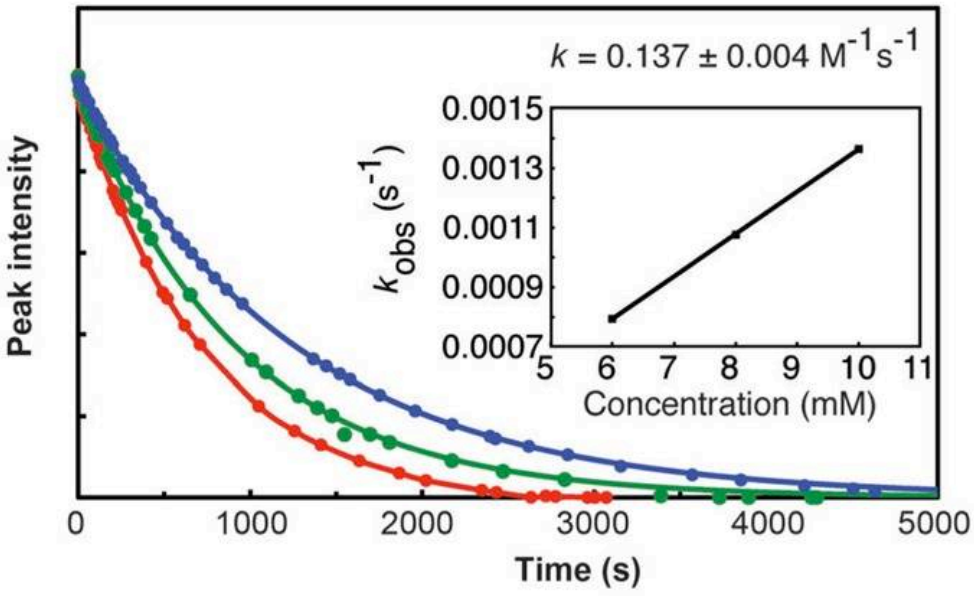

Figure 2.1 Plot of tetrazine absorbance versus time during the reaction between 0.6 mM tetrazine **3** and cyclopropene **2**, [6 (blue), 8 (green), or 10 mM (red)]. Data was fit to a first-order exponential decay. Inset: k_{obs} plotted against concentration with the slope taken as the second-order rate constant.

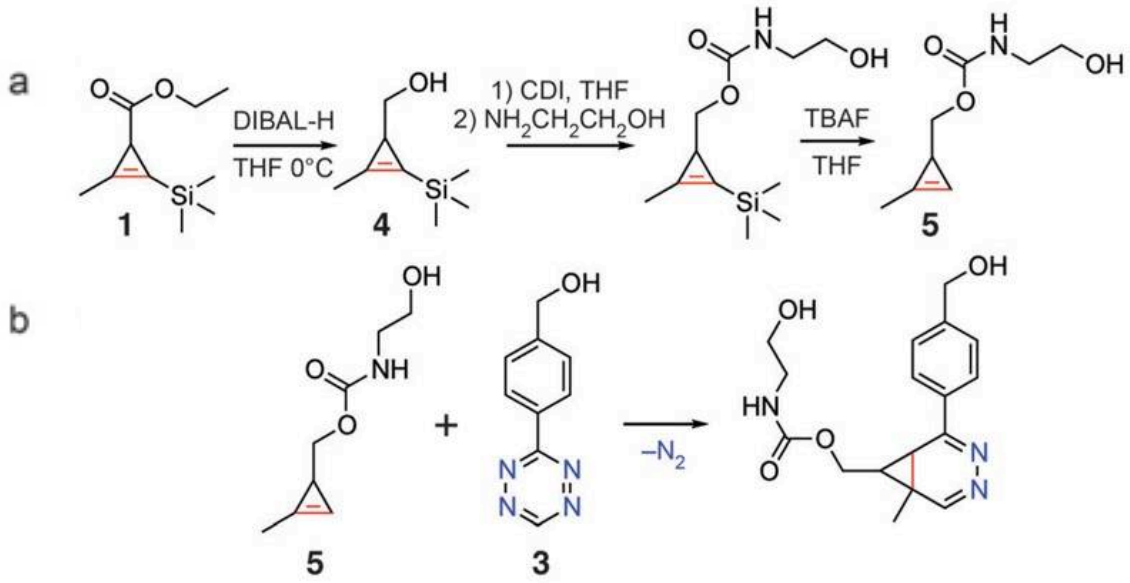

Scheme 2.3 a) Synthesis of 2-methylcyclopropene carbamate (**5**). DIBAL-H =diisobutylaluminum hydride; CDI =carbonyldiimidazole; THF =tetrahydrofuran; TBAF =tetra-*n*-butylammonium fluoride. b) Reaction of **5** with monoaryl tetrazine **3** leads to formation of diazanorcaradiene isomers (only one regioisomer is depicted).

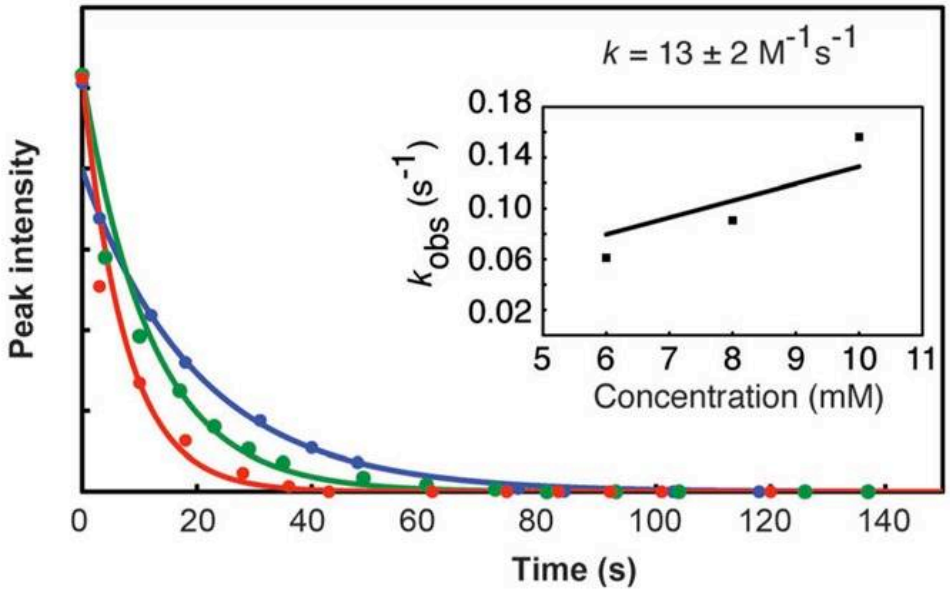

Figure 2.2 Plot of tetrazine absorbance versus time during the reaction between 0.6 mM tetrazine **3** and cyclopropene **5**, [6 (blue), 8 (green), or 10 mM (red)]. Data was fit to a first-order exponential decay. Inset: k_{obs} plotted against concentration with the slope taken as the second-order rate constant.

In an attempt to improve the kinetics of cycloaddition, we reduced the ester of precursor **1** to form [2-methyl-3-(tri-methylsilyl)cycloprop-2-en-1-yl]methanol (**4**; Scheme 2.2a). Compound **4** is a highly convenient synthon that can be made in two steps from commercially available starting materials. Methylcyclopropene**4** can be further conjugated to primary amines by carbamate formation, followed by deprotection of the trimethylsilyl protecting group to afford 2-methylcyclopropene carbamate (**5**). The synthesis of **5** required five steps from commercially available starting materials and was completed in 33% overall yield. Unlike the synthesis of *trans*-cyclooctene, the synthesis of cyclopropene **5** does not require the use of an ultraviolet reactor, silver nitrate trapping agent, or a metering pump.[52] We speculated that **5** would possess the stability afforded by the methyl derivatized alkene but display increased inverse Diels-Alder reactivity compared to **2** by elimination of the electron-withdrawing carbonyl. Indeed, carbamate **5** was highly reactive with tetrazine **3** (Scheme 2.2b), and cycloaddition proceeded with a second-order rate constant of 13 $\pm 2 M^{-1}s^{-1}$ at 37°C in a solution of water/DMSO (12% DMSO by volume; Figure 2.2). This is an improvement of approximately two orders of magnitude compared to cyclopropene carboxamide **2**. At 20°C, we measured a rate constant of 7 $\pm 1 M^{-1}s^{-1}$ (12% DMSO by volume; Figure 2.3). Methyl-cyclopropene **5** could be stored at −20°C without degradation and displayed excellent stability in aqueous solutions at 37°C for over 24 h (Figure 2.4). Furthermore, **5** was stable in aqueous solutions containing L-cysteine, both at room temperature and after heating at 60°C (Figure 2.5), in agreement with previous studies on related methylcyclopropenes.[53] Interestingly, when heated to 60°C in the presence

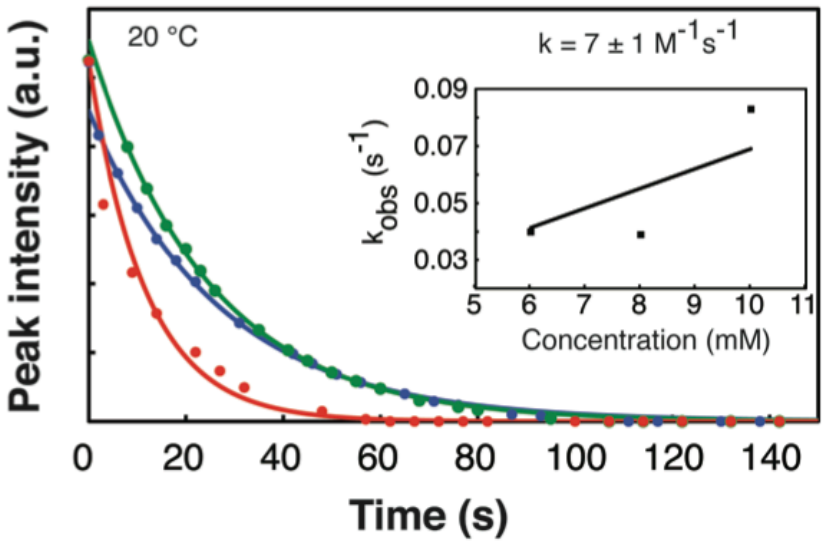

Figure 2.3 Kinetics of the tetrazine **3** reaction with cyclopropene **5** at 20 °C. Experiment was done with 0.6 mM tetrazine **3** and increasing excess of cyclopropene **5**: 6.0 mM (green), 8.0 mM (blue), 10.0 mM (red). Insert shows the corresponding observed reaction rates (k_{obs}) from the fitted data (individual fits shown as lines in the main graph) plotted against cyclopropene **5** concentrations. The slope of the resulting line was used to determine the second-order rate constant, indicated in the upper right corner.

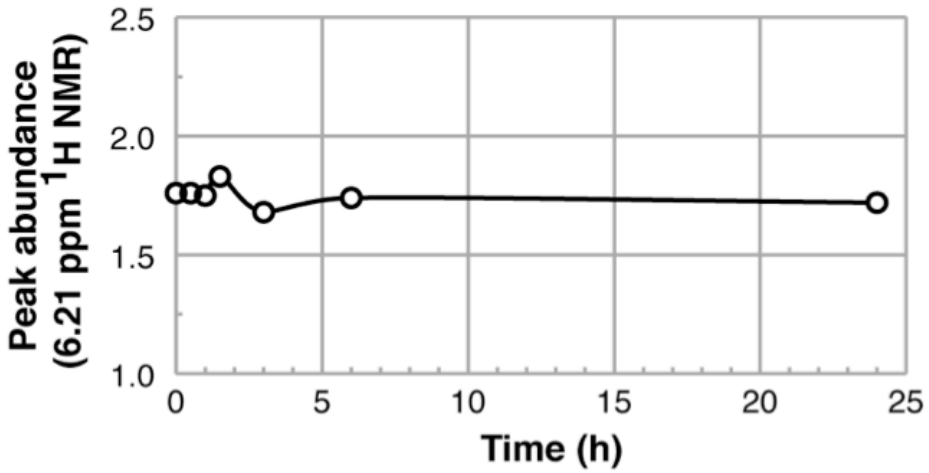

Figure 2.4 Time course of stability of cyclopropene carbamate **5** by ^{1}H NMR peak abundance at 6.21 ppm over 24 h.

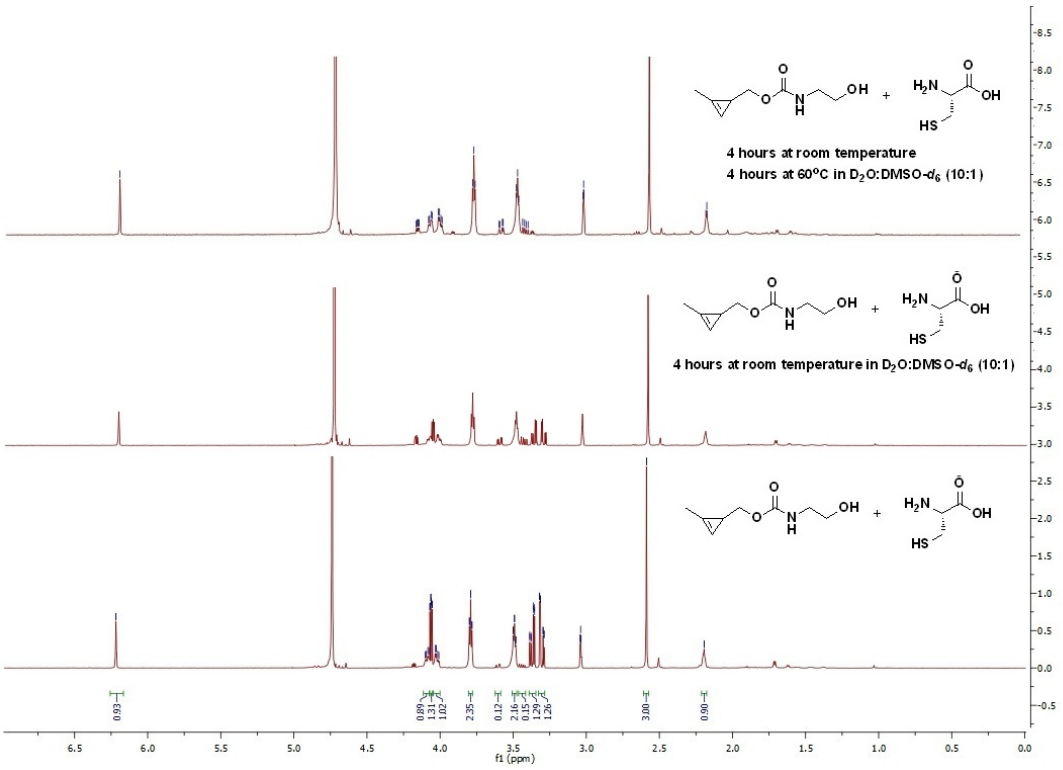

Figure 2.5 ^{1}HNMR spectrum of methyl cyclopropene **5** and L-cysteine after 4 hours at room temperature; 4 hours at room temperature and 4 hours at 60 °C in D_2O:DMSO-d_6 (10:1). L-cysteine slowly oxidizes to cystine over the time-course of the experiment.

of L-cysteine, we found that *trans*-cyclooctenol [*rel*-(1*R*,4*E*,p*R*)-cyclooct-4-enol] isomerized slowly to *cis*-cyclooctenol (Figure 2.6). Although further work will be needed to determine the relevance of this phenomenon for bioconjugation, it does illustrate that, under certain conditions, methylcyclopropenes may possess superior stability to *trans*-cyclooctenes, because cyclopropenes are not subject to this *cis*/*trans*-isomerization.

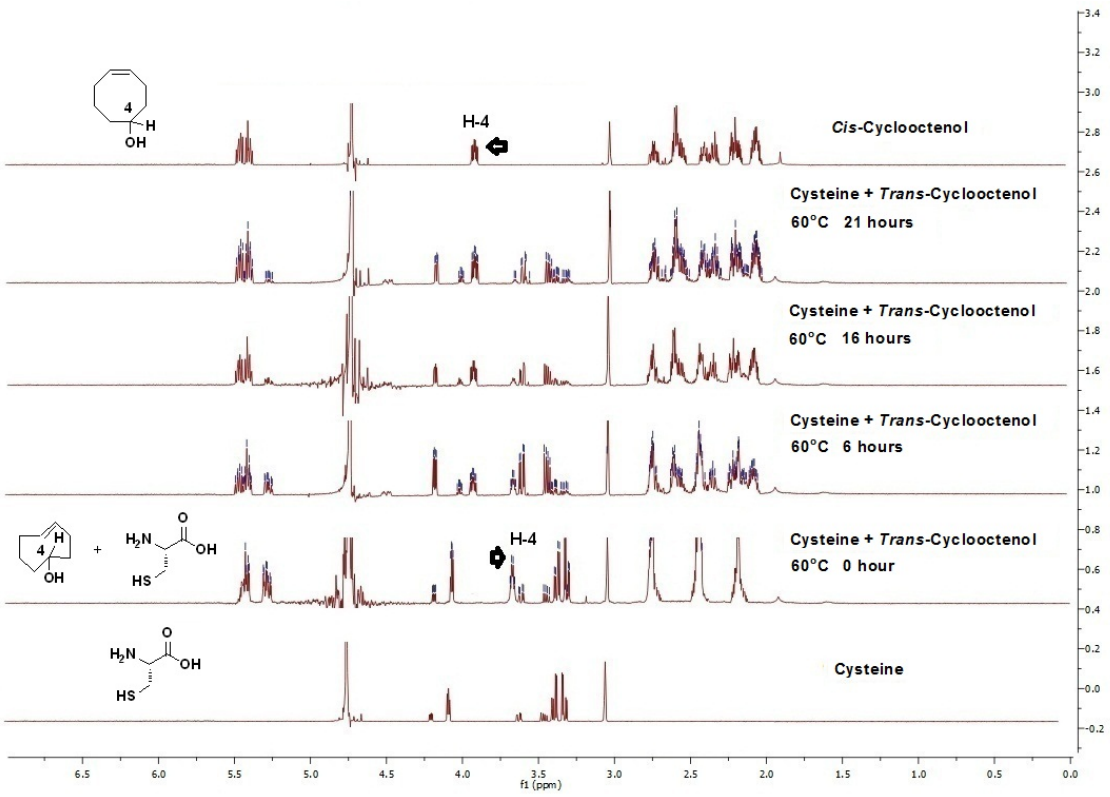

Figure 2.6 [1]HNMR spectra demonstrating the conversion of *trans*-cyclooctenol to *cis*-cyclooctenol in the presence of L-cysteine at 60 ºC. L-cysteine slowly oxidizes to cystine over the time-course of the experiment.

2.3 Fluorogenic "Turn-On" of Fluorophore-Conjugated Tetrazines with Methylcyclopropene

Fluorogenic probes are highly valuable in live-cell imaging applications owing to an inherently lower background fluorescence from nonspecific binding or accumulation.[35,54] This is particularly relevant for imaging intracellular molecules as washout can be problematic. Recent work has demonstrated that tetrazines are capable of significantly quenching several bright fluorescent probes, potentially through a resonant energy transfer mechanism.[55] These probes show significant fluorescent "turn-on" after reaction with dienophiles, can be synthesized from commercially

available reactive precursors, and use bright, conveniently excited fluorophores that are commonly used in cellular imaging, such as boron dipyrromethane (BODIPY) and Oregon Green. The combination of recently discovered high-quality fluorogenic

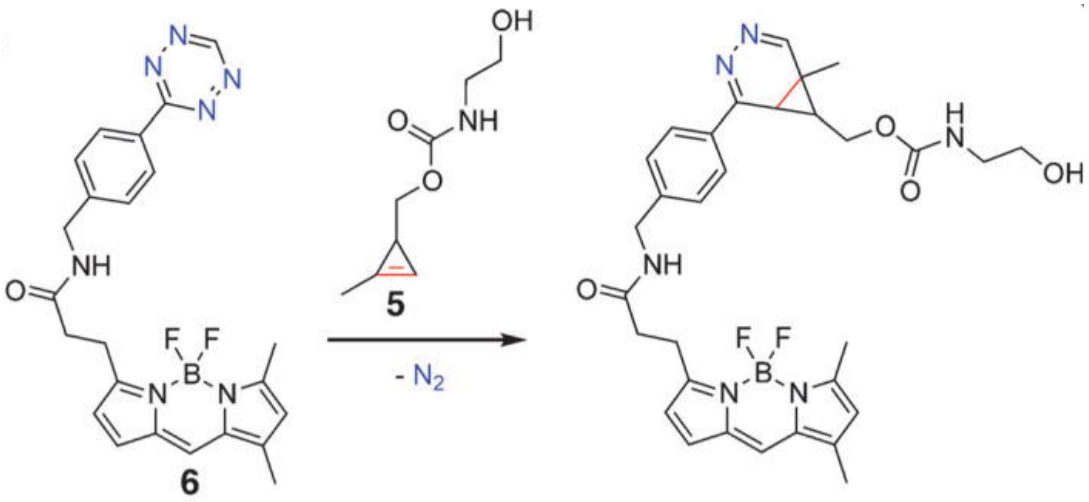

Scheme 2.4 Reaction of fluorogenic tetrazine-BODIPY FL **6** with **5.**

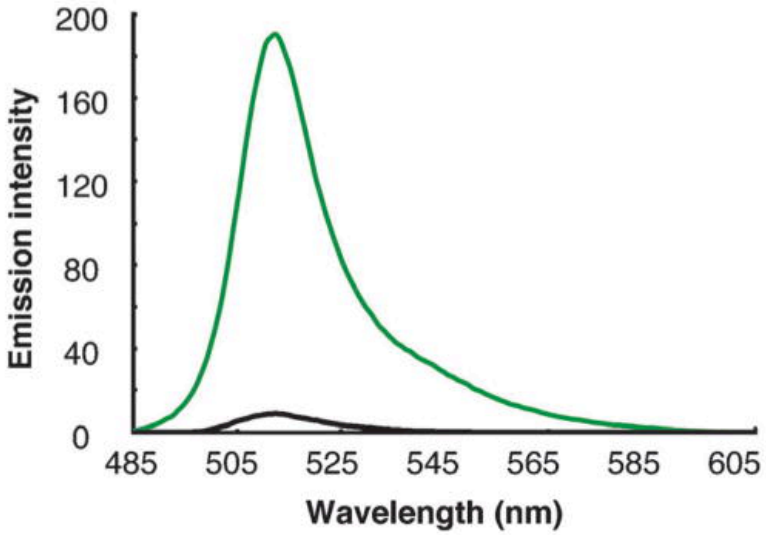

Figure 2.7 Emission spectra of tetrazine-BODIPY FL before reaction with **5** (black) and after reaction (green).

tetrazine probes, such as tetrazine-BODIPY FL, with small dienophile tags would advance bioorthogonal live-cell imaging. Tetrazine-BODIPY FL probe (**6**) reacts rapidly with **5**, with a concomitant increase in fluorescence (Figure 2.7, Scheme 2.4).[35] In phosphate-buffered saline at 20°C, there is a 22-fold increase in fluorescence intensity at 512 nm after addition of excess **5**, similar to previous measurements of fluorescence increase after reaction with other strained dienophiles.[35,36] The reaction can also be monitored by liquid chromatography/mass spectrometry. Addition of one equivalent of **5** results in complete reaction of the tetrazine-BODIPY FL and, as expected, the formation of multiple overlapping peaks all with the molecular mass of the diazanorcaradiene isomers (Figure 2.8).

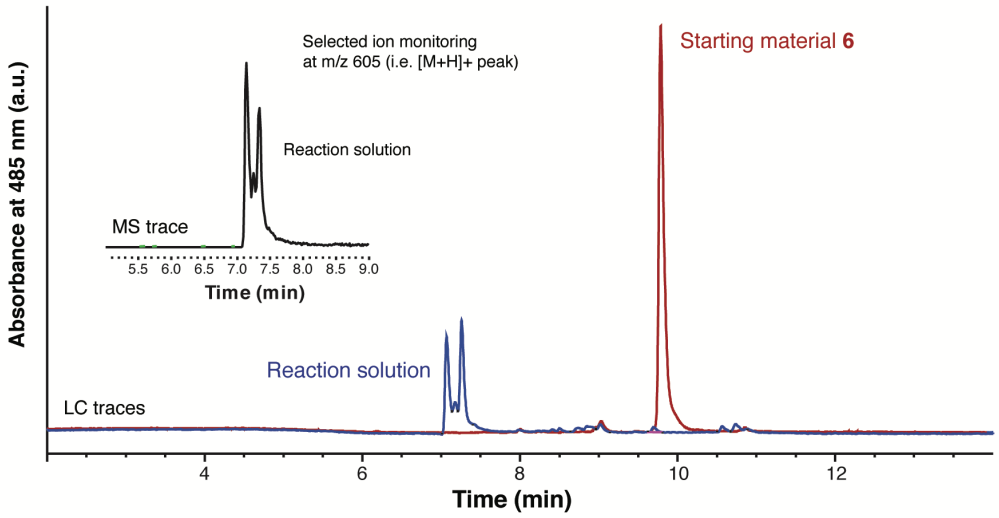

Figure 2.8 Reaction between tetrazine-BODIPY FL **6** with cyclopropene **5**. HPLC trace of purified tetrazine-BODIPY FL **6** (0.08 mM in 8% DMF/H_2O) (red line). HPLC trace of the reaction products from addition of cyclopropene **5** to tetrazine-BODIPY FL **6** (blue line). MS trace of the reaction solution, selected ion monitoring at m/z 605 (i.e. $[M+H]^+$ peak) (black insert line).

Live-cell labeling of bioorthogonal functional groups has emerged as a powerful tool for analyzing small molecule distributions in cells.[56] To demonstrate the applicability of cyclopropene tags for live-cell imaging using fluorogenic tetrazine cycloadditions, we synthesized a cyclopropene tagged phospholipid **7** (Scheme 2.5), which we characterized by NMR spectroscopy and high-resolution mass spectrometry.

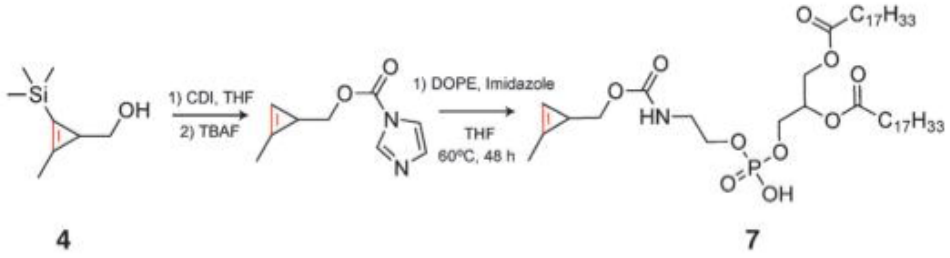

Scheme 2.5 Synthesis of cyclopropene phospholipid **7**.

Bioorthogonal reactions are increasingly used for lipid imaging and labeling, and there have been several exciting applications, such as metabolic labeling of choline phospholipids, high-throughput analysis of protein lipidation, and monitoring the trafficking of soluble lipids.[57–61] Cyclopropene–tetrazine cycloadditions would allow lipophilic fluorogenic tetrazines to be used, offering the important advantage of intracellular imaging in live cells (Figure 2.9). Additionally, in vitro applications would benefit from improved reaction kinetics and the lack of redox-active copper catalysts, which can potentially damage biomolecules while adding an extra layer of complexity.[62,63] To image the distribution of cyclopropene phospholipids in human cells, we incubated SKBR3 breast cancer cells in media (cDMEM) containing 50

μM **7** for one hour. After washing with media, the cells were subsequently incubated with 10 μM of tetrazine-BODIPY FL for one hour. Cells were then washed and imaged using confocal fluorescence microscopy (Figure 2.9b).

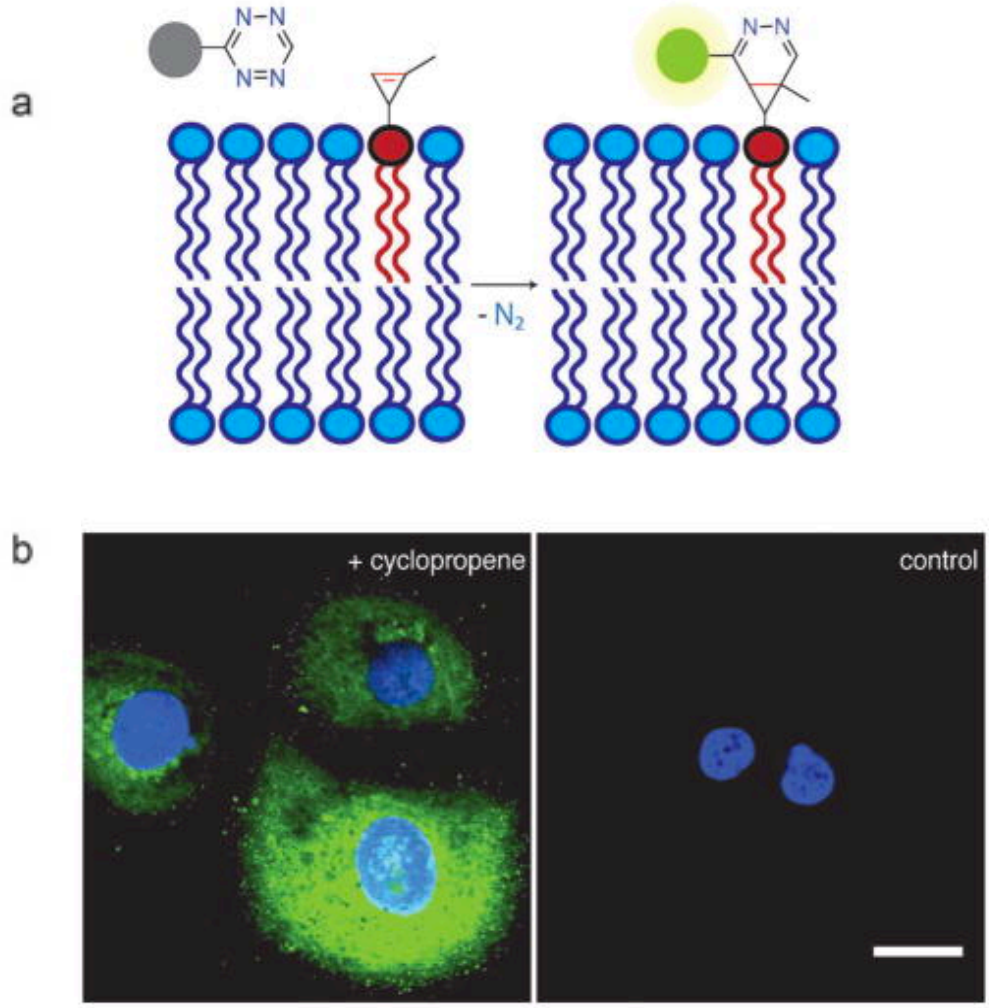

Figure 2.9 a) Reaction of fluorogenic tetrazine-BODIPY FL with membrane-bound **7**. The BODIPY chromophore is initially quenched by tetrazine with the fluorescence recovered after cycloaddition and formation of the coupling adduct. DOPE =1,2-dioleoyl-*sn*-glycero-3-phosphoethanol-amine. b) Live-cell confocal imaging of **7** distribution in SKBR3 cells with the fluorogenic probe tetrazine-BODIPY FL. Left: cells incubated (t=1 h) with 50 μM **7** followed by 10 μM tetrazine-BODIPY FL probe (t =1 h; green). Right: control in which SKBR3 cells were treated with 10 μM tetrazine-BODIPY FL (t =1 h; green). Cells were treated with 300 nM DAPI to visualize the nuclei (blue). Scale bar =20 μm.

Staining of membrane structures could be readily observed with a notable absence of staining within the nucleus (Figure 2.10). In contrast, control cells that were not exposed to **7** but were treated with the tetrazine-BODIPY FL probe showed relatively negligible background staining, demonstrating the benefit of using a fluorogenic cycloaddition, which significantly mitigates the signal from nonspecific binding. Images obtained with 7 were similar to images obtained with a modified *trans*-cyclooctene 1,2-Dioleoyl-sn-glycero-3-phosphoethanolamine (DOPE) lipid **9** (Figure 2.10), indicating that, under the conditions tested, the cyclopropene tag is of comparable quality for live-cell imaging with respect to previously introduced dienophiles. We are presently utilizing **7** to visualize phospholipid uptake in several model systems. Additionally, we are synthesizing additional cyclopropene lipid tags to image and detect specific lipid distribution and lipid post-translational modifications in live cells.

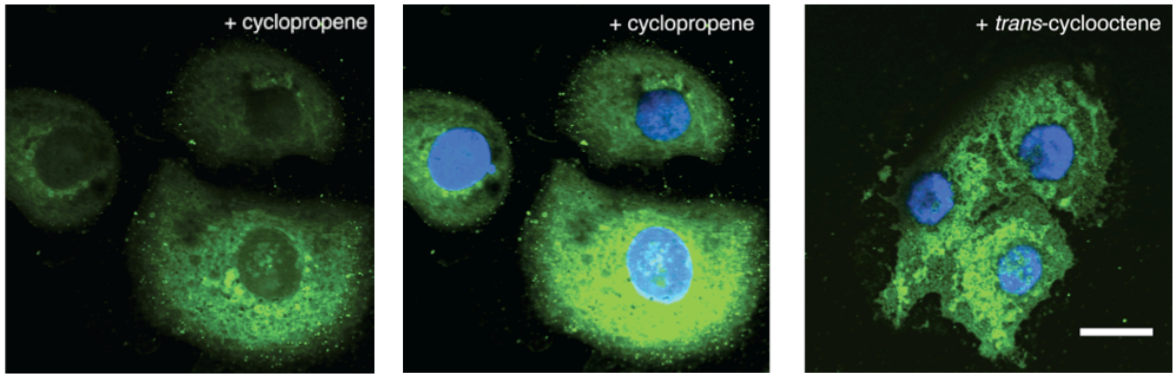

Figure 2.10 Staining of SKBR3 cells with cyclopropene **7 (**50 μM) by tetrazine-BODIPY FL (10 μM) with notable absence of staining within the nucleus (left panel). The green fluorescence (left panel and middle panel) is the result of the cycloaddition of the quenched tetrazine-BODIPY FL probe with the methyl-cyclopropene carbamate. Staining of *trans*-cyclooctene modified DOPE phospholipid **9** (50 μM) by tetrazine-BODIPY FL (10 μM)(right panel) Scale bar denotes 20 μm.

2.4 Concluding Remarks

In conclusion, we have studied the suitability of methyl-cyclopropene tags as small dienophiles for tetrazine bioconjugation chemistry. Modulating the substituents of cyclopropenes can have a dramatic effect on their stability and on the kinetics of tetrazine cycloaddition. Through synthetic modification of the cyclopropene scaffold, we have developed a methylcyclopropene derivative that is stable in aqueous solution but retains high reactivity with tetrazines. Cyclopropene derivatives are capable of eliciting a strong fluorogenic response from quenched tetrazine fluorescent probes, and this feature can be used to perform live-cell imaging, which we demonstrated by labeling cyclopropene-modified phospholipids. We believe the use of methylcyclopropenes will extend the advantages of tetrazine cycloadditions to small-molecule tracking applications that require minimal reaction partners. We are currently pursuing applications that incorporate cyclopropenes into metabolic and enzyme activity reporters, such as lipid, monosaccharide, and amino acid analogues.

2.5 Experimentals and Methods

2.5.1 Materials

All chemicals were received from commercial sources and used without further purification. Thin layer chromatography (TLC) was performed on silica gel. Chromatographic purifications were conducted using 40-63 μm silica gel. All mixtures of solvents are given in *v*/*v* ratio. ^{1}H and ^{13}C NMR spectroscopy was performed on a Varian NMR at 400 (^{1}H) or 100 (^{13}C) MHz and a Jeol NMR at 500 (^{1}H) or 125 (^{13}C) MHz. All ^{13}C NMR spectra were proton decoupled.

2.5.2 Synthesis of cyclopropene 2

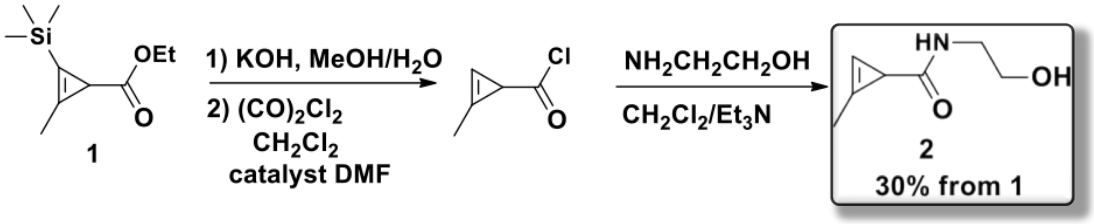

Scheme 2.6 synthesis of cyclopropene **2**

Compound **1** was synthesized according to a previously reported method[64] and was obtained in 70% yield. To a stirred solution of compound **1** (213.0 mg, 1.0 mmol) in MeOH (4.0 mL) at 0 ºC was slowly added a solution of KOH (140.0 mg, 2.5 mmol) in H_2O (1.0 mL) dropwise. After all the KOH was added, the reaction mixture was stirred overnight at room temperature before it was diluted with 10 mL H_2O and

extracted with EtOAc (10 mL×2). The pH value of the aqueous layer was adjusted to 3 by addition of 1M HCl, then extracted with EtOAc (10.0 mL×3), the combined organic layer was dried over Na_2SO_4 and evaporated to afford 72 mg of the crude methyl cyclopropene acid as a colorless oil.

The crude acid was dissolved in 5 mL CH_2Cl_2 and one drop of DMF was added, followed by $(CO)_2Cl_2$ (126 mg, 1.0 mmol). The resulting solution was stirred for 2 hours at room temperature and then evaporated to afford the crude methyl cyclopropene acid chloride.

To a stirred solution of ethanolamine (61 mg, 1.0 mmol) and Et_3N (101 mg, 1.0 mmol) in CH_2Cl_2 (2 mL) was added a solution of the above methyl cyclopropene acid chloride in CH_2Cl_2 (2 mL). The resulting reaction solution was stirred for 1 hour at room temperature and then evaporated to afford the crude product. The residue was purified using preparative TLC (EtOAc/Hexane = 1.5:1) to afford 42 mg of compound **2**. The overall yield is 30% from compound **1**.

^{1}H NMR (500 MHz, $CDCl_3$) δ 2.03 (1H, d, J = 5 Hz), 2.18 (3H, d, J = 5 Hz), 2.98 (1H, bs), 3.43 (2H, t, J = 5 Hz), 3.71 (2H, t, J = 5 Hz), 5.90 (1H, bs), 6.44 (1H, s); ^{13}C NMR (125 MHz, $CDCl_3$) 10.70, 22.35, 42.63, 62.41, 95.91, 113.57, 177.71; HRMS $[M+Na]^+$ m/z calcd. for $[C_7H_{11}NO_2Na]^+$ 164.0682, found 164.0684.

2.5.3 Synthesis of (2-methyl-3-(trimethylsilyl)cycloprop-2-en-1-yl)methanol 4

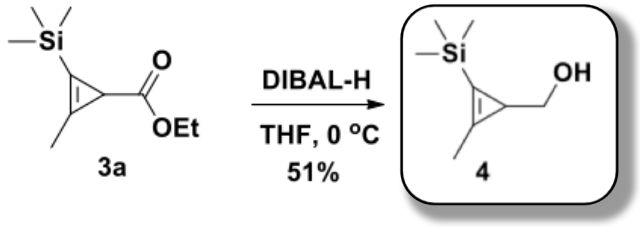

Scheme 2.7 Synthesis of (2-methyl-3-(trimethylsilyl)cycloprop-2-en-1-yl)methanol **4**

To a stirred solution of compound **1** (2.0 g, 10.0 mmol) in dry THF (25.0 mL) at 0 ^{o}C was slowly added a solution of 1.0 M $LiAlH_4$ in THF (25.0 mL, 25.0 mmol) dropwise. After addition of $LiAlH_4$, the reaction mixture was stirred 3 hours at 0 ^{o}C before it was quenched with H_2O carefully. The precipitate was filtered and the filtrate was concentrated to give the crude product. The residue was purified by flash silica column chromatography (Hexane/EtOAc = 5:1) to afford 0.8 g compound **4** as a colorless oil in 51% yield. ^{1}H NMR (500 MHz, $CDCl_3$) δ 0.17 (9H, s), 1.57 (1H, t, J = 5 Hz), 2.22 (3H, s), 3.48 (2H, d, J = 5 Hz); ^{13}C NMR (100 MHz, $CDCl_3$) 0.99, 13.56, 22.25, 69.60, 111.48, 135.86.

2.5.4 Synthesis of cyclopropene 5

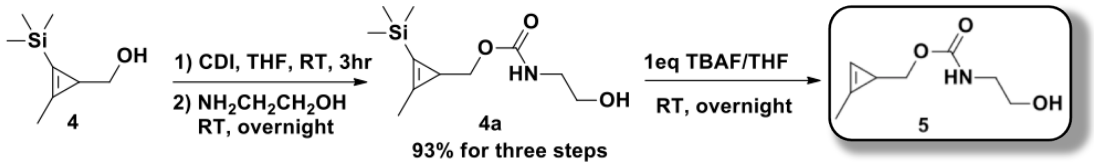

Scheme 2.8 Synthesis of cyclopropene **5**

Carbonyldiimidazole (CDI; 88 mg, 0.55 mmol) was added to a stirred solution of compound **4** (70 mg, 0.45 mmol) in dry THF (3.0 mL) at room temperature. The resulting solution was stirred for 3 hours and then ethanolamine (34 mg, 0.55 mmol) was added. The reaction solution was stirred overnight at room temperature and then evaporated to afford the crude product. The residue was purified by preparative TLC (Hexane/EtOAc = 2:1) to afford 0.08 g compound **4a** as colorless oil. The above compound **4a** was dissolved in dry THF (3.0 mL), followed by addition of 1.0 M TBAF in THF (0.5 mL, 0.5 mmol). The reaction solution was stirred at room temperature overnight until no starting material could be observed by TLC. The reaction solution was evaporated and purified by preparative TLC (Hexane/EtOAc = 1/1) to afford 71 mg of compound **5** as a colorless oil. Overall yield is 93% starting from compound **4**.

Compound **4a:** ^{1}H NMR (500 MHz, $CDCl_3$) δ 0.11 (9H, s), 1.50 (1H, t, J = 5 Hz), 2.15 (3H, d, J = 5 Hz), 3.21 (1H, bs), 3.30 (2H, dd, J = 10Hz, 5 Hz), 3.66 (2H, bs), 3.81 (1H, bs), 3.90 (1H, dd, J = 10 Hz, 5 Hz), 5.29 (1H, bs); ^{13}C NMR (125 Hz, $CDCl_3$) 14.29, 25.87, 30.10, 50.03, 64.99, 74.28, 104.07, 122.91, 141.60.

Cyclopropene **5:** ^{1}H NMR (500 MHz, $CDCl_3$) 1.61 (1H, t, J = 5 Hz), 2.10 (3H, d, J = 5 Hz), 3.16 (1H, bs), 3.30 (2H, dd, J = 10Hz, 5 Hz), 3.67 (2H, d, J = 5 Hz), 3.90 (2H, d, J = 5 Hz), 5.35 (1H, bs), 6.54 (1H, s); ^{13}C NMR (125 Hz, $CDCl_3$) 24.65, 29.05, 50.09, 65.13, 73.43, 97.04, 111.85, 141.58; HRMS $[M+Na]^+$ m/z calcd. for $[C_8H_{13}NO_3Na]^+$ 194.0788, found 194.0789.

2.5.5 Synthesis of lipid cyclopropene 7

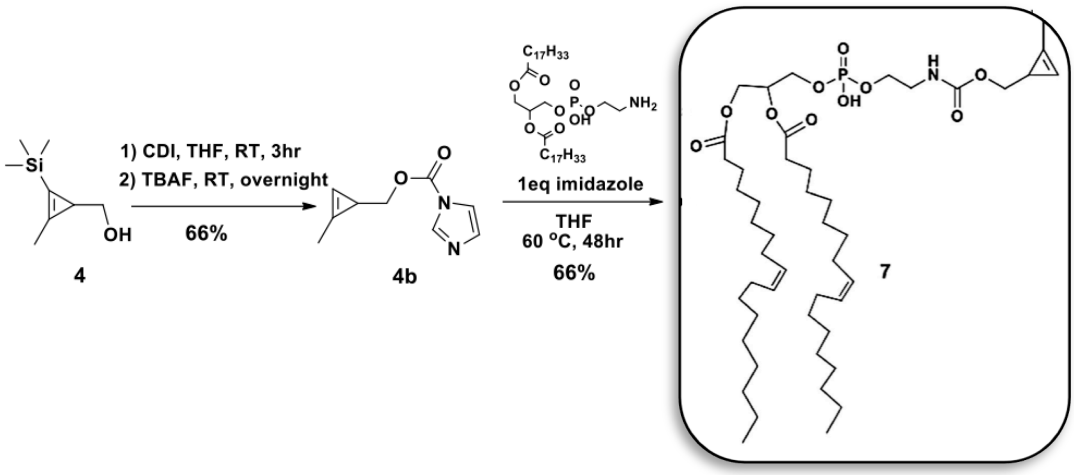

Scheme 2.9 Synthesis of lipid cyclopropene **7**

To a stirred solution of compound **4** (200 mg, 1.03 mmol) in dry THF (10.0 mL) at room temperature was added CDI (176 mg, 1.10 mmol). The resulting solution was stirred for 3 hours and then 1M TBAF in THF (1.1 mL, 1.10 mmol) was added. The reaction solution was stirred overnight at room temperature and then evaporated to afford the crude product. The residue was purified by flash silica column chromatography (Hexane/EtOAc = 1:1) to afford 110 mg compound **4b** as a colorless oil in 66% yield. The above compound **4b** was dissolved in dry THF (5.0 mL) and followed by addition of 1,2-dioleoyl-*sn*-glycero-3-phosphoethanolamine (DOPE) lipid (200 mg, 0.27 mmol) and imidazole (45 mg, 0.66 mmol). The reaction solution was stirred at 60 ^{o}C for 48 hours. The reaction solution was evaporated and the residue dissolved with 20 mL EtOAc and washed with 1 M HCl (20 mL×2), dried over the organic layer with Na_2SO_4 and evaporated to afford the crude product. The residue

was purified by flash silica column chromatography (CH_2Cl_2/MeOH = 10/1) to afford 150 mg compound **7** as colorless oil in 66% yield.

Compound **4b:** ^{1}H NMR (500 MHz, $CDCl_3$) δ 1.78 (1H, t, J = 5 Hz), 2.16 (3H, d, J = 5 Hz), 4.25 (1H, dd, J = 10Hz, 5 Hz), 4.33 (1H, dd, J = 10Hz, 5 Hz), 6.60 (1H, s), 7.07 (1H, s), 7.44 (1H, s), 8.55 (1H, s); ^{13}C NMR (125 Hz, $CDCl_3$) 11.68, 16.72, 76.22, 101.67, 117.22, 120.11, 130.56, 137.79.

Lipid cyclopropene **7:** ^{1}H NMR (500 MHz, $CDCl_3$) δ 0.87 (6H, t, J = 10 Hz), 1.25-1.31 (40H, m), 1.57-1.59 (5H, m), 2.00 (8H, m), 2.11 (3H, s), 2.88 (4H, dd, J = 20Hz, 10Hz), 3.38 (2H, bs), 3.88 (2H, bs), 3.93 (2H, bs), 3.97 (2H, bs), 4.13 (1H, m), 4.37 (1H, m), 5.22 (1H, bs), 5.33 (4H, m), 5.96 (1H, bs), 6.55 (1H, s); ^{13}C NMR (125 Hz, $CDCl_3$) 29.40, 31.34, 33.73, 38.21, 39.98, 41.84, 43.52, 43.88, 47.25, 53.12, 70.20, 71.50, 72.40, 76.20, 77.93, 101.90, 116.52, 123.58, 123.73, 123.82, 123.99, 145.96, 158.59, 158.75; HRMS $[M-H]^-$ m/z calcd. for $[C_{47}H_{83}NO_{10}P]^-$ 852.5760, found 852.5757.

2.5.6 Synthesis of *trans*-cyclooctene modified DOPE phospholipid 9

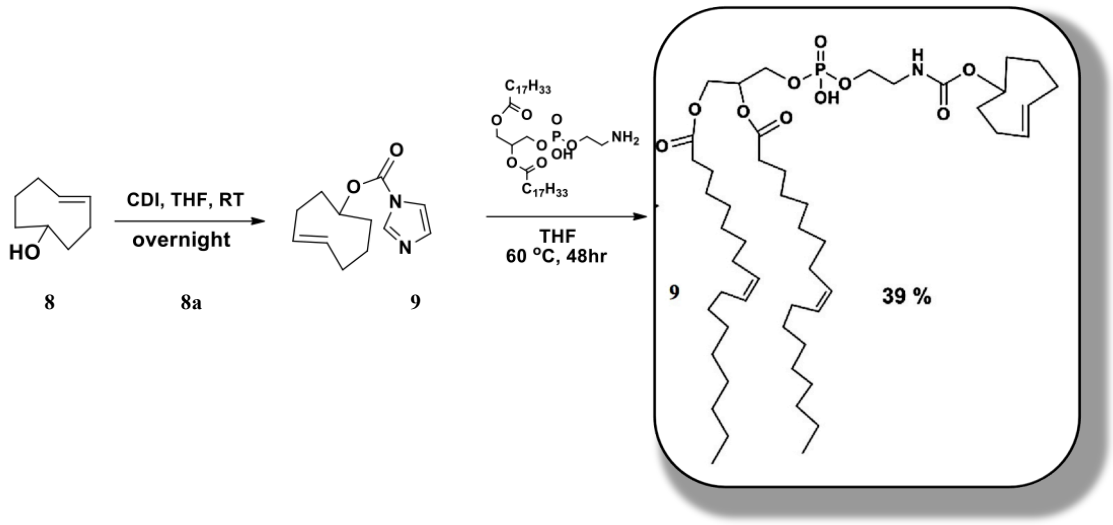

Scheme 2.10 Synthesis of *trans*-cyclooctene modified DOPE phospholipid **9**

To a stirred solution of *trans*-cyclooctene **8** (3.0 mg, 0.023 mmol) in dry THF (10.0 mL) at room temperature was added CDI (4.0 mg, 0.025 mmol). The resulting solution was stirred overnight at room temperature and then 1,2-dioleoyl-*sn*-glycero-3-phosphoethanolamine (DOPE, 15.0 mg, 0.020 mmol) was added. The reaction solution was stirred at 60 °C for 48 hours. The reaction solution was evaporated and the residue was purified by preparative TLC (DCM:MeOH=10:1) to afford 7.0 mg product (**9**) as colorless oil in 39 % yield. ^{1}H NMR (500 MHz, $CDCl_3$) δ 0.87 (6H, t, J = 10 Hz), 1.25-2.31 (72H, m), 3.23-3.36 (2H, m), 3.86-3.91 (4H, m), 4.13 (1H, m), 4.30-4.38 (2H, m), 5.22 (1H, bs), 5.31-5.39 (5H, m), 5.48-5.52 (1H, m); HRMS $[M-H]^-$ m/z calcd. for $[C_{50}H_{89}NO_{10}P]^-$ 894.6230, found 894.6231.

2.5.7 Stability of cyclopropene 5

Cyclopropene **5** was kept at 37 °C in D_2O: DMSO-d_6 = 10:1 and ^{1}H NMR was taken over a period of 24 h at the following time points: 0.0, 0.5, 1.0, 1.5, 3.0, 6.0 and 24 h. By comparing the peak abundance of the cyclopropene alkene proton (6.21 ppm) at different time points, we determined the stability of cyclopropene **5** (Figure 2.4).

2.5.8 Stability of methyl cyclopropene 5 and *trans*-cyclooctenol in the presence of L-cysteine

Cyclopropene **5** and *trans*-cyclooctenol [*rel*-(1*R*, 4*E*, p*R*)-cyclooct-4-enol] were separately combined with 1 equivalent of L-cysteine in D2O:DMSO-*d*6 (10:1) and kept at room temperature. ^{1}HNMR were taken over a period of 4 hours. The ^{1}HNMR showed both dienophiles are stable to L-cysteine at room temperature.

We next heated both mixtures to 60°C for 4 hours. ^{1}HNMR showed cyclopropene **5** remained stable at this temperature (Figure 2.5 shows the ^{1}HNMR for cyclopropene **5** after 4 hours incubation with L- cysteine at room temperature and after 4 hours at room temperature followed by 4 hours at 60 °C). However we observed that *trans*-cyclooctenol was being converted to *cis*-cyclooctenol under these conditions. After heating 4 hours, 34% of the *trans*-cyclooctenol was converted to *cis*-cyclooctenol. We studied the conversion of *trans*-cyclooctene to *cis*-cyclooctene over a period of 21 hours at 60 ^{o}C in the presence of L-cysteine. The ^{1}HNMR showed that after 21 hours, 88% of the *trans*-cyclooctenol was converted to *cis*-cyclooctenol (Figure 2.6).

2.5.9 HPLC characterization of the reaction between tetrazine-BODIPY FL 6 with cyclopropene 5

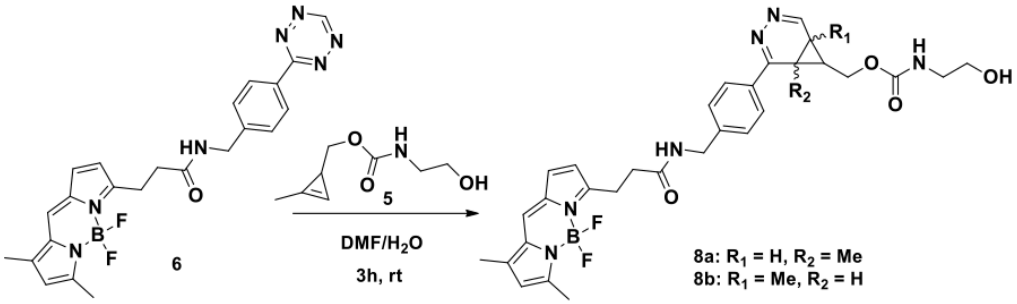

Scheme 2.11 tetrazine-BODIPY FL **6** reacting with cyclopropene **5**

Tetrazine-BODIPY FL **6** (1.0 mM in dry DMF, 20 μL) and Cyclopropene **5** (1.0 mM in H_2O, 20 μL) were combined in 210 μL of H_2O at a final concentration of 0.08 mM for tetrazine-BODIPY FL **6**. The reaction solution was agitated for 3 hours at room temperature and then analyzed by LC-MS. Multiple peaks were identified with molecular mass corresponding to diazanorcaradiene adducts (m/z 605 $[M+H]^+$). The multiple peaks are expected given the previously demonstrated potential to form several isomeric products. The reaction, based on the remaining signal from the tetrazine-BODIPY FL **6**, went to completion (Figure 2.8).

2.5.10 Characterization of reaction between tetrazine-BODIPY-FL 6 and cyclopropene phospholipid 7

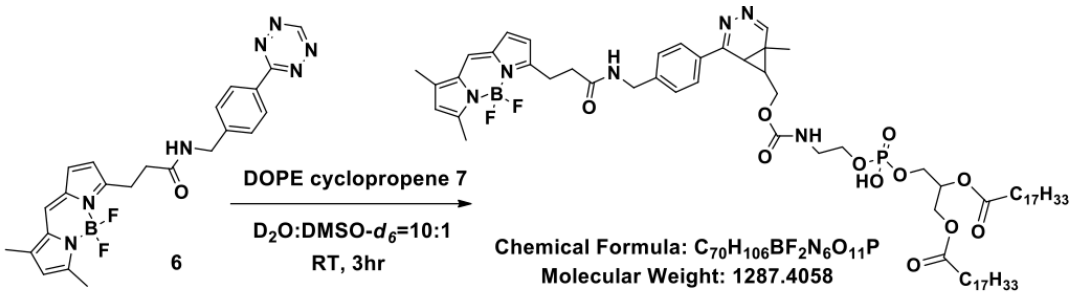

Scheme 2.12 tetrazine-BODIPY FL **6** reacting with cyclopropene phospholipid **7**

Tetrazine-BODIPY FL **6** (1.0 mM in dry DMF, 20 μL) and DOPE cyclopropene **7** (1.0 mM in DMSO, 20 μL) were combined in 60 μL of H_2O at a final concentration of 0.2 mM for tetrazine-BODIPY FL **6**. The reaction solution was agitated for 3 hours at room temperature and then analyzed by negative ion electrospray mass spectrometry in order to identify the molecular mass corresponding to diazanorcaradiene adducts (m/z 1286 $[M-H]^-$).

2.5.11 Fluorescence unquenching measurements

Freshly-purified tetrazine-BODIPY FL **6** was dissolved in DMF and reacted with 10-fold excess cyclopropene **5** at the final concentrations of 10 μM tetrazine and 100 μM cyclopropene in 1% v/v DMF/dH_2O. The reaction mixture was kept at room temperature (20 °C). Emission scans were recorded using a Perkin Elmer LD-45 spectrometer, with the excitation wavelength of 470 nm (2.5-nm slit width), and emission signal was tracked over the 485-640 nm range (5.0-nm slit width). Emission

was measured over time and compared against a control sample lacking cyclopropene. There was no emission change observed over the initial 2 h timeframe for the control sample. The resulting unquenching of the BODIPY FL fluorescence increased as measured at 30, 90, and 120 min intervals (Figure 2.5.1). The measurements were stopped after 2 h, as the rate of change in fluorescence peak intensity was decreasing.

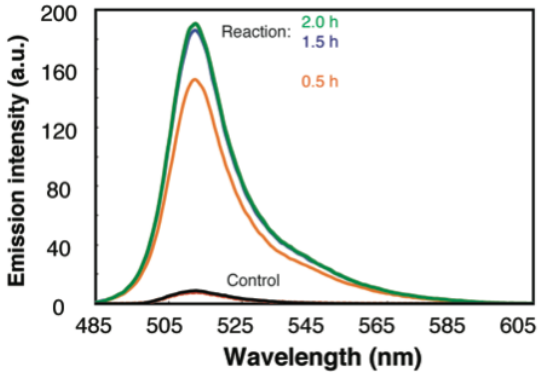

Figure 2.5.1 Emission intensity measurements of the tetrazine-BODIPY FL **6** reaction with cyclopropene **5**. Emission of the reaction mixture is shown at 30 min (orange line), 90 min (blue), and 120 min (green). Corresponding control sample lacking cyclopropene **5** was measured initially at 0 min (dashed red line) and 120 min (black line).

2.5.12 Reaction rate determination

A tetrazine **3** stock solution was prepared in DMSO and used to prepare tetrazine solutions at 0.6 mM final concentration in 12% v/v DMSO in ddH_2O. Reactions were initiated with excess cyclopropene at final concentrations of 6.0, 8.0, and 10.0 mM. The disappearance of the tetrazine absorption peak at 520 nm was tracked over the reaction timeframe by measuring the absorption spectra using a NanoDrop 2000c spectrophotometer (Thermo Scientific). Samples were placed in a

quartz cuvette with 10-mm pathlength and stirred at the maximum speed setting of the instrument. The temperature was uncontrolled by the instrument for room temperature (20 °C) measurements, and set and equilibrated at 37 °C for the higher temperature experiments.

Absorption spectra were measured manually over time. Absorption peak signal was taken as the average of measurements at 519-521 nm. Baseline signal was determined as the sloping line connecting the measured background levels preceding and following the tetrazine peak (410-430 nm and 590-610 nm, respectively). Final peak intensity value was taken as the signal above the baseline.

Reaction rates were obtained by fitting the exponential decays of tetrazine peak absorption intensity as a pseudo first order reaction. Nonlinear data fits were performed with GraphPad Prism. Tetrazine reactions with cyclopropene carbamate **5** were carried out at 20 and 37 °C (data points and corresponding fitted curves at 20 °C in Figure 2.3, 37 °C in Figure 2.1). Tetrazine reactions with cyclopropene carboxamide **2** were done at 37 °C (Figure 2.2).

2.5.13 Live-cell microscopy

Human breast cancer SKBR3 cells were received from Professor Jered Haun (University of California, Irvine). The cells were incubated overnight on a Lab-Tek chamber slide maintained in cDMEM medium (10% fetal bovine serum, 1% L-glutamine, 1% penicillin/streptomycin). Cells were washed with phosphate-buffered saline (PBS) and incubated in cDMEM with 100 μM of cyclopropene **5** for 1 hour at 37 °C. The media was aspirated, and cells were washed twice with PBS. Cells were

then incubated in cDMEM and 10 μM tetrazine-BODIPY FL **6** probe for 1-2 hours at 37 °C. In the last 30 min of incubation 300 nM DAPI was added to the incubation media. Cells were washed twice with PBS before imaging. All photos were collected with an Olympus FV1000 confocal microscope using ImageJ 1.45j software package.

Notes About the Chapter:

Chapter two, in full, is a reprint (with co-author permission) of the material as it appears in the publication; J. Yang, J. Seckute, **C. M. Cole**, N. K. Devaraj. "Live-Cell Imaging of Cyclopropene Tags with Fluorogenic Tetrazine Cycloadditions," *Angew. Chem. Int. Ed.*, 2012, 51(30), 7476-7479. My contribution to this chapter was in the preparation of one of the precursors to compound **6.** Additionally, I spectroscopically monitored the reaction between compound **5** and compound **6** and took all the live-cell images. I thank Jun Yang, Jolita Seckute, and Neal Devaraj for their invaluable contributions to this chapter: Jun Yang synthesized and characterized all the compounds presented in this chapter; Jolita Seckute monitored the kinetics between compound **3** and the methylcyclopropene derivatives. In addition, she prepared the majority of the manuscript; and I would like to thank Neal Devaraj for directing the research and in the preparation of the manuscript.

~ CHAPTER 3 ~

3 Fluorescent Live-Cell Imaging of Metabolically Incorporated Unnatural Cyclopropene-Mannosamine Derivatives

3.1 General Overview of glycan labeling techniques

Glycomics is the latest emerging macromolecule network in systems biology, encompassing polysaccharides, glycolipids and glycoproteins. Glycans perform fundamental roles in nearly all cellular operations, including inflammation[65], cancer[65], immunity[66] and cell signaling. Despite glycans widespread presence in biological systems, their molecular functions have remained obscured. This is in part due to the heterogeneity of monosaccharides giving rise to a large diversity of possible glycosidic-linkages and additional cross linkages.

Previous glycan labeling techniques have required the use of rather harsh labeling methods. The current gold standards for labeling glycans are the compounds 2-aminobenzamide (2-AB), 2-aminopyridine (PA) & 2-aminobenzoic acid (2-AA), which require the reducing end of the saccharides to be free.[67] This often necessitates additional steps such as de-glycosylation and reductive amination.[68] Other methods employ the use of hydrazine[68] or copper catalysts[67] both of which are cytotoxic. A major limitation in the study of glycans is the paucity of *in vivo* labeling agents that are non-toxic to cells. For live-cell applications, the azide-cyclooctyne catalyst-free cycloaddition has been useful in labeling azide bioorthogonal molecules with fluorescent probes.[34]

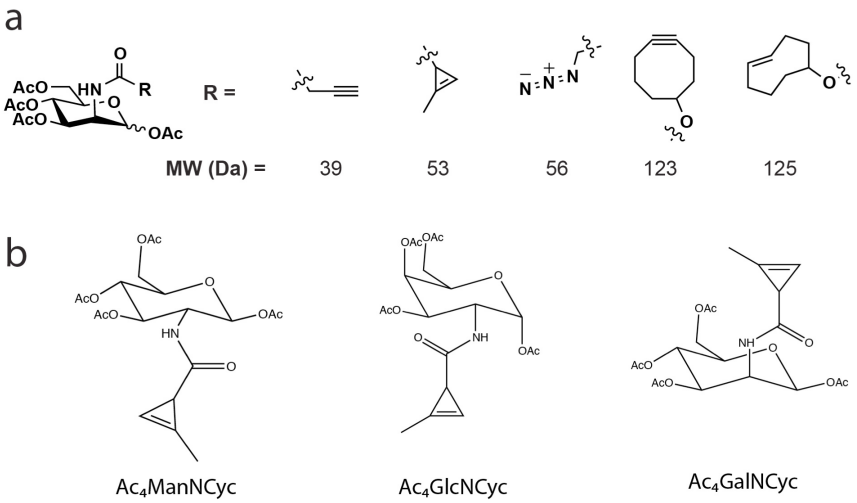

Figure 3.1 a) Comparison of N-acyl substituents on unnatural mannosamine derivatives. b) N-Acetyl- glucosamine (GlcNAc), N-Acetyl-galactosamine (GalNAc), N- Acetyl mannosamine (ManNAc) cyclopropene analogs.

The advent of click chemistry for modifying glycans with an azide functional group has allowed for the in vivo detection and visualization of azidosugars, which are metabolically incorporated on extra-/intra-cellular glycoproteins.[69] It has been previously established that the sialic acid biosynthetic pathway is tolerant of monosaccharide derivatives with small *N*-acyl substituents.[70]

N-acetyl-neuraminic acid is the most common sialic acid found in mammalian cells[71], where it can be found in the glycosylphosphatidylinositol anchor (GPI) that links glycolipids to their respective proteins. Thus, this negatively charge amino sugar is commonly found on the plasma membrane, where they prevent foreign pathogens from gaining entry into the cell.[66] N-acetylneuraminic acid bearing azide handles provide the real-time distribution of polysialic acids on the membranes of neurons.[72] Allowing researchers to compare baseline cellular glycosylation events with altered

levels of glycosylation due to gene expression and metabolism.

N-Acetyl-galactosamine, N-Acetyl-glucosamine, & N-Acetyl-mannosamine chemical reporters bearing a ketone or azide were the original bioorthogonal-labeling agents pioneered by Bertozzi and coworkers which could mimic their natural analogs.[16,73–75] This elegant methodology, combines metabolic engineering and bioorthogonal reactions, for in situ imaging or even proteomic enrichment. This technology has been applied to numerous immortal cell lines (e.g., Jurkat, HeLa, CHO, and neuron-like blastoma cells) and organisms (e.g., zebrafish, mice, and microbes) for the selective labeling of sialic acid on membranes.

Recently, there has been growing attention in exploring tetrazine bioorthogonal cycloadditions for improved temporal resolution in live-cell imaging applications. Tetrazines have been shown to react rapidly via inverse Diels-Alder reaction with a variety of strained alkenes and alkynes including *trans*-cyclooctene, norbornene, and cyclooctynes.[34] In addition, tetrazines are uniquely suited for live-cell imaging using fluorogenic imaging probes that utilize BODIPY and fluorescein conjugated tetrazines, which remain quenched prior to cycloaddition. However, the use of tetrazine cycloadditions has been impeded due to the size of these paired dienophiles, which are large compared to the azide and alkyne tags commonly used in bioorthogonal chemistry. In this chapter we show that glycans with a minimal methyl-cyclopropene tag can react irreversibly and quickly with tetrazines via cycloaddition[41,43].

In terms of molecular weight, methylcyclopropenes are comparable to azides (Figure 3.1). The monosaccharides that are common constituents of protein glycans

are N-Acetyl-glucosamine (GlcNAc), N-Acetyl-galactosamine (GalNAc), N-Acetyl-mannosamine (ManNAc) and N-Acetyl-neuraminic acid (NANA). By modifying these amino monosaccharides with our fast reacting methylcyclopropene probe we hope to expand the versatility of the tetrazine ligation, a general overview can be seen in Figure 3.2.

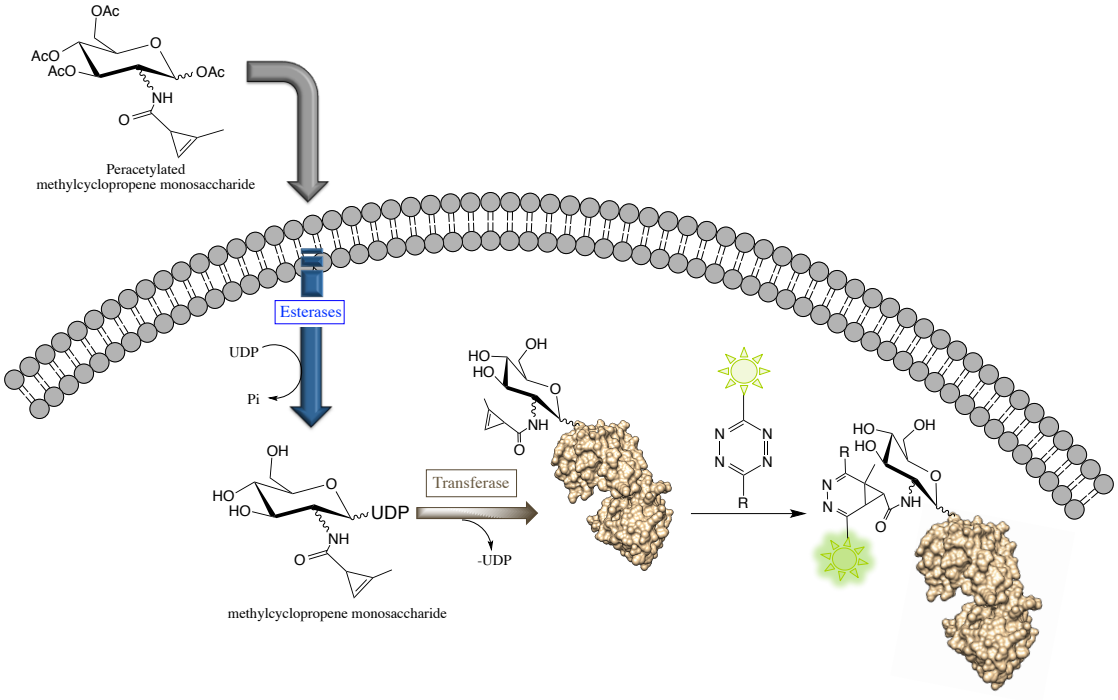

Figure 3.2 General concept of using peracetylated monosaccharide derivatives to pass through the cell membrane and label glycoproteins on the cellular membrane. Once in side the cell the derivative will readily get deacetylated followed by coupling to a glycoprotein via a transferase.

Currently, unnatural sugar derivatives for use in cellular and animal labeling have yielded powerful new tools for glycobiologists. Engineering these monosaccharide derivatives has assisted in our understanding of glycan biosynthesis and their metabolic flux. For the first time fluorogenic tetrazines in combination with

methylcyclopropenes will be used to probe the highly complex world of glycans. Furthermore, it is well documented that these monosaccharides participate in many protein-protein interactions, which may prove to be a furtive area for future inquiries in pathways responsible for nutrient acquisition, apoptosis, immunity and the stress response.

Metabolic oligosaccharide engineering offers a chemoselective and a simple means to label cellular glycans. In this chapter we will take precautions to ensure that the staining is due to glycan uptake of the probes by setting up controls with N-linked / O-linked glycosylation inhibitor to knockdown the signal. In addition, it will be of relevance to set up competition reactions between the modified monosaccharide analog and their respective naturally occurring monosaccharide to confirm there is the expected knockdown of labeling. Finally, flow cytometry will be employed for quantitative analyses of the incorporation of the proposed sugar derivative. These experiments will provide evidence that the staining patterns are due to glycosylation and uptake of the unnatural methylcyclopropene sugars.

3.2 Introduction

There is tremendous interest in the use of bioorthogonal reactions for imaging of unnatural building blocks that are metabolically incorporated into biosynthetic pathways. Applications include visualizing glycans, imaging proteins tagged with unnatural amino acids, monitoring cellular proliferation, and tracking lipid analogues.[29,76–79] For live-cell imaging applications, the azide–cyclooctyne catalyst-free cycloaddition has been extremely useful in providing a rapid and biocompatible method to label small azide tags with fluorophore.[29] Recently, there has been growing interest in exploring bioorthogonal cycloadditions involving tetrazines for live-cell imaging applications.[31] Tetrazines have been shown to react rapidly through inverse-electron-demand Diels–Alder reactions with a variety of strained alkenes and alkynes including *trans*-cyclooctenes, norbornenes, and cyclooctynes. These reactions can be used for live-cell imaging, and tetrazines can quench the fluorescence of commonly used imaging probes such as BODIPY dyes and fluoresceins.[35,37] This leads to a fluorogenic response after reaction, which can improve signal-to-background, which is particularly useful for intracellular live-cell imaging applications.[39,76,80] Though tetrazine cycloadditions would be exciting developments for a wide array of metabolic imaging applications, the large size of both the tetrazine and cycloalkene coupling partners has limited their ability to be incorporated into small bioactive molecules. In response to this challenge, we recently developed small and stable methylcyclopropenes as coupling partners for fluorogenic tetrazines.[81] The molecular weight of these tags rivaled those of azides and were used to fluorogenically image

lipids in live mammalian cells. However, we were interested in whether methylcyclopropenes could substitute for azides in metabolic imaging applications with stringent steric constraints. Here we demonstrate that unnatural cyclopropene-mannosamine derivatives can be used to image glycans on live human cancer cell lines.

Tetrazine-based cycloadditions are an emerging class of bioorthogonal reactions that can proceed with rapid rate constants, enable imaging of dienophile tags in live-cells and animals, and be mutually orthogonal to azide–alkyne cycloadditions.[23,34,82–84] Despite these applications, the use of tetrazine cycloadditions has been limited in metabolic imaging. This is due to the size of tetrazines and paired dienophiles such as *trans*-cyclooctene and norbornene, which are large compared to the azide and alkyne tags commonly used in bioorthogonal chemistry. We recently developed methylcyclopropenes as tetrazine-reactive cellular imaging tags that are comparable to azides in terms of molecular weight (Scheme 3.1a).[81] Following our work, others have shown that cyclopropene-containing amino acids and cyclopropene derivatized neuraminic acid analogues can be incorporated into cellular

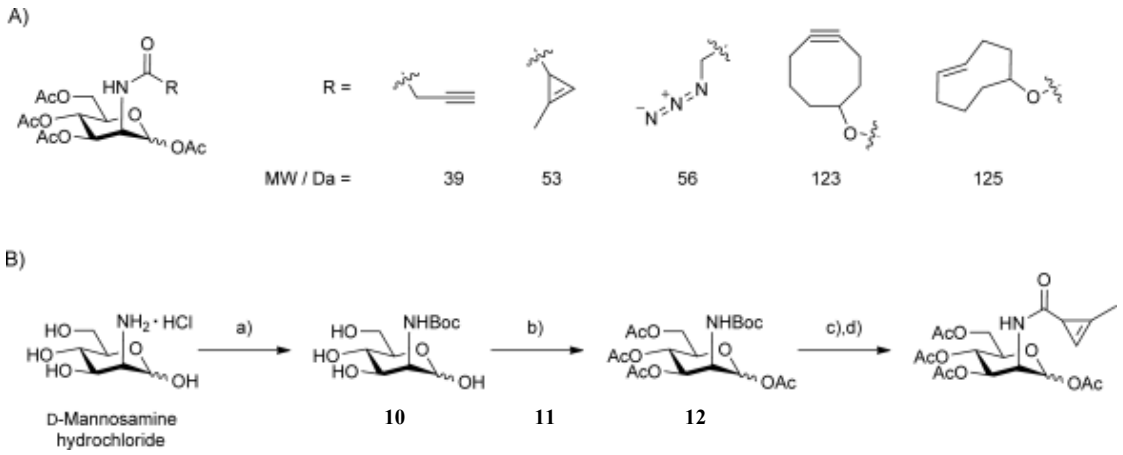

Scheme 3.1 A) Comparison of N-acyl substituents on unnatural mannosamine derivatives. The cyclopropene handle is similar in size to the commonly used azide handle. B) Synthesis of peracetylated $Ac_4ManNCyc$ (**12**). a) 1.0 eq. NaOH, dioxane, sat. $NaHCO_3$, Boc_2O; b) pyridine, Ac_2O, 20 % (2 steps); c) 20 % TFA, CH_2Cl_2; d) CH_2Cl_2, Et_3N, DMAP, 2-methyl-2-cyclopropenyl-1-carbonyl chloride, 60 % (2 steps).

macromolecules and later tagged using photoinitated reactions or tetrazine-biotin–avidin coupling.[85,86] However, although the experiments demonstrated cellular uptake of the chosen analogues, these systems are well known to tolerate larger substituents.[87,88] For instance, past work has demonstrated that *trans*-cyclooctene-containing unnatural amino acids and aryl-azide-containing neuraminic acid analogues can be taken up by cells.[39,89] Thus, in those studies, the cyclopropene would not be a necessary dienophile for inverse-electron-demand Diels–Alder chemistry. Seeking to provide a more stringent test, we attempted to metabolically label human cancer cell lines with an unnatural cyclopropene-mannosamine derivative.

3.3 Metabolically Incorporating Mannosamine Analogues into SK-BR-3 Cells

Mannosamine analogues are classic bioorthogonal metabolic labeling agents, as pioneered by the Bertozzi group.[15,16,29] It has been well demonstrated that the sialic acid biosynthetic pathway is tolerant of unnatural mannosamines bearing small unnatural N-acyl substituents.[70,90] Mannosamines bearing short azide-modified acyl chains (ManNAz) are readily accepted in the pathway and have been elegantly labeled by fluorescent cyclooctynes and Staudinger ligation probes after incorporation into glycans.[16,29] Several studies have established that lengthy or branched substituents are not well tolerated and extending the N-acyl substituent by more than five carbon atoms severely decreases uptake.[90,91] This work has demonstrated that cellular metabolism is likely limited by phosphorylation of the unnatural analogues by ManNAc 6-kinase.[91] Thus, large norbornene- and *trans*-cyclooctene-*N*-acylmannosamine derivatives are not expected to be taken up by the biosynthetic machinery. Based on this prior work, we decided to test if cyclopropene-mannosamine analogues could be incorporated by live human cancer cells. Successful incorporation would provide evidence that methylcyclopropene tags can substitute for azides in stringent metabolic imaging or engineering applications.

We synthesized unnatural peracetylated mannosamine analogue bearing an N-acyl cyclopropene (Ac_4ManNCyc, **12**) by coupling peracetylated mannosamine to a highly reactive methylcyclopropene acid chloride that we previously described (Scheme 3.1B).[81] Initially, we approached the synthesis of **12** by reacting unprotected mannosamine with highly reactive electrophilic methylcyclopropene precursors. This yielded multiple products and was not practical for isolating the desired compound.

Instead, we first protected the amine functional group of mannosamine (to afford intermediate **10**) followed by acetylation of the remaining alcohols, using acetic anhydride, and chromatographic separation to afford compound **11**. Deprotection of the amine using trifluoroacetic acid yielded peracetylated mannosamine **12**, which readily reacted with a methylcyclopropene acid chloride to yield the desired peracetyled cyclopropene-sugar **12**. Alternatively, we could also react the primary amine with a methylcyclopropene-NHS derivative followed by peracetylation. We chose to utilize the peracetylated derivatives given the well-known ability of such lipophilic precursors to enter cells and accumulate in glycans, dramatically lowering the concentration of probe the cells are required to be exposed to.[92]

Methylcyclopropene-amides are known to react slower with tetrazine handles compared to faster methylcyclopropenyl carbamates.[81] However, the reported reaction rates for the methylcyclopropene-amides are comparable to alternative bioorthogonal reactions used for live-cell imaging. Additionally, the molecular weight of the methylcyclopropene-amide handle is similar to the azide handles that have been previously used for imaging glycans, making it an attractive derivative (Scheme 3.1A).[29] We and others have demonstrated that one of the benefits of tetrazine-based cycloadditions is the ability to utilize fluorogenic probes that increase in emission intensity after cycloaddition.[35] Indeed, reaction of **12** elicits fluorogenic responses from quenched tetrazine probes such as tetrazine-Alexa Fluor 488 (Figure 3.3). Such fluorogenic reactions are valuable for live-cell imaging and can improve the signal to background by diminishing signal from nonspecifically bound or trapped fluorescent probes.

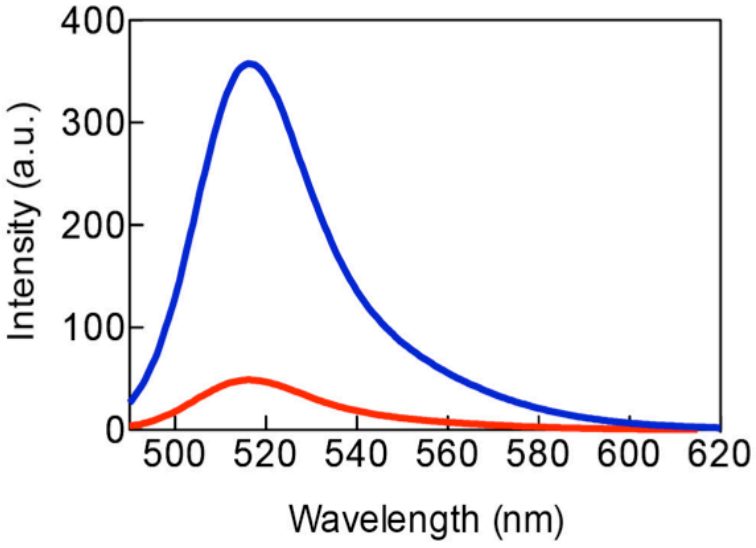

Figure 3.3 Emission spectra demonstrating the fluorogenic response of tetrazine-Alexa Fluor 488 before (red) and after incubation with Ac_4ManNCyc **3** (blue).

In order to determine if Ac_4ManNCyc was incorporated effectively by cells, we incubated adherent human breast cancer (SK-BR-3) and colon cancer (LS-174T) cell lines with **12** (100 μm) for 48 h in cell medium and serum. After incubation, cells were thoroughly washed and then reacted for one hour with fluorogenic Alexa Fluor 488 tetrazine (10 μm; Figure 3.4). After a second wash, cells were imaged by confocal microscopy (Olympus FV1000). Cells that were exposed to **12** showed bright surface staining (Figure 3.6A) while control cells that were not treated with unnatural sugar had a complete absence of staining (Figure 3.5). In order to ensure that the staining was due to glycan uptake of the probe, we also performed controls by exposing cells to **3** (100 μm) and inhibiting uptake by using glycosylation inhibitors (tunicamycin or αBnGalNAc) or ManNAc (20 mm) as a competitive substrate.[93] Inhibitors severely diminished staining to levels that were similar to controls (Figure 3.6B). The use of

ManNAc as competitor also lowered the fluorescent signal, with faint surface staining visible (Figure 3.6C).

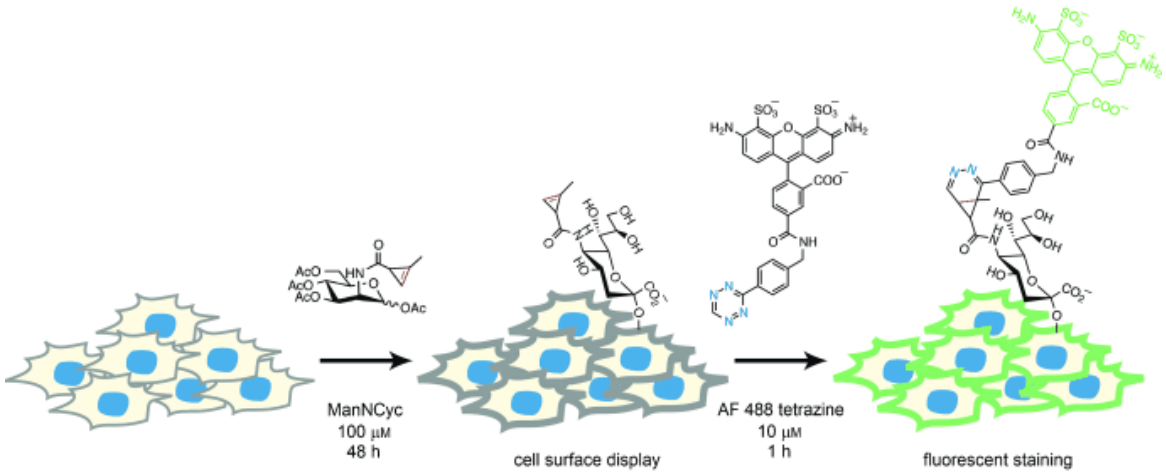

Figure 3.4 Cartoon outlining proposed fluorescent staining of glycans using tetrazine–cyclopropene chemistry. Ac_4ManNCyc (**12**) is incubated with live cells for 48 h. If the unnatural mannosamine derivative is processed by the cell, methylcyclopropenes will be displayed on the surface and tagged by fluorogenic tetrazine-Alexa Fluor 488. This staining pattern will be visible by confocal microscopy.

These experiments provide evidence that the staining patterns are reporting on glycosylation and uptake of the unnatural cyclopropene-mannosamine. We also performed additional studies using flow cytometry to quantitate the relative uptake of sugars, which corroborated the imaging data (Figure 3.7). Cells exposed to **12** followed by the tetrazine imaging probe showed increased fluorescence intensity compared to controls, which only received the tetrazine imaging probe.

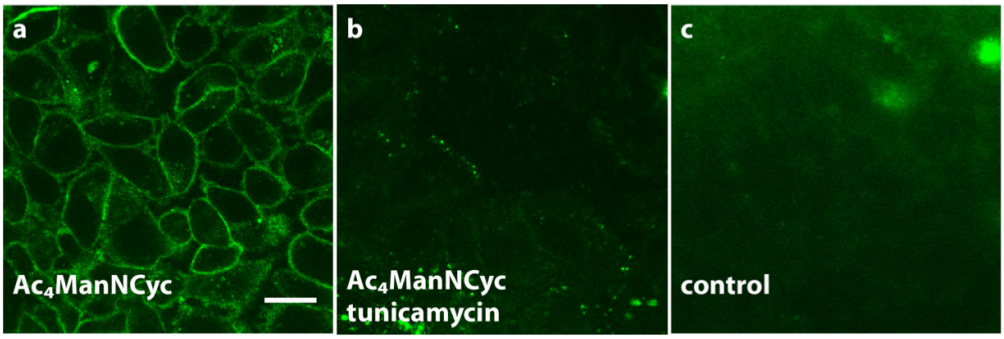

Figure 3.5 Imaging SKBR3 cells. Separate populations of SKBR3 cells were incubated for 48 hours with (a) Ac_4ManNCyc, (b) Ac_4ManNCyc and 1.2 μM tunicamycin, and (c) a control solution lacking a mannosamine derivative. The cells were then reacted with 10 μM tetrazine-Alexa Fluor 488 and imaged by confocal microscopy. Cells receiving only Ac4ManNCyc showed bright surface staining while the other control populations had minimal surface staining. Scale bar denotes 20 microns.

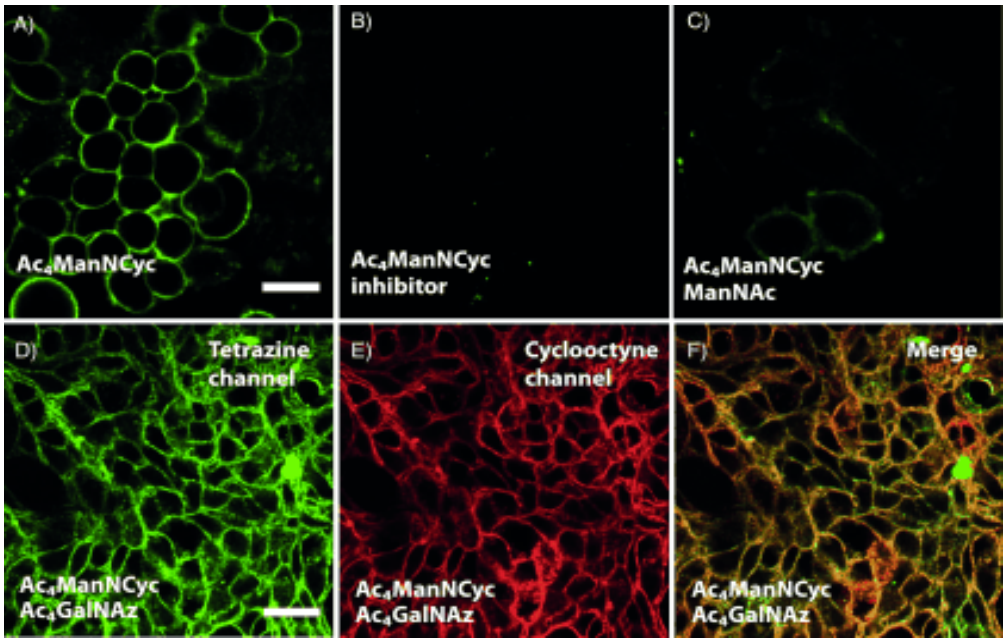

Figure 3.6 Imaging glycans using cyclopropene-mannosamine derivatives. A) SKBR3 cell surfaces were stained by incubation with Ac_4ManNCyc (**12**; 100 μm) followed by reaction with tetrazine-Alexa Fluor 488 (10 μm). B) Staining was significantly lower when SKBR3 cells were incubated with **12** as well as tunicamycin (1.2 μm), a glycosylation inhibitor. C) Staining was also reduced when SKBR3 cells were incubated with **12** as well as of ManNAc (20 mm) as a competitor. Simultaneous imaging of **12** and Ac_4GalNAz incorporation. LS174T cells were incubated with of **12** (100 μm) and Ac_4GalNAz (100 μm) for 48 h. After incubation, cells were reacted sequentially with tetrazine-Alexa Fluor 488 (10 μm) and DIBO 647 (15 μm). Confocal microscopy revealed extensive surface staining in the D) 488 nm channel and E) 647 nm channel with good colocalization of surface staining (F). Controls revealed minimal cross staining of tetrazine-Alexa Fluor 488 with cells incubated only with Ac_4GalNAz and DIBO 647 with cells incubated only with **12** (Figure 3.8). Scale bars: 20 μm.

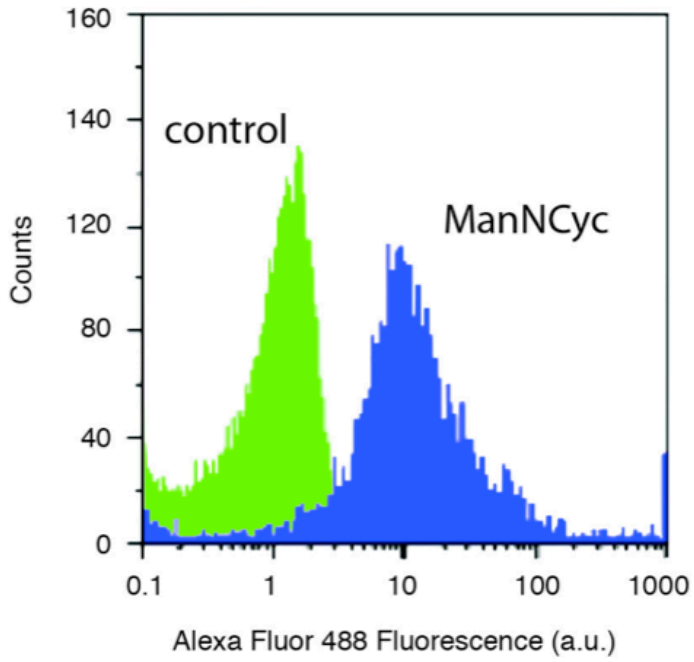

Figure 3.7 Flow cytometry indicates fluorescent staining of SKBR3 cells incubated with Ac_4ManNCyc **12** followed by tetrazine-Alexa Fluor 488. Control cells not exposed to the cyclopropene registered significantly less fluorescence intensity.

3.4 Duel Labeling of Peracetylated *N*-azidoacetylgalactosamine and N-Methylcyclopropene Mannosamine in SKBR3 Cells

Finally, we tested whether or not we could simultaneously image two different metabolically incorporated unnatural sugar derivatives (Figure 3.6D-F), **12** and peracetylated *N*-azidoacetylgalactosamine (Ac_4GalNAz). The latter unnatural galactosamine azide has been shown to incorporate into O-linked mucins and can be tagged using commercially available fluorescent cyclooctynes.[30,94] Recent experimental work has shown that alkenes and azides can be mutually orthogonal to each other, even when using highly strained *trans*-cyclooctenes.[69] Additionally, the Houk group has calculated that methylcyclopropene handles, such as those we have

previously developed, should be mutually orthogonal to azide in reactions with cyclooctynes.[95] We incubated LS174T human colon cancer cells with 100 μm **12** and $Ac_4GalNAz$ for two days. After incubation, we sequentially stained the cells with tetrazine-Alexa Fluor 488 (10 μm) and dibenzocyclooctyne (DIBO) 647 (15 μm). Fluorescent microscopy demonstrated cell-surface staining in both the fluorescent channels. Similar results were obtained with the SKBR3 cell line. Cells that were incubated with only **12** and DIBO 647 or **12** and tetrazine-Alexa Fluor 488 showed minimal surface staining (Figure 3.8). The ability to simultaneously label two different metabolically incorporated molecules using live-cell compatible inverse-electron-demand Diels–Alder and Huisgen reactions expands the capabilities of bioorthogonal metabolic imaging.

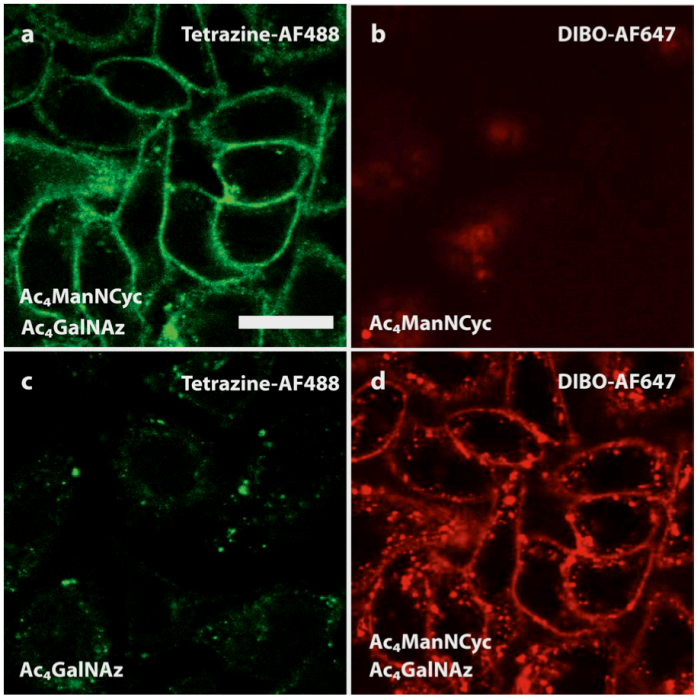

Figure 3.8 Cross reactivity studies. LS174T cell surfaces were incubated for 48 hours with Ac_4ManNCyc and Ac_4GalNAz reacted with both tetrazine-Alexa Fluor 488 and DIBO Alexa Fluor 647 and imaged by confocal microscopy in (a) the 488 channel and (d) the 647 channel. Cells that were incubated for 48 hours with Ac4ManNCyc and reacted with DIBO Alexa Fluor 647 (b) or incubated with Ac4ManNAz and reacted with tetrazine-Alexa Fluor 488 (c) showed minimal surface staining, similar to the background signal due to nonspecific binding of dye. Scale bar denotes 20 microns.

3.5 Concluding Remarks

In conclusion, we have demonstrated that recently developed methylcyclopropene bioorthogonal handles can be used for metabolic imaging of unnatural mannosamine derivatives on live-cell surfaces. The ability of methylcyclopropenes to substitute for azides should significantly expand the use of bioorthogonal reactions for metabolic imaging applications.[89] This technology also enables multicolor imaging of two different metabolically incorporated mini-tags. These results highlight the potential utility of cyclopropenes as reactive mini-tags for a myriad of applications in the profiling and imaging of small molecules.

3.6 Experimentals and Methods

3.6.1 Tissue culture/cell growth conditions

SK-BR-3 and LS174T cells were grown in cDMEM media supplemented with 10% fetal bovine serum, 1% L- glutamine, 1% penicillin/streptomycin. Cells were incubated in 5.0% carbon dioxide, 95% humidity at 37 °C. Generally, cells were grown in T-75 tissue culture flasks, seeded at densities between 500,000 and 750,000 cells per flask (cells were quantified with the Life Technologies Countess automated cell counter). The cells were trypsinized with TrypLE Express and resuspended in cDMEM. Cells were allowed to incubate for two days before supplementing with Ac_4ManNCyc (N-cyclopropeneacetylmannosamine) or Ac_4GlcNAz (N-azidoacetylglucosamine). The cells were then analyzed via confocal microscopy and flow cytometry as described below.

3.6.2 Live-cell microscopy

The SK-BR-3 and LS174T cells were incubated for two days in the presence of 100 μM of Ac4ManNCyc and/or 50 μM Ac_4GlcNAz on a Lab-Tek chamber slide maintained in cDMEM medium. Treatment of cells with tunicamycin was done by preparing a 0.2 mg/mL stock in DMSO, which was diluted to a final working concentration of 1.2 μM tunicamycin in cDMEM (0.5% DMSO). Cells were washed 3x with phosphate-buffered saline (PBS) and incubated for 1 hour at 37 °C in 10 μM tetrazine-BODIPY TMR-X, 10 μM tetrazine-Alexa flour 488 and/or 15 μM dibenzocyclooctyne (DIBO)- Alexa Fluor 647 in cDMEM. The media was aspirated,

and cells were washed twice with PBS before imaging. All photos were collected with an Olympus FV1000 confocal microscope using ImageJ 1.45j software package.

3.6.3 Analysis of cell surface cyclopropenes by flow cytometry

After the incubating the adherent SK-BR-3 cells in 100 μM of Ac4ManNCyc (1.2 μM tunicamycin and/or 1 mM αBnGalNAc was used in experiments requiring glycosylation inhibitors) they were washed twice in PBS and then incubated in 10 μM of tetrazine-Alexa flour 488 for 1 hour at 37 °C. Control cells were not exposed to Ac_4ManNCyc and incubated in 10 μM of tetrazine-Alexa flour 488 for 1 hour at 37 °C. Cells were then resuspended in 1-2 ml of cDMEM (5.0x105 to 1.0x106 per ml) using a rubber policeman. The cells were passed through a 25-gauge syringe to ameliorate excessive clumping, and subjected to analysis by flow cytometry using a 200mW 488nm blue solid-state laser on the Partec Space Flow Cytometer (Partec).

3.6.4 Fluorescence turn-on spectroscopy

Mannosamine-cyclopropene (Ac_4ManNCyc) and tetrazine-Alexa-Fluor 488 stocks were prepared at 1 and 0.1 mM, respectively, in phosphate-buffered saline (PBS) pH 7.4. Fluorescence turn-on was measured using a Perkin Elmer LD-45 spectrometer, with the excitation wavelength set to 480/5 nm, and emission scanned over 490-620 nm (5-nm slit width) at a rate of 50 nm/min. Reaction conditions were 50 μM tetrazine-Alexa-Fluor 488 and 100 μM Ac_4ManNCyc in PBS pH 7.4 buffer at room temperature.

3.6.5 Synthesis of 1,3,4,6-Tetra-*O*-acety-*N*-Boc-D-mannosamine 12

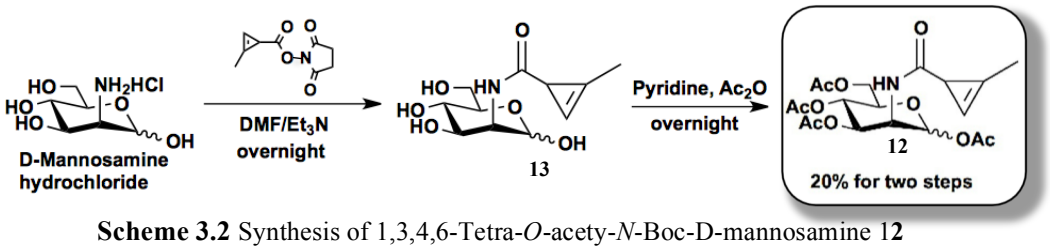

Scheme 3.2 Synthesis of 1,3,4,6-Tetra-*O*-acety-*N*-Boc-D-mannosamine 1**2**

A mixture of D-mannosamine hydrochloride (5.0 mg, 0.023mmol), *N*-succinimidyl methyl cyclopropenoate **14** (5.0 mg, 0.026 mmol), and triethylamine (5.0 mg, 0.046 mmol) in DMF (0.3 ml) was stirred at room temperature overnight. The reaction mixture was concentrated *in vacuo*, and the residue was dissolved in pyridine (0.3 mL) and Ac_2O (25 mg) was added. The reaction was stirred at room temperature overnight and then was concentrated *in vacuo*; the residue was purified by prepared TLC (Hexane/EtOAc=1/1) to afford 2.0 mg of compound **12**, in 20% yield.

^{1}H NMR (400 MHz, $CDCl_3$) δ 1.97 (32H, m), 3.99-4.07 (4H, m), 4.19-4.22 (2H, m), 4.63-4.68 (2H, m), 5.10-5.16 (2H, m), 5.25-5.31 (2H, m), 5.64-5.72 (2H, m), 5.97-5.98 (2H, m), 6.43 (1H, s), 6.45 (1H, s); ^{13}C (100 MHz, $CDCl_3$) δ 10.70, 10.85, 20.86, 20.90, 20.92, 20.96, 20.98, 21.08, 22.53, 22.56, 49.19, 49.24, 62.14, 62.30, 65.40, 65.66, 69.12, 69.30, 70.25, 92.06, 95.50, 95.99, 113.63, 114.64, 168.44, 169.87, 169.94, 170.26, 170.69, 176.22; HRMS $[M+Na]^+$ m/z calculated for $[C_{19}H_{25}NO_{10}Na]^+$ 450.1371, found 450.1373.

3.6.6 Synthesis of tetrazine-Alexa Flour 488 (15)

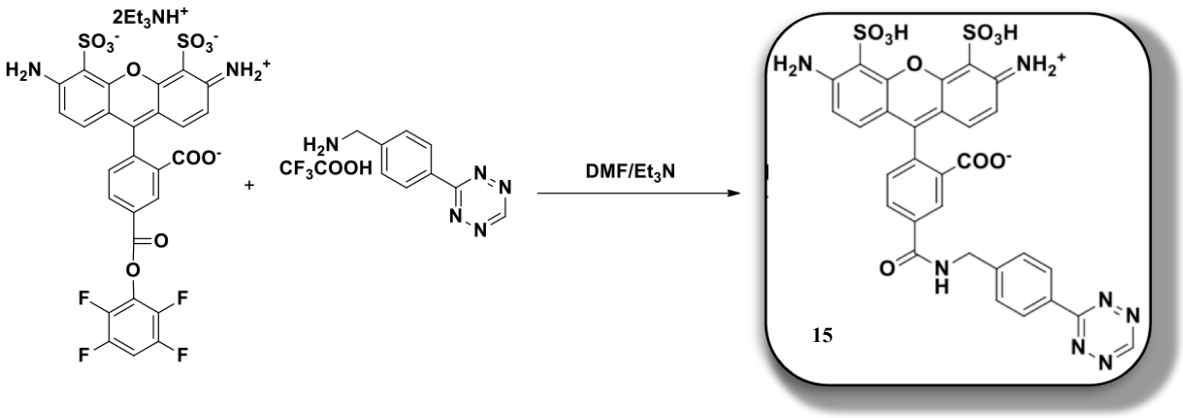

Scheme 3.3 Synthesis of tetrazine-Alexa Flour 488 **(15)**

To a stirred solution of Alexa Fluor 488 5-TFP (0.5 mg) in DMF (0.5) at room temperature was added (4-(1,2,4,5- tetrazin-3-yl)phenyl)methanamine1 (0.5 mg) and Et_3N (0.5 mg). The reaction solution was stirred at room temperature for 30 minutes. The product **15** was purified by reverse phase TLC (MeOH:H_2O=1:3) directly without work-up to afford 0.4 mg product as an orange solid in quantitative yield. HRMS [M-H]$^-$ m/z calculated for $[C_{30}H_20N_7O_{10}S_2]^+$ 702.0719, found 702.0718.

Notes about the Chapter:

Chapter three, in full, is a reprint (with co-author permission) of the material as it appears in the publication; **Christian M. Cole**, Dr. Jun Yang, Dr. Jolita Šečkutė and Prof. Neal K. Devaraj "Fluorescent Live-Cell Imaging of Metabolically Incorporated Unnatural Cyclopropene-Mannosamine Derivatives" *ChemBioChem*, 2013, 14(2), 205-208. I would like to thank Jun Yang, Jolita Seckute, and Neal Devaraj for their invaluable contributions to this chapter: Jun Yang synthesized and characterized all

the compounds presented in this chapter; Jolita Seckute measured the fluorogenic response of tetrazine-Alexa Fluor 488 and its derivatives. I would like to thank Neal Devaraj for directing the research and for preparing the majority of the manuscript. The author of the dissertation is the primary author of this manuscript.

~ CHAPTER 4 ~

4 Encapsulation of Living Cells within Giant Phospholipid Liposomes Formed by the Inverse-Emulsion Technique

4.1 Brief history: Liposomes

The history of liposomes originated early in the seventeenth century by a young neurologist named Hensing who identified a substance in brain matter, which upon burning in a crucible left behind a "greasy oil" that was highly enriched in phosphorous. [96] Decades later in 1846, Gobley realized that egg yolk contained the same phosphorous compound previously identified by Hensing. Working with hen's egg yolk Gobley was the first to isolate phospholipid lecithin[97], shortly thereafter Stricker correctly deduced its structure.[98] However, it would take another hundred years before Dawson's and Bangham's work on phospholipase indirectly elucidates the existence of liposomes.[99] First correctly described by Bangham in the 1960s[100], liposomes are synthetic analogues to vesicles in which an aqueous volume is enclosed by a bilayer of natural or synthetic amphipathic molecules, commonly phospholipids. The lipid bilayer is a supermolecular structure with the all-important task of separating "inside" from "outside" or "self" from "non-self". When dissolved in aqueous environments phospholipids spontaneously form stable phospholipid bilayers due to their intrinsic amphiphilic characteristics. This is a rare and unique trait in biology, where most macromolecular complexes are meticulously orchestrated and controlled at all steps by enzymes; the main driving force behind the assembly of the lipid bilayer

is thermodynamics, which is further enhanced by hydrogen bonding, van der Waals forces and other electrostatic interactions.[101]

Considering the ease of lipid membrane formation, liposomes have an extensive history in drug delivery and other therapeutic applications. They provide an excellent delivery system because they can be easily outfitted with antibodies for targeting cells in vivo[102], have a low immune response and are biodegradable.[103] Currently, liposomes are utilize for subcutaneous or sub-dermal drug delivery, but due to a short half-life in serum they need to be additionally modified with polyethylene glycol (PEG) to prevent immediate detection by monocytes.[104] However, once modified liposomes have the ability to diffuse throughout the whole body and even can be adapted to transverse the blood brain barrier (BBB) making them suitable for releasing treatments for brain repair or anti-cancer therapies. As a consequence, new types of liposomes have been developed (e.g., nanosomes and niosome), although the drawback associated with liposomes still remain; notably, their small payloads and the relatively short time-release of therapeutics.

One problem that researchers have encountered when packaging larger molecular weight compounds in liposomes is poor or even no observable encapsulation efficiency.[105] In the next two chapters we will look at two powerful strategies to encapsulate large biomolecules easily and efficiently (i.e. invert emulsion technique to engulf live cells (Figure 4.1) and the NCL *in situ* vesicle formation to encapsulate eGFP).

4.2 Encapsulation of Live-Cells in Liposomes

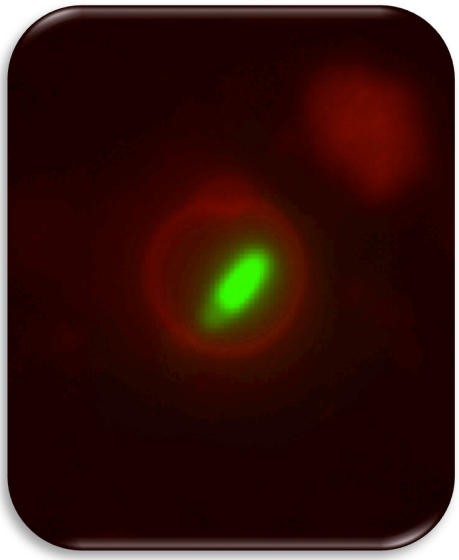

Figure 4.1 Encapsulation of fluorescent GFP bacteria in a liposome stained with Texas red-DHPE by the inverse emulsion method.

Liposomes form spontaneously by the assimilation of phospholipids, the primary component of cell membranes. Due to their unique ability to form selectively permeable bilayers in situ, they are widely used as nanocarriers for drug and small-molecule delivery. However, there is a lack of straightforward methodologies to encapsulate living microorganisms. Here we demonstrate the successful encapsulation of whole cells in phospholipid vesicles by using the inverse-emulsion technique of generating unilamellar vesicles. This method of liposome preparation allows for a facile encapsulation of large biomaterials that previously was not easily attainable. Using *Escherichia coli* as a model organism, we found that liposomes can protect the bacterium against external protease degradation and from harsh biological

environments. Liposomes prepared by the inverse-emulsion method were also capable of encapsulating yeast and were found to be naturally susceptible to hydrolysis by enzymes such as phospholipases, thus highlighting their potential role as cell delivery carriers.

The encapsulation of live cells has commonly been employed in the field of tissue engineering and drug delivery,[106,107] but more recently this technology has been adapted for applications in biofuel production,[108] environmental sensors,[109] probiotics delivery,[110] cultivation,[111] and in the preservation and immobilization of bacteria.[112] Consequently, there is a growing need for suitable biomaterials that can achieve high encapsulation efficiency of live cells, but still provide select advantages, such as non-immunogenicity, biodegradability, biocompatibility, mutable permeability, and protection from the environment. We have exploited the intrinsic characteristics of liposomes to confer several of these benefits when encapsulating *Escherichia coli* bacteria.

Liposomes are a well-studied synthetic transporter used in many applications in a broad range of disciplines (e.g., colloid science, theoretical physics, biophysics, chemistry, biochemistry, and biology).[113] Liposomes are an effective vehicle for packaging and delivering payloads because liposomes can be readily modified with antibodies or ligands for targeting,[114] adapted to cross the blood–brain barrier,[115] or made permeable by using pore-forming proteins.[113] Additionally, liposomes have a low immune response and are biodegradable.[116] As a consequence, natural and synthetic lipids used for encapsulation holds great promise for live-cell delivery.

Unfortunately, there are some drawbacks associated with several popular methods of liposome formation, such as poor encapsulation efficiency and an inability to engulf large-molecular-weight compounds efficiently. For instance, electroformation and rehydration cannot efficiently encapsulate relatively large biomolecules such as proteins or DNA.[102] One of the few methods to achieve high encapsulation efficiency is microfluidic encapsulation.[117] However, this technique requires the manufacturing of either polydimethylsiloxane (PDMS) or capillary systems, which are relatively challenging and time consuming.[118] In addition, these systems are prone to clogging when cells are used, unless special precaution is taken.[119]

4.3 The Inverse-Emulsion Method: GUV Formation

The inverse-emulsion method of creating giant unilamellar vesicles (GUVs) has previously been reported to encapsulate large biomolecules, such as proteins, with high efficiency.[120] Additionally, in contrast to microfluidics, electroformation, and rehydration methods, this technique is a fairly simple approach requiring few materials, while still maintaining scalability and a relatively high efficiency of encapsulation. We adapted a protocol published by the Weitz lab[121] to form GUVs capable of encapsulating bacteria. Briefly, we created an inverse-emulsion by mixing an aqueous solution containing *E. coli* with oil of dissolved surfactants.

The lipids present in the oil formed a monolayer around the drops of the dispersed aqueous solution; this trapped bacteria in the hydrophilic core of the inverted micelle. During centrifugation, the aqueous droplets in the emulsion collide

with the oil/water interface to form large unilamellar vesicles filled with bacteria (Figure 4.2).[121] In order to use this method to encapsulate *E. coli* and yeast, it was necessary to increase the viscosity of the buffer substantially by either using glycerol or adjusting the final concentration of sucrose/glucose to approximately 1 m. On average, we obtained 500 liposomes in 0.1 µL of sample. This corresponds to a production efficiency of five liposomes per rectangular volume of 180×140×30 µm. We counted over 230 liposomes and found that more then 30 % of them contained at least ten live bacteria per liposome (Graph 4.1) with an encapsulation efficiency (EE) of 1.4 % as determined by:

$$\mathrm{EE}\ [\%] = \frac{\mathrm{bacteria}_{[\mathrm{total}]} - \mathrm{bacteria}_{[\mathrm{free}]}}{\mathrm{bacteria}_{[\mathrm{total}]}} \times 100$$

Graph 4.1 Abundance of encapsulated bacteria per liposome when formed by the inverse-emulsion technique. 152 liposomes from three independent preps were counted and the number of bacteria encapsulated per liposome is graphed above. The concentration of bacteria in the upper buffer was at 0.8 OD600. At this concentration less then 15% of the liposomes were empty and 30% had greater then 10 bacteria / liposome. Liposomes smaller then 1 μm were not counted.

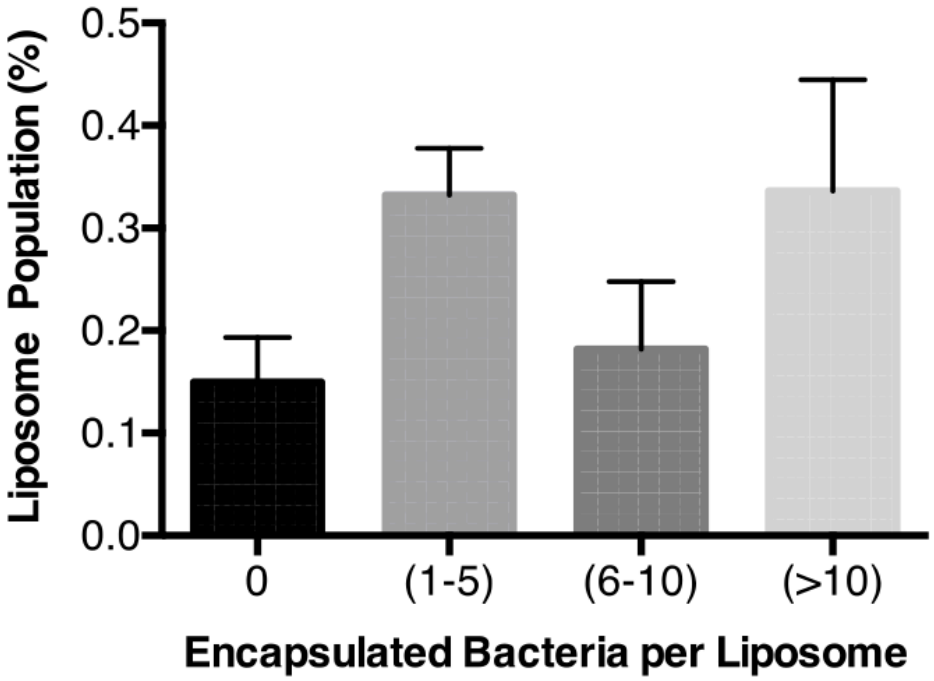

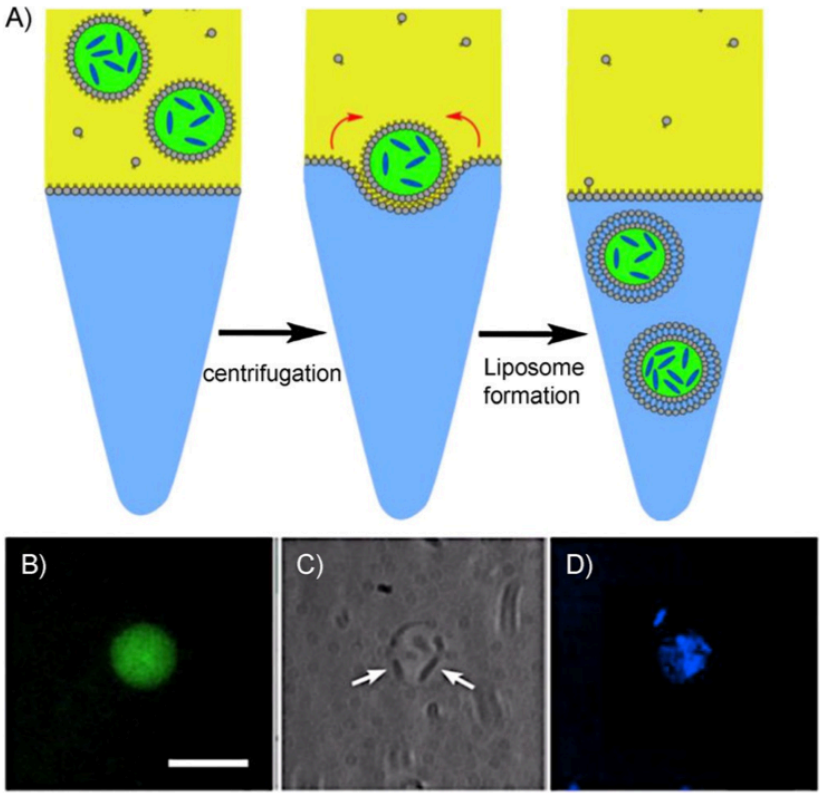

Figure 4.2 Encapsulation of bacteria in vesicles. A) Schematic representation of the inverse-emulsion method to form vesicles. Water droplets containing live cells are added to a solution of heavy mineral oil containing POPC phos- pholipids to generate a water/oil emulsion. Each droplet is surrounded by a monolayer of phospholipid. The entire emulsion is then layered over water. After centrifuging, the water droplets pass through the bulk oil and gain another phospholipid leaflet as they transverse the water-oil interface to become bilayer vesicles. B) Fluorescence microscopy image of a vesicle filled with HPTS, a water-soluble dye. Scale bar: 10 mm. C) Bright-field microscopy image that shows the outline of the vesicle along with encapsulate bacteria (white arrows). D) Fluorescence microscopy image of a liposome encapsulated with Hoechst-stained bacteria.

where $bacteria_{[total]}$ is the initial amount of bacteria added to the upper buffer and $bacteria_{[free]}$ is the number of free bacteria that were not encapsulated. At OD=0.8, several bacteria per liposome can be encapsulated (Figure 4.3). Encapsulation efficiency can be improved to ~13 % if the initial OD_{600} is less than 0.1 absorbance. However, this results in a lower density of bacteria per liposome and more empty liposomes. This is similar to the results reported by Tan et al., who demonstrated using

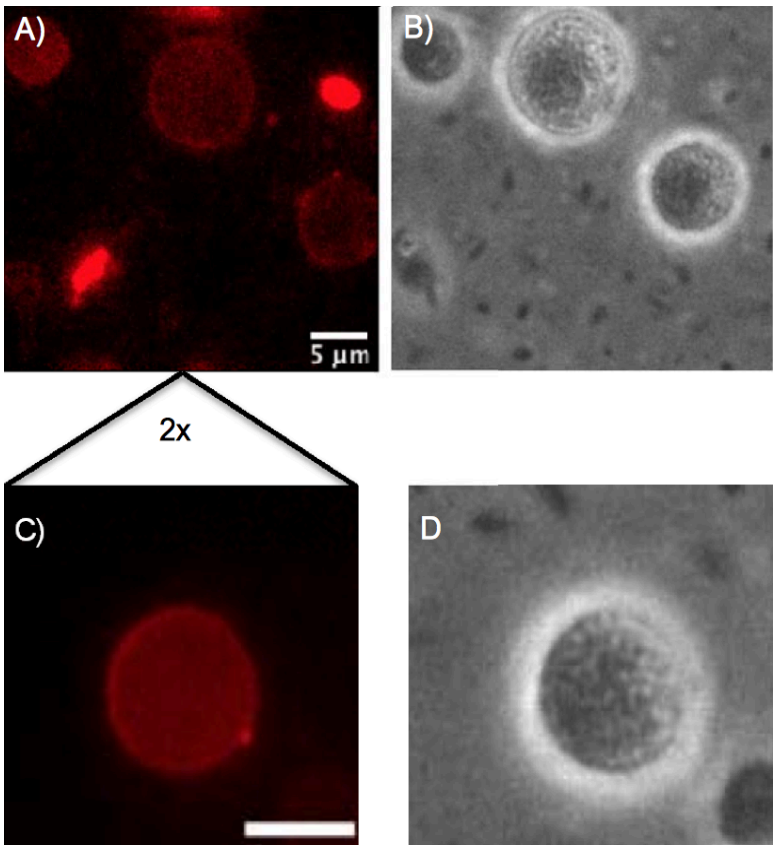

Figure 4.3 Encapsulation of E. *coli* in POPC liposomes using the inverse-emulsion method. The liposomes are texturized from the encapsulated bacteria. Figures A & C are membrane stained liposomes using 1 mole percent of Texas Red-DHPE. B & D are phase contrast images of the liposomes displaying a high yield of encapsulated E. *coli*. C & D are enlarged to better visualize the interior.

microfluidics encapsulation efficiencies of between 5–15 % according to the flow rate.[117]

To determine if the amount of bacteria encapsulated is correlated to the size of the liposome, we used hydroxypyrene-1,3,6-trisulfonic acid (HPTS) dye as an indicator of internal volume. When a high density of cells is encapsulated, the fluorescent intensity of HPTS is low due to the buffer being secluded; when

comparatively few bacteria are encapsulated, the fluorescent intensity is high (Figure 4.4). Surprisingly, there was no correlation between the radius of a liposome and the amount of encapsulated bacteria. Under visual observation, the encapsulated bacteria appear to be randomly distributed among various sizes of liposomes. We additionally explored the use of divalent salts to increase our encapsulation efficiency.[122]

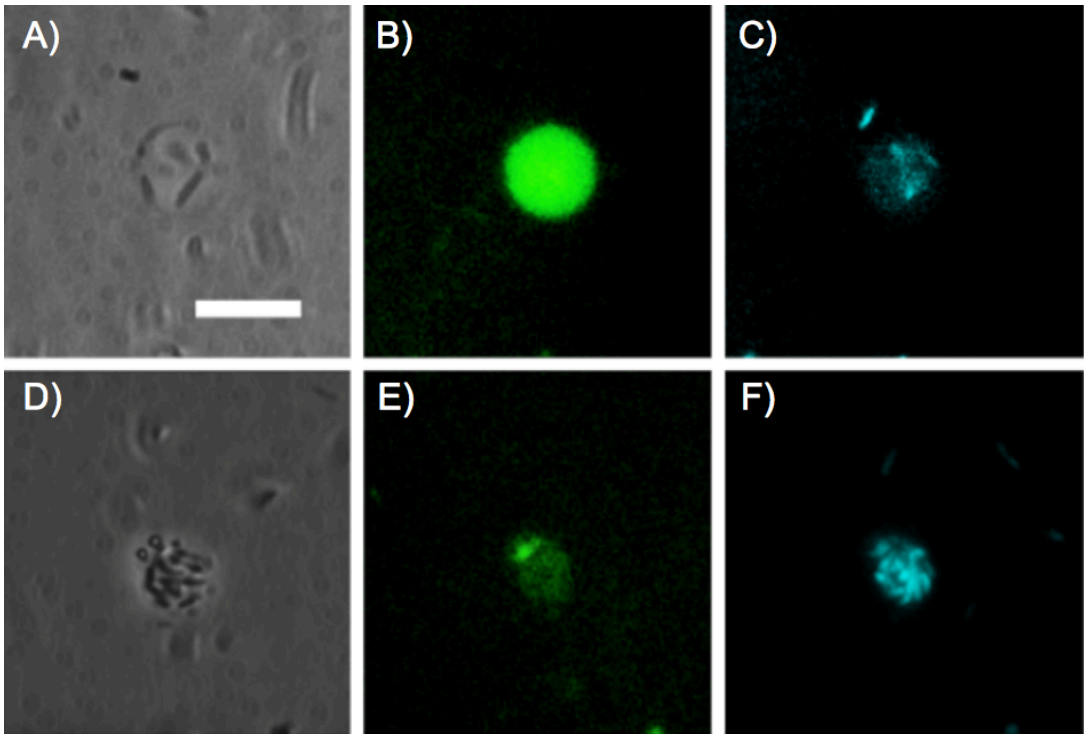

Figure 4.4 Encapsulation of E. *coli* in POPC liposomes using HPTS as a volume indicator. A) Phase contrast image of a liposome containing little encapsulated bacteria. B) Fluorescent image of HPTS inside a liposome containing a low concentration of bacteria, thus illustrating a high amount of encapsulated HPTS. C) Hoechst stained bacteria. The image sequence A-C appears in Fig. 1 of the manuscript. D) Phase contrast image of a liposome containing a high concentration of bacteria. E) Fluorescent image of HPTS inside a liposome containing many bacteria, thus a high void volume lowers the amount of HPTS, which can be present. F) Hoechst stained bacteria. Scale bar is 10 μm.

We observed a drastic decrease in liposome formation when an equivalent amount of divalent or monovalent salts relative to buffer concentration was added (Graph 4.2). To maximize encapsulation, 0.1 % nonyl phenoxypolyethoxylethanol (NP-40) detergent was added to the upper buffer to help stabilize larger GUVs and to avoid premature rupturing. This is a nonionic, non-denaturing detergent chemically identical to IGEPAL CA-630.

Graph 4.2 Graph showing the effect that divalent and monovalent salt has on the formation of liposomes using the inverse-emulsion method. The upper buffer was 100 mM HEPES pH 7.5, 200 mM sucrose, and 100 mM salt (NH_4Cl, $MgCl_2$, $CaCl_2$ or NaCl). This was pull downed into the lower buffer consisting of 200 mM HEPES pH 7.5 and 200 mM glucose. The control was supplemented with an addition of 100 mM HEPES pH to 7.5 to both the upper and lower buffers. Liposomes contained in an area of 90 μm^2 were counted and the number of liposomes was plotted on the graph, error bars represent data from triplicate results.

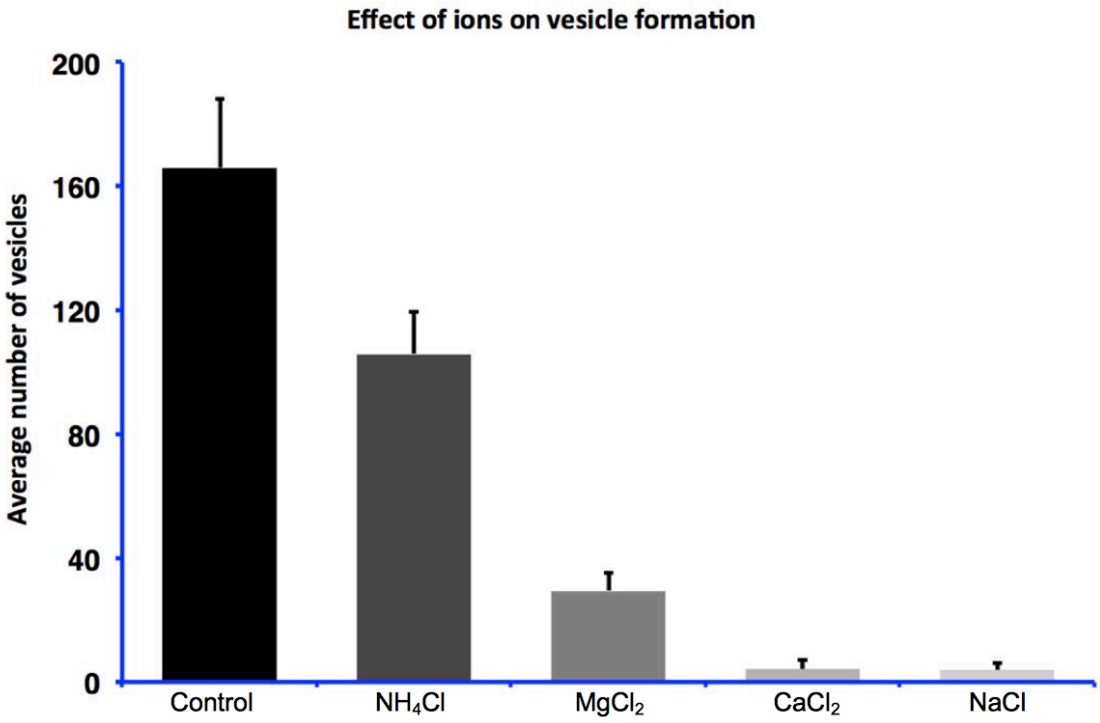

4.4 Liposomes Protect Live-Cells from Harsh Environments

We hypothesized that liposomes could protect bacteria by ensuring that the internal compartment is separated from the external biological environment, protecting them from any damaging effects of enzymes. In addition, the internal liposome solution has some buffering capacity and can even resist small changes in the external pH. In order to observe the beneficial effects, *E. coli* or yeast (Figure 4.5) was first encapsulated in 1-palmitoyl-2-oleoyl-*sn*-glycero-3-phosphocholine (POPC) liposomes by using the standard encapsulation method described in the Experimental Section.

To authenticate that *E. coli* were encapsulated in liposomes, we initially stained the liposome with 1.0 mol % of Texas Red-DHPE (Figures 4.3 and 4.6). Pepsin and hydrochloric acid were subsequently added to the mixture of encapsulated and free *E. coli* to measure the level of protection afforded by the liposome.

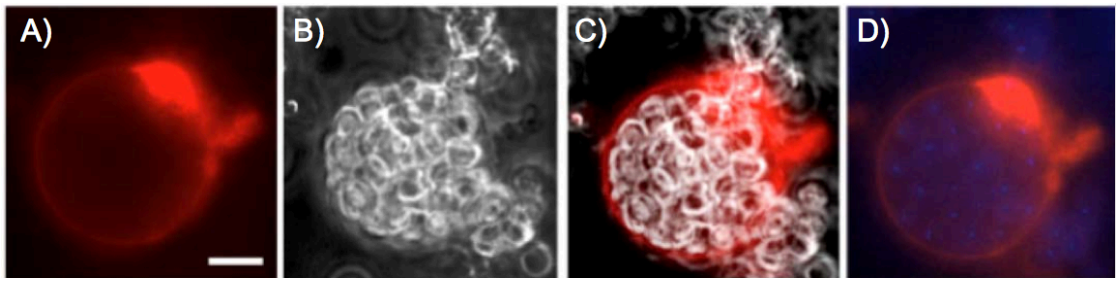

Figure 4.5 Encapsulation of yeast in POPC liposomes using the inverse-emulsion method. A) Shows a liposome made using the inverse-emulsion method by employing an upper buffer (100 mM HEPES pH to 7.5, 0.05% NP40 detergent, and 1M sucrose) and a lower buffer (100 mM HEPES pH to 7.5, 0.05% NP40 detergent and 1M glucose). This liposome was stained with 1 mole percent of Texas Red-DHPE to better illustrate the membrane. B) Phase contrast image of a giant liposome completely filled with yeast. C) Merge fluorescent image of the membrane stained liposome and the phase contrast image. D) Merge image of the encapsulated yeast stained with hoechst and the Texas- red DHPE membrane of the liposome. Scale bar is 12μm

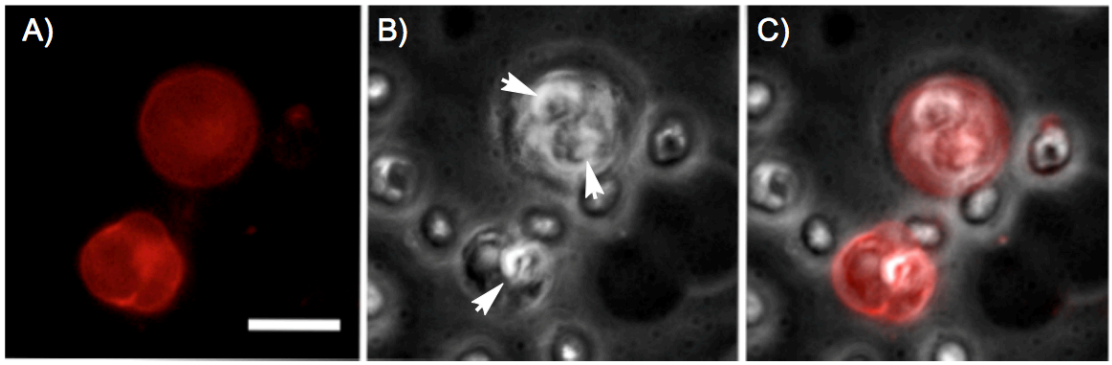

Figure 4.6 Encapsulation of yeast in POPC liposomes using the inverse-emulsion method with the same conditions as described in Figure 4.3. A) Liposomes stained with 1 mole percent of Texas Red-DHPE. B) Phase contrast image of the liposome and encapsulated yeast (arrows). C) Merge image of encapsulated yeast and the liposome stain. Scale bar is 12 μm

The presence of bacteria or yeast inside a liposome was determined by using epi-fluorescence and phase-contrast microscopy. The DNA of the cells was stained with Hoechst stain, a cell-permeable dye able to stain both live and dead cells. This dye was used in combination with propidium iodide (PI) stain. PI was used exclusively to visualize damaged *E. coli* with compromised membranes. Thus, the co-localization of Hoechst and PI allows for the unambiguous determination of live and dead bacteria in liposomes. We estimated that 94 % of the encapsulated bacteria did not exhibit PI staining for over 6 h, but maintained viability for up to 24 h. These imaging results illustrate the effectiveness of liposomes in protecting encapsulated bacteria from enzymatic degradation and acidic environments (Figure 4.7).

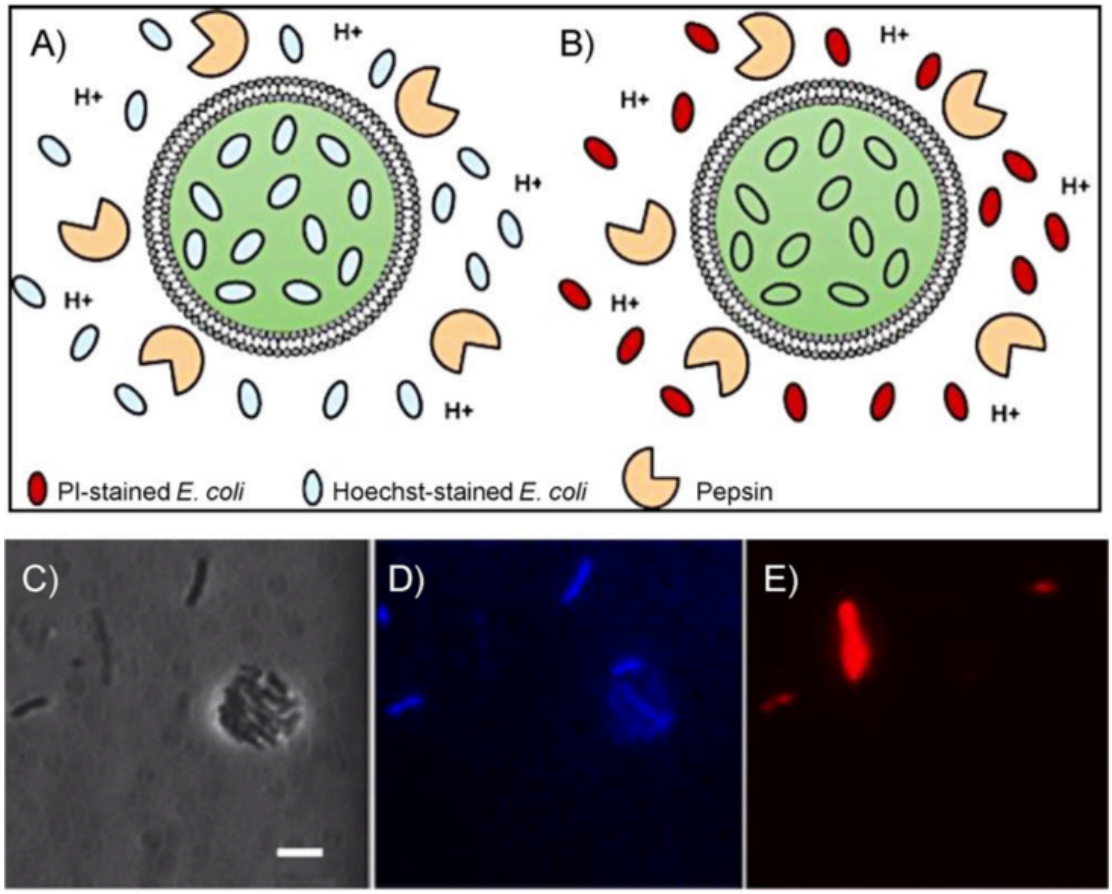

Figure 4.7 Viability of *E. coli* encapsulated in liposomes. A)–B) Illustration of the microscopy images (D–E) that depicts a phospholipid membrane secluding the encapsulated bacteria from pepsin, while the internal buffer system delays the damage from the external acidity. A) Hoechst stain allows for the visualization of all bacteria, encapsulated and free. B) Propidium iodide will stain only the external bacteria, as these will have compromised membranes due to the pepsin activity. C) Phase-contrast image of a liposome with multiple bacteria encapsulated. Scale bar: 5 μm. D) Visualization of internal and external bacteria by using Hoechst stain. E) The solution was treated with hydrochloric acid in order to lower the pH of the solution and with pepsin in order to disrupt membrane proteins on the bacteria. The propidium iodide stain locates the bacteria with compromised membranes and it can be seen that only the external bacteria have been stained.

In order to better quantify the viability of encapsulated *E. coli*, we plated the solution containing the encapsulated bacterial liposomes on an agar plate and counted the colony-forming units (CFUs) of the pepsin- and HCl-treated *E. coli*. For these experiments, BL21 *E. coli* was grown to OD=0.6 and then aliquoted to both the

liposome and control samples, matching their respective ODs before liposome formation. We observed that the control samples, which contained only free *E. coli*, produced no colonies, thus resulting in a 100 % loss of viability (Graph 4.3). Interestingly, increasing the amount of encapsulated *E. coli* produced a dose-responsive increase in CFUs. This further highlights the suitability of liposomes as carriers for live cells even under harsh biological conditions.

Graph 4.3 Increase in CFUs from the protective effect of liposomes. We tested the viability of E. coli encapsulated in vesicles treated with pepsin and HCl in comparison to unprotected E. coli. The control, unprotected sample had no growth. There was a linear increase in CFU/mL in relation to the final amount of vesicle suspension in each sample. This demonstrates that the vesicles not only prevented the membranes of the bacteria from being compromised, but also ensured that the bacteria would remain viable after undergoing the treatment with pepsin in an acidic environment.

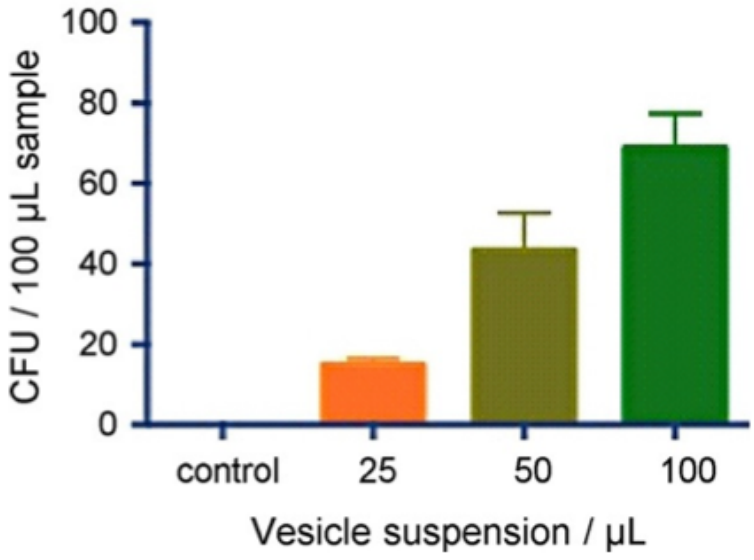

To show the potential use of liposomes as cell-delivery carriers that could release a payload, we used phospholipase A2 (PA2) to hydrolyze the liposome

membrane. To observe the effects of PA2, we encapsulated *E. coli* and HPTS dye together in liposomes, and monitored the hydrolysis of the phospholipid membrane by time-lapse microscopy (Figure 4.8). The liposomes began to hydrolyze within 10 min, as observed by the loss of HPTS fluorescence. This event is also corroborated in the phase-contrast channel, as the bacteria can be observed to disperse as they are released from their liposome carrier.

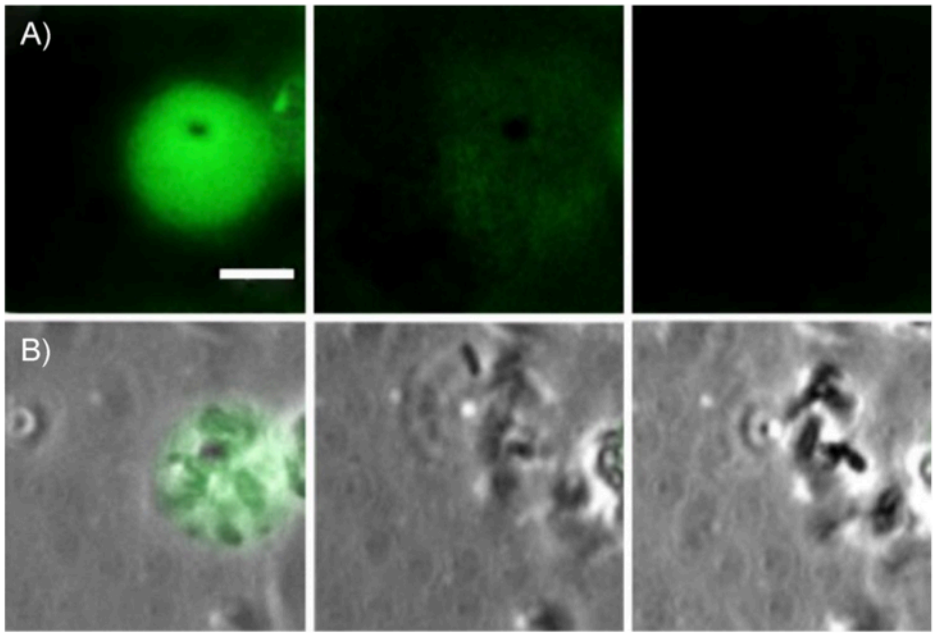

Figure 4.8 Time-lapse microscopy of liposome hydrolysis. Bacteria-encapsulated vesicles were observed in A) the fluorescence channel and B) the phase-contrast channel. The brightness of HPTS dye was used as an indicator of vesicle integrity. At 8 min, the liposome was still intact, and the bacteria were encapsulated. At 10 min, the vesicle membrane was hydrolyzed by phospholipase A2, which caused the vesicle to rupture and leak HPTS. Scale bar: 10 μm.

4.5 Summary of Encapsulation of Live-Cells

In summary, we have demonstrated the suitability of the inverse-emulsion method for the effective encapsulation of living cells in liposomes. This approach generates 1–30 μm-sized GUVs that confine live cells into a micrometer-sized space.

The size restriction could potentially benefit many applications, including tissue engineering, as highlighted by Uludag and co-workers[123] who showed that more protein is secreted in smaller capsules than in larger ones. The food industry routinely encapsulates probiotics for fortification in food and discovered that a larger capsule size (≥100 μm) can negatively influence the texture and "mouth-feel" of a food product,[124,125] Additionally, smaller capsules with higher surface-to-volume ratios might be desired if the secretion of biomolecules is governed by pumps or pores.[126] Functionally, these liposomes provide environmental protection from enzymes and pH changes. Although there are a variety of methods for the production of synthetic vesicles, there are many issues associated with each method. Rehydration suffers from liposome heterogeneity and aggregation.[127] Moreover, rehydration and electroformation techniques are incapable of encapsulating large entities (i.e., bacteria). Microfluidic encapsulation does achieve high encapsulation efficiency, but requires the use of complex PDMS or capillary systems, which are generally time consuming and challenging to set up and run. The inverse-emulsion method provides a solution to all of these issues, creating a simple yet effective way of protecting living cells from harmful environments. The encapsulated cells prepared by this method retain their viability after being exposed to hazardous environments, such as changes in external pH and proteases. Lastly, we have shown a proof-of-concept liposome delivery system that can release encapsulated bacteria in the presence of phospholipase A2, thus mimicking probiotic delivery to the gut.

4.6 Experimental Section

4.6.1 Standard encapsulation

All chemicals and reagents were of reagent grade, obtained from Sigma Aldrich, unless otherwise stated. POPC was purchased from Avanti Inc. as a powder. POPC (5 mg) was dissolved in chloroform (100 μL, Fisher Scientific), and this mixture was dried under compressed nitrogen for 30 min to obtain a lipid film. The film was dissolved in heavy mineral oil (1 mL, Fisher Scientific) by using a bath sonicator for up to 1 h or until the solution was completely clear. Vesicles were prepared by adapting a previously published protocol.[118] In brief, the upper buffer was prepared by using HEPES (100 mM, pH 7.5), sucrose (900 mM) and 0.1 % NP40 detergent; according to the manufacturer (Sigma–Aldrich) it contains <0.5 % water. An aliquot (3 μL) of BL21 *E. coli* (Invitrogen) at OD=1.2 was added to the upper buffer (10 μL) and the oil/lipid solution (150 μL). A water-in-oil emulsion was created out of these solutions by agitating the mixture until it appeared homogeneous and turbid. The resulting emulsion was then layered over the lower buffer of HEPES (100 mM, pH 7.5) and glucose (900 mM) by gently pipetting the emulsion. This was then centrifuged for 5 min at 7200 *g* at room temperature. The oil layer was aspirated off from the top of the solution, and the vesicles were collected from the resulting pellet near the bottom.

4.6.2 Staining experiment

The standard encapsulation method was used, except that HPTS (10 mM) and PI (5 $\mu g\,mL^{-1}$) were added to the upper buffer. After the vesicles had been synthesized, pepsin (10 $mg\,mL^{-1}$) and Hoechst stain (2 $\mu g\,mL^{-1}$, Invitrogen) were added. The addition of HCl (12 M) brought the pH of the resulting solution to 3.5. The vesicle solution was then incubated for 1 h at room temperature, and the sample was centrifuged at 5000 *g* for 10 min. The resulting pellet and solution (5 μL) were put onto a slide to be examined under a microscope.

4.6.3 Colony formation

After the vesicles had been formed according to the discussed method, pig pepsin (10 $mg\,mL^{-1}$, Spectrum, New Jersey) was added, and hydrochloric acid was used to bring the resulting solution to pH 3.5. The solution was then incubated for 1 h at room temperature. In parallel, a control solution of *E. coli* was created that had the same optical density as the vesicle solution; this was also incubated for 1 h in the presence of pepsin at pH 3.5. The bacterial solution containing vesicles was aliquoted (0, 25, 50 and 100 μL) into four tubes, and the control solution was used to bring the final volume to 100 μL. All four samples were plated on LB agar culture plates. The plates were left to grow overnight, and the colonies were counted the next day. This experiment was repeated in order to account for experimental errors.

4.6.4 Phospholipase hydrolysis

The previous method of encapsulation was used, with the addition of KCl (10 mM) and $CaCl_2$ (35 mM) to both the upper and lower buffers and HPTS (1 mM, Sigma–Aldrich) dye was added to the upper buffer. After the vesicles had been made, the sample (3 μL) was added to a microscope slide, then phospholipase A2 (5 $\mu g\, mL^{-1}$, Sigma–Aldrich) was added directly to the slide in order to hydrolyze the vesicles. The sample was then observed under the microscope every 2 min for 30 min.

4.6.5 Encapsulation efficiency

Liposomes were prepared with a bacterial concentration of OD_{600}=0.8. The solution containing the liposomes and free bacteria were dialyzed against HEPES (100 mM, pH 7.5) and glucose (900 mM) for 3 h in a Slide-A-Lyzer dialysis cassette (Thermo Fisher) containing a Whatman membrane filter with a nylonpore size of 1 μm. The ODs of the free bacteria and that of the initial solution were compared on a NanoDrop 2000c UV/Vis spectrophotometer (Thermo Scientific). Alternatively, microscopy images were used to manually count a total of 589 bacteria to find the ratio of encapsulated bacteria compared with free bacteria.

Notes about the Chapter:

Chapter four, in full, is a reprint (with co-author permission) of the material as it appears in the publication; Sampreeti Chowdhuri, **Christian M. Cole** and Prof. Neal K. Devaraj "Encapsulation of Living Cells within Giant Phospholipid Liposomes Formed by the Inverse-Emulsion Technique" *ChemBioChem*, 2016, 17(10), 886-889. I

would like to thank Sampreeti Chowdhuri for her invaluable contributions to this chapter: Sampreeti Chowdhuri prepared the encapsulated E. coli samples and carried out the CFU viability assay. I would like to thank Neal Devaraj for funding the research. The author of the dissertation is co-primary author of this manuscript and directed the research.

~ CHAPTER 5 ~

5 In Vas: Studying Biological Systems in Vesicles

5.1 Introduction

One of the more seductive goals of biochemistry is to understand the functional basic unit of living organisms, the cell. Our remarkable success in elucidating cellular function and dynamics is an impressive accomplishment; however, the complexity of our model is exponentially rising.[128] The current cellular archetype has been evolving from past systems; with every iteration becoming more convoluted than the last. By analogy it is seeking to understand the fundamental workings of a central processing unit by looking inside the worlds most advance super computer. Thus, the current conception of a cell does not lend itself well to fundamental questions or computational modeling of its individual components. Taking steps to build a simplified system or a protocell can facilitate our understanding behind the fundamental biology, and may also provide insights into the emergence of intrinsic self-replicating & self-directing systems.

Two complementary approaches are taken to construct artificial cells. The top-down approach, being pioneered by scientists such as Craig Venter, focuses on the minimal genome. This is achieved by synthesizing genes that are essential for life and transplanting them into a host cell.[129,130] The bottom-up approach starts at the molecular level and adds elements to the system until it takes on life-like qualities.

Our lab has taken the latter approach in the development of a hybrid artificial protocell. The current development of the bottom-up approach is encapsulating cell-free transcription–translation systems inside vesicles, consequently treating them as a micron-size flask for gene expression. This category of scientific inquiry really belongs to a new space in between the more traditional concepts of in vivo and in vitro. The Latin word *vas* is fitting to use since the original word is translated to mean "a vessel holding biological fluid". In this chapter we will coalesce liposomes with a more dynamic system akin to living systems by employing bioorthogonal chemistry and the inclusion of genetic circuits, thus engendering a *in vas* framework to study artificial cells. The end goal is to progress this artificial cellular model using an engineering approach for its modular design and construction with known components and concentration of reagents.

5.2 In Vitro Cell-Free TX-TL Reactions

To begin development of an artificial cell model using the canonical biological dogma for transcription–translation (TX-TL), we first have to optimize gene expression of the cell-free systems (i.e. S30 cell lysate or PURExpress recombinant lysate). These systems offer a variety of benefits to build basic and complex networks: no cytotoxicity, mRNA lifetimes can be adjusted, high co-expression levels and finally additives can be added for added specialization (i.e. detergent, unnatural amino acids, metals, and stabilizers). [131] However, it is important to optimize the reaction to provide the best platform for robust and adaptable gene expression. This will later become significant, when a greater number of genes have to be expressed simultaneously to

form sophisticated protein networks and genetic circuits. The preferred readout for these experiments is fluorescence, which relies on the expression of fluorescent proteins (FP) to obtain real-time rates of the TX-TL system.

Cell-free systems that employ prokaryotic elements (i.e. S30 cell lysate or PURExpress recombinant lysate) tend to provide a poor environment for the folding of recombinant proteins, especially ones derived from eukaryotes. To help ameliorate this problem we turned to high expressing plasmids. Accordingly, we primarily used plasmid constructs of eGFP controlled by a T7 promoter or the eGFP-Del6 reporter protein. The eGFP-Del6 gene was cloned on a pBEST plasmid, previously optimized by Vincent Noireaux for cell-free expression.[132] This plasmid included a PtacI promoter, which is one of the strongest *E. coli* sigma factor 70 promoters.[133] The untranslated region (UTR) was replaced by UTR1. The UTR1 sequence includes the T7 gene*10* leader RNA, containing a strong ribosome binding site.[134] Finally, the pBEST plasmid included the lac operator overlapping the -10 part of the promoter; Noireaux found that this modification increased expression by a factor of five to ten fold on average.[132] Before characterizing the expression of eGFP-Del6 inside giant unilamellar vesicles (GUV's), we compared the expression of three commercially available lysates; S30 lysate from Promega, S30 lysate from Invitrogen and a completely recombinant lysate, PURExpress from New England Biosciences (NEB).

All of the discussed lysates come pre-equipped and are optimized to express genes off the T7 promoter. The lysates were tested with an eGFP plasmid containing a pT7, as expected the PURExpress resulted in lower expression of the reporter protein relative to its S30 counterparts (Figure 5.1).

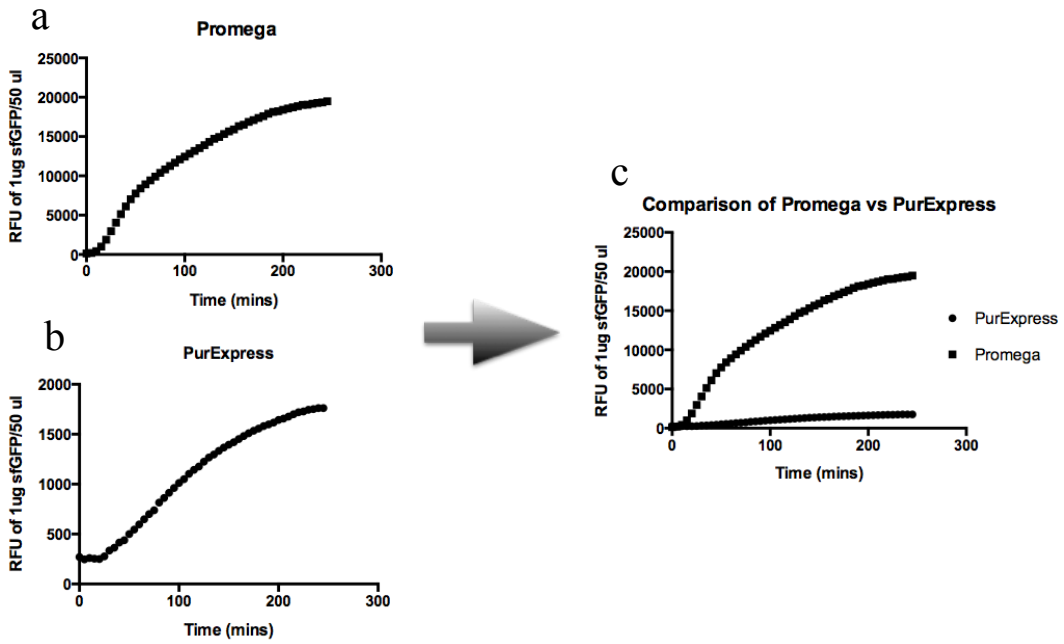

Figure 5.1 In vitro cell-free transcription – translation assay comparing commercially purchase S30 lysate to PURExpress. a) 1 µg of GFPuv plasmid under control of pT7 in Promega lysate. b) 1 µg of GFPuv plasmid under control of pT7 in PURExpress lysate. c) Overlay of the Promega and PURExpress assays

Invitrogen's lysate performed slightly better then PURExpress (data not shown), but its performance was underwhelming, therefore we employed Promega's S30 lysate for all future experiments (excluding the thiol-galactose experiments, which required a S30 lysate free of the additive IPTG). However, from the perspective of

bioengineering the PURExpress system is appealing due to its transparency and ease of modification.

For this reason we investigated the possibility to improve the effectiveness of PURExpress by increasing the concentration of RNA polymerase holoenzyme. As shown in Figure 5.2a, as RNA polymerase concentration increases there is a respective increase in eGFP fluorescence until 1.5 units of RNA polymerase is added, at which point there is a resulting downward trend. The decrease in eGFP expression from the addition of RNA polymerase was reasoned to be due to the increasing concentration of stabilizing ingredients (i.e. glycerol) in the enzymes buffer. This was addressed by removing glycerol via buffer exchange in a 10 kDa spin column to afford RNA

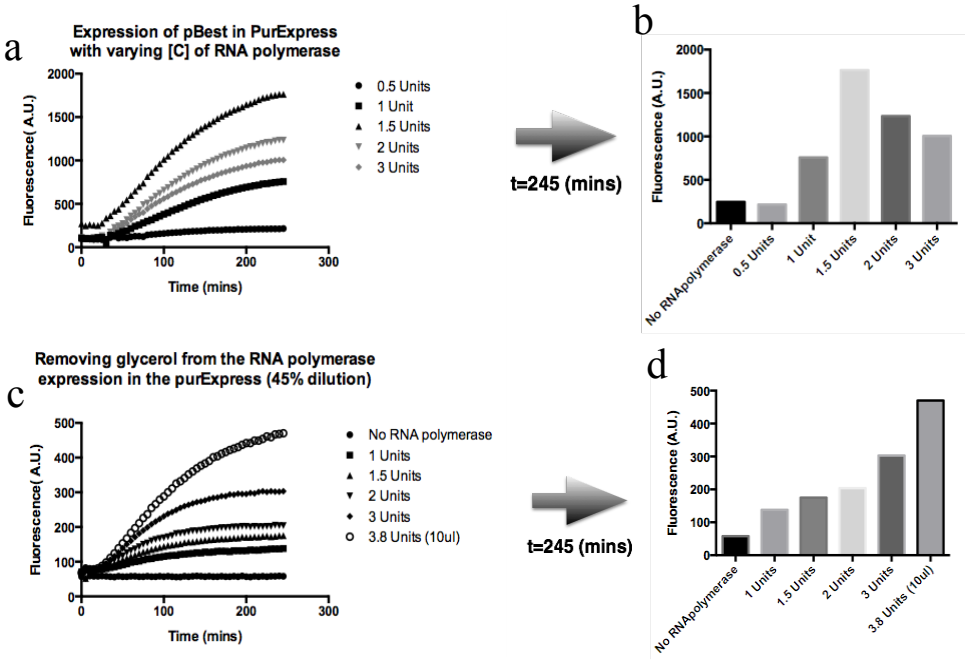

Figure 5.2 In vitro cell-free transcription – translation assay of PURExpress a) 1 µg of eGFP-Del6 (pBEST plasmid) under control of an endogenous E. coli promoter (λ pL) with varying amounts of RNA polymerase. b) Graph representing the instantaneous fluorescence of the expression curves at time = 245 minutes. c) 1 µg of eGFP-Del6 (pBEST plasmid) under control of an endogenous E. coli promoter (λ pL) with varying amounts of RNA polymerase after removal of glycerol. Samples are 45% diluted d) Graph showing the instantaneous fluorescence at time = 245 minutes. A correlation between intensity and [RNA polymerase] is observed.

polymerase without the glycerol contamination. This sample demonstrated an increase of fluorescence relative to RNA polymerase for all concentrations, but was still low relative to bacterial lysate. With further improvements to this system it could serve as a viable replacement for the less informative S30 lysate.

5.3 *In Vas* Cell-Free TX-TL Reactions

One of the considerations of designing a system *in vas* is to know the passive diffusion rates of small molecules and how they influence gene expression and changes to osmotic pressure. The first small molecules we studied that directly influence gene expression were the 20 amino acids. To investigate cell-free expression of eGFP relative to the flux of amino acids across a bilayer we packaged PURExpress and plasmid DNA in liposomes using the inverse pull down technique and either added the twenty amino acids to the inside or outside of the liposomes. To monitor the expression of eGFP in liposomes we either employed flow cytometry (Figure 5.3) or confocal microcopy (Figure 5.4).

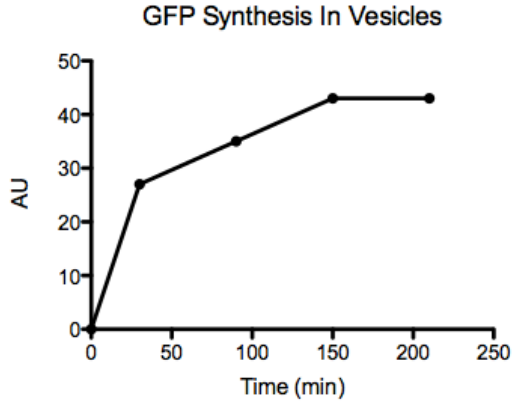

Figure 5.3 Monitoring eGFP-del6 expression *in vas* using flow cytometry. During Expression a sample of liposomes were analyzed at different time points.

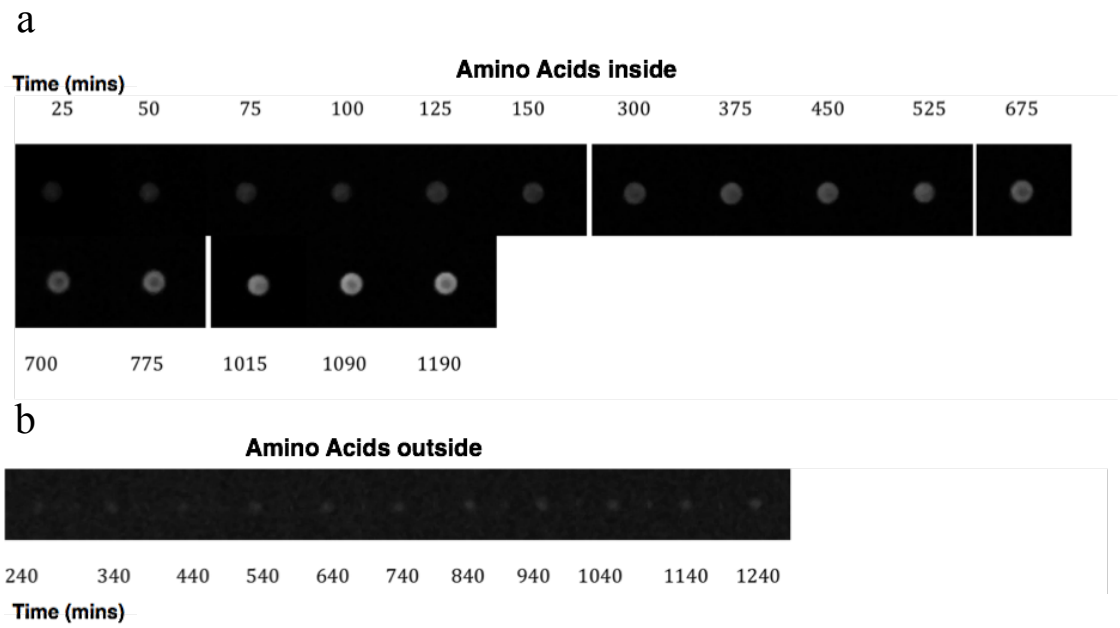

Figure 5.4 Monitoring eGFP-del6 expression *in vas* with POPC using confocal microscopy with a) amino acids on the inside or b) amino acids on the outside

The results of n > 100 liposomes are summarized in Graph 5.1 and representative liposomes are presented in Figure 5.5. This data agrees with previously published data[135], which indicates the type of lecithin and its degree of saturation/length has an impact on the diffusion of amino acids across the bilayer and consequently, on gene expression inside the liposome. This significance of diffusion is non-apparent if the amino acids are placed inside, as the diffusion is sufficiently slower then expression (Graph 5.1).

Graph 5.1 Quantification of the fluorescence intensity of eGFP-del6 expression *in vas* with various phosphatidylcholine lipids using confocal microscopy with amino acids on the inside or outside the liposomes, n > 100.

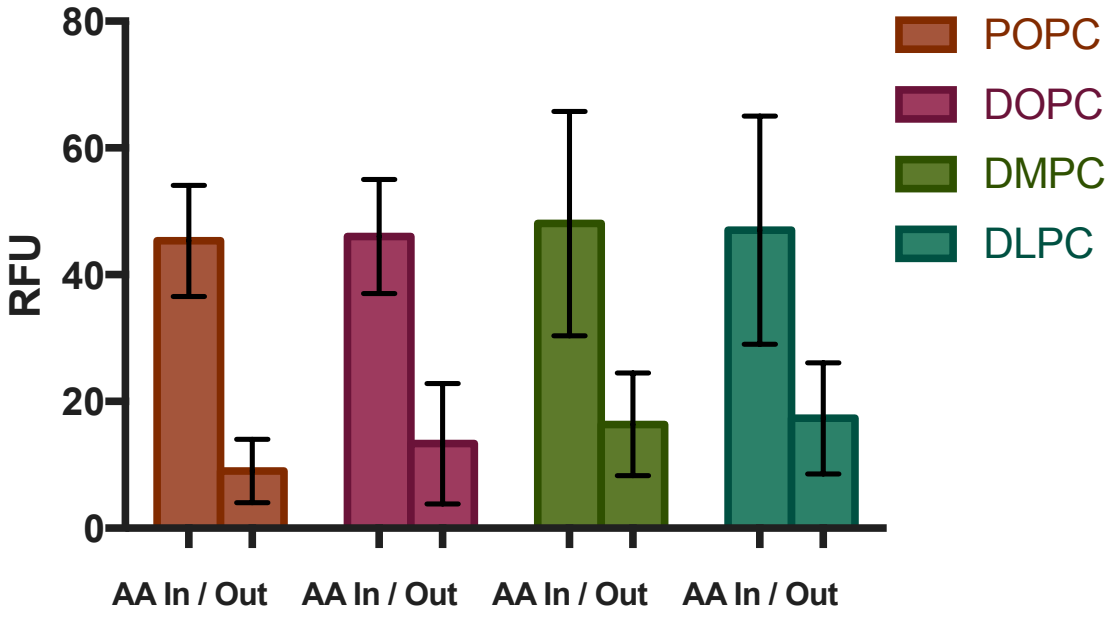

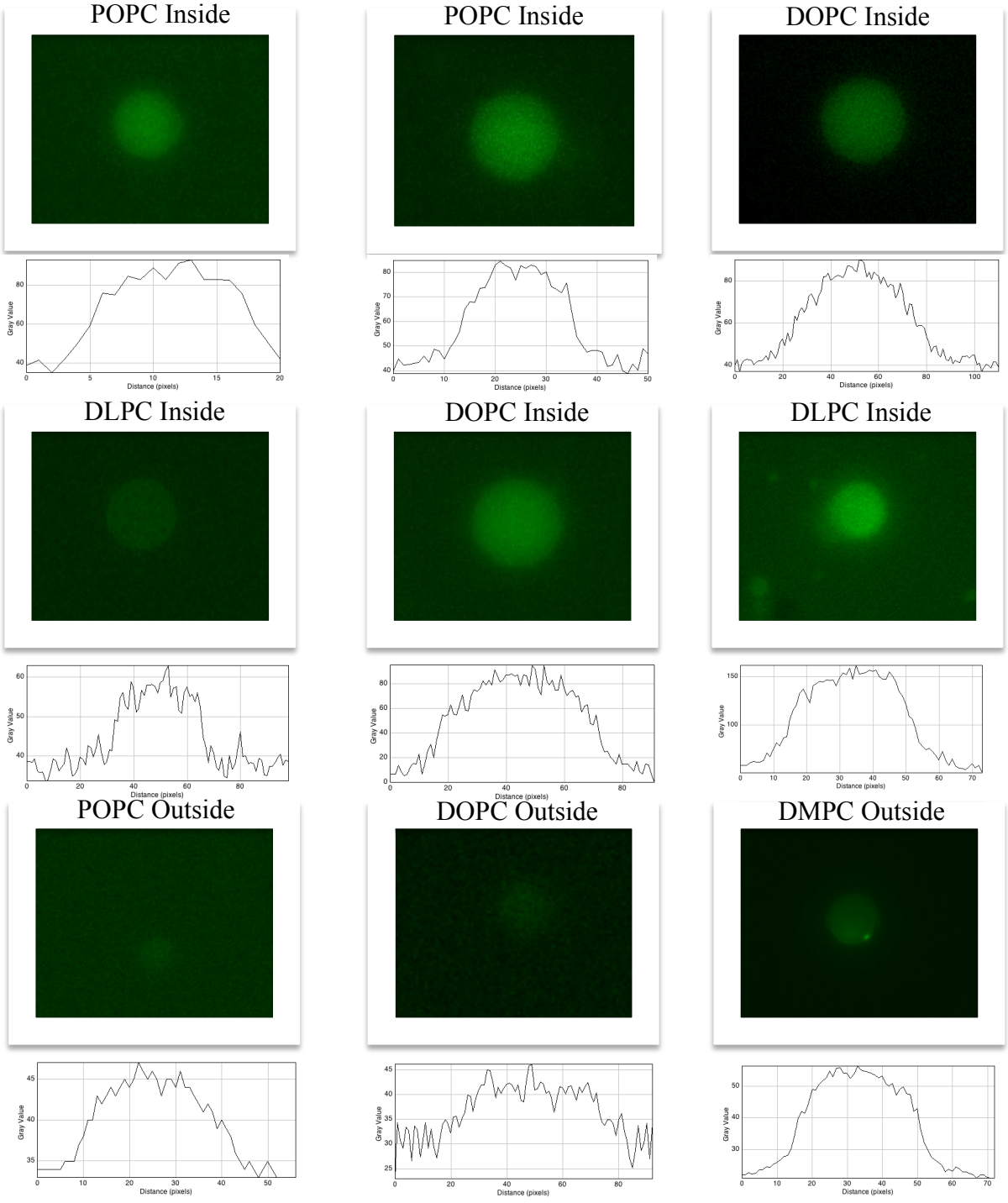

Figure 5.5 Confocal micrographs of liposomes expressing eGFP-del6 in PURExpress with amino acids either added to the inside or outside. These are representative images that were used for Graph 5.1

5.4 Negative Feedback Genetic Circuits:

Regulatory proteins in living systems are often dynamic and cyclic. Oscillations of biomolecules are necessary for the cell's temporal and spatial regulation.[136,137,138] To mimic this we incorporated oscillator gene circuits inside of the vesicle. In order to observe dynamic gene expression we needed protein degradation and expression to be simultaneously or intermittently linked. To achieve this we utilized the protein ClpXP and the ssrA recognition sequence to get time dependent degradation of our reporter protein. The buffered solution prepared to test the activity of ClpXP; and subsequently used as the "upper buffer" solution for the pull down method, was from single molecule experiments done by Lang et. al.[139] and then adapted based on considerations of Weber-Ban.[140] It is known from their experiments

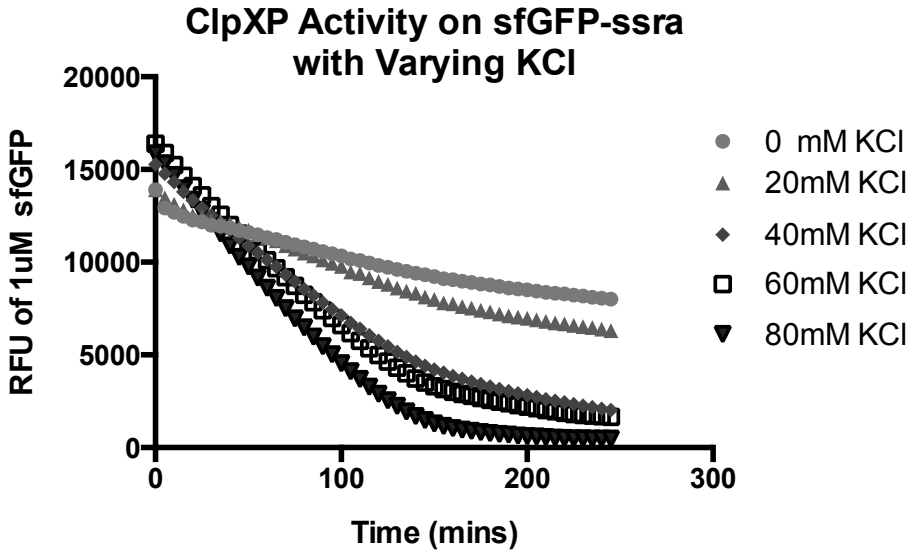

Figure 5.6 In vitro assay of the enzymatic degradation of eGFP by ClpXP's to optimize the concentration of KCl to make compatible with the inverse pull-down technique.

that the ionic concentration of sodium or potassium is necessary to help stabilize ClpXP; however, as discussed earlier in this chapter, high ionic concentrations can interfere with the pull-down technique preventing the formation of liposomes. To maximize liposome formation we found the lowest concentration of potassium chloride that could be used, while still maintaining high ClpXP activity (Figure 5.6). Next, we checked the activity of ClpXP at every stage of the pull down as shown in Figure 5.7. We concluded that ClpXP was losing activity from the emulsion stage and failed to recover activity after centrifugation. To combat this we added a low concentration of NP-40 detergent and BSA as a sacrificial protein to keep the ClpXP soluble and to prevent excess absorption and denaturation at the water-oil interface (Figure 5.8).

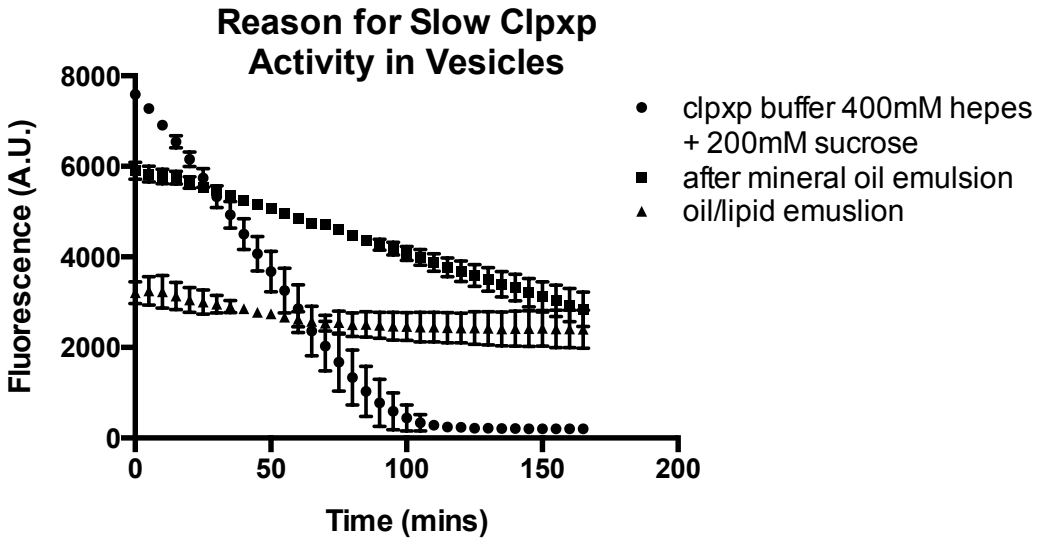

Figure 5.7 In vitro assay of the enzymatic degradation of eGFP by ClpXP's to evaluate activity for every step of the inverse pull-down technique.

With our current approach we have successfully encapsulated ClpXP close to its physiological concentration[141] and observed degradation of purified eGFP-ssrA in a liposome via confocal microscopy that closely corresponds to the rate of the in vitro studies (Figure 5.9 and Figure 5.10). Combining ClpXP with a simple negative feedback oscillator (Figure 5.11), which was previously shown to function in vivo.[142] We were anticipating dynamic behavior of gene expression inside a vesicle with tunable degradation; however, the oscillations observed were not repeatable and suffered from low amplitudes. As Henrike et. al. later revealed[143], cell-free circuits that employ a single form of feedback may fail to generate robust and measurable oscillations. This insight allows for future experiments to test genetic circuits, like the repressilator, inside liposomes with ClpXP to generate the first blinking liposomes.

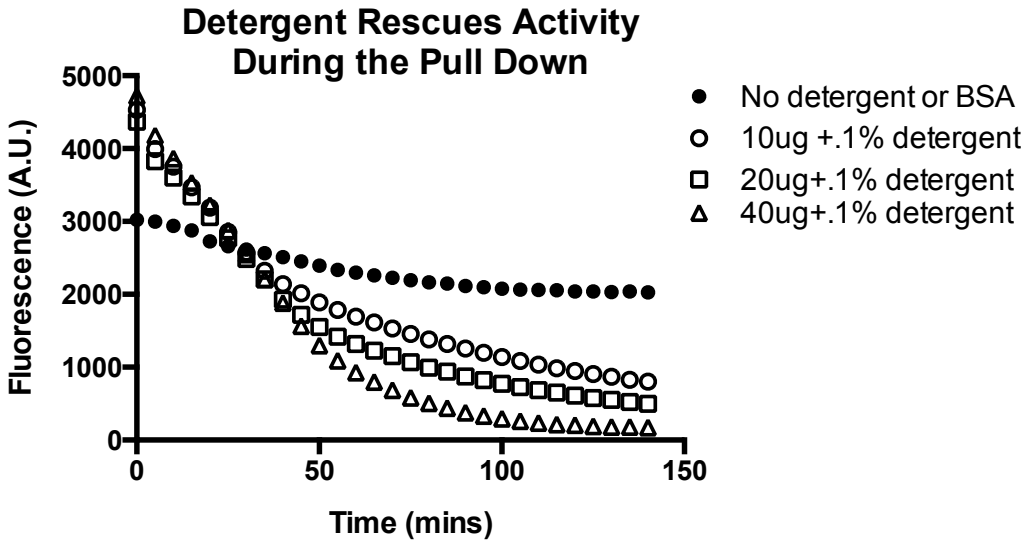

Figure 5.8 In vitro assay of the enzymatic degradation of eGFP by ClpXP showing a rescuing of activity after the emulsion step by the addition of np-40 detergent and the sacrificial protein BSA.

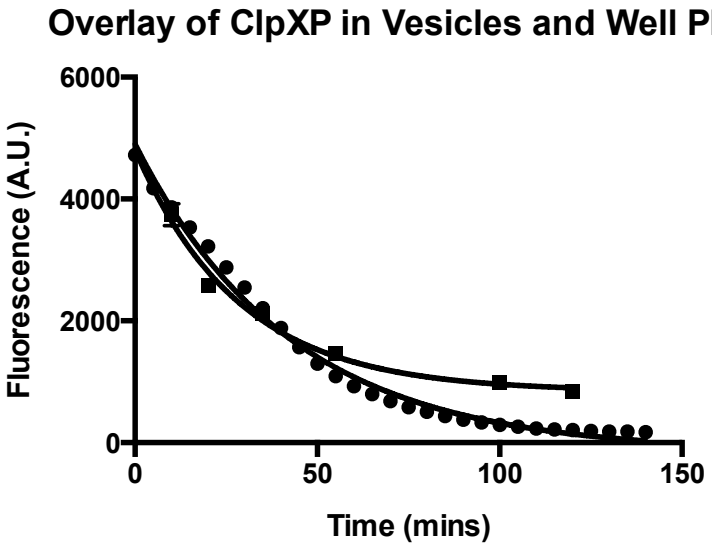

Figure 5.9 Comparing an in vitro assay with a *in vas* assay of the enzymatic degradation of eGFP by ClpXP showing similar rates

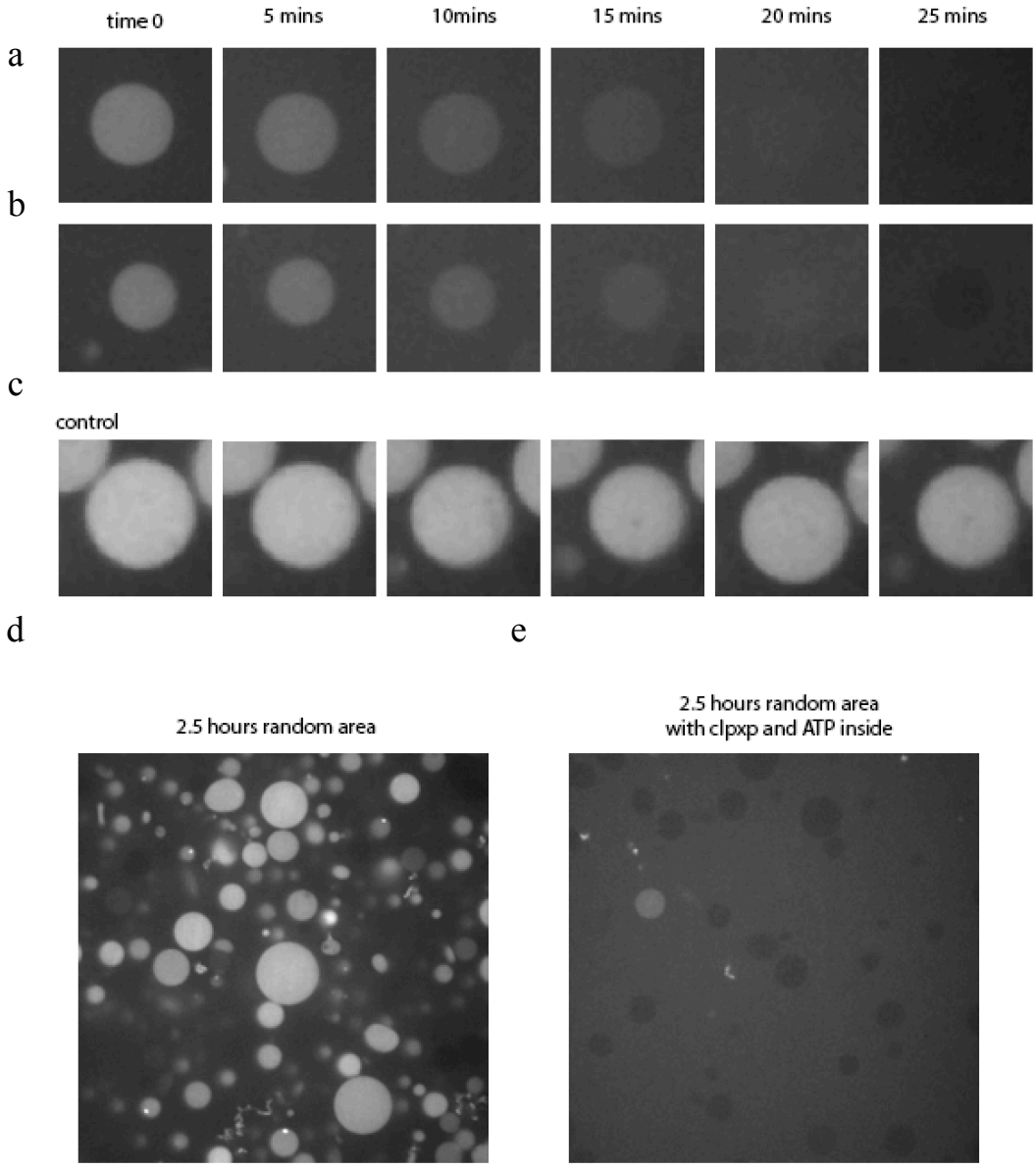

Figure 5.10 a-b) Time lapse of the degradation of eGFP by 0.3 μM ClpXP in a POPC liposome. c) Time lapse of the control population with no ClpXP. d) Random area on the control slide after 2.5 hours. e) Random area on the sample slide showing robust degradation of eGFP in POPC liposomes after 2.5 hours.

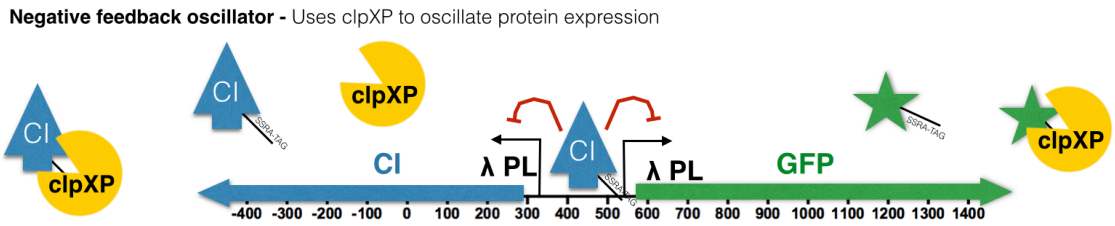

Figure 5.11 Diagram of a negative feedback circuit that utilizes ClpXP for the degradation of its genetic elements.

5.5 Coupling Growth and Expression - Copper Sensing Circuit:

One characteristic of all living cells is a semi-permeable barrier that separates the organisms from its environment; commonly the barrier is a phospholipid membrane. Our lab has been developing a biomimic of the phospholipid membrane by employing the copper catalyzed azide-alkyne cycloaddition reaction (CuAAC).[144] This Cu(I)-catalyzed click reaction between an oleoyl azide **16** and alkyne lysophospholipid **17** forms a triazole phospholipid **18** capable of spontaneous vesicle formation (Figure 5.12b). To achieve a system that couples both growth and gene expression, we utilized the copper catalyzed azide-alkyne cycloaddition reaction and coupled it with the copper sensitive elements, CueR and p-CopA.[145] This circuit design relies on the presence of copper to initiate both membrane growth and activate the copper sensitive polymerase CueR, which subsequently binds to p-CopA (Figure 5.12a). Initially, we sought to characterize the concentration range of copper and sodium ascorbate needed for the CuAAC reaction to proceed at the same time scale as eGFP expression. Utilizing azide-alkyne FRET pairs (Figure 5.13) and measuring

their emission intensity at 680 nm we were able to adjust all the relative parameters, providing the results in Figure 5.14.

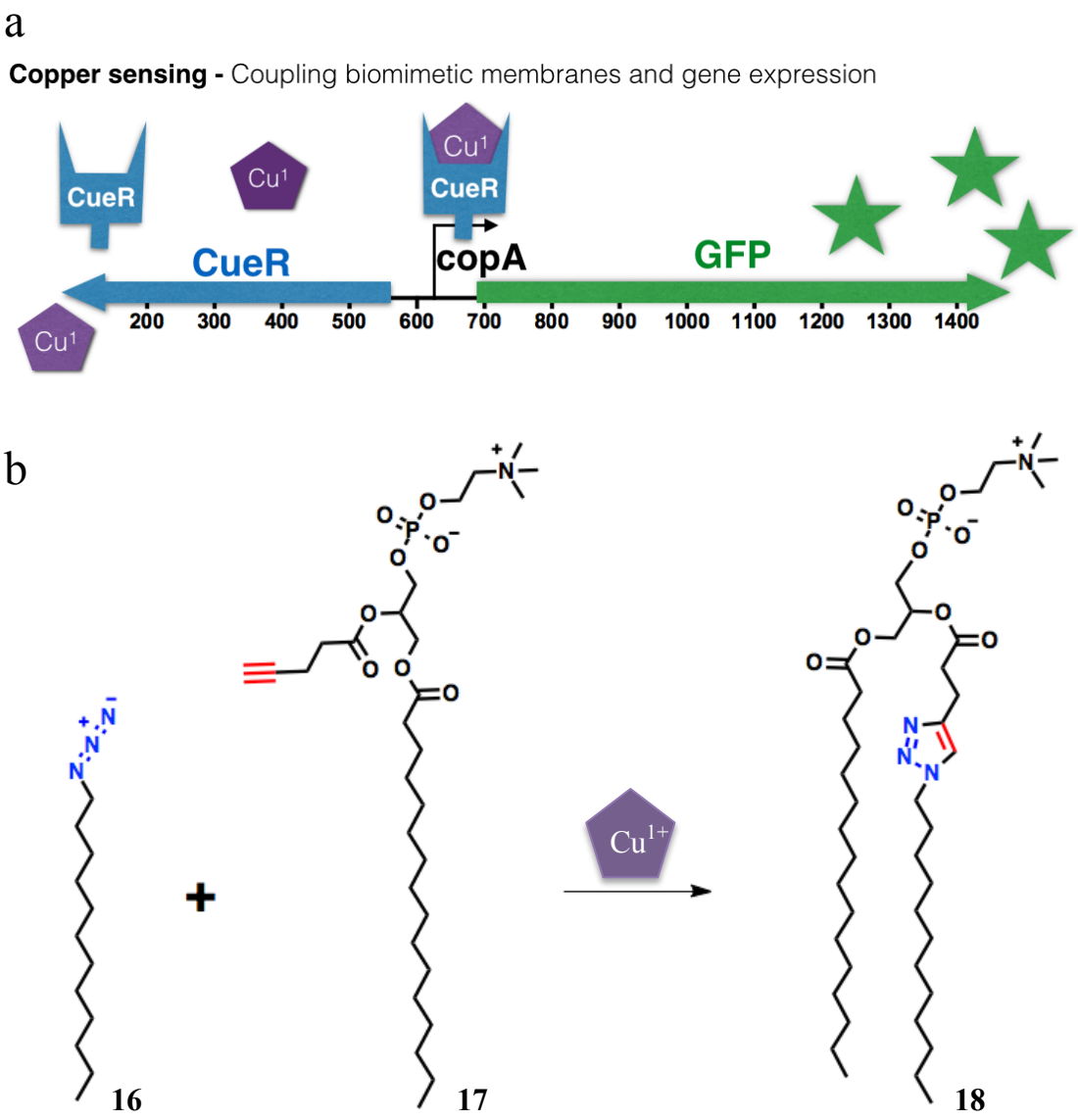

Figure 5.12 a) Diagram of a genetic circuit coupling gene expression and the CuAAC reaction. The circuit expresses CueR constitutively, which then binds to copper. The CueR copper complex then activates gene expression via CopA promoter. b) Cu(I)-catalyzed click reaction between the non-membrane forming precursors oleoyl azide **16** and alkyne lysophospholipid **17** to form the triazole phospholipid **18** capable of spontaneous vesicle formation.

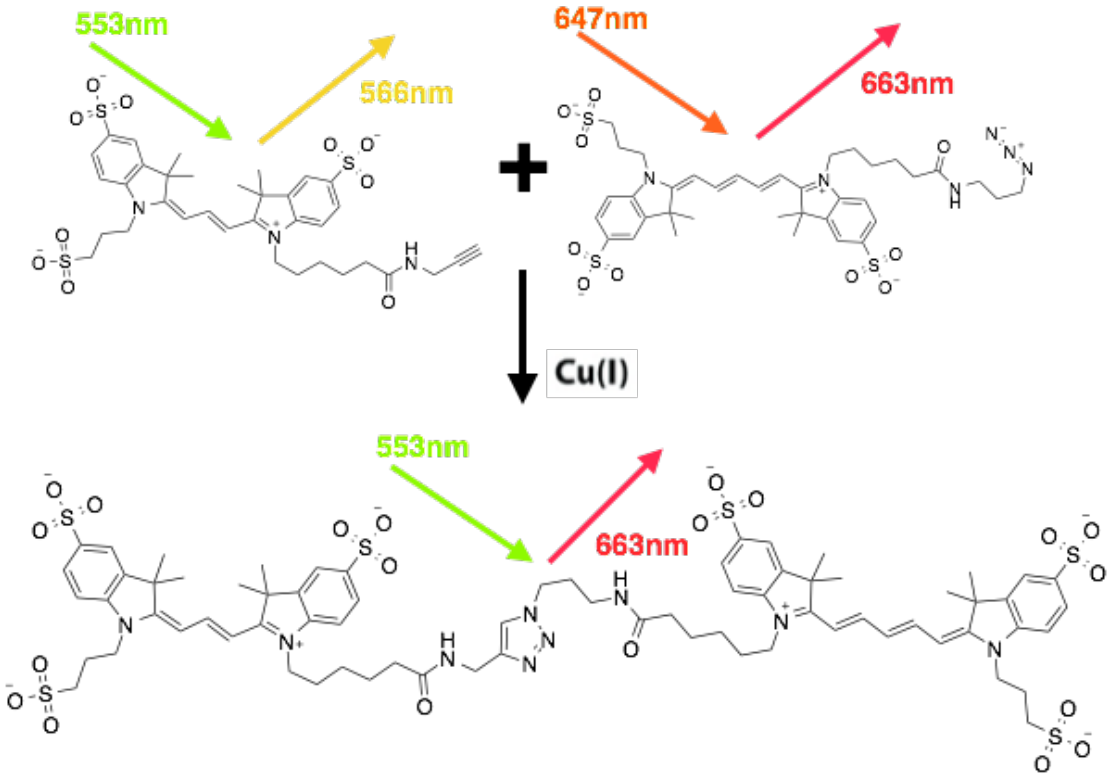

Figure 5.13 Azide-alkyne FRET pairs used to optimize the CuAAC reaction

Considering copper is highly cytotoxic and proteotoxic[63] we characterized eGFP expression under control of a endogenous E. coli sigma factor 70 promoter. As expected, higher copper concentrations completely knocked down expression, while a moderate concentration of a 100 µM resulted in approximate half of the expression of the control (no copper, Figure 5.15a). Considering this result we expected the CueR /

p-CopA system to behave similarly, in that there would be an upper limit of copper before the system attenuated. We therefore looked at these components and tested them in vitro with respect to copper concentrations (Figure 5.15b). Intriguingly, the rate of eGFP expression of this system was not logarithmic, but instead appeared more linear between the bonds of 0 - 300 minutes. We hypothesized that such a delay could arise from the need to express CueR first, followed by its subsequent binding to copper before eGFP could be expressed off the p-CopA. To validate this reasoning we pre-incubated CueR and lysate for 10 min or 20 min before adding copper; thereby triggering eGFP expression after CueR had been expressed. As shown in Figure 5.15c, this time delay was sufficient to recover the rate of eGFP expression in the CueR system.

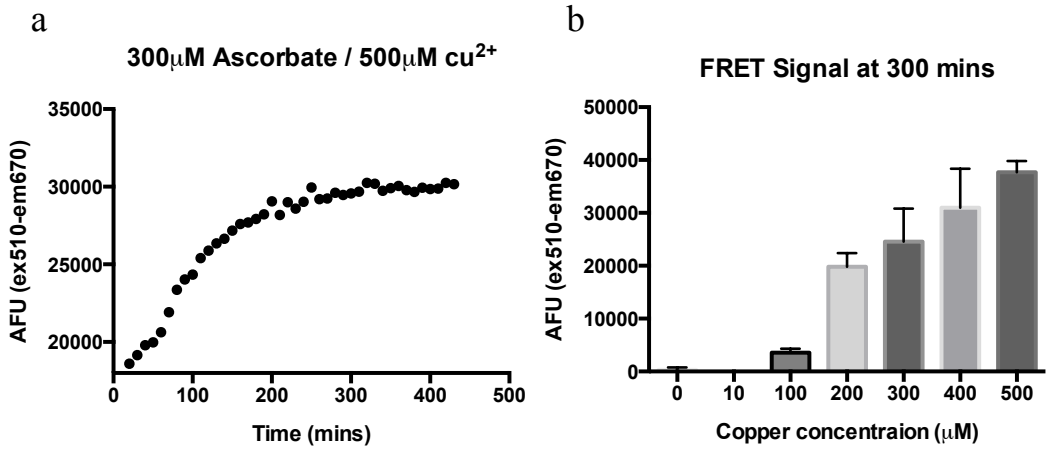

Figure 5.14 Azide-alkyne FRET pairs used to monitor the reaction kinetics and to optimize the copper concentration. All measurements were measured using ex510 nm and em670 nm. a) One representative kinetic assay using 1 μM FRET probes with 300 μM sodium ascorbate and 500 μM copper. b) Average fluorescent intensity after 300 minutes over a range of copper concentrations. n=3

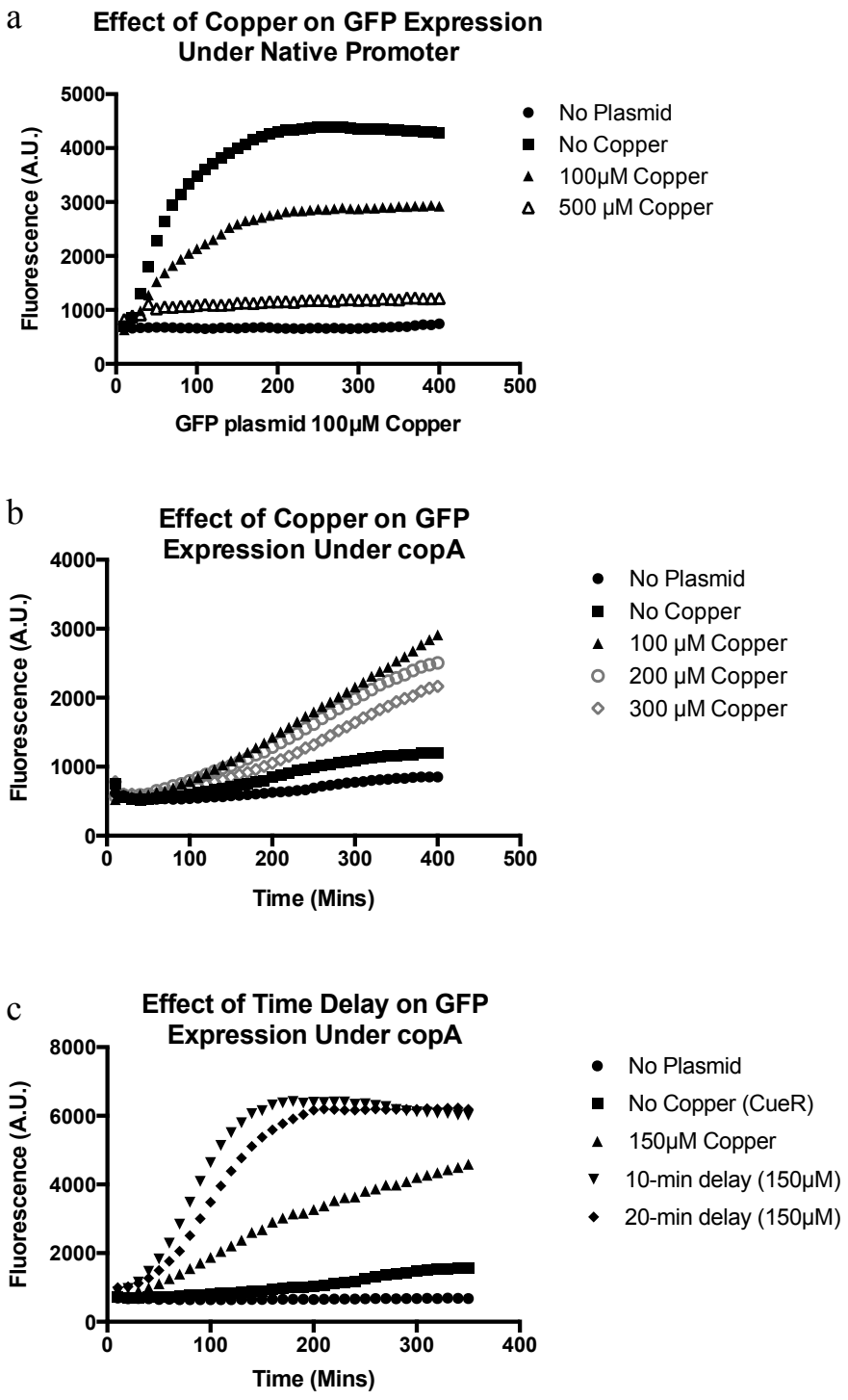

Figure 5.15 Effect of copper on gene expression. a) Effect that copper has on eGFP expression under control of the endogenous lambda promoter in Promega lysate. After 100 µM of copper the proteotoxicity results in decease fluorescence. b) Effect that copper has on eGFP expression under control of CueR and the CopA promoter in Promega lysate. Similarly after 100 µM of copper the proteotoxicity results in decease fluorescence. c) Shows altered kinetics of eGFP under control of CueR and the CopA promoter in Promega lysate. However, after waiting >10 min the kinetic shows a rate recovery presumable due to the build up of CueR.

Accordingly, we found the copper concentrations for both the CuAAC reaction and gene expression to be well matched. To explore these results *in vas*, we first made liposomes via the inverse emulsion method containing Promega's s-30 lysate, CueR plasmid, oleoyl azide **16** and alkyne phospholipid **17** with a fluorogenic

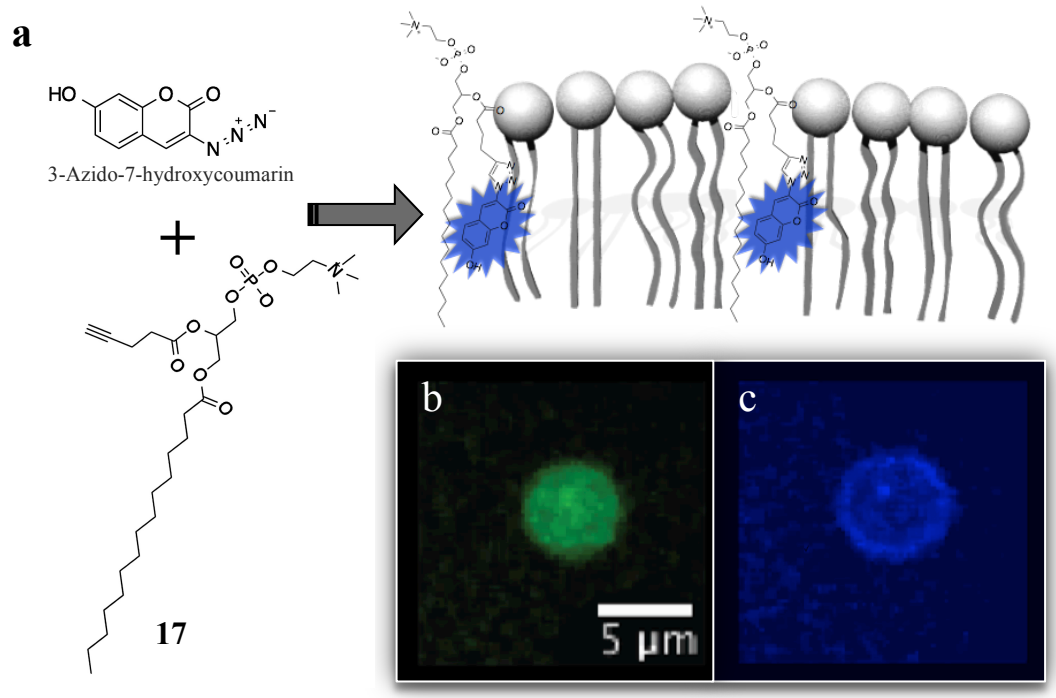

Figure 5.16 a) Diagram of the CuAAC reaction between 3-azido-7-hydroxycoumarin and an alkyne lysolipid **17**. After reaction the fluorogenic product inserts into the membrane of a pre-existing liposome. b) Confocal fluorescent micrograph of a liposome containing S30 promega lysate, and 100 µM copper. The eGFP is being expressed from p-CopA. c) The same liposome also has membrane staining indicating the reaction between 3-azido-7-hydroxycoumarin and an alkyne lysolipid **17** has taken place demonstrating both expression and CuAAC lipid formation.

3-azido-7-hydroxycoumarin dye to visualize the progression of the CuAAC. As shown in Figure 5.16, we coupled gene expression (eGFP) and remodeled the membrane (CuAAC), indirectly indicated by the membrane staining of 3-azido-7-hydroxycoumarin. These systems were coupled together through the availability of copper in the environment. However, the time scale of the reaction proved too slow to observe any discernable morphological changes to the membrane. This was further hindered by the presence of lysate, which also reduces the rate of the CuAAC (data not shown).

5.6 Coupling Growth and Expression – NCL Controlled Circuit:

The NCL system as described in the next chapter, *spontaneous incorporation of membrane proteins* does not require copper or another catalyst to initiate the ligation, in contrast to the previously explored CuAAC reaction. Thus, in order to link gene expression and membrane growth we employed an alternative system by modifying the NCL reaction between a c-16 lysolipid **19** with an oleoyl thio-galactose **20** (Figure 5.17).

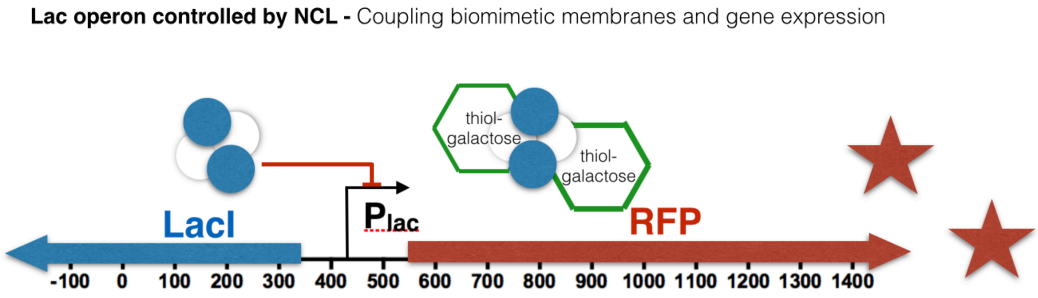

Figure 5.17 Diagram of a genetic circuit coupling gene expression and the NCL reaction. The circuit expresses LacI constitutively. The NCL reaction proceeds between oleoyl thio-galactose **20** and a c-16 cysteine lysolipid **19**, which subsequently releases IPTG. Gene expression initiates once LacI binds IPTG off of a lac promoter.

This effectively releases free IPTG upon coupling, which then induces gene expression under control of a lac repressor system (Scheme 5.1). The interaction between LacI and oleoyl thio-galactose **20** is low, probably due to the sterics of the oleoyl and sequestering of the thio-galactose in micelles. However, expression of the mCherry reporter under control of the lac promoter dramatically increased in the presence of lysolipid **19** (Figure 5.18). In addition, this reaction is completed in 10 min

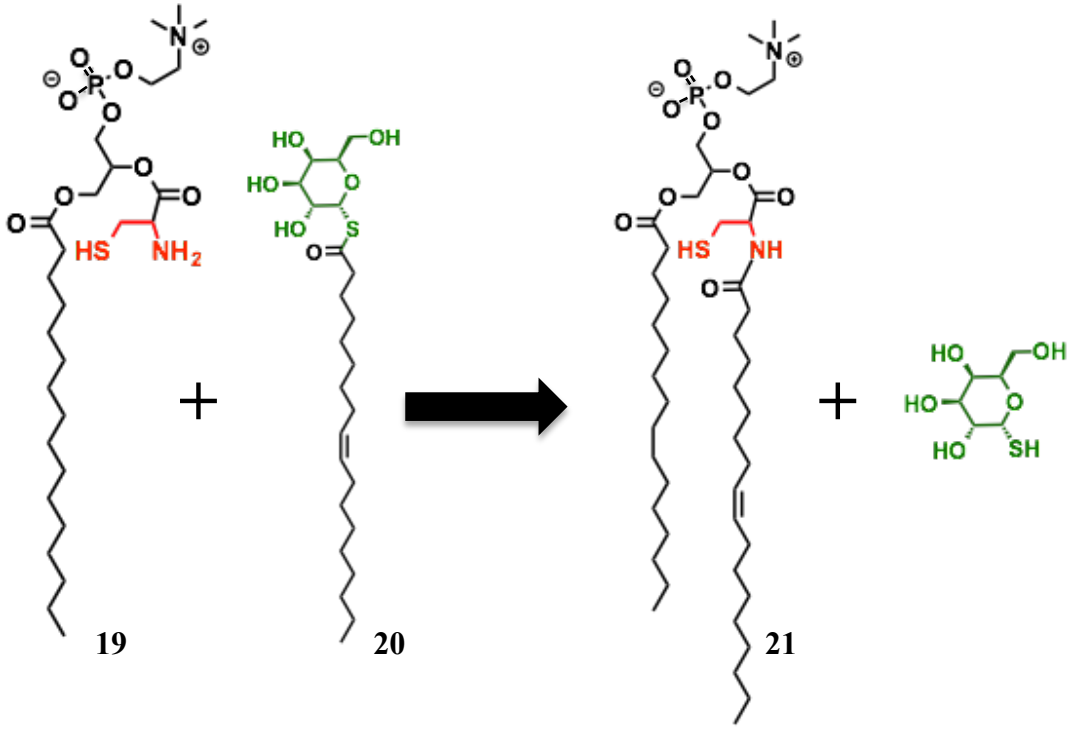

Scheme 5.1 Schematic of NCL reaction between lysolipid **19** and oleoyl thio-galactose **20** to produce the amide lipid **21** and an analogue of IPTG. Gene expression initiates once LacI binds the IPTG analogue and expresses eGFP off of a lac promoter.

allowing changes in liposome morphology to be visualized during the experiment.

These unique systems raise important questions in the areas of biophysical and medicinal sciences, providing insight into the concerted assimilation of complex systems bounded by a membrane. The networks discussed in this chapter coupled gene expression; either by the addition of copper or by the release of an analogue of IPTG, and the generation of membrane-forming products. While still in its infancy, more complex *in vas* systems could mimic the life-like qualities reminiscent of earlier protocells.

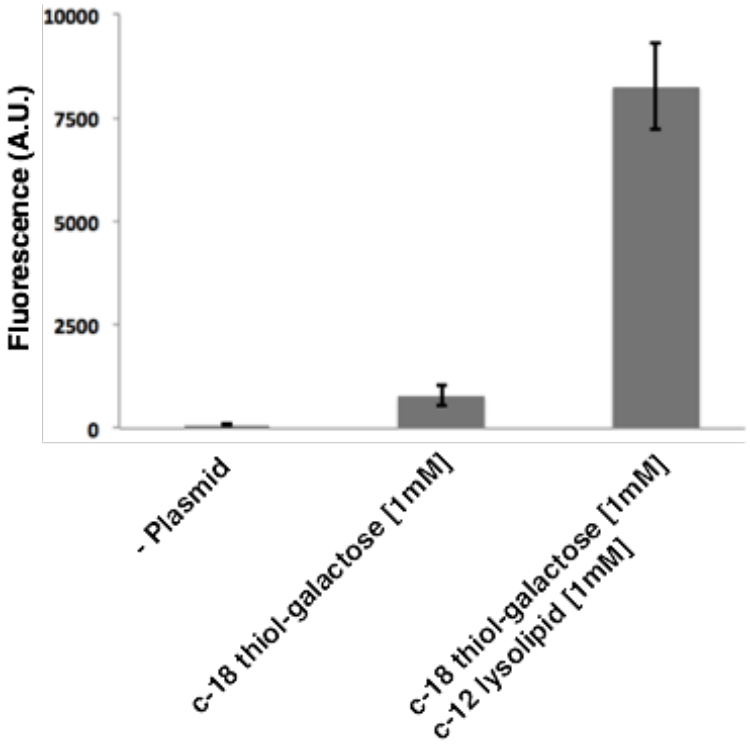

Figure 5.18 In vitro assay using in house S30 lysate monitoring fluorescent intensity of expressed eGFP at time = 4 hours. The eGFP is under control of the Lac promoter and constitutively express LacI. When only oleoyl thiol-galactose is present there is marginal background fluorescence. In contrast, there is a 10 fold increase in fluorescence when both NCL precursors are incubated together, cysteine lysolipid **19** and oleoyl thio-galactose **20.**

5.7 Experimentals and Methods

5.7.1 Materials

Commercially available 1-palmitoyl-2-hydroxy-*sn*-glycero-3-phosphocholine and 1-palmitoyl-2-oleoyl-*sn*-glycero-3-phosphocholine (POPC) were used as obtained from Avanti® Polar Lipids. 4-pentynoic acid, oleoyl bromide, sodium azide, N-Boc-Cys(Trt)-OH, *N,N'*-diisopropylcarbodiimide (DIC), 4-dimethylaminopyridine (DMAP), trifluoroacetic acid (TFA), triethylsilane (TES), oleic acid, *N*-(3-dimethylaminopropyl)-*N'*-ethylcarbodiimide hydrochloride (EDC.HCl), sodium 2-mercapto-ethanesulfonate (MESNA), dithiothreitol (DTT), phenylmethylsulfonyl fluoride (PMSF), 4-(2-hydroxyethyl)piperazine-1-ethanesulfonic acid (HEPES) sodium salt, Cy5-azide, Cy3-alkyne and 8-hydroxypyrene-1,3,6-trisulfonic acid (pyranine) were obtained from Sigma-Aldrich. Texas Red® 1,2-dihexadecanoyl-*sn*-glycero-3-phosphoethanolamine, triethylammonium salt (Texas Red® DHPE) and Alexa Fluor® 488 NHS Ester were obtained from Life Technologies. Isopropyl β-D-thiogalactoside (IPTG) was obtained from Teknova. Deuterated chloroform ($CDCl_3$), methanol (CD_3OD) and dimethyl sulfoxide (d_6-DMSO) were obtained from Cambridge Isotope Laboratories. All reagents obtained from commercial suppliers were used without further purification unless otherwise noted. Analytical thin-layer chromatography was performed on E. Merck silica gel 60 F_{254} plates. Compounds, which were not UV active, were visualized by dipping the plates by dipping the plates in a ninhydrin or potassium permanganate solution and heating. Silica gel flash chromatography was performed using E. Merck silica gel (type 60SDS, 230-400

mesh). Solvent mixtures for chromatography are reported as v/v ratios. HPLC analysis was carried out on an Eclipse Plus C8 analytical column with *Phase A*/*Phase B* gradients [*Phase A*: H_2O with 0.1% formic acid; *Phase B*: MeOH with 0.1% formic acid]. HPLC purification was carried out on Zorbax SB-C18 semipreparative column with *Phase A*/*Phase B* gradients [*Phase A*: H_2O with 0.1% formic acid; *Phase B*: MeOH with 0.1% formic acid]. Proton nuclear magnetic resonance (^{1}H NMR) spectra were recorded on a Varian VX-400 MHz, Varian VX-500 MHz or Jeol Delta ECA-500 MHz spectrometers, and were referenced relative to residual proton resonances in $CDCl_3$ (at 7.24 ppm), CD_3OD (at 4.87 or 3.31 ppm) or d_6-DMSO (at 2.50 ppm). Chemical shifts were reported in parts per million (ppm, d) relative to tetramethylsilane (d 0.00). ^{1}H NMR splitting patterns are assigned as singlet (s), doublet (d), triplet (t), quartet (q) or pentuplet (p). All first-order splitting patterns were designated on the basis of the appearance of the multiplet. Splitting patterns that could not be readily interpreted are designated as multiplet (m) or broad (br). Carbon nuclear magnetic resonance (^{13}C NMR) spectra were recorded on a Varian VX-400 MHz, Varian VX-500 MHz or Jeol Delta ECA-500 MHz spectrometers, and were referenced relative to residual proton resonances in $CDCl_3$ (at 77.23 ppm), CD_3OD (at 49.15 ppm) or d_6-DMSO (at 39.51 ppm). Electrospray Ionization-Time of Flight (ESI-TOF) spectra were obtained on an Agilent 6230 Accurate-Mass TOFMS mass spectrometer. Fluorescence measurements were performed on a LS 55 fluorescence spectrometer using a single cuvette reader. Absorbance readings were measured on a ThermoScientific NanoDrop 2000c UV-Vis spectrophotometer and fluorescence was measured using a 384-well Tecan Genios plate reader or a Tecan i200 plate reader.

.

5.7.2 *In Vitro* Cell-Free TX - TL Assay of eGFP-del6

The pBEST-OR2-OR1-Pr-UTR1-deGFP-T500 was a gift from Vincent Noireaux (Addgene plasmid # 40019)[132]. Promega's S30 T7 High-Yield Protein Expression System was used as directed, with 1 μg of vector per half-reaction (25 μL). The PURExpress was used according to manufacturer's protocol containing 1 μg of vector per reaction (25 μL). Fluorescence of eGFP-del6 was then measured in a 384-well plate spectrophotometer (Genios), incubated at 32ºC.

5.7.3 RNA polymerase Assay

The same conditions were used as in the eGFP-del6 assay with the addition of 0.5 – 3 units of E. coli RNA Polymerase, Holoenzyme (NEB, MA). Glycerol was removed from the RNA polymerase by using a 10 kDa spin column (Millipore, MA). The final concentration was 500 units per mL. All the reaction volumes were diluted to ddH_2O to a final reaction volume of 35 μL.

5.7.4 CueR Assay

The pRC03-luxI plasmid containing the eGFP gene under control of p-CopA and CueR was donated by Robert Copper (Jeff Hasty, UCSD). Promega's S30 T7 High-Yield Protein Expression System was used as directed supplemented with 0 – 300 μM copper sulfate, 50 – 100 μM sodium ascorbate and 2 μg of vector per reaction

(50 μL). Fluorescence of eGFP was then measured in a 384-well plate spectrophotometer (Genios), incubated at 32ºC.

5.7.5 ClpXP Assay

Purified ClpXP protein and eGFP superfolder-ssrA plasmid and protein was donated by Shi Xinying (Joseph lab, UCSD). The degradation of eGFP-ssrA by ClpXP was monitored at 488 nm in a 384-well plate spectrophotometer (Genios). ClpXP at a final concentration of 0.3 μM was added to a buffer solution containing 400 mM HEPES, pH 7.5, 0 – 400 mM KCl and 1 μM eGFP. 200 mM sucrose, 0-100 μg BSA, and 0% – 0.5% NP-40 was added during liposome formation.

5.7.6 *In Vitro* Cell-Free TX - TL Assay of Thiol-Galactose

The constitutively expressed LacI and RFP under control of the lac promoter was donated by Robert Copper (Jeff Hasty, UCSD). The S30 Lysate (without IPTG) was donated by Shi Xinying (Joseph lab, UCSD). The reaction was conducted in 15 μL S30 lysate, 10 μL DNA (final concentration 1 μg / 50 μL) and 25 μL small molecule mix (50 mM K-HEPES, pH 8.2, 0.9 mM NTP (pH 7.0 with KOH), 0.6 mM ATP and GTP (pH 7.0 with KOH), 30 mM phosphoenol pyruvate, pH 7.0, 3 mM of each of the 20 amino acids, 2% w/v PEG 8000, 0.068 mg/mL folinic acid, 0.048 units / mL pyruvate kinase, 0.2 mg / mL tRNA from E. coli, 1 mM putrescine, 4 mM Mg-glutamate, 120 mM K-glutamate). The reactions included a final concentration of 1 mM of c-18 thiol-galactose **67** and c-12 lysolipid **67**. The reaction was monitored at ex530 in a 384-well plate spectrophotometer (i200).

5.7.7 FRET Assay

The commercially available Cy5-azide and Cy3-alkyne were added to a HEPES buffer solution (10 mM HEPES, pH 7.5, 0 – 1 mM copper sulfate, 0 – 1 mM sodium ascorbate) at a final concentration of 1 μM. The reaction was monitored at ex510 nm and em670 nm in a 384-well plate spectrophotometer (i200).

5.7.8 3-Azido-7-Hydroxycoumarin Assay

Liposomes containing the S30 Promega lysate supplemented with 200 mM sucrose were made as previously discussed. The small molecule 3-azido-7-hydroxycoumarin was dissolved in the mineral oil until it was saturated and precipitated out. The alkyne lysolipid **23** and oleoyl azide **23** were packaged either on the inside or outside of the liposome at a final concentration of 500 μM. The reaction was incubated at 32ºC up to 4 hours.

5.7.9 Preparation of Giant Unilamellar Vesicles

Liposomes were prepared by adapting the previously discussed inverse pull down method in chapter 4. Briefly, POPC was dissolved in chloroform at a concentration of 50 mg/mL and then dried using compressed nitrogen for 30 min to obtain a lipid film. Heavy mineral oil (1 mL, Fisher Scientific) was added to the lipid film to bring the final lipid concentration to 5 mg/mL. An aliquot of 10 μL of the upper solution was added to 100 μL of the oil-lipid mixture. These mixtures were forcibly agitated to form w/o emulsions that was then placed gently on top of 400 μL

of the lower solution, and centrifuged at 7200*g*, 24 °C, for 5 min. The pelleted vesicles were collected after aspirating off the top oil layer.

The inner solution was the PURE system (0.3 mM each amino acid, 3.75 mM ATP, 2.5 mM GTP, 1.25 mM CTP and UTP, 1.5 mM spermidine, 25 mM creatine phosphate, 1.5 mM dithiothreitol (DTT), 0.01 μg/μL N5-formyl-5,6,7,8-tetrahydropteroyl-L-glutamic acid (FD), 280 mM potassium glutamate, 18.9 mM $Mg(OAc)_2$, 100 mM HEPES) and cell lysate supplemented with 200 mM sucrose, 1 μg plasmid DNA, and 0.2 U/μL RNasin in place of ddH_2O. The lower solution was either the PURE system supplemented with 200 mM glucose or 400 mM HEPES, pH 7.5 with 200 mM glucose. Glucose was added at the same molarity as the sucrose in the inner solution to adjust the osmolarity. The amino acid solution was just included inside the upper solution or lower solution.

5.7.10 Flow Cytometric Analysis

The fluorescent signal for GFP was measured by FCM (Partec, Germany). We obtained 50 000 data samples for each measurement. GFP was excited with a 488 nm semiconductor laser, and the emission was detected through a 510 nm bandpass filter. Prior to the measurement, vesicles were diluted to an appropriate concentration with the lower buffer (400 mM HEPES, pH 7.5 with 200 mM glucose). Fluorescence intensities of GFP were plotted over time.

5.7.11 Fluorescence Microscopy

All Images were acquired on a Yokagawa spinning disk system (Yokagawa, Japan) built around an Axio Observer Z1motorized inverted microscope (Carl Zeiss Microscopy GmbH, Germany) with a 63x, 1.40 NA oil immersion objective to an Evolve 512x512 EMCCD camera (Photometrics, Canada) using ZEN imaging software (Carl Zeiss Microscopy GmbH, Germany). Fluorophores were excited with a 405nm, 50 mW DPSS laser and a 488 nm, 100 mW OPSL laser.

5.7.12 Synthesis of Oleoyl Azide (16).[146]

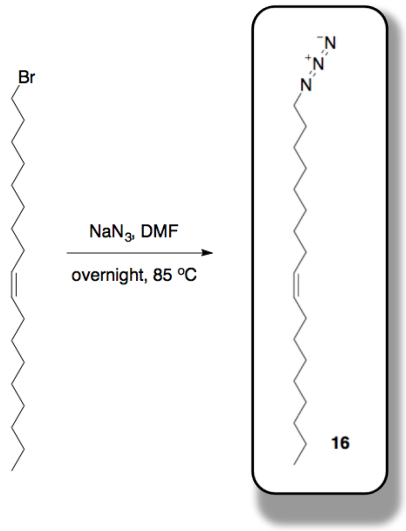

Scheme 5.2 Synthesis of Oleoyl Azide **(16)**

A solution of oleoyl bromide (150.0 mg, 0.45 mmol) in DMF (1 mL) was reacted with sodium azide (100.0 mg, 1.54 mmol) overnight at 85 ºC under N_2 atmosphere. After the reaction, H_2O (5 mL) was added, and the organic phase was extracted with CH_2Cl_2 (3 × 3 mL). After drying with $MgSO_4$, the solvent was removed

by rotary evaporation and the product isolated by flash column chromatography, affording 105.6 mg of **2a** as a pale yellow oil [80%]. **^{1}H NMR** ($CDCl_3$, 400.13 MHz, d): δ 5.40-5.30 (m, 2H, 1 × CH_2), 3.30-3.20 (t, 2H, 1 × CH_2), 2.10-1.95 (m, 4H, 2 × CH_2), 1.70-1.50 (m, 2H, 1 × CH_2) 1.40-1.20 (m, 22H, 11 × CH_2), 0.90 (t, 3H, 1 × CH_3).

5.7.13 Synthesis of 1-palmitoyl-2-[pent-4-ynoyl]-*sn*-glycero-3-phosphocholine (17).[144]

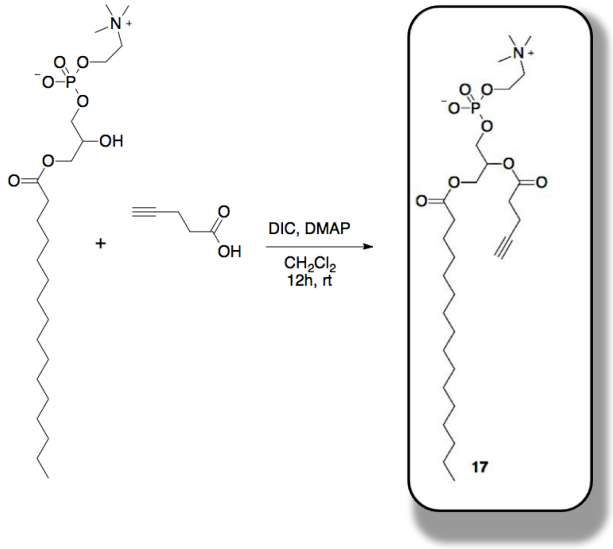

Scheme 5.3 Synthesis of 1-palmitoyl-2-[pent-4-ynoyl]-*sn*-glycero-3-phosphocholine **(17)**

A solution of 1-palmitoyl-2-hydroxy-*sn*-glycero-3-phosphocholine (70.0 mg, 141.2 mmol) in CH_2Cl_2 (10 mL) was stirred at rt for 10 min, and then 4-pentynoic acid (70.0 mg, 713.6 mmol), DIC (774.1 mL, 1.11 mmol) and DMAP (25.0 mg, 204.6 mmol) were successively added. After 12 h stirring at rt, the solvent was removed under reduced pressure, and the crude was purified by flash column

chromatography ($CHCl_3$/MeOH/H_2O), affording 57.2 mg of **1a** as a white solid [70%]. **^{1}H NMR** ($CDCl_3$, 400.13 MHz, d): δ 5.25-5.20 (m, 1H, 1 × CH), 4.40-4.30 (m, 3H, 1.5 × CH_2), 4.20-4.10 (m, 2H, 1 × CH_2), 4.05-4.00 (m, 1H, 0.5 × CH_2) 3.95-3.90 (m, 2H, 1 × CH_2), 3.40 (s, 9H, 3 × CH_3), 2.60-2.40 (m, 4H, 2 × CH_2), 2.35-2.25 (t, 2H, 1 × CH_2), 2.05 (t, 1H, 1 × CH), 1.60-1.50 (m, 2H, 1 × CH_2), 1.35-1.20 (m, 24H, 12 × CH_2), 0.90-0.80 (t, 3H, 1 × CH_3). **MS (ESI-TOF)** [m/z (%)]: 576 ($[MH]^+$, 100). **HRMS (ESI-TOF) calculated** for $C_{29}H_{55}NO_8P$ ($[MH]^+$) 576.36, **found** 576.48.

5.7.14 Triazole phospholipid 1-palmitoyl-2-[triazole-(oleoyl)]-*sn*-glycero-3-phosphocholine (18).[144]

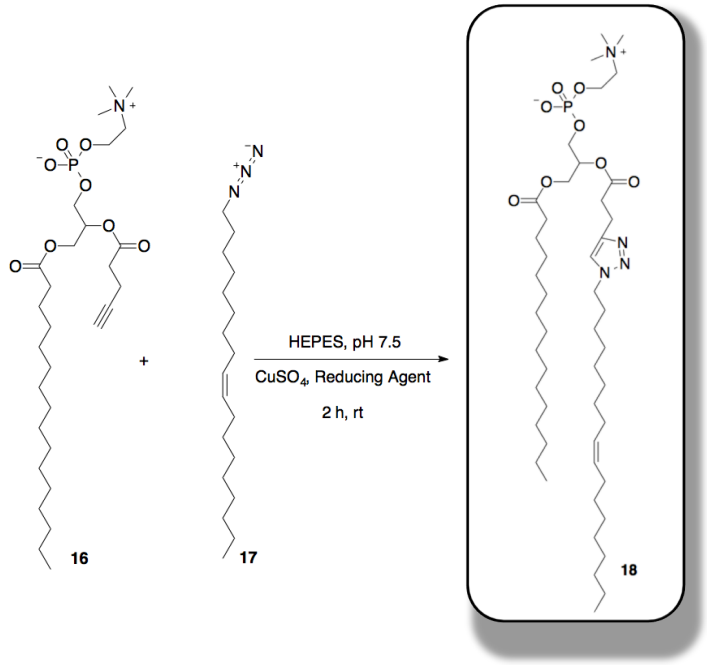

Scheme 5.4 Synthesis of 1-palmitoyl-2-[triazole-(oleoyl)]-*sn*-glycero-3-phosphocholine (**18**)

A solution of 1-palmitoyl-2-[pent-4-ynoyl]-*sn*-glycero-3-phosphocholine (**17**, 24 mg, 41.7 mmol) and oleoyl azide (**16**, 13.0 mg, 44.3 mmol) in 20 mM HEPES pH 7.5

buffer (100 mL) was stirred for 2 h in the presence of 1 mM $CuSO_4.5H_2O$ and 2 mM reducing agent (hydroquinone or sodium *L*-ascorbate). The solvent was evaporated and the resulting triazole phospholipid isolated by flash column chromatography, affording 23.6 mg of **18** as a white powder [65%]. **^{1}H NMR** ($CDCl_3$, 400.13 MHz, d): δ 7.50 (s, 1H, 1 × CH), 5.40-5.30 (m, 2H, 1 × CH_2), 5.25-5.20 (m, 1H, 1 × CH), 4.50-4.25 (m, 5H, 2.5 × CH_2), 4.20-4.10 (m, 1H, 0.5 × CH_2), 4.05-4.00 (m, 2H), 3.90-3.80 (m, 2H, 1 × CH_2), 3.40 (s, 9H, 3 × CH_3), 3.00 (m, 2H, 1 × CH_2), 2.80-2.70 (m, 2H, 1 × CH_2), 2.60-1.00 (56H, 28 × CH_2), 0.90-0.80 (t, 6H, 2 × CH_3). **MS (ESI-TOF**) [m/z (%)]: 869 ($[MH]^+$, 100). **HRMS (ESI-TOF**) **calculated** for $C_{47}H_{90}N_4O_8P$ 869.64 found 869.73.

5.7.15 Synthesis of galactopyranosyl thiooleate (20)

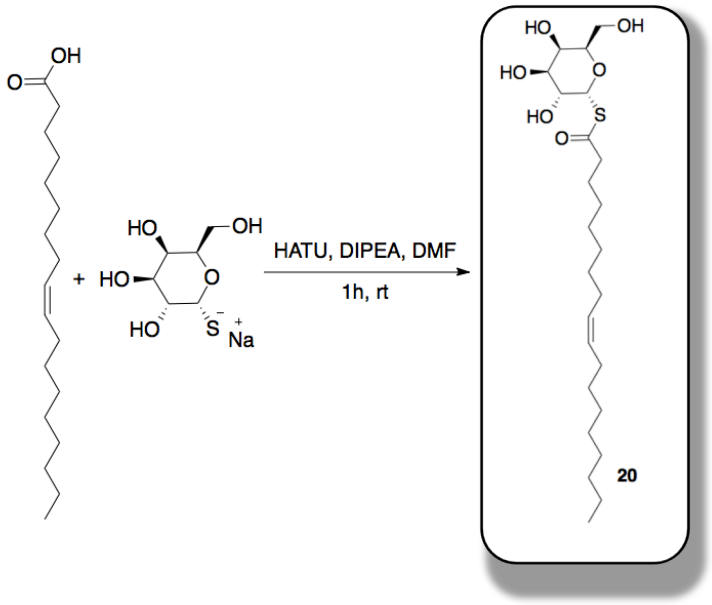

Scheme 5.5 Synthesis of galactopyranosyl thiooleate **(20)**

A solution of oleic acid (14.5 μL, 45.8 μmol) in DMF (500 μL) was stirred at 0 ºC for 10 min, and then HATU (19.2 mg, 50.4 μmol) and DIEA (31.9 μL, 183.3 μmol) were successively added. After 10 min stirring at 0 ºC, 1-thio-b-D-galactopyranose sodium salt (10.0 mg, 45.8 μmol) was added. After 1 h stirring at rt, the solvent was removed under reduced pressure. The corresponding residue was dissolved in MeOH (500 μL), filtered using a 0.2 mm syringe-driven filter, and the crude solution was purified by HPLC, affording 18.1 mg of galactopyranosyl thiooleate as a colorless film [86%, R_t = 8.2 min (Zorbax SB-C18 semipreparative column, 95% *Phase B*, 15.5 min)]. MS (ESI-TOF) [m/z (%)]: 483 ($[M+Na]^+$, 100), 460 ($[MH]^+$, 20). HRMS (ESI-TOF) calculated for $C_{24}H_{44}O_6SNa$ ($[M+Na]^+$) 483.2751, found 483.2748.

Notes about the Chapter:

I would like to thank Roberto Brea, Hoaxing Wu, Robert Cooper, Shi Xinying and Neal Devaraj for their invaluable contributions to this chapter: Roberto Brea synthesized and characterized all the NCL compounds presented in this chapter; Hoaxing Wu synthesized and characterized all the CuAAC compounds; Shi Xinying purified ClpXP protein, eGFP superfolder-ssrA protein, and prepared the S30 lysate and reaction mix; Robert Cooper provided the CueR plasmid and the LacI plasmid. I would like to thank Neal Devaraj for help funding the research.

~ CHAPTER 6 ~

6 In Situ Vesicle Formation by Native Chemical Ligation

6.1 Introduction

Phospholipid vesicles are of intense fundamental and practical interest, yet methods for their de novo generation from reactive precursors are limited. A non-enzymatic and chemoselective method to spontaneously generate phospholipid membranes from water-soluble starting materials would be a powerful tool for generating vesicles and studying lipid membranes. Here we describe the use of native chemical ligation (NCL) to rapidly prepare phospholipids spontaneously from thioesters. While NCL is one of the most popular tools for synthesizing proteins and nucleic acids, to our knowledge this is the first example of using NCL to generate phospholipids de novo. The lipids are capable of in situ synthesis and self-assembly into vesicles that can grow to several microns in diameter. The selectivity of the NCL reaction makes in situ membrane formation compatible with biological materials such as proteins. This work expands the application of NCL to the formation of phospholipid membranes.

Phospholipid membranes are routinely employed in several practical applications such as the study of protein–membrane interactions,[147–150] drug-delivery,[151] origin-of-life studies,[152–154] bottom-up synthetic biology,[155] and synthetic reactors.[156,157] While the capability of phospholipids to self-assemble into membranes is well studied,[103,158] the de novo synthesis and assembly of membranes from simple

non-membrane-forming reactive precursors is poorly understood. Living organisms are capable of synthesizing lipid membranes in situ by utilizing membrane-bound acyltransferases and reactive thioester precursors.[159,160] Given the well-documented challenges associated with reconstituting lipid-synthesizing membrane proteins into vesicles,[161,162] several groups have explored methods to generate lipid membranes de novo from reactive amphiphilic precursors.[144,163,164] However, these methods generally suffer from a range of issues, including the necessity of catalysts, lack of soluble starting materials, use of biologically incompatible reactive precursors, and the formation of lipids that have limited structural similarity to natural phospholipids.[144,164] Phospholipid membranes are often advantageous in complex environments due to their stability and biocompatibility.[165] Simpler and more robust methods for phospholipid synthesis could also find use as drivers for the growth and division of primitive protocells.[80,165,166] Therefore, it would be exciting to develop a catalyst-free method to generate and grow phospholipid membrane vesicles from reactive soluble precursors. Furthermore, it would be interesting to utilize water-soluble thioester precursors, analogous to living cells.[159,160,167] Here we demonstrate that the chemoselective native chemical ligation (NCL)[168,169] is capable of in situ synthesis of phospholipid vesicles from long-chain thioesters. The lipids can self-assemble in situ to form vesicles that can grow to several microns in diameter. Moreover, the chemoselectivity of the NCL reactions ensures that the phospholipid vesicles are compatible with biological materials such as proteins,[170] and we demonstrate this by encapsulating green fluorescent protein (GFP) in situ.

6.2 NCL: Liposome Formation

The native chemical ligation is one of the most popular tools for the synthesis of large peptides and small proteins.[171–175] The mechanism of NCL involves a two-step process consisting of a thiol-exchange step between a C-terminal peptide thioester and the sulfhydryl moiety of an N-terminal cysteine residue in another peptide, which prompts an intramolecular nucleophilic attack by the α-amino group of the cysteine (S→N acyl rearrangement) to form the final amide bond (Figure 6.1). Further acylation of the resulting sulfhydryl ("reloading") is also possible under specific conditions.[176] NCL is extensively used for the synthesis of native proteins, because it efficiently and non-enzymatically connects two peptides to generate a protein with an amide linkage at the reaction site.[177–180] Due to its exquisite chemoselectivity, the applications of NCL extend well beyond the scope of protein synthesis.[181–191] Here, we demonstrate the use of NCL as a method to couple long-chain acyl thioesters to cysteine-functionalized lysolipids in a highly specific and chemoselective way to form the corresponding phospholipids.

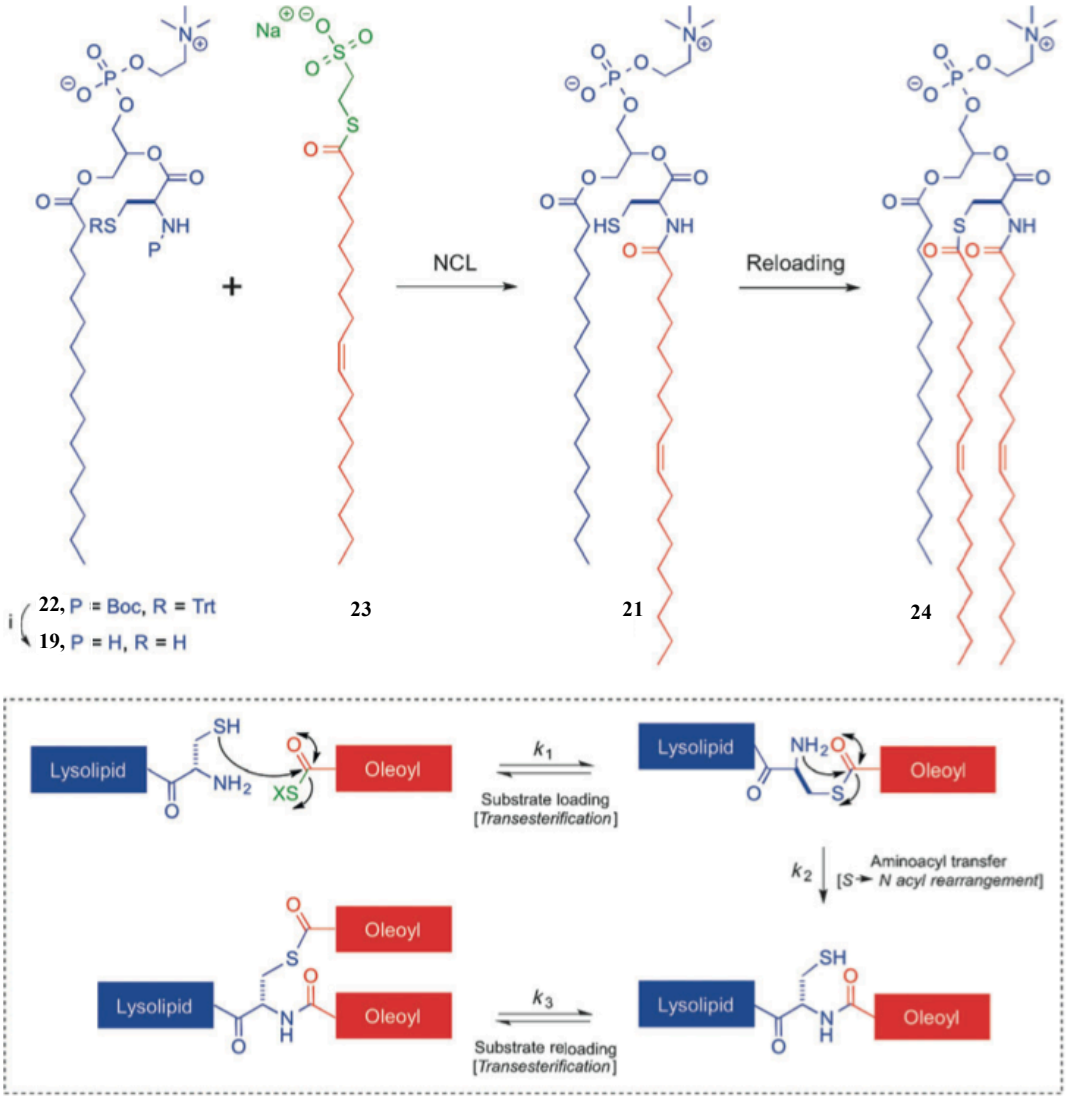

Figure 6.1 Top: Synthesis of phospholipids by NCL reaction of a cysteine-functionalized lysolipid and MESNA oleoyl thioester. Conditions: i) TFA/CH2Cl2/TES (1:1:0.1). Bottom: the mechanism of the NCL and the possible substrate reloading.

We initially designed two substrates to mimic the native precursors of the common phospholipid 1-palmitoyl-2-oleoyl-*sn*-glycero-3-phosphocholine (POPC): a cysteine-functionalized analogue of the lysolipid 1-palmitoyl-*sn*-glycero-3-

phosphocholine **19** and a sodium 2-mercaptoethanesulfonate (MESNA) oleoyl thioester **23** in lieu of oleoyl-CoA (Figure 6.1). Precursors **19** and **23** are both water-soluble amphiphiles, forming micelles of approximately 5.3 and 3.8 nm in diameter, respectively, with critical micelle concentrations (cmc values) below 100 μM (for **19**) and 10 μM (for **23**) (Graph 6.1).[192] The high water solubility of both precursors facilitated NCL at mild conditions in the millimolar concentration range. Under typical NCL conditions [(4-(2-hydroxyethyl)-1-piperazineethanesulfonic acid (HEPES) buffer, pH 7.0 containing tris(2-carboxyethyl)phosphine hydrochloride (TCEP·HCl) as reducing agent], unprotected segments **19** and **23** coupled to afford amidophospholipid **21**, a novel class of phospholipid that resembles POPC, with the exception of a cysteine-amido linker (Figure 6.1).

Graph 6.1 Micelle sizes estimated from DLS studies corresponding to 1.0 mM aqueous solution of 1-palmitoyl-2-hydroxy-sn-glycero-3-phosphocholine Lysolipid OH (7.32 nm in diameter), 1-palmitoyl- 2-(L-Cys)-sn-glycero-3-phosphocholine **19** (5.32 in diameter) and MESNA thiooleate **23** (3.79 nm in diameter).

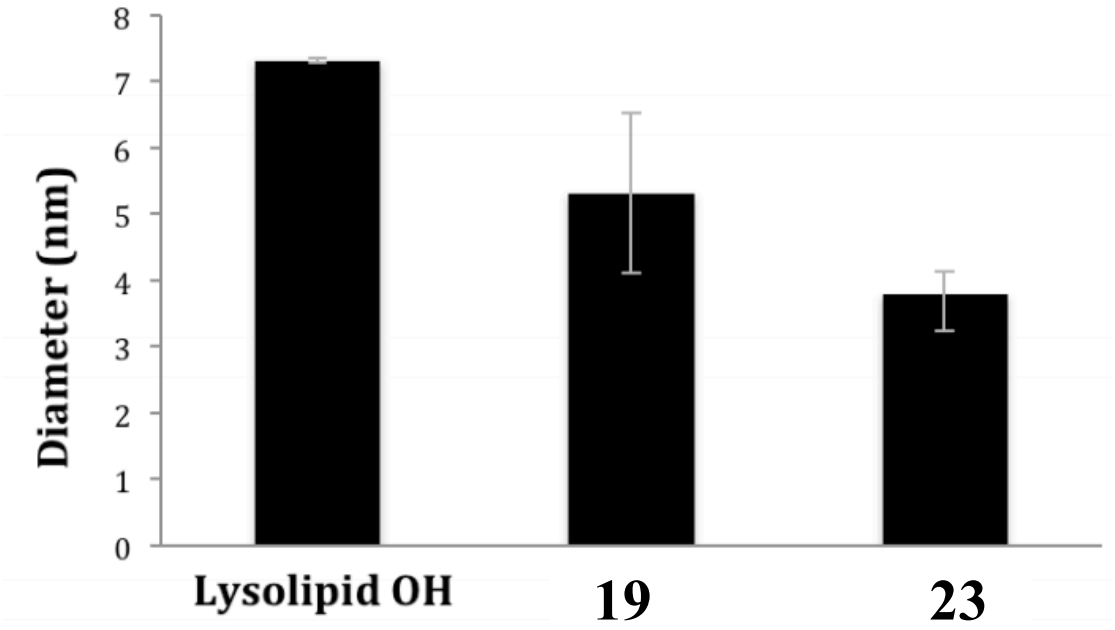

Alternatively, addition of precursors in imidazole buffer at neutral pH allowed the NCL ligation and subsequent MESNA thioester reloading,[176] leading to the formation of amidophospholipid **24**, albeit in relatively lower yield, possibly because multiple reaction steps were required (Figure 6.1). This phospholipid, which incorporates a second oleoyl chain in the phospholipid architecture, is a novel membrane-forming phospholipid containing three alkyl chains and is reminiscent of unique multi-chain phospholipids such as 3-*O*-acyl-D-*erythro*-sphingomyelin.[193]

Phospholipid synthesis was analyzed over time using combined liquid chromatography (LC), mass spectrometry (MS), and evaporative light-scattering detection (ELSD) measurements. Addition of MESNA thioester to the cysteine-based lysolipid in the appropriate buffer immediately led to amidophospholipid formation, and this process progressed to near completion over a period of 30 min using millimolar concentrations of reactants.

As expected, neither the cysteine-modified lysolipid **19** nor the MESNA thioester **23** formed membranes in aqueous solution. However, the purified amidophospholipid products **21** and **24**, when hydrated, readily formed membrane-bound vesicles. Lipid vesicular structures were initially identified by fluorescence microscopy using the membrane-staining dye 1,2-dihexadecanoyl-*sn*-glycero-3-phosphoethanolamine, triethylammonium salt (Texas Red DHPE) (Figure 6.2a). Confirmation that the resulting structures were membrane compartments was also achieved by transmission electron microscopy (TEM) (Figure 6.2b). In this case, aliquots of the hydrated and sonicated phospholipid samples were collected over 400 mesh Cu/Rh grids, which were then negatively stained with uranyl acetate. Under

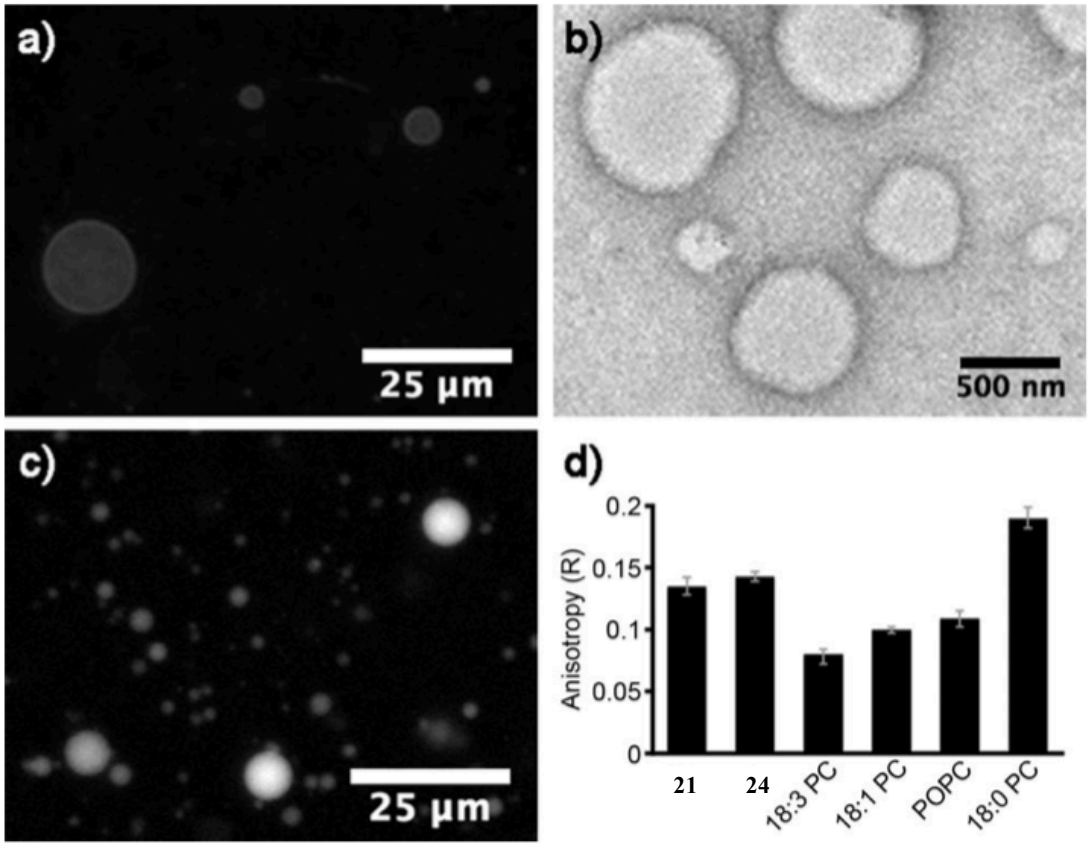

Figure 6.2 Characterization of the amidophospholipid vesicular structure. a) Fluorescence microscopy image of membrane-containing vesicles formed by hydration of a thin film of phospholipid **21**. Membranes were stained using 1 µM Texas Red DHPE dye solution. b) TEM image of negatively stained self-assembled vesicular structures formed from amidophospholipid **21**. c) Fluorescence microscopy image demonstrating the encapsulation of HPTS in membrane vesicles of phospholipid **21**. d) Steady-state anisotropy of DPH in membranes formed from amidophospholipids **21** and **24** compared with those from native phosphatidylcholines with the indicated acyl chains. The unitless anisotropy ratio (R) is a measure of the acyl packing of the bilayer, with higher values indicating a more ordered membrane.

these conditions, electron microscopy revealed the presence of several populations of spherical compartments that were between 50–900 nm wide, consistent with the vesicle architecture. The efficient encapsulation ability of the vesicles was determined by inclusion of a polar fluorophore, 8-hydroxypyrene-1,3,6-trisulfonic acid (HPTS), in the hydration media, followed by vesicle characterization using fluorescence

microscopy (Figure 6.2c). Finally, we determined the phase transition temperature of the lipids chains by performing steady-state anisotropy measurements as a function of temperature with the membrane fluidity probe 1,6-diphenyl-1,3,5-hexatriene (DPH).[194] The measurements indicate that the amidophospholipid membranes composed of **21** and **22** are well-ordered, with fluidity and chain-melting temperatures comparable to those of native POPC membranes (*T*c=270 K) (Figure 6.2d).[195]

6.3 NCL Liposome Encapsulation

We next explored de novo lipid vesicle formation in aqueous solvent. Remarkably, we found that the NCL coupling reaction is capable of driving the highly efficient in situ self-assembly of phospholipid membranes into vesicular structures (Figure 6.3a). When we combined an aqueous solution of **19** with thioester **23** in the presence of TCEP, we observed the formation of large vesicular structures, both spherical and tubular, by fluorescence microscopy (Figure 6.3b). One advantage of NCL-driven lipid formation compared to previous techniques used for the de novo assembly of vesicles is the chemoselectivity of the reaction, even in the presence of common biologically relevant functional groups. The selectivity of the reaction should enable compatibility with biological molecules such as proteins. To check for orthogonality and biocompatibility of the lipid-forming NCL reaction, as well as the functional stability of the vesicles, GFP was spontaneously encapsulated in situ. A 220 μM solution of GFP was diluted in a small volume of HEPES buffer containing lysolipid **19** and TCEP, and thioester **23** was subsequently added. After 30 min of reaction, non-encapsulated GFP was removed by spin filtration. When the lipid

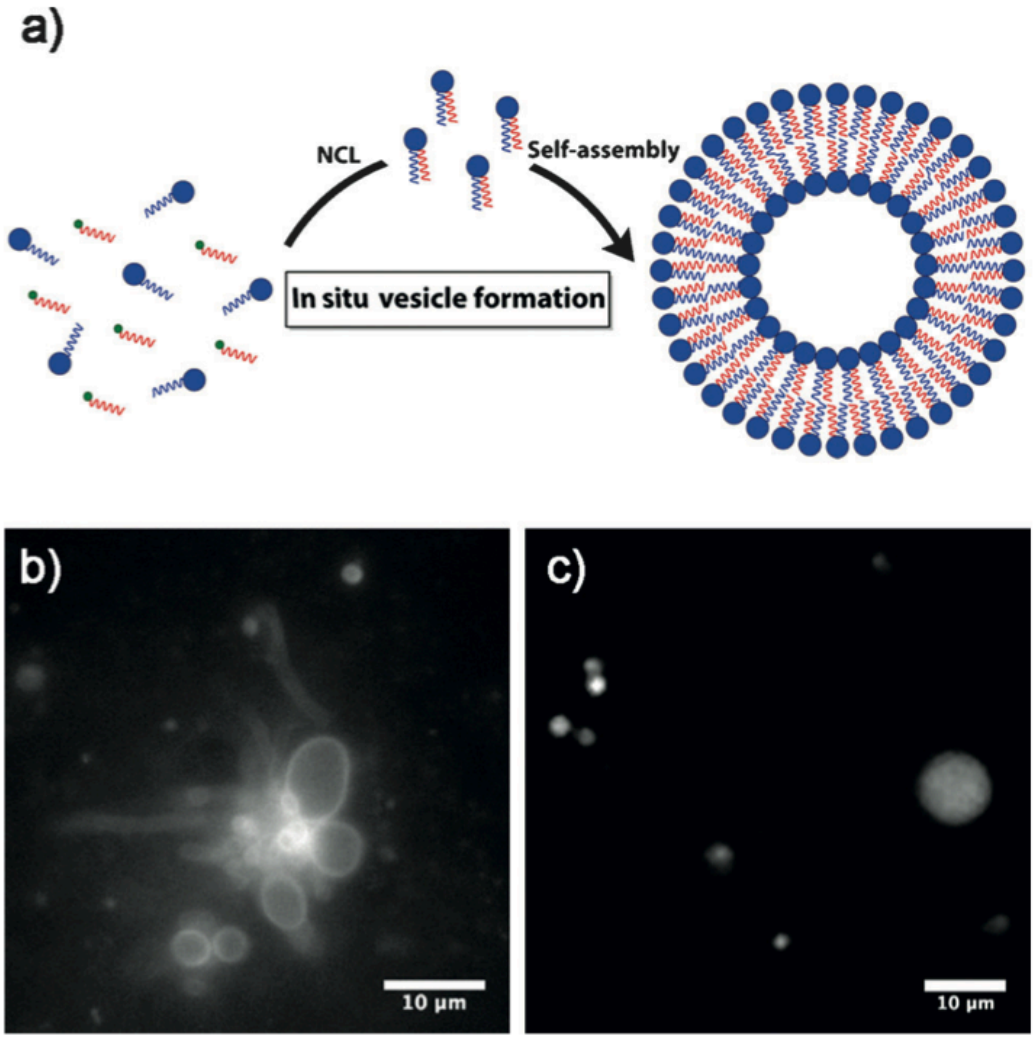

Figure 6.3 In situ assembly of phospholipid membranes driven by a non-enzymatic reaction. a) Model of spontaneous vesicle assembly induced by NCL-based amidophospholipid synthesis. b) Fluorescence microscopy image of the membrane-containing vesicles formed by spontaneous assembly directed by NCL-based synthesis of phospholipid **21**. Membranes were stained using 1µM Texas Red DHPE dye solution. c) Fluorescence microscopy image demonstrating the encapsulation of GFP in vesicles driven by the in situ self-assembly of phospholipid **21** membranes.

containing solution was examined by fluorescence microscopy, stable vesicles containing GFP were observed (Figure 6.3c). The compatibility of the lipid formation with biological molecules could lead to applications involving the packaging of therapeutic proteins or the use of these vesicles as compartments for enzymatic reactions.

6.4 NCL: Time-Lapse of Liposome Formation

The morphological transformations of the vesicle assemblies were also monitored by time-lapse phase-contrast microscopy at room temperature (Figure 6.4). No observable aggregates were found immediately after **19** and **23** (1 mM for each) had been combined in the presence of TCEP (20 mM). Approximately 5 min after mixing, small granular aggregates began to appear, and then tubular vesicles grew, which were converted into spherical vesicles. This morphological conversion is analogous to the spontaneous transformation of some amphiphilic molecules from micelles to giant vesicles in aqueous dispersions.[163] We also observed that the NCL between **19** and **23** frequently sustained the growth of vesicles present in the reaction medium (Figure 6.4). As a prototypical example, we specifically checked a population of two vesicles of 18 and 15 μm in diameter. We found that the size of the vesicles increased steadily, up to final values of 37 and 24 μm in diameter, respectively, after 15 min. This result corresponds to an approximate quadrupling of the surface area and is possibly due to continued formation of phospholipid **21** within the bilayer of the in situ formed vesicles. Our observations of in situ vesicle formation correlate well with

our LC-MS characterization, which showed that the NCL reaction takes place in a fast, chemoselective, and highly specific fashion at neutral pH.

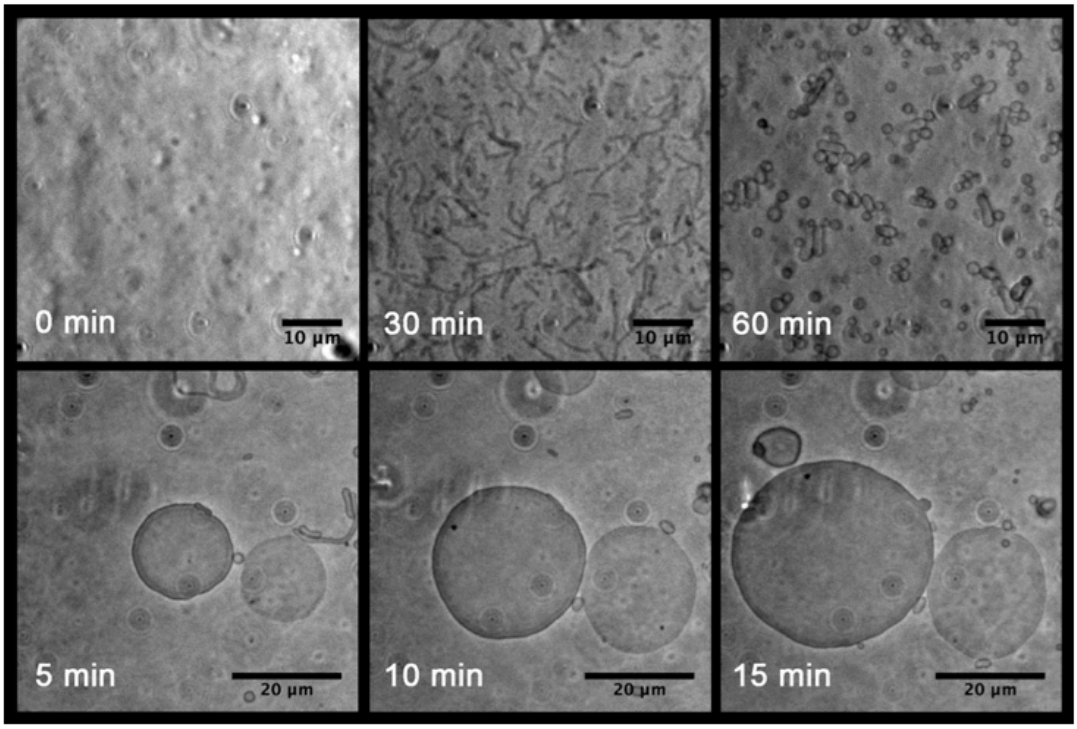

Figure 6.4 In situ vesicle formation (top) and growth (bottom). An aqueous buffer solution of cysteine-functionalized lysolipid **19** (1 mM) and MESNA oleoyl thioester **23** (1 mM) in the presence of TCEP.HCl (20 mM) was imaged at different times after initial mixing. The top panels show phase-contrast images corresponding to the vesicle formation. Initially, phospholipid membranes were not present. However, shortly after the two precursors had been mixed, the spontaneous formation and growth of vesicle and tubular structures was observed. After 30 min, the starting materials were consumed and replaced with large fields of vesicles. The bottom panels are phase-contrast micrographs of vesicles growing over a period of 10 min in the presence of reactive lipid precursors.

6.5 Concluding Remarks

In summary, we have explored the suitability of NCL for the de novo synthesis of phospholipid membranes. This highly specific and chemoselective approach has allowed the preparation and full characterization of a new class of

amidophospholipids, which self-assemble in situ to form membrane-bound vesicles. Such amidophospholipids could also be utilized in applications involving protocells. Thus, the NCL reaction can be efficiently used as a non-enzymatic method to drive the de novo self-assembly of phospholipid membranes. Importantly, this protocol uses thioester precursors, analogous to enzymatically driven lipid synthesis. Moreover, the orthogonality, the high reaction rate, and the biocompatibility of this approach are key features that make it a powerful option for the efficient encapsulation of relevant biomolecules, such as proteins. We foresee future applications of the NCL membrane assembly in advanced synthetic cell studies utilizing phospholipid vesicles as well as in the construction of liposomal drug-delivery systems and bioreactors.

6.6 Experimental and Methods

6.6.1 Materials

Commercially available 1-palmitoyl-2-hydroxy-sn-glycero-3-phosphocholine and 1-palmitoyl-2-oleoyl-sn-glycero-3-phosphocholine (POPC) were used as obtained from Avanti® Polar Lipids. N-Boc-Cys(Trt)-OH, N,N'-diisopropylcarbodiimide (DIC), 4-dimethylaminopyridine (DMAP), trifluoroacetic acid (TFA), triethylsilane (TES), oleic acid, N-(3-dimethylaminopropyl)-N'- ethylcarbodiimide hydrochloride (EDC.HCl), sodium 2-mercapto-ethanesulfonate (MESNA), tris(2-carboxyethyl)phosphine hydrochloride (TCEP.HCl), 8-hydroxypyrene-1,3,6-trisulfonic acid (HPTS), dithiothreitol (DTT), 4-(2-hydroxyethyl)piperazine-1-ethanesulfonic acid (HEPES) sodium salt and 1,6-diphenyl-1,3,5-hexatriene (DPH)

were obtained from Sigma-Aldrich. Texas Red® 1,2-dihexadecanoyl-sn-glycero-3-phosphoethanolamine, triethylammonium salt (Texas Red® DHPE) was obtained from Life Technologies. Deuterated chloroform ($CDCl_3$), methanol (CD_3OD) and dimethyl sulfoxide (d_6-DMSO) were obtained from Cambridge Isotope Laboratories. All reagents obtained from commercial suppliers were used without further purification unless otherwise noted. Analytical thin-layer chromatography was performed on E. Merck silica gel 60 F_{254} plates. Compounds, which were not UV active, were visualized by dipping the plates in a ninhydrin or potassium permanganate solution and heating. Silica gel flash chromatography was performed using E. Merck silica gel (type 60SDS, 230-400 mesh). Solvent mixtures for chromatography are reported as v/v ratios. HPLC analysis was carried out on an Eclipse Plus C8 analytical column with Phase A/Phase B gradients [Phase A: H_2O with 0.1% formic acid; Phase B: MeOH with 0.1% formic acid]. HPLC purification was carried out on Zorbax SB-C18 semipreparative column with Phase A/Phase B gradients [Phase A: H_2O with 0.1% formic acid; Phase B: MeOH with 0.1% formic acid]. Proton nuclear magnetic resonance (^{1}H NMR) spectra were recorded on a Varian VX-500 MHz or Jeol Delta ECA-500 MHz spectrometers, and were referenced relative to residual proton resonances in $CDCl_3$ (at 7.24 ppm), CD_3OD (at 4.87 or 3.31 ppm) or d_6-DMSO (at 2.50 ppm). Chemical shifts were reported in parts per million (ppm, δ) relative to tetramethylsilane (δ 0.00). ^{1}H NMR splitting patterns are assigned as singlet (s), doublet (d), triplet (t), quartet (q) or pentuplet (p). All first-order splitting patterns were designated on the basis of the appearance of the multiplet. Splitting patterns that could not be readily interpreted are designated as multiplet (m) or broad (br). Carbon

nuclear magnetic resonance (^{13}C NMR) spectra were recorded on a Varian VX-500 MHz or Jeol Delta ECA-500 MHz spectrometers, and were referenced relative to residual proton resonances in $CDCl_3$ (at 77.23 ppm), CD_3OD (at 49.15 ppm) or d_6-DMSO (at 39.51 ppm). Electrospray Ionization-Time of Flight (ESI-TOF) spectra were obtained on an Agilent 6230 AccurateMass TOFMS mass spectrometer. Anisotropy measurements were obtained on a SPEX FluoroMax-3 spectrofluorometer. Transmission electron microscopy images were recorded on a FEI TecnaiTM Sphera 200 kV microscope equipped with a LaB_6 electron gun, using the standard cryotransfer holders developed by Gatan, Inc.

6.6.2 Synthesis of 1-palmitoyl-2-[N-Boc-L-Cys(Trt)]-sn-glycero-3-phosphocholine (22)

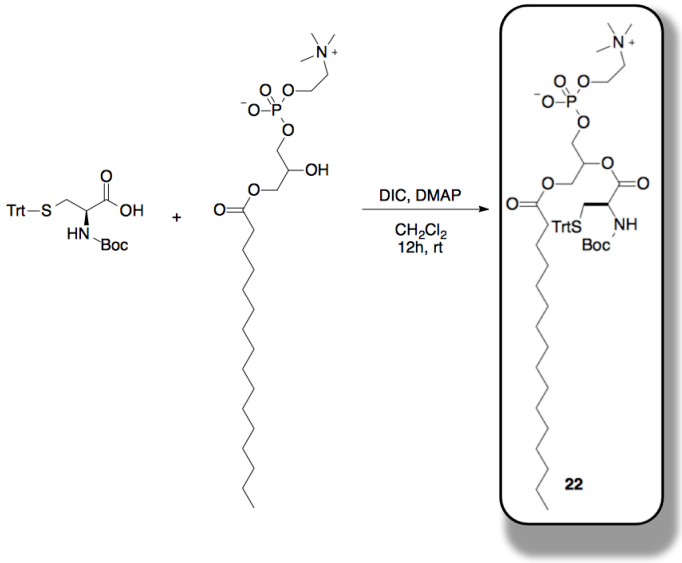

Scheme 6.1 Synthesis of 1-palmitoyl-2-[N-Boc-L-Cys(Trt)]-sn-glycero-3-phosphocholine **(22)**

A solution of N-Boc-LCys(Trt)-OH (93.7 mg, 201.6 µmol) in CH_2Cl_2 (7.5 mL) was stirred at rt for 10 min, and then DIC (47.0 µL, 302.4 µmol) and DMAP (12.3 mg,

100.8 μmol) were successively added. After 10 min stirring at rt, 1-palmitoyl-2-hydroxy-sn-glycero-3-phosphocholine (25.0 mg, 50.4 μmol) was added. After 12 h stirring at rt, the solvent was removed under reduced pressure, and the crude was purified by HPLC, affording 29.6 mg of **22** as a colorless foam [88%, Rt = 12.5 min (Zorbax SB-C18 semipreparative column, 5% Phase A in Phase B, 15.5 min)]. ^{1}H NMR ($CDCl_3$, 500.13 MHz, δ): 7.38-7.31 (d, J = 8.0 Hz, 6H, 6 × CH_{Ar}), 7.30-7.23 (m, 6H, 6 × CH_{Ar}), 7.22-7.16 (m, 3H, 3 × CH_{Ar}), 5.25-5.13 (m, 1H, 1 × CH), 5.10 (d, J = 7.8 Hz, 0.3H, 1 × NH), 5.01 (d, J = 7.8 Hz, 0.7H, 1 × NH), 4.38-4.21 (m, 3H, 1.5 × CH_2), 4.20-4.11 (m, 1H, 1 × CH), 4.10-3.87 (m, 3H, 1.5 × CH_2), 3.86-3.66 (m, 2H, 1 × CH_2), 3.25 (s, 9H, 3 × CH_3), 2.73-2.45 (m, 2H, 1 × CH_2), 2.33-2.06 (m, 2H, 1 × CH_2), 1.62-1.43 (m, 2H, 1 × CH_2), 1.38 (s, 9H, 3 × CH_3), 1.31-1.16 (m, 24H, 12 × CH_2), 0.85 (t, J = 7.0 Hz, 3H, 1 × CH_3). ^{13}C NMR ($CDCl_3$, 125.77 MHz, δ): 173.6, 170.4, 163.9, 155.3, 144.5, 129.7, 128.3, 121.2, 80.2, 72.2, 67.3, 66.4, 64.1, 62.6, 59.9, 54.7, 52.8, 34.2, 34.1, 32.1, 29.9, 29.9, 29.9, 29.7, 29.6, 29.5, 29.4, 29.3, 28.6, 24.9, 22.9, 14.3. MS (ESI-TOF) [m/z (%)]: 941 ($[MH]^+$, 100). HRMS (ESI-TOF) calculated for $C_{51}H_{78}N_2O_{10}PS$ ($[MH]^+$) 941.5109, found 941.5111.

6.6.3 Synthesis of 1-palmitoyl-2-(L-Cys)-sn-glycero-3-phosphocholine (19)

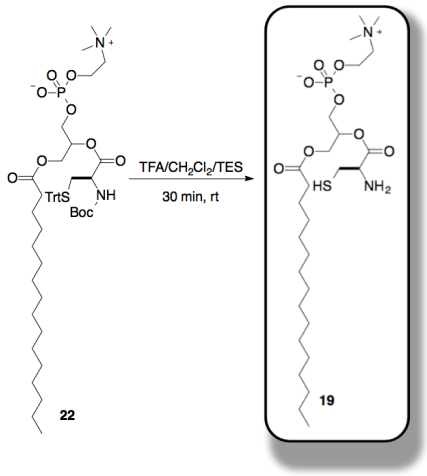

Scheme 6.2 Synthesis of 1-palmitoyl-2-(L-Cys)-sn-glycero-3-phosphocholine (**19**)

A solution of 1-palmitoyl-2-[N-Boc-LCys(Trt)]-sn-glycero-3-phosphocholine (**22**, 30.0 mg, 31.9 µmol) in 6 mL of TFA/CH_2Cl_2/TES (2.85:2.85:0.3) was stirred at rt for 30 min. After removal of the solvent, the residue was dried under high vacuum for 3 h. Then, the corresponding residue was diluted in MeOH (1 mL), filtered using a 0.2 µm syringe-driven filter, and the crude solution was purified by HPLC, affording 14.2 mg of the lysolipid **19** as a colorless foam [64%, Rt = 9.0 min (Zorbax SB-C18 semipreparative column, 50% Phase A in Phase B, 5 min, and then 5% Phase A in Phase B, 10 min)]. ^{1}H NMR ($CDCl_3$, 500.13 MHz, δ): 5.37 (m, 1H, 1 × CH), 4.43-4.36 (m, 1H, 0.5 × CH_2), 4.35-4.28 (m, 1H, 1 × CH), 4.27-4.14 (m, 3H, 1.5× CH_2), 4.13-3.98 (m, 2H, 1 × CH_2), 3.63-3.56 (m, 2H, 1 × CH_2), 3.17 (s, 9H, 3 × CH_3), 3.16-2.99 (m, 2H, 1 × CH_2), 2.33-2.25 (m, 2H, 1 × CH_2), 1.60-1.49 (m, 2H, 1 × CH_2), 1.31-1.19 (m, 24H, 12 × CH_2), 0.84 (t, J = 6.9 Hz, 3H, 1 × CH_3). ^{13}C NMR ($CDCl_3$, 125.77 MHz, δ): 175.0, 168.5, 75.0, 67.5, 65.1, 63.3, 60.7, 55.9, 54.8, 34.9, 33.2, 31.0, 31.0,

30.9, 30.9, 30.9, 30.8, 30.7, 30.6, 30.4, 26.1, 25.5, 25.3, 23.9, 14.6. MS (ESI-TOF) [m/z (%)]: 599 ([MH] $^{+}$, 10). HRMS (ESI-TOF) calculated for $C_{27}H_{56}N_2O_8PS$ ([MH]$^{+}$) 599.3490, found 599.3484.

6.6.4 Synthesis of MESNA thiooleate (**23**)

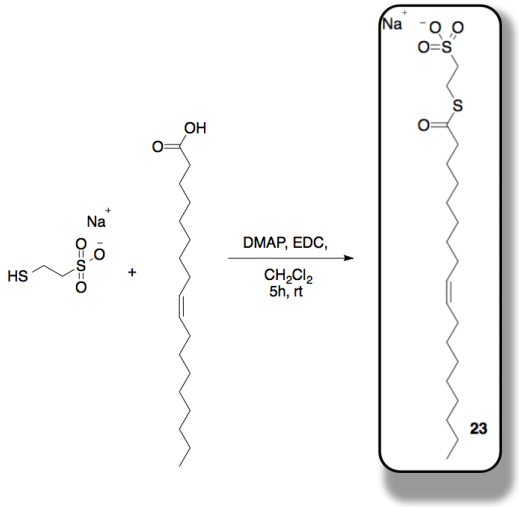

Scheme 6.3 Synthesis of MESNA thiooleate (**23**)

A solution of oleic acid (189.2 mg, 670.0 µmol) in CH_2Cl_2 (5 mL) was stirred at 0 ºC for 10 min, and then DMAP (7.4 mg, 60.9 µmol) and EDC.HCl (128.4 mg, 670.0 µmol) were successively added. After 10 min stirring at 0 ºC, sodium 2-mercaptoethanesulfonate [196] (MESNA, 100.0 mg, 609.1 µmol) was added. After 5 h stirring at rt, the mixture was extracted with H_2O (2 × 3 mL) and the combined aqueous phases were washed with EtOAc (3 mL). After evaporation of H_2O under reduced pressure, the residue was washed with CH_3CN (5 mL), and then filtered to yield 194.7 mg of **23** as a white solid [75%]. ^{1}H NMR (d_6-DMSO, 500.13 MHz, δ): 5.36-5.27 (m, 2H, 2 × CH), 3.05-2.99 (m, 2H, 1 × CH_2), 2.60-2.51 (m, 4H, 2 × CH_2),

2.02-1.92 (m, 4H, 2 × CH_2), 1.58-1.49 (m, 2H, 1 × CH_2), 1.34-1.18 (m, 20H, 10 × CH_2), 0.85 (t, J = 6.9 Hz, 3H, 1 × CH_3). ^{13}C NMR (d_6-DMSO, 125.77 MHz, δ): 198.7, 129.8, 129.7, 51.0, 43.4, 31.4, 29.2, 29.1, 28.9, 28.8, 28.7, 28.6, 28.5, 28.3, 26.7, 26.6, 25.1, 24.4, 22.2, 14.1. MS (ESI-TOF) [m/z (%)]: 429 ($[MH]^+$, 100). HRMS (ESI-TOF) calculated for $C_{20}H_{38}NaO_4S_2$ ($[MH]^+$) 429.2104, found 429.2105.

6.6.5 Synthesis of Phospholipids Amidophospholipid 1-palmitoyl-2-[β-Cys-(oleoyl)]-sn-glycero-3-phosphocholine (21).

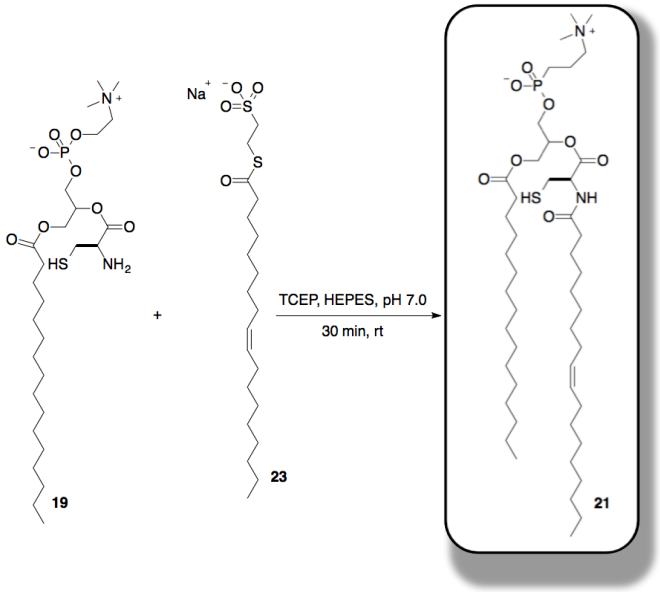

Scheme 6.4 Synthesis of Phospholipids Amidophospholipid 1-palmitoyl-2-[β-Cys-(oleoyl)]-sn-glycero-3-phosphocholine (**21**).

1-palmitoyl- 2-(β-Cys)-sn-glycero-3-phosphocholine (**19**, 5.00 mg, 7.18 μmol) and MESNA-thiooleate (**23**, 3.07 mg, 7.18 μmol) were dissolved in 1.44 mL of 20 mM TCEP.HCl in 150 mM HEPES pH 7.0 buffer and stirred under N_2 at rt. After 30 min, the corresponding mixture was filtered using a 0.2 μm syringe-driven filter, and the crude solution was purified by HPLC, affording 4.2 mg of the amidophospholipid

21 as a white solid [68%, Rt = 12.7 min (Zorbax SB-C18 semipreparative column, Phase B, 15.5 min)]. ^{1}H NMR ($CDCl_3$, 500.13 MHz, δ): 6.87 (d, ^{1}H, 1 × NH, J = 7.5 Hz), 5.37-5.29 (m, 2H, 2 × CH), 5.28-5.18 (m, 1H, 1 × CH), 4.88-4.77 (m, 1H, 1 × CH), 4.46-4.24 (m, 3H, 1.5 × CH_2), 4.23-3.99 (m, 3H, 1.5 × CH_2), 3.98-3.80 (m, 2H, 1 × CH_2), 3.36 (s, 9H, 3 × CH_3), 3.08-2.81 (m, 2H, 1 × CH_2), 2.34-2.17 (m, 4H, 2 × CH_2), 2.04-1.87 (m, 4H, 2 × CH_2), 1.67-1.48 (m, 4H, 2 × CH_2), 1.35-1.16 (m, 45H, 22 × CH_2 + 1 × SH), 0.85 (t, J = 6.8 Hz, 6H, 2 × CH_3). ^{13}C NMR ($CDCl_3$, 125.77 MHz, δ): 173.7, 169.9, 163.5, 130.7 and 130.4, 130.2 and 129.9, 72.3, 66.3, 64.6, 62.4, 60.2, 54.7, 53.7, 36.5, 34.2, 32.9, 32.1, 30.0, 29.9, 29.9, 29.9, 29.8, 29.7, 29.6, 29.6, 29.6, 29.5, 29.4, 29.4, 29.3, 27.4, 26.9, 25.9, 25.0, 22.9, 14.4. MS (ESI-TOF) [m/z (%)]: 863 ($[MH]^+$, 100), 885 ($[M +Na]^+$, 60). HRMS (ESI-TOF) calculated for $C_{45}H_{88}N_2O_9PS$ ($[MH]^+$) 863.5943, found 863.5948.

6.6.6 Amidophospholipid 1-palmitoyl-2-[β-Cys(oleoyl)-(oleoyl)]-sn-glycero-3-phosphocholine (24).

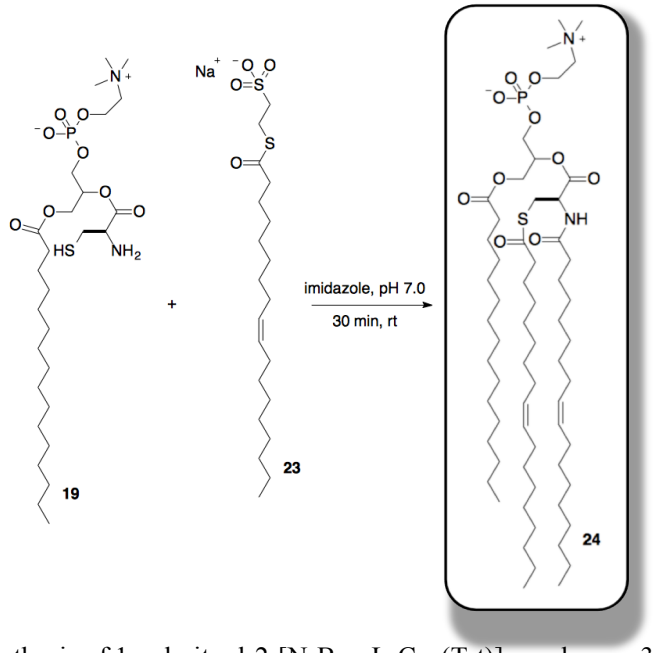

Scheme 6.5 Synthesis of 1-palmitoyl-2-[N-Boc-L-Cys(Trt)]-sn-glycero-3-phosphocholine **(22)**

1-palmitoyl-2-(β-Cys)-sn-glycero-3-phosphocholine (**19**, 5.00 mg, 7.18 μmol) and MESNA-thiooleate (**23**, 6.14 mg, 14.36 μmol) were dissolved in 1.44 mL of 500 mM imidazole pH 7.0 buffer and stirred under N_2 at rt. After 30 min, the corresponding mixture was filtered using a 0.2 μm syringe-driven filter, and the crude solution was purified by HPLC, affording 4.3 mg of the amidophospholipid **24** as a white solid. [53%, Rt = 13.5 min (Zorbax SB-C18 semipreparative column, Phase B, 15.5 min)]. ^{1}H NMR ($CDCl_3$, 500.13 MHz, δ): 6.82 (d, 1H, 1 × NH, J = 7.6 Hz), 5.49-5.24 (m, 4H, 4 × CH), 5.23-5.16 (m, 1H, 1 × CH), 4.87-4.73 (m, 1H, 1 × CH), 4.48-4.24 (m, 3H, 1.5 × CH_2), 4.23-3.96 (m, 3H, 1.5 × CH_2), 3.95-3.76 (m, 2H, 1 × CH_2), 3.36 (s, 9H, 3 × CH_3), 3.28-2.94 (m, 2H, 1 × CH_2), 2.36-2.15 (m, 6H, 3 × CH_2), 2.09-

1.86 (m, 8H, 4 × CH_2), 1.69-1.44 (m, 6H, 3 × CH_2), 1.35-1.16 (m, 64H, 32 × CH_2), 0.86 (t, J = 6.9 Hz, 9H, 3 × CH_3). ^{13}C NMR ($CDCl_3$, 125.77 MHz, δ): 198.9, 173.4, 170.0, 163.7, 130.5, 130.2, 130.1, 129.6, 72.2, 66.5, 64.8, 62.3, 60.2, 54.5, 53.7, 42.1, 36.5, 34.2, 32.9, 32.8, 32.1, 32.0, 30.0, 29.9, 29.9, 29.8, 29.8, 29.7, 29.6, 29.6, 29.6, 29.5, 29.5, 29.4, 29.4, 29.4, 29.3, 29.2, 27.4, 26.9, 26.9, 25.8, 25.0, 22.9, 14.3. MS (ESI-TOF) [m/z (%)]: 1127 ($[MH]^+$, 100), 1149 ($[M +Na]^+$, 40). HRMS (ESI-TOF) calculated for $C_{63}H_{120}N_2O_{10}PS$ ($[MH]^+$) 1127.8401, found 1127.84035.

6.6.7 Micelle sizes: critical micelle concentrations (cmc)

100 μL of aqueous solutions (10 mM, 1 mM, 100 μM, 10 μM and 1 μM) of the control (1-palmitoyl-2- hydroxy-sn-glycero-3-phosphocholine Lysolipid OH) and the precursors (**19** or **23**) were analyzed by Dynamic Light Scattering (DLS) in order to determine the micelle sizes and the critical micelle concentrations (cmc's).

6.6.8 LC/MS Analysis

LC/MS Analysis Membrane assembly was performed in the appropriate buffer (150 mM HEPES pH 7.0 buffer containing 20 mM TCEP.HCl for phospholipid **21**; 500 mM imidazole pH 7.0 buffer for phospholipid **24**) as described above. Aliquots of 1.5 μL of sample were taken at various time points, diluted with 50 μL of MeOH and analyzed using an Eclipse Plus C8 analytical column (5% Phase A in Phase B, 5.5 min) with an Evaporative Light Scattering Detector (ELSD) at a flow of 1.0 mL/min. For all LC/MS runs, solvent Phase A consisted of H_2O with 0.1% formic acid and solvent Phase B of MeOH with 0.1% formic acid.

6.6.9 NCL Fluorescence Microscopy: Hydration Method

10 μL of a 20 mM solution of phospholipid (**21** or **24**) in $CHCl_3$ was added to a 1 mL vial, placed under N_2 and dried for 15 min to prepare a lipid film. Then, 200 μL of H_2O was added and the solution was tumbled at 25 ºC for 1 h. Afterward, to 10 μL of this 1 mM aqueous solution of phospholipid (**21** or **24**) was added 0.1 μL of a 100 μM Texas Red® DPHE dye solution in EtOH, and the mixture was briefly agitated. The corresponding mixture was finally monitored by fluorescence and phase contrast microscopy in order to determine the vesicle structure.

6.6.10 NCL Fluorescence Microscopy: Sonication Method.

10 μL of a 20 mM solution of phospholipid (**21** or **24**) in $CHCl_3$ was added to a 1 mL vial, placed under N_2 and dried for 15 min to prepare a lipid film. Then, 200 μL of H_2O was added, and the resulting mixture was sonicated with heat (≈55ºC) for 1 h. Afterward, to 10 μL of this 1 mM aqueous solution of phospholipid (**21** or **24**) was added 0.1 μL of a 100 μM Texas Red® DPHE dye solution in EtOH, and the mixture was briefly agitated. The corresponding mixture was finally monitored by fluorescence and phase contrast microscopy in order to determine the vesicle structure

6.6.11 Transmission Electron Microscopy (TEM) Studies

A deposition System Balzers Med010 was used to evaporate a homogeneous layer of carbon. The samples were collected over 400 mesh Cu grids. The grids were then negatively stained with a solution of 1% (w/w) uranyl acetate. Micrographs were

recorded on a FEI TecnaiTM Sphera microscope operating at 200 kV and equipped with a LaB6 electron gun, using the standard cryotransfer holders developed by Gatan, Inc. For image processing, micrographs were digitized in a Zess SCAI scanner with different sampling windows.

TEM measurements. Copper grids (formvar/carbon-coated,, 400 mesh copper) were prepared by glow discharging the surface at 20 mA for 1.5 min. Once the surface for vesicle adhesion is ready, 3.5 μL of a 5 mM solution of phospholipid 3 in H_2O (previously sonicated at ≈55ºC C for 1 h) was deposited on the grid surface. This solution was allowed to sit for 10 seconds before being washed away with 10 drops of glass distilled H_2O and subsequent staining with 3 drops of 1% w/w uranyl acetate. The stain was allowed to sit for 10 seconds before wicking away with filter paper. All grid treatments and simple depositions were on the dark/shiny/glossy formvar-coated face of the grid (this side face up during glow discharge). Samples were then imaged via TEM, revealing the presence of several populations of spherical compartments (50-900 nm in diameter), consistent with the vesicle architecture.

6.6.12 Encapsulation Experiments

Encapsulation of HPTS. 60 μL of a 20 mM solution of phospholipid (**21** or **24**) in $CHCl_3$ was added to a 1 mL vial, placed under N_2 and dried for 15 min to prepare a lipid film. Then, 200 μL of mineral oil was added and placed under N_2 to displace the air above the mineral oil. The resulting mixture was sonicated with heat (≈55ºC) for 1 h. Afterward, 100 μL of the amidophospholipid oil was added to a 1 mL eppendorf. Then, 10 μL of the upper buffer [1mM HPTS + 1 mM DTT + 50 mM NaCl + 200 mM

sucrose in 100 mM HEPES buffer pH 7.5 solution] was added, and the resulting mixture was flicked and vortexed till it was a cloudy emulsion. The corresponding emulsion was added to a 1 mL eppendorf containing 100 μL of the lower buffer [1 mM DTT + 50 mM NaCl + 200 mM glucose in 100 mM HEPES buffer pH 7.5 solution], so it floated on top. Then, we waited for 10 min. After this time, the sample was centrifuged for 10 min at 9000-10000 rcf. The sample was separated from the oil (either aspirating off the oil or using a syringe/needle to collect the sample from the bottom). The corresponding sample contained vesicles encapsulating HPTS that were observed using fluorescence microscopy.

In situ encapsulation of GFP. 1-palmitoyl-2-(β-Cys)-sn-glycero-3-phospho-choline (**19**, 0.50 mg, 0.72 μmol) was dissolved in 66 μL of a 220 μM solution of previously purified Green Fluorescent Protein (GFP) in 20 mM HEPES buffer pH 7.0. Then, 79 μL of a 20 mM TCEP.HCl solution in 300 mM HEPES pH 7.0 was added. Finally, MESNA-thiooleate **23** (0.31 mg, 0.72 mmol) was added and the resulting mixture was stirred under N_2 at rt. After 30 min, the reaction was transferred to a 100 kDa spin filter and centrifuged for 10 min at 9000-10000 rcf in order to remove the non-encapsulated GFP. Then, the sample was washed and centrifuged with a 150 mM solution of HEPES buffer pH 7.0 (5 × 250 μL). The lipid containing solution was finally examined by fluorescence microscopy, observing vesicles containing the desired GFP

6.6.13 Anisotropy Studies

Vesicle preparation and extrusion. 50 μL of a 20 mM solution of phospholipid (POPC, **21** or **24**) in $CHCl_3$ was added to a 1 mL vial, placed under N_2 and dried for 15 min to prepare a lipid film. The dried film was hydrated in 500 μL of H_2O [Final concentration of phospholipid: 2 mM]. The lipid solution was briefly vortexed and then sonicated with heat (≈55ºC) for 45 min. Once the sample was fully hydrated, the vesicles were extruded through 100 nm membrane. Extruded vesicles were finally analyzed by Dynamic Light Scattering (DLS).

Anisotropy measurements. 2 μL of a 500 μM solution of DPH in EtOH was added to 198 μL of 100 nm phospholipid (POPC, **21** or **24**) extruded vesicles [Final concentration of DPH: 5 μM, 1% v/v]. The solution was tumbled at 25 ºC overnight. Steady-state anisotropy was measured at different temperatures (from -10 to 40 ºC) on a Perkin spectrophotometer with a manual polarizer accessory and peltier temperature controller.

6.6.14 Membrane Assembly

in situ vesicle formation and growth 5.0 μL of a 40 mM TCEP.HCl solution in 150 mM HEPES buffer pH 7.0 was added to 2.5 μL of a 4 mM solution of free cysteine-based lysolipid **19** in 150 mM HEPES buffer pH 7.0. Then, 2.5 μL of a 4 mM solution of MESNA thiooleate **23** in 150 mM HEPES buffer pH 7.0 was added, and the mixture was briefly agitated. The corresponding mixture was then monitored by fluorescence and phase contrast microscopy in order to analyze the in situ formation and growth of the resulting vesicles.

Notes about the Chapter:

Chapter six, in full, is a reprint (with co-author permission) of the material as it appears in the publication; Dr. Roberto J. Brea, **Christian M. Cole**, Prof. Neal K. Devaraj "In Situ Vesicle Formation by Native Chemical Ligation" *Angew. Chem. Int. Ed.*, 2014, 53(51), 14102-14105. I would like to thank Roberto Brea and Neal Devaraj for their invaluable contributions to this chapter: Roberto Brea synthesized and characterized the majority of compounds presented in this chapter and characterized all the phospholipid analogues; I would like to thank Neal Devaraj for directing the research. I purified eGFP, assisted in the synthesis of **19, 21** and helped with all microscopy.

~ CHAPTER 7 ~

7 Spontaneous Reconstitution of Functional Transmembrane Proteins During Bioorthogonal Phospholipid Membrane Synthesis

7.1 Introduction

Transmembrane proteins are critical for signaling, transport, and metabolism, yet their reconstitution in synthetic membranes is often challenging. Non-enzymatic and chemoselective methods to generate phospholipid membranes in situ would be powerful tools for the incorporation of membrane proteins. Herein, the spontaneous reconstitution of functional integral membrane proteins during the de novo synthesis of biomimetic phospholipid bilayers is described. The approach takes advantage of bioorthogonal coupling reactions to generate proteoliposomes from micelle-solubilized proteins. This method was successfully used to reconstitute three different transmembrane proteins into synthetic membranes. This is the first example of the use of non-enzymatic chemical synthesis of phospholipids to prepare proteoliposomes.

Membrane proteins are key regulators of communication between cellular compartments, functioning primarily as receptors and transporters.[197,198] They also determine the distinctive architecture and adhesion properties of cells.[199,200] Membrane proteins are targeted by the majority of approved pharmaceuticals;[201] loss of their function can lead to numerous disease states, including metabolic dysfunction,[202] neurodegenerative disorders,[203] and cardiovascular malfunctions.[204] To study their

structure, dynamics, and function, membrane proteins are often reconstituted into lipid bilayers to create proteoliposomes.[205] The conventional reconstitution of membrane proteins into proteoliposomes is achieved by using organic extraction, mechanical fragmentation, or detergent solubilization to remove the proteins from native bilayers.[205] The ensuing membrane proteins are subsequently introduced into a liposome. This often requires high concentrations of detergent to solubilize proteins from the native bilayer, followed by depletion of the detergent in the presence of phospholipids.[206] However, while effective for select membrane proteins, this method is generally time-consuming, and remnants of detergent often remain absorbed on the proteoliposome after detergent removal.[207] Therefore, it would be exciting to develop a strategy to spontaneously reconstitute membrane proteins into synthetic lipid bilayers in a highly specific and chemoselective manner.

7.2 Spontaneous Liposome Formation

In searching for methods to spontaneously form proteoliposomes, we were attracted to the possibility of harnessing bioorthogonal coupling reactions.[15,178,208] We previously demonstrated the de novo synthesis of non-natural phospholipid membranes from bioorthogonally reactive precursors (Figure 7.1A).[144,209,210] Synthetic membranes capable of forming vesicles and entrapping polar molecules are rapidly generated by exploiting chemoselective reactions, such as copper catalyzed azide–alkyne cycloaddition (CuAAC)[144,209,211–213] or native chemical ligation (NCL; Figure 7.1A).[168,177,181,210] However, it was unknown whether integral membrane proteins could incorporate or remain functional in artificial membranes formed through these

bioorthogonal coupling reactions. Herein, we describe the spontaneous reconstitution of a variety of membrane proteins during bioorthogonal lipid membrane synthesis, with retention of functionality (Figure 7.1B). Bioorthogonal proteoliposome formation could be a powerful method for the study of membrane proteins and/or their incorporation into synthetic cells.

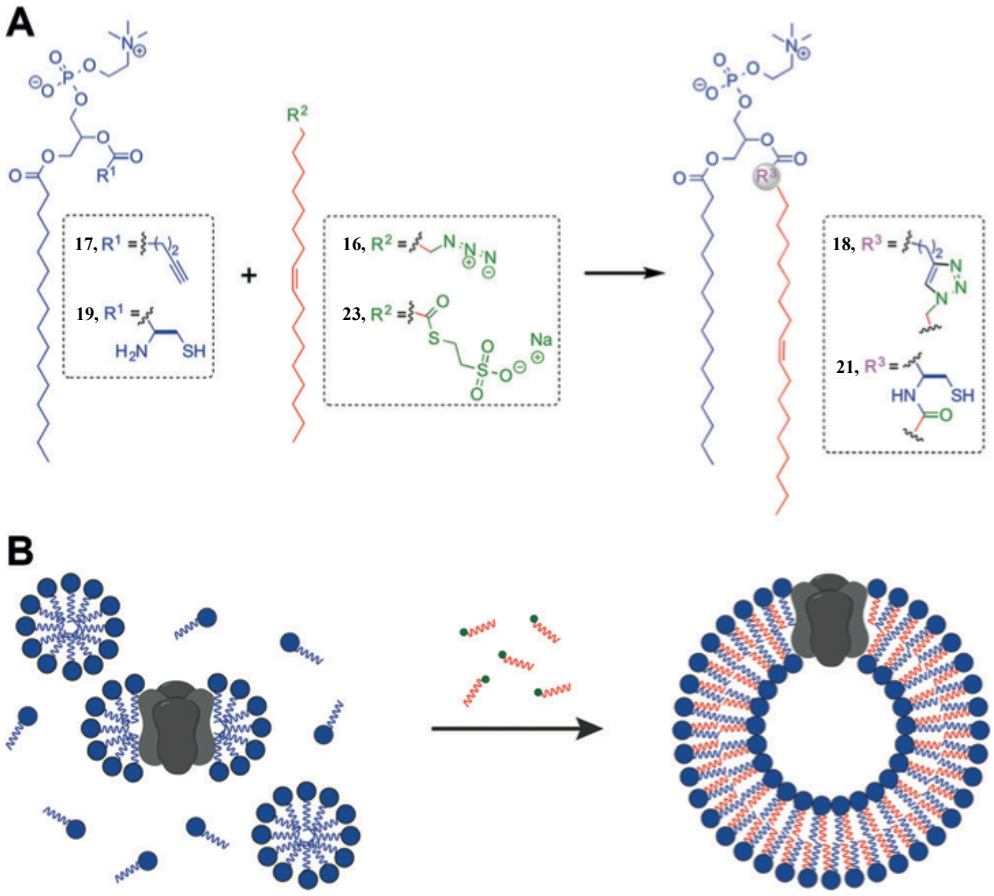

Figure 7.1 De novo synthesis of phospholipid membranes and concurrent in situ incorporation of proteins. A) Two unique bioorthogonal routes to produce synthetic analogues of POPC. Phospholipid **18** is formed by CuAAC between alkyne lysolipid **17** and alkyl azide **16**. Phospholipid **21** is formed via NCL between cysteine lysolipid **19** and thioester **23**. B) Model for spontaneous reconstitution of transmembrane proteins during the non-enzymatic formation of phospholipid membrane. Protein is solubilized with synthetic mimetics of lysophosphatidylcholine, which act as the detergent to form micelle-solubilized protein complexes. Addition of the reactive alkyl precursor and subsequent coupling results in the spontaneous generation of the corresponding proteoliposomes.

We initially designed analogues of palmitoyl lysophosphatidylcholine that were conveniently functionalized at the sn2 position with a bioorthogonal reactive group (**17** or **19**; Figure 7.1A). The corresponding reactive lysolipid detergents can be used to solubilize membrane proteins. Upon addition of an alkyl chain bearing a mutually reactive functional group (**16** or **2 3**), a chemoselective coupling reaction transforms the non-membrane-forming precursors into a synthetic mimetic (**18** or **21**) of the common phospholipid 1-palmitoyl-2-oleoyl-*sn*-glycero-3-phosphocholine (POPC), which is capable of spontaneously self-assembling to form bilayer membranes. As previously mentioned, CuAAC between an alkyne-modified lysolipid (**17**) and an oleoyl azide (**16**) can be employed to efficiently construct a triazole-containing phospholipid (**18**; Figure 7.1A and Figure 7.2).[144,209] Alternatively, the NCL approach can be also utilized to rapidly form phospholipids from a cysteine-modified lysolipid (**19**) and a thioester derivative of oleic acid (**23**) to produce an amide-containing phospholipid (**21**; Figure 7.1A, Figure 7.3).[210] Both non-natural phospholipids (**18** and **21**) share many characteristics with native POPC,[144,209,210] including their structure, fluidity, and ability to encapsulate small molecules, thus leading us to hypothesize that the reconstitution of membrane proteins would be possible.

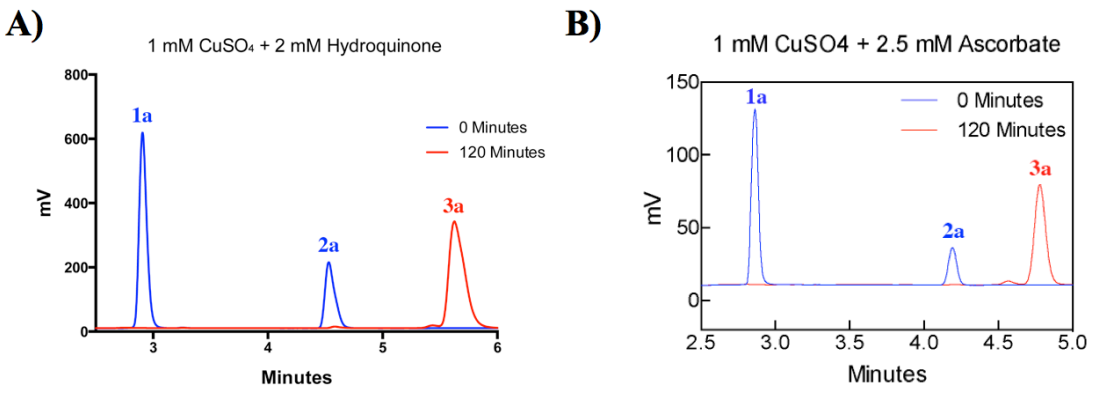

Figure 7.2 HPLC/ELSD spectra monitoring the progress of the CuAAC reaction. **A)** Using hydroquinone as reducing agent (for the reconstitution of CcO). **B)** Employing sodium *L*-ascorbate as reducing agent (for the reconstitution of MsbA or PMCA2). Retention times (R_t's) for lysolipid (**17**), oleoyl azide (**16**) and triazole phospholipid (**18**) were verified by mass spectrometry.

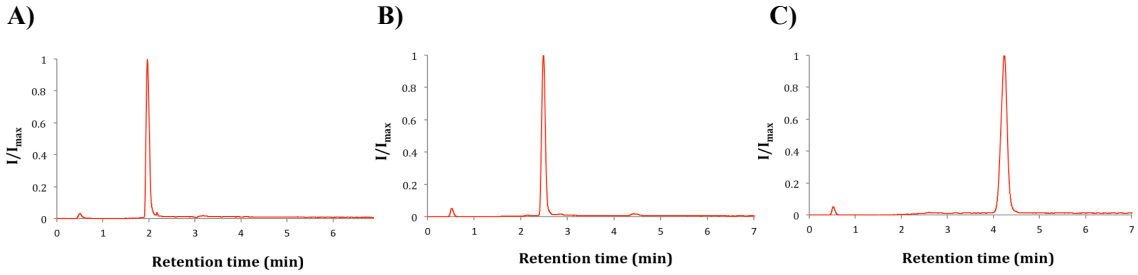

Figure 7.3 HPLC/ELSD spectra corresponding to lysolipid **19** (A), MESNA thiooleate **23** (B) and phospholipid **21** (C). Retention times (R_t's) were verified by mass spectrometry.

7.3 Reconstitution of cytochrome *c* oxidase

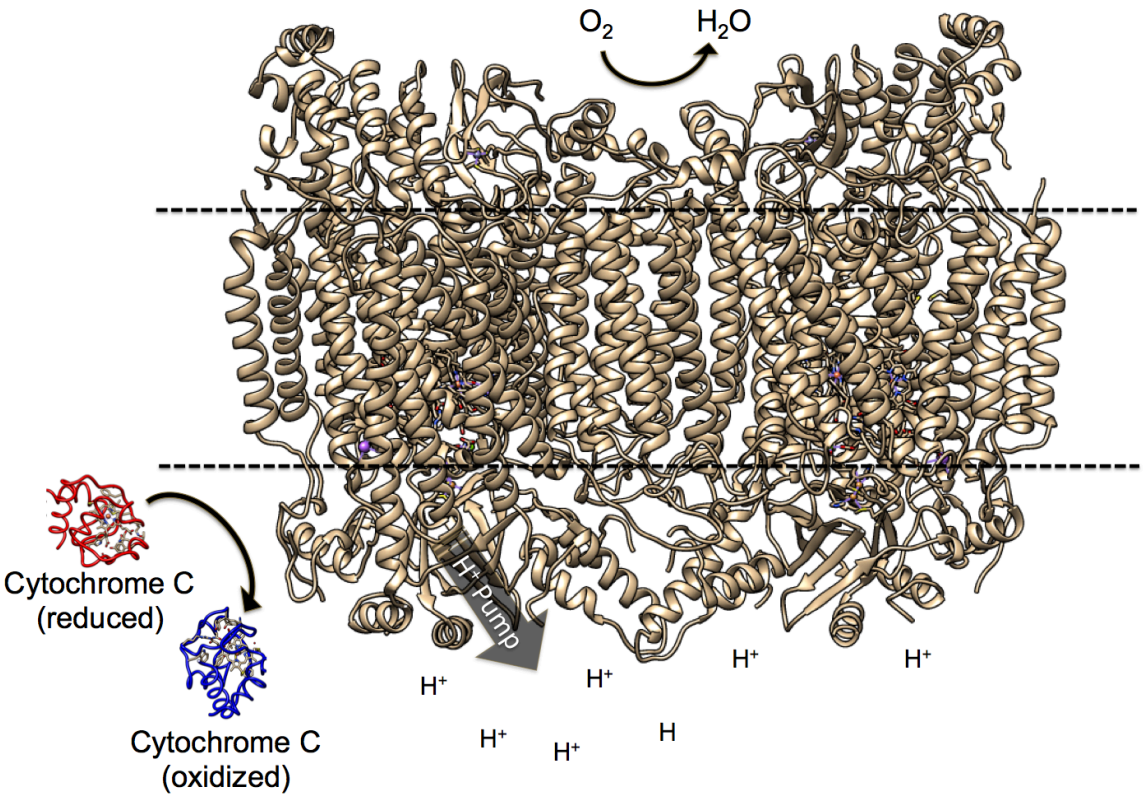

Figure 7.4 Ribbon Structure of CcO oxidizing its endogenous substrate cytochrome C. During this process diatomic oxygen is reduced to water and protons get shuttled across the membrane

The feasibility of incorporating transmembrane proteins during lipid preparation was demonstrated by synthesis of the triazole phospholipid **18** in the presence of commercially purified cytochrome *c* oxidase (CcO) from bovine heart.[214] The active CcO dimer is an approximately 200 kDa transmembrane protein complex found in bacteria and mitochondria.[214] CcO is the terminal protein in aerobic respiration, coupling the reduction of oxygen to proton pumping.[215] Despite its large size, CcO can be reconstituted in natural lipid membranes with minimal loss of

activity,[216] thus making it an appealing choice for initial proof-of-concept studies.

We first measured the activity of CcO by monitoring the decrease in absorbance of its substrate, cytochrome *c*, as it undergoes CcO catalyzed oxidation (Figure 7.4).[217] CcO was initially solubilized with *n*-dodecyl β-d-maltoside (DDM).[218] This detergent possesses stabilizing properties that can maintain 100 % of the CcO as a highly active monodisperse dimer.[218] Measurement of the activity of CcO in DDM was used as a positive control (Figure 7.5A, (+) DDM). We next removed the DDM with Bio-Beads SM-2[219] and overnight dialysis, which led to a significant drop in activity (Figure 7.5A, (−) DDM). CcO could be reconstituted into POPC liposomes by introducing POPC into the DDM–protein complexes (POPC/CcO molar ratio of 1400:1). The excess DDM detergent was then removed with Bio-Beads SM-2 and overnight dialysis to create functional proteoliposomes containing highly active CcO (Figure 7.5A, POPC). In situ triazole reconstitution was accomplished by first exchanging the DDM with the lysolipid **17**. The bioorthogonal CuAAC coupling reaction was carried out with an equimolar concentration of the oleoyl azide **16**, 1 mm $CuSO_4$, and 2 mm hydroquinone. After 2 h, the copper-catalyzed process resulted in

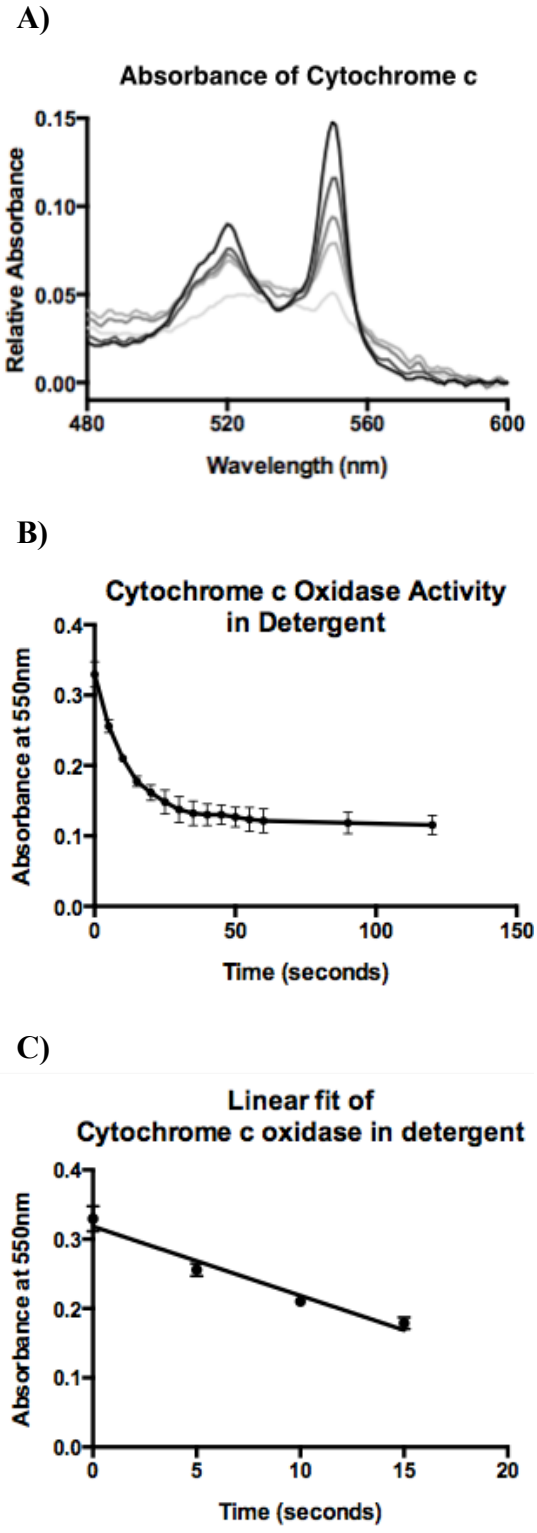

Figure 7.5 A) Representative absorbance scans showing the change in absorption of cytochrome *c* in the presence of 0.39 mM DDM with cytochrome *c* oxidase over an interval of 2 min. B**)** Absorbance at 550 nm plotted against time showing the kinetics of C*c*O in the presence of 0.39 mM DDM. C) Linear phase of C*c*O kinetics. The slope was used as the measure of the change in cytochrome *c* activity.

the formation of compound **18** and complete disappearance of **17**, as judged using combined liquid chromatography (LC), mass spectrometry (MS), and evaporative light scattering detection (ELSD) measurements (Figure 7.2). To further ensure that the observed CcO activity was not due to residual lysophospholipid detergent, the vesicles were treated with Bio-Beads SM-2 and dialyzed overnight. Remarkably, the activity of the CcO that was spontaneously reconstituted during triazole lipid synthesis closely mirrors the activity of CcO reconstituted in POPC by using the more traditional methods (Figure 7.5A, in situ CuAAC; Graph 7.1). This demonstrates that the bioorthogonal triazole reaction can spontaneously reconstitute active CcO into a bilayer. Solubilizing detergent is consumed during phospholipid formation and is thus eliminated. We estimated the yield of reconstituted CcO using the CuAAC methodology to be 3.0 μg, which corresponds to 60 % incorporation. CcO reconstitution using traditional methods and POPC gave us yields closer to 3.4 μg, which corresponds to 70 % incorporation.

Graph 7.1 Effect of sonication on CuAAC proteoliposomes with reconstituted C*c*O. Sonication of triazole liposomes further increases the observed activity, probably due to the breakup of multilamellar vesicles and the creation of smaller unilamellar vesicles, which facilitates the ability of cytochrome *c* to react with incorporated CcO.

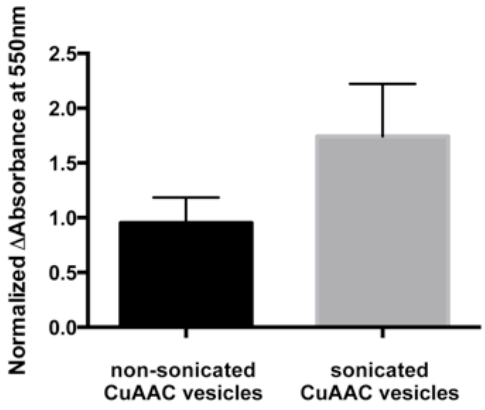

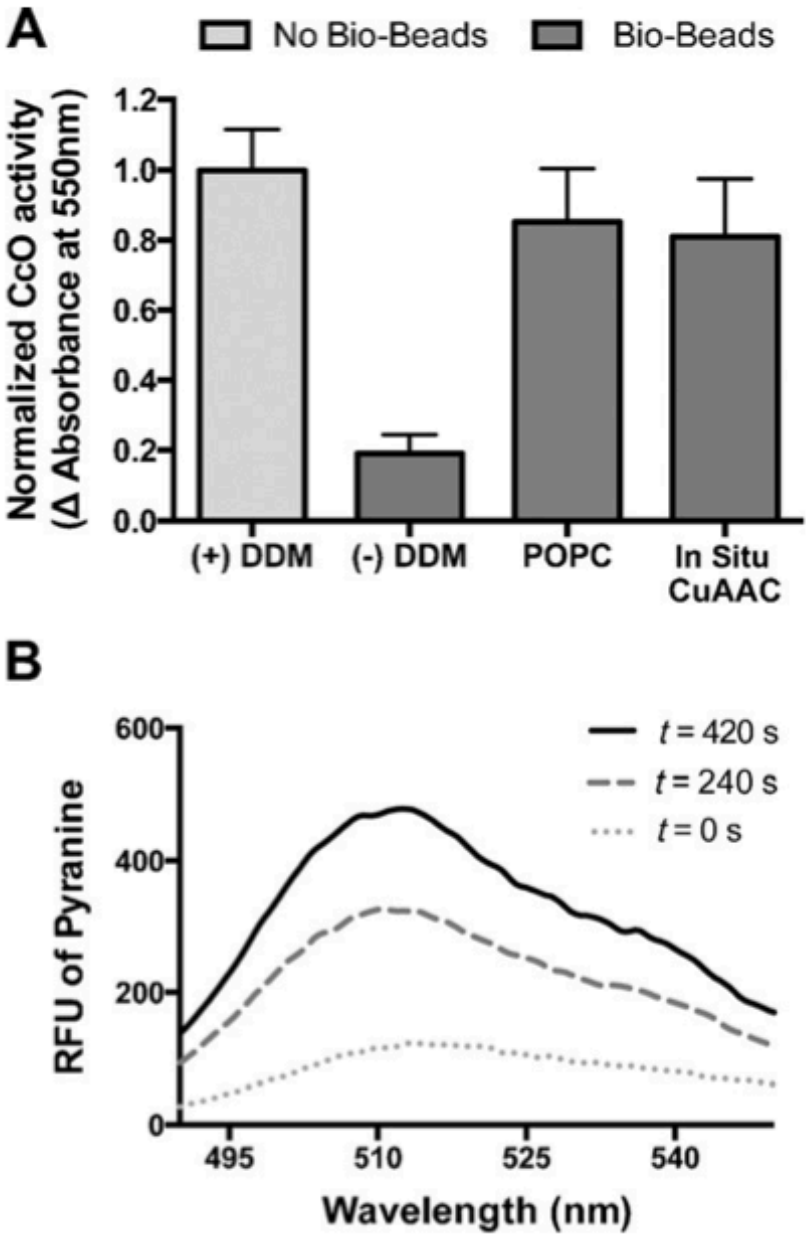

Figure 7.6 Characterization of CcO activity. A) Normalized activity of CcO determined by measuring the absorption peak of cytochrome *c* at 550 nm. (+) DDM: CcO activity as measured in *n*-dodecyl β-d-maltoside (DDM) [positive control]. (−) DDM: CcO activity in DDM following detergent removal using Bio-Beads SM-2 and dialysis [negative control]. POPC: CcO activity after reconstitution in POPC and the removal of detergent with Bio-Beads SM-2 and dialysis. In situ CuAAC: CcO activity after spontaneous reconstitution in the triazole-containing phospholipid membranes. As a precaution, membranes were treated with Bio-Beads SM-2 and dialyzed. B) Fluorescence in relative fluorescence units (RFUs) of the pH sensitive dye (pyranine) encapsulated in CcO proteoliposomes formed in situ by the CuAAC approach. Upon adding cytochrome *c*, there is a gain in fluorescence at 515nm, thus indicating that pyranine is being deprotonated as a result of the shuttling of protons across the membrane.

One of the advantages of studying proteins in well-defined membranes is the ability to evaluate functions that rely on the selective permeability of phospholipid membranes. Although we demonstrated that CcO retained its ability to oxidize cytochrome *c*, we were interested in analyzing whether the triazole membranes could support the proton-pumping function of CcO. Adapting a previously published procedure,[220] we employed the pH-sensitive dye pyranine on the inside of the in situ generated vesicles to test the proton-pumping activity of the transmembrane protein complex (Figure 7.5B). While monitoring fluorescence at 515 nm, cytochrome *c* was added. We observed an increase in fluorescence with time, which is indicative of protons being pumped across the membrane. This experiment demonstrates that CcO proton pumping remains functional and that the membranes formed via CuAAC coupling can maintain a proton gradient.

We next investigated the morphology and type of membrane structures formed during in situ bioorthogonal proteoliposome synthesis by using spinning-disk confocal microscopy (Figure 7.6, CcO; Figure 7.7). CcO was labeled using 10 equivalents of the AlexaFluor488 N-hydroxysuccinimide (NHS) ester before the maltoside detergent was exchanged with **17**. The fluorophore-modified CcO was then used for the in situ CuAAC coupling as previously described. After proteoliposome formation, the lipid-staining dye Texas Red DHPE was added at 1.0 mol %. As expected for a reconstituted membrane protein, we observed strong colocalization of CcO with Texas Red DHPE, thus indicating that CcO is primarily localized to the triazole-containing phospholipid membranes (Figure 7.6, CcO; Figure 7.7).

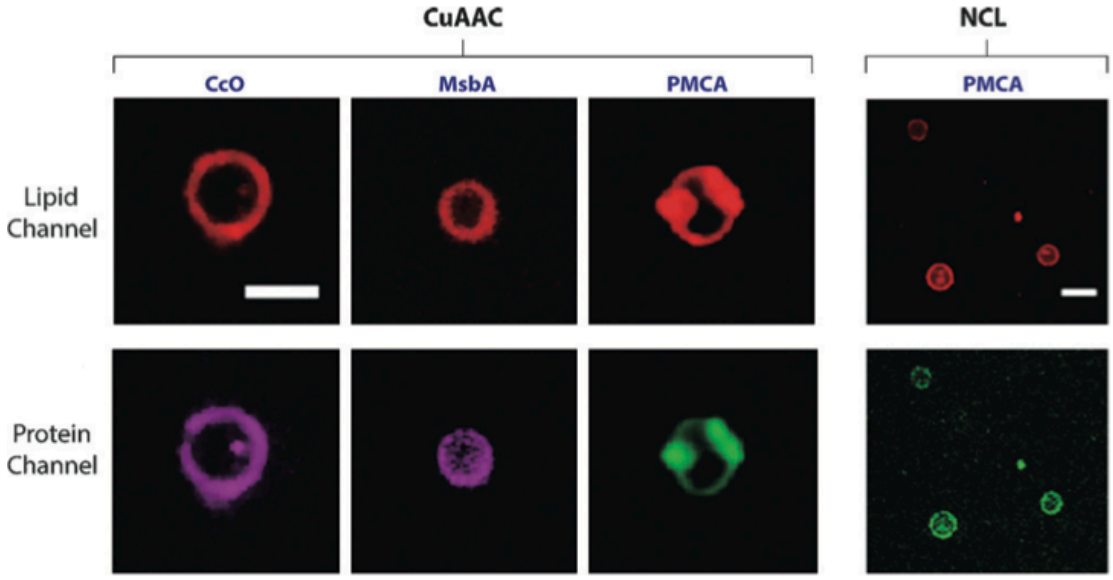

Figure 7.7 Spinning-disk confocal fluorescence microscopy images of spontaneously reconstituted proteoliposomes produced by using either CuAAC (left) or NCL (right). The lipid channel shows the location of the lipid membrane staining dye Texas Red DHPE. The protein channel shows the location of fluorescent transmembrane proteins [Proteins modified with AlexaFluor488 NHS ester (CcO and MsbA) or EGFP (PMCA2)]. CuAAC scale bar: 5 μm. NCL scale bar: 10μm.

7.4 Reconstitution of Membrane Proteins

Having shown that purified proteins could be spontaneously reconstituted, we next determined whether it would be possible to directly reconstitute membrane proteins overexpressed in bacteria into artificial membranes. To answer this question, we synthesized the membrane protein MsbA,[221–223] which is a member of a class of ABC transporters responsible for multiple-drug resistance, in *E. coli* cells. After protein production, cells were lysed and proteins were solubilized with 500 μm of reactive lysolipid **17**. Subsequent affinity purification allowed us to obtain the pure

protein, which was then modified by using 10 equivalents of the AlexaFluor488 NHS ester. The labeled protein/alkyne-lysolipid micelles were reacted by CuAAC with an equimolar concentration of oleoyl azide **16**. Fluorescently modified MsbA showed excellent colocalization with the synthetic membrane, thus indicating that the protein can be reconstituted successfully into proteoliposomes directly from cell lysate (Figure 7.6, MsbA).

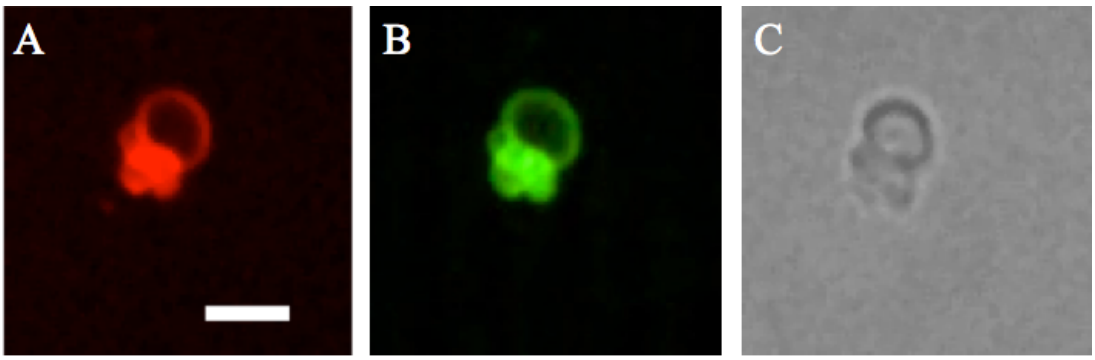

Figure 7.8 Spinning disk confocal microscopy of spontaneously reconstituted C*c*O proteoliposomes using the CuAAC methodology. **A)** Fluorescence microscopy image of a C*c*O proteoliposome. Membranes were stained using 1 μM Texas Red® DHPE dye solution. **B)** Fluorescence microscopy image of a C*c*O proteoliposome fluorescently modified with AlexaFluor® 488-NHS ester. **C)** Phase contrast image of a CcO proteoliposome, showing a darken bilayer. Scale bar denotes 5 μm.

As a final test, we reconstituted a mammalian plasma membrane calcium ATPase fusion protein (PMCA2-EGFP) into proteoliposomes (Figure 7.6, PMCA).[224,225] Calcium ATPases are key components in the regulation of cellular calcium ion homeostasis and signaling.[226] Owing to its ten membrane-spanning segments, PMCA2 can be a challenging protein to reconstitute into membranes.[227]

Furthermore, expression is typically performed in mammalian cells, which often results in unsatisfactory protein yields.[228] We utilized a recombinant PMCA2 fused to EGFP to aid in visualizing membrane incorporation.[229] HeLa cells expressing the protein were physically lysed, and high-speed centrifugation was used to collect the insoluble membrane fraction, which was solubilized with 600 μm of alkyne lysolipid **19**. The His-tagged protein was then purified using Ni-NTA resin. The elution buffer contained 300 mM imidazole in order to elute the PMCA2-EGFP. However, we found that the protein required extensive washing to remove free imidazole, since millimolar concentrations of imidazole can coordinate the copper catalyst and inhibit the CuAAC reaction. The incompatibility of CuAAC with high concentrations of imidazole is a limitation when working with His-tagged proteins. However, after the removal of excess imidazole, CuAAC was successfully used to reconstitute the mammalian protein (Figure 7.6, CuAAC/PMCA).

Since it would be useful to enable spontaneous proteoliposome formation in the presence of imidazole, we explored the reconstitution of PMCA2 into synthetic membranes produced through NCL. NCL does not require metal catalysts and is compatible with high concentrations of imidazole.[230] Reconstitution of PMCA2 by using NCL was performed in a similar manner to that described above, except that 600 μm of compound **19** was used for solubilization. After elution from the Ni-NTA resin, the NCL reaction was initiated by addition of equimolar amounts of oleoyl thioester **23** in the presence of 10 mm DTT. In situ vesicle formation took place and PMCA2-EGFP incorporation was verified by fluorescence microscopy (Figure 7.6, NCL PMCA).

PMCA2 is a complex transmembrane protein that has been previously shown to mediate transient current fluctuations of calcium ions across membranes.[224,225] To determine whether PMCA2-EGFP was active within membranes composed of amide-containing phospholipid **21**, we monitored calcium ion transport by using a standard black lipid membrane (BLM) setup (Figure 7.8 and Figure 7.9).[231,232] A bilayer of phospholipid **21** in *n*-decane was painted onto a Teflon pore separating two aqueous chambers as described previously.[233,234] The painted membranes formed from phospholipid **21** were stable for at least 2 h and exhibited a constant membrane capacitance of approximately 60 pF. This membrane capacitance value provides an estimate for the membrane thickness of approximately 3 nm,[235] which suggests that **21** forms a single bilayer rather than a multilayered structure in these BLM experiments. The BLM studies also demonstrate that the membrane characteristics of synthetic phospholipid **21** are comparable to those of other typical phospholipids in terms of the formation of stable suspended lipid bilayers.[236,237] After determining that the suspended membranes formed from **21** are stable, PMCA2-EGFP proteoliposomes were then fused with the bilayer. To verify that PMCA2 could mediate a flux of calcium ions across the membrane, we monitored the current versus time across the membrane in the presence of an 80 mV applied potential and observed transient ion current fluctuations that resembled previously reported ion current events from purified PMCA2 in proteoliposomes (Figure 7.8 and Figure 7.9).[224,225] Measurement of the current at different applied potentials revealed at least two conductance states for PMCA2-EGFP under our recording conditions, with estimated conductance values of 10 and 31 pS (Figure 7.9). These conductance values are similar to previously

reported divalent conductance states of PMCA2 as estimated from patch-clamp recordings.[238] On the other hand, when Na^+ ions were introduced to the recording media instead of Ca^{2+} ions, no ion-current events were observed under the same recording conditions (Figure 7.8B and Figure 7.9). These BLM recording experiments

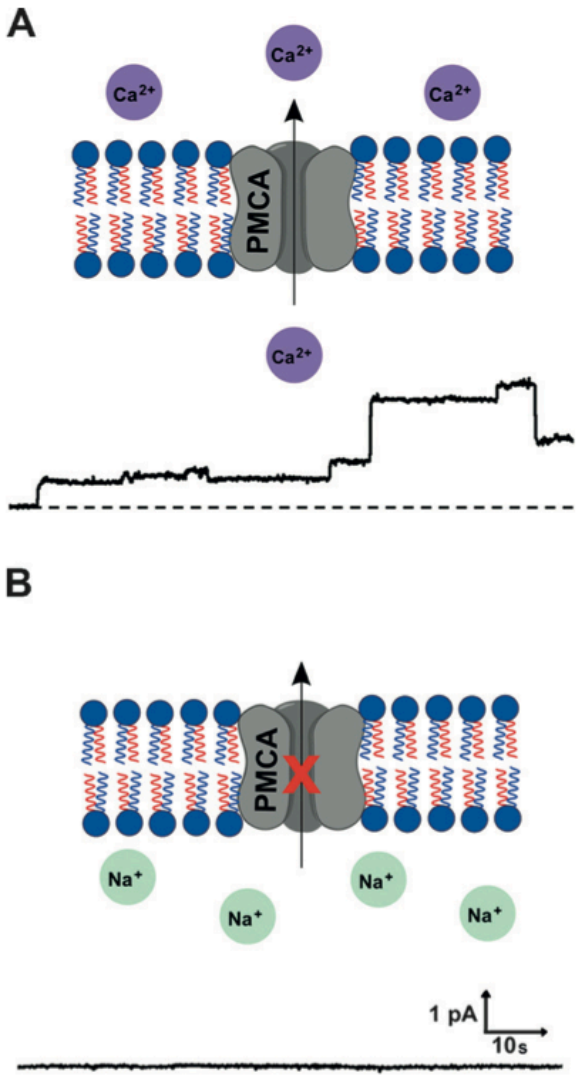

Figure 7.9 Monitoring the activity of the selective calcium ion transport protein PMCA2 by measuring the change in conductance across a planer lipid bilayer. A) The flux of Ca2+ through PMCA2 was observed in a black lipid membrane (BLM) system with synthetic phospholipid 3 b. Ca2+ ion flux across the membrane mediated by PMCA2 was measured under an applied potential of 80 mV. B) In comparison, no ion current events were observed when Ca2+ ions were replaced by Na+ ions in the recording medium. The dashed line in A corresponds to the current trace in B.

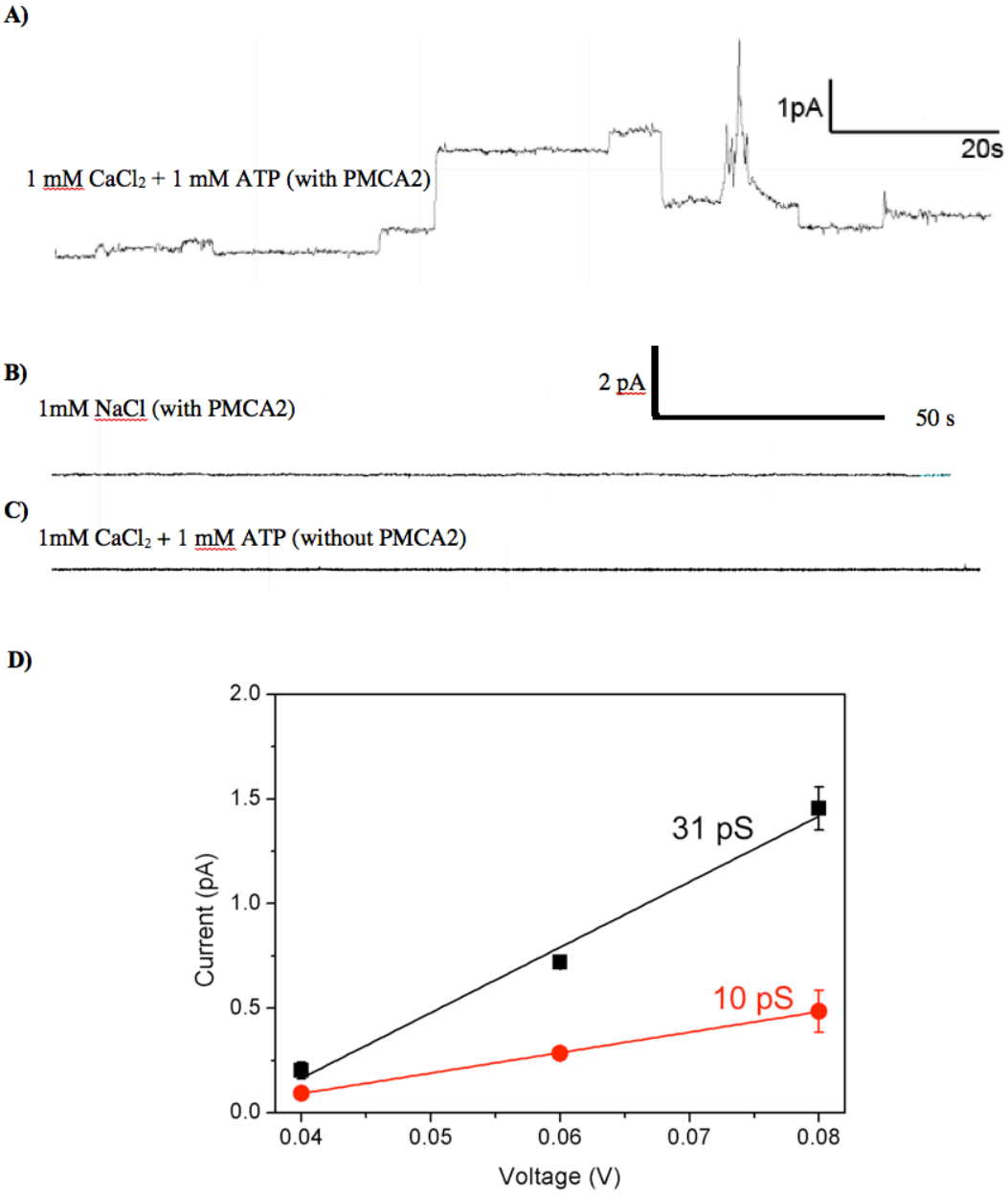

Figure 7.10 A) Planar lipid experiment done by painting compound **21** onto a Teflon® pore and fusing NCL formed proteoliposomes containing PMCA2 with an applied voltage of 80mV in the presence of 1 mM ATP and 1 mM $CaCl_2$. **B)** Negative control using 1 mM NaCl instead of $CaCl_2$. **C)** Membranes comprised of **3b** were stable and quiescent for hours in the presence of 1 mM ATP and 1 mM $CaCl_2$, but lacking PMCA2. **D)** Current-voltage (I-V) curves for two observed conductance states of PMCA2-EGFP.

demonstrate that PMCA2-EGFP retains its ability to mediate the transport of calcium (and not sodium) ions when embedded in synthetic membranes formed through NCL.

7.5 Concluding Remarks

In summary, we have explored the suitability of bioorthogonal coupling reactions for driving the in situ formation phospholipid membranes and concomitant spontaneous reconstitution of functional membrane proteins. This method should be compatible with alternative reactive lipids to create specific compositions of lipid membranes. Additionally, lysolipid derivatives could be used to solubilize and incorporate natural lipids. We are currently exploring the in situ synthesis of more-complex lipid membranes, as well as developing a small library of lysolipid and thioester detergents that can be used to optimize the reconstitution of alternative membrane proteins. We foresee biotechnological applications that make use of the spontaneous reconstitution of transport proteins to control the composition inside synthetic cells, which could be used as chemical microreactors or biosensors.

7.6 Experimental and Methods

7.6.1 Materials

Commercially available 1-palmitoyl-2-hydroxy-*sn*-glycero-3-phosphocholine and 1-palmitoyl-2-oleoyl-*sn*-glycero-3-phosphocholine (POPC) were used as obtained from Avanti® Polar Lipids. 4-pentynoic acid, oleoyl bromide, sodium azide, N-Boc-Cys(Trt)-OH, *N,N'*-diisopropylcarbodiimide (DIC), 4-dimethylaminopyridine (DMAP), trifluoroacetic acid (TFA), triethylsilane (TES), oleic acid, *N*-(3-dimethylaminopropyl)-*N'*-ethylcarbodiimide hydrochloride (EDC.HCl), sodium 2-mercapto-ethanesulfonate (MESNA), dithiothreitol (DTT), phenylmethylsulfonyl fluoride (PMSF), 4-(2-hydroxyethyl)piperazine-1-ethanesulfonic acid (HEPES) sodium salt, *n*-dodecyl β-D-maltoside (DDM), 8-hydroxypyrene-1,3,6-trisulfonic acid (pyranine), cytochrome *c* and cytochrome *c* oxidase (C*c*O) were obtained from Sigma-Aldrich. Texas Red® 1,2-dihexadecanoyl-*sn*-glycero-3-phosphoethanolamine, triethylammonium salt (Texas Red® DHPE), Penicillin-Streptomycin and Alexa Fluor® 488 NHS Ester were obtained from Life Technologies. Bio-Beads® SM-2 was obtained from Bio-Rad. Isopropyl β-D-thiogalactoside (IPTG) was obtained from Teknova. McCoy's 5A high glucose media was purchased from Corning Cellgro. *L*-Glutamine was obtained from Carl Roth. Fetal bovine serum (FBS) was purchased from Thermo Fisher Scientific Inc. Deuterated chloroform ($CDCl_3$), methanol (CD_3OD) and dimethyl sulfoxide (d_6-DMSO) were obtained from Cambridge Isotope Laboratories. All reagents obtained from commercial suppliers were used without further purification unless otherwise noted. Analytical thin-layer chromatography was

performed on E. Merck silica gel 60 F_{254} plates. Compounds, which were not UV active, were visualized by dipping the plates in a ninhydrin or potassium permanganate solution and heating. Silica gel flash chromatography was performed using E. Merck silica gel (type 60SDS, 230-400 mesh). Solvent mixtures for chromatography are reported as v/v ratios. HPLC analysis was carried out on an Eclipse Plus C8 analytical column with *Phase A*/*Phase B* gradients [*Phase A*: H_2O with 0.1% formic acid; *Phase B*: MeOH with 0.1% formic acid]. HPLC purification was carried out on Zorbax SB-C18 semipreparative column with *Phase A*/*Phase B* gradients [*Phase A*: H_2O with 0.1% formic acid; *Phase B*: MeOH with 0.1% formic acid]. Proton nuclear magnetic resonance (^{1}H NMR) spectra were recorded on a Varian VX-400 MHz, Varian VX-500 MHz or Jeol Delta ECA-500 MHz spectrometers, and were referenced relative to residual proton resonances in $CDCl_3$ (at 7.24 ppm), CD_3OD (at 4.87 or 3.31 ppm) or d_6-DMSO (at 2.50 ppm). Chemical shifts were reported in parts per million (ppm, d) relative to tetramethylsilane (d 0.00). ^{1}H NMR splitting patterns are assigned as singlet (s), doublet (d), triplet (t), quartet (q) or pentuplet (p). All first-order splitting patterns were designated on the basis of the appearance of the multiplet. Splitting patterns that could not be readily interpreted are designated as multiplet (m) or broad (br). Carbon nuclear magnetic resonance (^{13}C NMR) spectra were recorded on a Varian VX-400 MHz, Varian VX-500 MHz or Jeol Delta ECA-500 MHz spectrometers, and were referenced relative to residual proton resonances in $CDCl_3$ (at 77.23 ppm), CD_3OD (at 49.15 ppm) or d_6-DMSO (at 39.51 ppm). Electrospray Ionization-Time of Flight (ESI-TOF) spectra were obtained on an Agilent 6230 Accurate-Mass TOFMS mass spectrometer. Fluorescence measurements

were performed on a LS 55 fluorescence spectrometer using a single cuvette reader. Absorbance readings were measured on a ThermoScientific NanoDrop 2000c UV-Vis spectrophotometer.

See Chapter 5 for synthesis of oleoyl azide (**16**), 1-palmitoyl-2-[pent-4-ynoyl]-*sn*-glycero-3-phosphocholine (**17**), Triazole phospholipid 1-palmitoyl-2-[triazole-(oleoyl)]-*sn*-glycero-3-phosphocholine (**18**)

See Chapter 6 for synthesis of 1-palmitoyl-2-(*L*-Cys)-*sn*-glycero-3-phosphocholine (**19**), Amidophospholipid 1-palmitoyl-2- [*L*-Cys-(oleoyl)]-*sn*-glycero-3-phosphocholine (**21**), 1-palmitoyl-2-[N-Boc-*L*-Cys(Trt)]-*sn*-glycero-3-phosphocholine (**22**), MESNA thiooleate (**23**),

7.6.2 Spectroscopic Cytochrome c Oxidase Activity Assay

Cytochrome c reduction: Reduced cytochrome *c* was prepared by dissolving 100.0 mg of cytochrome *c* in 8 mL of 20 mM HEPES pH 7.0 buffer containing 4.0 mg of sodium *L*-ascorbate. The excess ascorbate was removed by dialyzing in 2 L of 20 mM HEPES pH 7.0 buffer with two exchanges over a 16 h period. The sample was brought up to 10 mL to give a final concentration of 0.83 mM reduced cytochrome *c*.

Cytochrome c oxidase labeling: C*c*O was labeled using 10 equivalents of Alexa Fluor® 488 NHS Ester in 20 mM HEPES pH 8.2 buffer for 2 h at rt. The modified protein was then washed with 20 mM HEPES pH 7.5 buffer, 150 mM NaCl and 400 μM of compound **17** in a spin column.

Cytochrome c oxidase activity: CcO activity was measured spectrophotometrically by quantifying the change in absorbance of reduced

cytochrome *c* at 550 nm. To calculate incorporation we assume activity of CcO to be 20 units / mg protein and the unit definition is 1 unit CcO will oxidize 1.0 μmole of cytochrome c per min. at 25 °C.

The positive control sample [*(+) DDM*] contained 100 mU of cytochrome *c* oxidase in 20 mM HEPES pH 7.5 buffer containing 0.39 mM *n*-dodecyl β-D-maltoside (DDM). A final concentration of 140 μM of cytochrome *c* was added to the cuvette and measurements were immediately made at 5 s intervals during the linear phase of cytochrome *c* oxidase.

The negative control sample [*(-) DDM*] was prepared by incubating the *(+) DDM* for 2 h with 30.0 mg of pre-washed Bio-Beads® SM-2. Bio-Beads SM-2® were then washed with 2-3 volumes of MeOH, distilled H_2O, and 20 mM HEPES pH 7.5. This was followed by overnight dialysis in 20 mM HEPES pH 7.5. The *(-) DDM* sample was then measured as previously described for the *(+) DDM* sample. The POPC sample (*POPC*) was prepared by first incubating the *(+) DDM* for 2 h with 150.0 mg of pre-washed Bio-Beads® SM-2 and 400 μM of POPC, followed by overnight dialysis in 20 mM HEPES pH 7.5 buffer. Prior to measuring, the vesicles were sonicated in a bath sonicator for 30 min.

7.6.3 Spectroscopic Cytochrome c: *In situ* CUAAC

In situ copper catalyzed azide alkyne cycloaddition reconstituted sample (*in situ CuAAC*) was accomplished by exchanging the DDM with compound **17**. This was done by lowering the concentration of DDM near its critical micelle concentration (cmc) (0.17 mM) with Bio-Beads® SM2 for 2 h as previously described, and then

using a spin filter to exchange the DDM with 400 μM of **17**. Once exchanged, the coupling reaction was carried out with equal molar of compound **16**, 1 mM $CuSO_4.5H_2O$, and 2 mM hydroquinone. After 2 h, the copper catalyzed cycloaddition resulted in the formation of compound **18**. This was also dialyzed overnight to remove any remaining DDM. Before measuring the C*c*O activity in the vesicles, they were sonicated for 30 min. Additional $CuSO_4.5H_2O$ solution was then added (final concentration: 1 mM) to replace any Cu(II) that may have been reduced in the active site of C*c*O during CuAAC. Appropriate control experiments showed that this additional amount of $CuSO_4.5H_2O$ did not change the activity of C*c*O.

7.6.4 Cytochrome c Oxidase Proton Pump Activity

POPC/Bio-Beads® SM-2 methodology (Traditional methodology): 10 mL of a 20 mM solution of POPC in $CHCl_3$ was added to a 1 mL vial, placed under N_2 and dried for 15 min to prepare a lipid film. Then, 200 mL of *hydrating buffer* [5 mM HEPES pH 7.1, 10 mM pyranine, 0.5 U C*c*O and 3.9 mM DDM] was added and the solution was tumbled for 2 h at rt. Afterward, the DDM was removed by incubating the resulting solution for 2 h with pre-washed Bio-Beads® SM-2. The corresponding proteoliposomes were then washed with 5 mM HEPES pH 7.1 buffer containing 10 mM glucose, and centrifuged in a 100 kDa spin filter (6 × 5 mL). The mixture was subsequently added to a quartz cuvette and the C*c*O pump activity was directly measured by monitoring the fluorescence at 515 nm. Finally, 10 μL of the previously prepared reduced cytochrome *c* solution was added, and then immediately fluorescence scans were acquired every 30 s. Control experiments were performed

demonstrating that reduced cytochrome *c* in the presence of pyranine had no observable change in fluorescence without C*c*O proteoliposomes.

CuAAC methodology: C*c*O (1.0 U) was initially exchanged with 1 mL of *exchanging buffer* [5 mM HEPES pH 7.1, 1 mM $CuSO_4.5H_2O$, 2 mM hydroquinone and 1 mM lysolipid **17**]. The protein was then mixed with a stock solution of pyranine (final concentration: 35 mM) and 1 mM of oleoyl azide **16**. The mixture was subsequently tumbled for 2 h at rt. The corresponding proteoliposomes were then washed with 5 mM HEPES pH 7.1 buffer containing 38 mM glucose, and centrifuged in a 100 kDa spin filter (6 × 3 mL). The mixture was subsequently added to a quartz cuvette and the C*c*O pump activity was directly measured by monitoring the fluorescence at 515 nm. Finally, 10 μL of the previously prepared reduced cytochrome *c* solution was added, and then immediately fluorescence scans were acquired every 30 s. Control experiments were performed demonstrating that reduced cytochrome *c* in the presence of pyranine had no observable change in fluorescence without C*c*O proteoliposomes.

7.6.5 MsbA Expression and Purification

The MsbA pET19b plasmid[239] was initially transformed into Rosetta™ (DE3) Competent Cells (Novagen) and an overnight cell culture was grown at 37 °C in Luria-Bertani (LB) broth, supplemented with 100 μg/mL ampicillin. This was used to inoculate a 4 L culture of fresh medium. Cells were grown at 37 °C until the O*D*600 reached ≈ 0.6 A. MsbA overexpression was then induced by the addition of 1 mM IPTG. The cells grew for an additional 4 h at 37 °C, and then were harvested by

centrifugation at 10000 *g* for 10 min at 4 °C. Cell pellets were re-suspended in *lysis buffer* [50 mM HEPES pH 7.5, 150 mM NaCl, 5 mM DTT, 400 μM **17** and 1 mM PMSF], and passed through a French pressure cell disrupter at 1200 psi. Cell debris was removed by centrifugation at 15000 *g* for 20 min at 4 °C. The supernatant was incubated for 2 h at 4 °C with Ni-NTA (Ni^{2+}-nitrilotriacetate) agarose pre-equilibrated with *wash buffer* [50 mM HEPES pH 7.5, 150 mM NaCl, 400 μM **17** and 10 mM imidazole]. After incubation, the resin was washed in a gravity column with 3 volumes of wash buffer. MsbA was eluted with *elution buffer* [50 mM HEPES pH 7.5, 150 mM NaCl, 400 μM **17** and 300 mM imidazole]. Fractions containing MsbA, as determined by SDS/PAGE analysis and coomassie blue staining, were pooled and washed to remove traces of imidazole.

7.6.6 MsbA Labeling and Reconstitution into Proteoliposomes

Purified MsbA was labeled using 10 equivalents of Alexa Fluor® 488 NHS Ester in 50 mM HEPES pH 8.2 buffer for 2 h at rt. The protein solution was then washed with 50 mM HEPES pH 7.5, 150 mM NaCl and 400 μM of compound **17** in a spin column. Alexa Fluor® 488 modified MsbA was diluted to a final concentration of 0.4 μM with 50 mM HEPES pH 7.5, 150 mM NaCl, and 400 μM **17**. To reconstitute MsbA into proteoliposomes, 100 ml of previously Alexa Fluor® 488 modified MsbA solubilized with **17** micelles was reacted with 400 μM of **16,** 1 mM $CuSO_4.5H_2O$, and 2 mM hydroquinone for 2 h at rt.

7.6.7 Cell Culture Conditions

HeLa cells were cultured in McCoy's supplemented media with 2 mM *L*-Glutamine, 10% FBS, 100 U/mL penicillin, and 100 μg/mL streptomycin. Cultures were incubated at 37 °C with 5% CO_2 and 95% humidity.

7.6.8 PMCA2 Purification

HeLa cells were grown to ≈ 90% confluency and transfected with EGFP-hPMCA2z/b plasmid,[240],with Lipofectamine® 2000 following the manufacturer's instructions. After 2 days, the cells were physically detached using a rubber policeman, and counted with the Countess® (Invitrogen), yielding ≈ $5.1x10^6$ cells. Cells were then centrifuged and the supernatant discarded. Cells were kept on ice for the remaining procedure. Cells were then re-suspended in 1 mL of *lysis buffer* [20 mM HEPES, 100 mM NaCl, SIGMAFAST™ Protease Inhibitor Tablet, and 1 mM DTT], and lysed with a homogenizer or vortexing with glass beads for 10 min. The mixture was ultracentrifuged at 130000 *g* for 2 h. The supernatant was discarded and the pellet was placed on a magnetic stirrer with either 500 μl of *solubilization buffer CuAAC* [20 mM HEPES, 100 mM NaCl, SIGMAFAST™ Protease Inhibitor Tablet, 1 mM DTT, 10 mM imidazole and 500 μM **17**] or *solubilization buffer NCL* [20 mM HEPES, 100 mM NaCl, SIGMAFAST™ Protease Inhibitor Tablet, 1 mM DTT, 10 mM imidazole and 600 μM **19**] for 6 h. The solution was left for an additional 2 h or overnight with Ni-NTA agarose pre-equilibrated with the corresponding solubilization buffer for batch binding. The resin was washed with 3 volumes of solubilization buffer *via* gravity column, and then eluted with the solubilization buffer containing 300 mM

imidazole. In the case of the CuAAC methodology (using compound **17** as a detergent), the protein needed to be washed 10 times using a spin column with 20 mM HEPES, 100 mM NaCl, 1 mM DTT, and 500 μM **17**, to remove excess imidazole. In the case of the NCL methodology (using compound **19** as a detergent), no additional washes to remove excess imidazole were performed.

7.6.9 PMCA2 Reconstitution

CuAAC methodology: To reconstitute purified PMCA2 into CuAAC proteoliposomes, the micelle-solubilized protein (PMCA2-**17**) (final concentration of lysolipid **17**: 500 mM) was reacted with 1 mM $CuSO_4.5H_2O$, 2.5 mM sodium *L*-ascorbate and 500 μM oleoyl azide (**16**) for 2 h at rt. The concentration of PMCA2 was adjusted to maximize fluorescent signal without forming protein/lipid aggregations as observed with microscopy.

NCL methodology: To reconstitute purified PMCA2 into NCL proteoliposomes, the micelle-solubilized protein (PMCA2-**19**) (final concentration of lysolipid **19**: 600 mM) was reacted with a 600 mM solution of MESNA oleoyl thioester (**23**) in the presence of 20 mM HEPES pH 7.5 buffer containing 10 mM DTT and 300 mM imidazole for 20 min at rt.

7.6.10 Fluorescence Microscopy

Images were acquired on a Yokagawa spinning disk system (Yokagawa, Japan) built around an Axio Observer Z1motorized inverted microscope (Carl Zeiss Microscopy GmbH, Germany) with a 63x, 1.40 NA oil immersion objective to an

Evolve 512x512 EMCCD camera (Photometrics, Canada) using ZEN imaging software (Carl Zeiss Microscopy GmbH, Germany). Fluorophores were excited with a 561 nm, 40 mW DPSS laser and a 488 nm, 100 mW OPSL laser. Large un-sonicated vesicles were chosen to highlight the fluorescent membrane stain of the proteins. However, the mixtures consist of a heterogeneous population of vesicles with the majority being small vesicles.

7.6.11 Measurement of Ion Transport Across Planar Lipid Bilayers

The "painting method" was used for formation of planar lipid membrane by dissolving phospholipid **21** in *n*-decane (final concentration: 10 mg mL^{-1}). We used a customized Teflon® chamber with two 4 mL wells separated by a thin Teflon® film containing a100 μm pore. The aperture was pre-treated by a drop of 10 mg mL^{-1} phospholipids **21** in *n*-decane and dried under vacuum before membrane formation. 10 mM HEPES buffer containing 150 mM KCl, pH 7 with either 1 mM $CaCl_2$ or NaCl were first filled into both parts of the chamber symmetrically. To check the membrane stability for every measurement, 80 mV was applied for 10 min before adding PMCA2 proteoliposomes with 1 mM ATP on one side of the chamber. The solution was stirred using a small magnetic bar (SPIN-2, Warner Instruments) for 15-20 min. Ion transport across the membrane was monitored in voltage clamp mode using Ag/AgCl electrodes (Warner Instruments). Data was acquired by customized software connected to the patch clamp amplifier (Warner Instruments, 10 mV pA-1 gain and 3 kHz cutoff filter). When Ca^{2+} ions were in the solution, we observed PMCA2 ion transport activity in the

presence of an applied voltage. Conversely when Na^+ ions were added into the recording media (instead of calcium ions) no channel activity was observed.

7.6.12 Future Directions

Membrane proteins are the key regulators of communication between cellular compartments, functioning primarily as receptors and transporters[197]. They also determine the distinctive architecture and adhesion properties of cells[197,241]. Loss of their function can lead to numerous disease states, including metabolic dysfunction[202], neurodegenerative diseases[203], and cardiovascular diseases,[242] thus making them the major target of the pharmaceutical industry[201]. Although the proteome is comprised of approximately 25% membrane proteins, less than 1% have known structures in the Protein Data Bank.[243] The lack of structural insight is one of the major challenges associated with the study of membrane proteins and has motivated the need to develop additional characterization tools.

We have demonstrated successful transmembrane protein reconstitution using the CuAAC precursors; oleoyl azide **16** / alkyne lysophosphatidylcholine **17** and the NCL precursors; cysteine lysolipid **19** / thioester **23**; however, both employ a lysophospholipid mimic acting as the detergent to solubilize the membrane proteins. This is far less than ideal considering lysophospholipids, in general, are poor detergents for the isolation of membrane proteins. Their cmc ranges between 4-20 μM, this particularly low cmc results in their intrinsic ability to make micelles before fully solubilizing the protein. As consequence this requires excess lysophospholipid to saturate the binding capacity of the protein in order to obtain micelle-solubilized

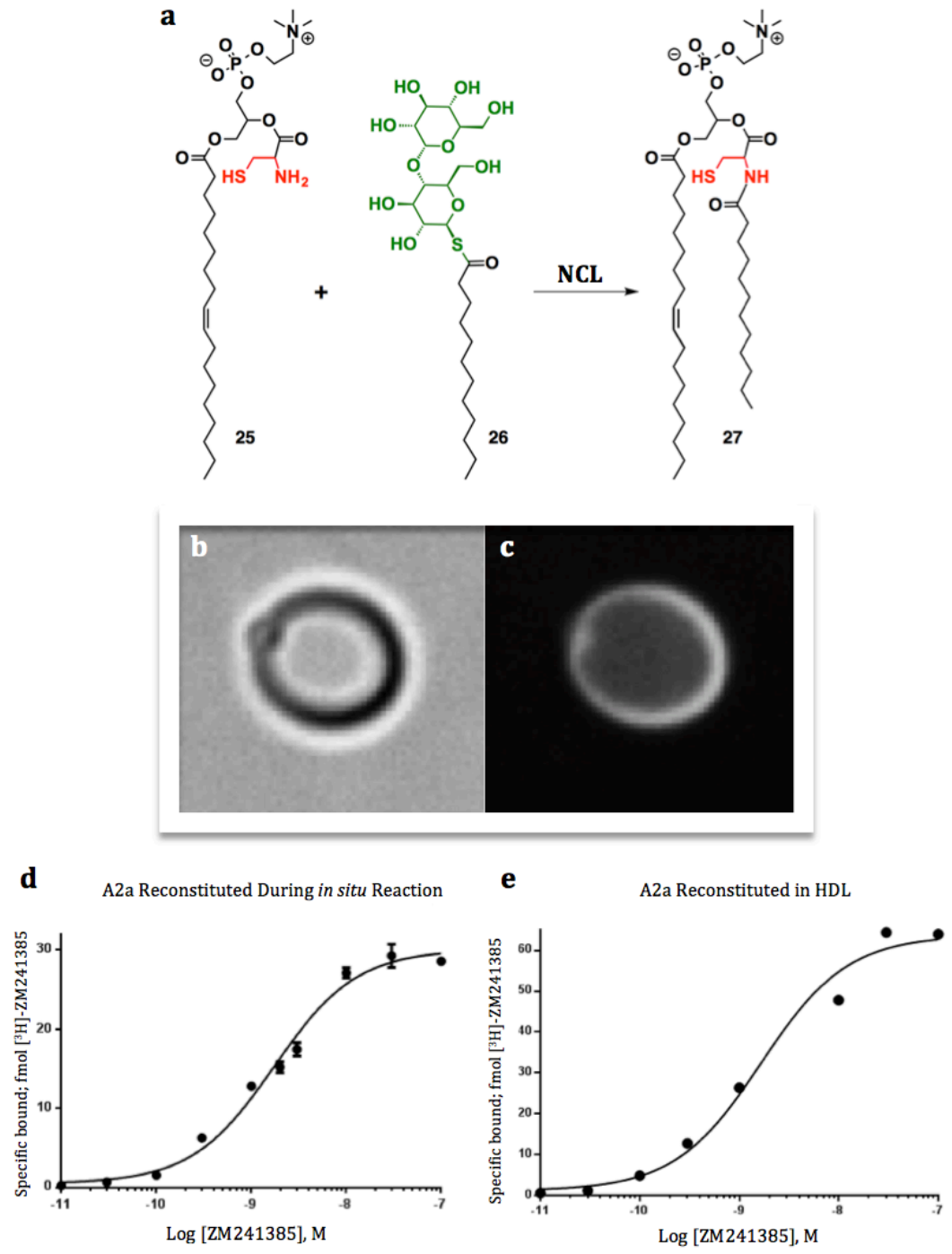

Figure 7.11 a) Scheme of NCL reaction between a C-18 cysteine lysophospholipid (**25**) and a C-12 DDM analogue modified with a thioester linkage (**26**) to produce the membrane forming product (**27**). b-c) Reconstituted A2a protein that was labeled with a 488 nm NHS-ester dye. The liposome was visualized in phase contrast (b) and fluorescence (c), illustrating membrane staining. d) Binding assay of A2a with its antagonist ZM241385 after *in situ* reconstitution and (e) in HDL particles, which is the current gold standard for activity assays. The curves show good agreement only differing in their EC_{50} by ± 0.06 nM

protein. Furthermore, if the lysophospholipid's head group is ionic or zwitterionic it has a greater potentially of denaturing a protein of interest, thereby abolishing its native function.

N-dodecyl-β-D-maltoside (DDM) is a glycosidic surfactant, increasingly employed in transmembrane protein isolations, especially when protein activity needs to be preserved. It was previously demonstrated to be more efficient than CHAPS, or NP-40.[244] Correspondingly, we designed a DDM thioester precursor to be utilized with the NCL methodology (Figure 7.11) to achieve high yielding protein reconstitution by improving both the solubilization and stability of the membrane proteins.

Notes about the Chapter:

Chapter seven, in part, is a reprint (with co-author permission) of the material as it appears in the publication; **Cole C.M.**, Brea R.J., Kim Y.H., Hardy M.D., Yang J., Devaraj N.K. "Spontaneous Reconstitution of Functional Transmembrane Proteins During Bioorthogonal Phospholipid Membrane Synthesis" *Angew. Chem. Int. Ed.*, 2015, 54(43), 12738-12742. I would like to thank Roberto Brea, Young Hun Kim, Michael Hardy, Hoaxing Wu, Jerry Yang and Neal Devaraj for their invaluable contributions to this chapter: Roberto Brea assisted in the synthesis of the NCL compounds; Young Hun Kim preformed the electrophysiology experiments; Michael Hardy assisted in the purification of compound **16** and **17**; Hoaxing Wu did the original CuAAC synthesis; I would like to thank Jerry Yang and Neal Devaraj for directing the research. The author of the dissertation is the primary author of this manuscript.

For the “Future Directions” in this chapter I would like to thank my collaborator Brent Lyda for his invaluable contributions for preforming the binding assays of A2a and for providing aliquots of the purified A2a protein. I would also like to thank Roger Sunahara for his insight and consultation and Roberto Brea for helping synthesize **26**.

References

1. Morrison, K. L. & Weiss, G. A. The origins of chemical biology. *Nat. Chem. Biol.* **2,** 3–6 (2006).

2. E. Kay, L. *The Molecular Vision of Life: Caltech, The Rockefeller Foundation, and the Rise of the New Biology*. (Oxford University Press, 1993).

3. Kay, L. E. Molecular Biology and Pauling's Immunochemistry: A Neglected Dimension *. *Hist Phil. Life Sci* **11,** 211–219 (1989).

4. Pauling, L. It's in the Blood, pictures and Illustarions. *Oregon State* 1 (2015).

5. Collins, B. J. ATP, not glucose, is energy currency. *Behav. Brain Sci.* **4,** 579 (1981).

6. Bertozzi, C. R., A decade of bioorthogonal chemistry. *Acc. Chem. Res.* **44,** 651–3 (2011).

7. Lodish H, Berk A, Zipursky SL, Matsudaira P, Baltimore D, Darnell, Bacterial Gene Control: The Jacob-Monod Model. (2000).

8. Ptashne, M. Specific Binding of the λ Phage Repressor to λ DNA. *Nature* **214,** 232–234 (1967).

9. Fersht, A. R. From the first protein structures to our current knowledge of protein folding: delights and scepticisms. *Nat. Rev. Mol. Cell Biol.* **9,** 650–654 (2008).

10. Ramil, C. P. & Lin, Q. Bioorthogonal chemistry: strategies and recent developments. *Chem. Commun. (Camb).* **49,** 11007–22 (2013).

11. Liu, Y., Patricelli, M. P. & Cravatt, B. F. Activity-based protein profiling: the serine hydrolases. *Proc. Natl. Acad. Sci. U. S. A.* **96,** 14694–9 (1999).

12. Lavis, L. D. & Raines, R. T. Bright Ideas for Chemical Biology. doi:10.1021/cb700248m

13. Staudinger, H. & Meyer, J. Über neue organische Phosphorverbindungen III. Phosphinmethylenderivate und Phosphinimine. *Helv. Chim. Acta* **2,** 635–646 (1919).

14. Köhn, M. & Breinbauer, R. The Staudinger Ligation—A Gift to Chemical Biology. *Angew. Chemie Int. Ed.* **43,** 3106–3116 (2004).

15. Sletten, E. M., Bertozzi, C.R. From mechanism to mouse: a tale of two bioorthogonal reactions. *Acc. Chem. Res.* **44,** 666–76 (2011).

16. Saxon, E. Bertozzi, C.R., Cell surface engineering by a modified Staudinger reaction. *Science* **287,** 2007–10 (2000).

17. Huisgen, R. 1,3-Dipolar Cycloadditions. Past and Future. *Angew. Chemie Int. Ed. English* **2,** 565–598 (1963).

18. Agard, N. J., Prescher, J. A., Bertozzi, C.R. A Strain-Promoted [3 + 2] Azide−Alkyne Cycloaddition for Covalent Modification of Biomolecules in Living Systems. *J. Am. Chem. Soc.* **126,** 15046–15047 (2004).

19. Tasdelen, M. A. & Yagci, Y. Light-induced click reactions. *Angew. Chem. Int. Ed. Engl.* **52,** 5930–8 (2013).

20. Ning, X., Temming, R., Dommerholt, J., Guo, J., Ania, D., Debets, M., Wolfert, M., Boons, G., van Delft, F., Protein modification by strain-promoted alkyne-nitrone cycloaddition. *Angew. Chem. Int. Ed. Engl.* **49,** 3065–8 (2010).

21. Yokoyama, Y., Takagi, N., Hikawa, H., Kaneko, S., Tsubaki, N., Okuno, H Chemoselective palladium-catalyzed reaction in aqueous media: Selectivity in the reaction of haloanilines with 1,1-dimethylallyl alcohol. *Adv. Synth. Catal.* **349,** 662–668 (2007).

22. Lin, Y. A., Chalker, J. M., Floyd, N., Bernardes, G. J. L. & Davis, B. G. Allyl Sulfides Are Privileged Substrates in Aqueous Cross-Metathesis: Application to Site-Selective Protein Modification. *J. Am. Chem. Soc.* **130,** 9642–9643 (2008).

23. Blackman, M. L., Royzen, M. & Fox, J. M. Tetrazine Ligation: Fast Bioconjugation Based on Inverse-Electron-Demand Diels−Alder Reactivity. *J. Am. Chem. Soc.* **130,** 13518–13519 (2008).

24. Ruhemann, S. VII.—The action of chloroform and alcoholic potash on hydrazines.(Part III.). *J. Chem. Soc. Trans.* (1890).

25. Ruhemann, S. XXXII.—Action of chloroform and alcoholic potash on hydrazines. Part II. *J. Chem. Soc. Trans.* (1889).

26. Auden, H. A. Some new osazones and tetrazones. *Proc. Chem. Soc.* **Xl,** 231 (1895).

27. Carboni, R. A. & Lindsey, R. V. Reactions of Tetrazines with Unsaturated Compounds. A New Synthesis of Pyridazines. *J. Am. Chem. Soc.* **81,** 4342–4346 (1959).

28. Thalhammer, F., Wallfahrer, U. & Sauer, J. Reaktivitt einfacher offenkettiger und cyclischer dienophile bei Diels-Alder-reaktionen mit inversem elektronenbedarf. *Tetrahedron Lett.* **31,** 6851–6854 (1990).

29. Baskin J.M., Prescher J.A., Laughlin S.T., Agard N.J., Chang P. V., Miller I.A., Lo A., Codelli J.A., Bertozzi C.R. Copper-free click chemistry for dynamic in vivo imaging. *Proc. Natl. Acad. Sci. U. S. A.* **104,** 16793–7 (2007).

30. Ning, X., Guo, J., Wolfert, M. A. & Boons, G. J. Visualizing metabolically labeled glycoconjugates of living cells by copper-free and fast huisgen cycloadditions. *Angew. Chemie - Int. Ed.* **47,** 2253–2255 (2008).

31. Devaraj, N. K. & Weissleder, R. Biomedical applications of tetrazine cycloadditions. *Acc. Chem. Res.* **44,** 816–27 (2011).

32. Karver, M. R., Weissleder, R. & Hilderbrand, S. A. Synthesis and Evaluation of a Series of 1,2,4,5-Tetrazines for Bioorthogonal Conjugation. *Bioconjug. Chem.* **22,** 2263–2270 (2011).

33. Sečkutė, J. & Devaraj, N. K. Expanding room for tetrazine ligations in the in vivo chemistry toolbox. *Curr. Opin. Chem. Biol.* **17,** 761–7 (2013).

34. Devaraj, N. K., Weissleder, R. & Hilderbrand, S. A. Tetrazine-based cycloadditions: application to pretargeted live cell imaging. *Bioconjug. Chem.* **19,** 2297–9 (2008).

35. Devaraj, N. K., Hilderbrand, S., Upadhyay, R., Mazitschek, R. & Weissleder, R. Bioorthogonal turn-on probes for imaging small molecules inside living cells. *Angew. Chemie - Int. Ed.* **49,** 2869–2872 (2010).

36. Liu D.S, Tangpeerachaikul, A., Selvaraj, R, Taylor, M.T., Fox, J.M., Ting, A.Y. Diels-alder cycloaddition for fluorophore targeting to specific proteins inside living cells. *J. Am. Chem. Soc.* **134,** 792–795 (2012).

37. Devaraj, N. K., Upadhyay, R., Haun, J. B., Hilderbrand, S. A. & Weissleder, R. Fast and sensitive pretargeted labeling of cancer cells through a tetrazine/trans-cyclooctene cycloaddition. *Angew. Chemie - Int. Ed.* **48,** 7013–7016 (2009).

38. Chen, W., Wang, D., Dai, C., Hamelberg, D. & Wang, B. Clicking 1,2,4,5-tetrazine and cyclooctynes with tunable reaction rates. *Chem. Commun.* **48,**

1736 (2012).

39. Plass, T., Milles, S., Koehler C., Szymański J., Mueller, R., Wießler, M., Schultz, C., Lemke, E.A. Amino acids for diels-alder reactions in living cells. *Angew. Chemie - Int. Ed.* **51,** 4166–4170 (2012).

40. Kaya, E., Vrabel, M., Deiml, C., Prill, S., Fluxa, V.S., Carell, T. A genetically encoded norbornene amino acid for the mild and selective modification of proteins in a copper-free click reaction. *Angew. Chemie - Int. Ed.* **51,** 4466–4469 (2012).

41. Sauer, J. & Heinrichs, G. Kinetik und umsetzungen von 1.2.4.5-tetrazinen mit winkelgespannten und elektronenreichen doppelbindungen. *Tetrahedron Lett.* **7,** 4979–4984 (1966).

42. Maier, G. Das Norcaradien-Problem. *Angew. Chemie* **79,** 446–458 (1967).

43. Maier, G. The Norcaradiene Problem. *Angew. Chemie Int. Ed. English* **6,** 402–413 (1967).

44. Sauer, J., Bäuerlein, P., Ebenbeck, W., Gousetis, C., Sichert, H., Troll, T., Utz, F., Wallfahrer, U. [4+2] Cycloadditions of 1,2,4,5-Tetrazines and Cyclopropenes − Synthesis of 3,4-Diazanorcaradienes and Tetracyclic Aliphatic Azo Compounds. *European J. Org. Chem.* **2001,** 2629–2638 (2001).

45. Carter, F. L. & Frampton, V. L. Review of the Chemistry of Cyclopropene Compounds. *Chem. Rev.* **64,** 497–525 (1964).

46. Dowd, P. & Gold, A. The thermal dimerization of cyclopropene. *Tetrahedron Lett.* **10,** 85–86 (1969).

47. von E. Doering, W. & Mole, T. Stereo-selectivity in the reaction of carbomethoxycarbene with cis-butene. *Tetrahedron* **10,** 65–70 (1960).

48. Closs, G. L., Closs, L. E. & Boll, W. A. The Base-Induced Pyrolysis of Tosylhydrazones of α,β-Unsaturated Aldehydes and Ketones. A Convenient Synthesis of Some Alkylcyclopropenes. *J. Am. Chem. Soc.* **85,** 3796–3800 (1963).

49. Yan, N., Liu, X., Pallerla, M. K. & Fox, J. M. Synthesis of stable derivatives of cycloprop-2-ene carboxylic acid. *J. Org. Chem.* **73,** 4283–6 (2008).

50. Petiniot, N., Anciaux, A. J., Noels, A. F., Hubert, A. J. & Teyssié, P. Rhodium catalysed cyclopropenation of acetylenes. *Tetrahedron Lett.* **19,** 1239–1242 (1978).

51. Yang, J., Karver, M. R., Li, W., Sahu, S. & Devaraj, N. K. Metal-catalyzed one-pot synthesis of tetrazines directly from aliphatic nitriles and hydrazine. *Angew. Chemie - Int. Ed.* **51,** 5222–5225 (2012).

52. Royzen, M., Yap, G. P. A. & Fox, J. M. A photochemical synthesis of functionalized trans-cyclooctenes driven by metal complexation. *J. Am. Chem. Soc.* **130,** 3760–1 (2008).

53. Matsuura, M., Saikawa, Y., Inui, K., Nakae, K., Igarashi, M., Hashimoto, K., Nakata, M. Identification of the toxic trigger in mushroom poisoning. *Nat. Chem. Biol.* **5,** 465–7 (2009).

54. Jewett, J. C. & Bertozzi, C. R. Synthesis of a fluorogenic cyclooctyne activated by Cu-free click chemistry. *Org. Lett.* **13,** 5937–5939 (2011).

55. Dumas-Verdes, C., Miomandre, F., Lépicier, E., Galangau, O., Vu, T.T., Clavier, G., Méallet-Renault, R., Audebert, P. BODIPY-Tetrazine Multichromophoric Derivatives. *European J. Org. Chem.* **2010,** 2525–2535 (2010).

56. Sletten, E. M. & Bertozzi, C. R. Bioorthogonal chemistry: fishing for selectivity in a sea of functionality. *Angew. Chem. Int. Ed. Engl.* **48,** 6974–98 (2009).

57. Hang, H. C. & Linder, M. E. Exploring protein lipidation with chemical biology. *Chem. Rev.* **111,** 6341–58 (2011).

58. Hang, H. C., Wilson, J. P. & Charron, G. Bioorthogonal chemical reporters for analyzing protein lipidation and lipid trafficking. *Acc. Chem. Res.* **44,** 699–708 (2011).

59. Best, M. D., Rowland, M. M. & Bostic, H. E. Exploiting bioorthogonal chemistry to elucidate protein-lipid binding interactions and other biological roles of phospholipids. *Acc. Chem. Res.* **44,** 686–98 (2011).

60. Jao, C. Y., Roth, M., Welti, R. & Salic, A. Metabolic labeling and direct imaging of choline phospholipids in vivo. *Proc. Natl. Acad. Sci. U. S. A.* **106,** 15332–7 (2009).

61. Neef, A. B. & Schultz, C. Selective fluorescence labeling of lipids in living cells. *Angew. Chem. Int. Ed. Engl.* **48,** 1498–500 (2009).

62. Chiou, S. H. DNA- and protein-scission activities of ascorbate in the presence of copper ion and a copper-peptide complex. *J. Biochem.* **94,** 1259–67 (1983).

63. Kennedy D.C., McKay, C.S., Legault, M.C.B., Danielson, D.C., Blake, J.A., Pegoraro, A.F., Stolow, A., Mester, Z., Pezacki, J.P. Cellular consequences of copper complexes used to catalyze bioorthogonal click reactions. *J. Am. Chem. Soc.* **133,** 17993–8001 (2011).

64. Cho, S. H. & Liebeskind, L. S. Practical organic synthesis with strained ring molecules. Rhodium catalyzed carbonylation of cyclopropenecarboxylate esters and cyclopropenyl ketones to .alpha.-pyrones and of vinylcyclopropenes to phenols. *J. Org. Chem.* **52,** 2631–2634 (1987).

65. Dube, D. H. & Bertozzi, C. R. Glycans in cancer and inflammation--potential for therapeutics and diagnostics. *Nat. Rev. Drug Discov.* **4,** 477–488 (2005).

66. van Kooyk, Y. & Rabinovich, G. a. Protein-glycan interactions in the control of innate and adaptive immune responses. *Nat. Immunol.* **9,** 593–601 (2008).

67. Laughlin, S.T., Agard, N.J., Baskin, J.M., Carrico, I.S., Chang, P. V., Ganguli, A.S., Hangauer, M.J., Lo, A., Prescher, J.A., Bertozzi, C.R. Metabolic Labeling of Glycans with Azido Sugars for Visualization and Glycoproteomics. *Methods in Enzymology* **415,** 230–250 (2006).

68. Ruhaak, L.R., Zauner, G., Huhn, C., Bruggink, C., Deelder, A.M., Wuhrer, M. Glycan labeling strategies and their use in identification and quantification. *Analytical and Bioanalytical Chemistry* **397,** 3457–3481 (2010).

69. Karver, M. R., Weissleder, R. & Hilderbrand, S. A. Bioorthogonal reaction pairs enable simultaneous, selective, multi-target imaging. *Angew. Chemie - Int. Ed.* **51,** 920–922 (2012).

70. Kayser, H., Zeitler, R., Kannicht, C., Grunow, D., Nuck, R., Reutter, W. Biosynthesis of a nonphysiological sialic acid in different rat organs, using N-propanoyl-D-hexosamines as precursors. *J. Biol. Chem.* **267,** 16934–16938 (1992).

71. Scholler, N., Hayden-Ledbetter, M., Hellstrom, K.-E., Hellstrom, I. & Ledbetter, J. A. Erratum for 'CD83 is a sialic acid-binding Ig-like lectin (Siglec) adhesion receptor that binds monocytes and a subset of activated CD8_+_ T cells'. *J Immunol* **182,** 1772–1773 (2009).

72. Kang, K., Joo, S., Choi, J.Y., Geum, S., Hong, S-P., Lee, S-Y., Kim, Y.H., Kim, S-M., Yoon, M-H., Nam, Y., Lee, K-B., Lee, H-Y., Choi, I.S. Tissue-based metabolic labeling of polysialic acids in living primary hippocampal

neurons. *Proc. Natl. Acad. Sci. U. S. A.* **112,** E241–8 (2015).

73. Mahal, L. K. Engineering Chemical Reactivity on Cell Surfaces Through Oligosaccharide Biosynthesis. *Science (80-.).* **276,** 1125–1128 (1997).

74. Shieh, P., Hangauer, M. J. & Bertozzi, C. R. Fluorogenic azidofluoresceins for biological imaging. *J. Am. Chem. Soc.* **134,** 17428–31 (2012).

75. Chang, P. V, Prescher, J. A., Hangauer, M. J. & Bertozzi, C. R. Imaging cell surface glycans with bioorthogonal chemical reporters. *J. Am. Chem. Soc.* **129,** 8400–1 (2007).

76. Lang, K., Davis, L., Torres-Kolbus, J., Chou, C., Deiters, A., Chin, J.W. Genetically encoded norbornene directs site-specific cellular protein labelling via a rapid bioorthogonal reaction. *Nat. Chem.* **4,** 298–304 (2012).

77. Ngo, J. T. & Tirrell, D. A. Noncanonical amino acids in the interrogation of cellular protein synthesis. *Acc. Chem. Res.* **44,** 677–685 (2011).

78. Rangan, K. J., Yang, Y. Y., Charron, G. & Hang, H. C. Rapid visualization and large-scale profiling of bacterial lipoproteins with chemical reporters. *J. Am. Chem. Soc.* **132,** 10628–10629 (2010).

79. Salic, A. & Mitchison, T. J. A chemical method for fast and sensitive detection of DNA synthesis in vivo. *Proc. Natl. Acad. Sci. U. S. A.* **105,** 2415–20 (2008).

80. Budin, G., Yang, K. S., Reiner, T. & Weissleder, R. Bioorthogonal probes for polo-like kinase 1 imaging and quantification. *Angew. Chemie - Int. Ed.* **50,** 9378–9381 (2011).

81. Yang, J., Sečkutė, J., Cole, C. M. & Devaraj, N. K. Live-Cell Imaging of Cyclopropene Tags with Fluorogenic Tetrazine. *Angew. Chemie Int. Ed.* **51,** 7476–9 (2012).

82. Wiessler, M., Waldeck, W., Pipkorn, R., Kliem, C., Lorenz, P., Fleischhacker, H., Hafner, M., Braun, K. Extension of the PNA world by functionalized PNA monomers eligible candidates for inverse diels alder click chemistry. *Int. J. Med. Sci.* **7,** 213–223 (2010).

83. Devaraj, N. K., Thurber, G. M., Keliher, E. J., Marinelli, B. & Weissleder, R. Reactive polymer enables efficient in vivo bioorthogonal chemistry. *Proc. Natl. Acad. Sci. U. S. A.* **109,** 4762–4767 (2012).

84. Rossin, R., Verkerk, P.R., Bosch, S.M., Van, D., Vulders, R.C.M, Verel, I., Lub J., Robillard, M.S. In vivo chemistry for pretargeted tumor imaging in live

mice. *Angew. Chemie - Int. Ed.* **49,** 3375–3378 (2010).

85. Yu, Z., Pan, Y., Wang, Z., Wang, J. & Lin, Q. Genetically encoded cyclopropene directs rapid, photoclick-chemistry-mediated protein labeling in mammalian cells. *Angew. Chemie - Int. Ed.* **51,** 10600–106004 (2012).

86. Patterson, D. M., Nazarova, L. A., Xie, B., Kamber, D. N. & Prescher, J. A. Functionalized cyclopropenes as bioorthogonal chemical reporters. *J. Am. Chem. Soc.* **134,** 18638–18643 (2012).

87. Luchansky, S. J., Goon, S. & Bertozzi, C. R. Expanding the diversity of unnatural cell-surface sialic acids. *ChemBioChem* **5,** 371–374 (2004).

88. Oetke C, Brossmer R, Mantey LR, Hinderlich S, Isecke R, Reutter W, Keppler OT, Pawlita M. Versatile biosynthetic engineering of sialic acid in living cells using synthetic sialic acid analogues. *J Biol Chem* **277,** 6688–6695 (2002).

89. Han, S., Collins, B. E., Bengtson, P. & Paulson, J. C. Homomultimeric complexes of CD22 in B cells revealed by protein-glycan cross-linking. *Nat. Chem. Biol.* **1,** 93–7 (2005).

90. Keppler, O. T., Horstkorte, R., Pawlita, M., Schmidt, C. & Reutter, W. Biochemical engineering of the N-acyl side chain of sialic acid: biological implications. *Glycobiology* **11,** 11R–18R (2001).

91. Jacobs, C. *et al.* Substrate specificity of the sialic acid biosynthetic pathway. *Biochemistry* **40,** 12864–12874 (2001).

92. Jacobs, C. L. *et al.* Metabolic labeling of glycoproteins with chemical tags through unnatural sialic acid biosynthesis. *Methods Enzymol.* **327,** 260–275 (2000).

93. Saxon E, Luchansky SJ, Hang HC, Yu C, Lee SC, Bertozzi CR. Investigating cellular metabolism of synthetic azidosugars with the Staudinger ligation. *J. Am. Chem. Soc.* **124,** 14893–14902 (2002).

94. Hang, H. C., Yu, C., Kato, D. L. & Bertozzi, C. R. A metabolic labeling approach toward proteomic analysis of mucin-type O-linked glycosylation. *Proc. Natl. Acad. Sci. U. S. A.* **100,** 14846–14851 (2003).

95. Liang, Y., MacKey, J. L., Lopez, S. A., Liu, F. & Houk, K. N. Control and design of mutual orthogonality in bioorthogonal cycloadditions. *J. Am. Chem. Soc.* **134,** 17904–17907 (2012).

96. Tower, D. B. *Hensing, 1719 : an account of the first chemical examination of the brain and the discovery of phosphorus therein : set against the background of Europe in the 17th and early 18th centuries : a source book in the history of neurochemistry*. (Raven Press, 1983).

97. Gobley, N. *Recherches chimiques sur le jaune d'oeuf Rapport sur un mémoire ayant pour titre "Recherches chimiques sur le jaune d'oeuf*. (impr. de Fain et Thunot, 1846).

98. oats. Vol29-1. *Bull. Hist. Chem* **29,** (2004).

99. Lasic, D. D. & Barenholz, Y. *Handbook of nonmedical applications of liposomes*. (CRC Press, 1996).

100. Bangham, A. D., Standish, M. M. & Watkins, J. C. Diffusion of univalent ions across the lamellae of swollen phospholipids. *J. Mol. Biol.* **13,** 238–IN27 (1965).

101. Israelachvili, J. N., Marcelja, S. & Horn, R. G. Physical principles of membrane organization. *Q. Rev. Biophys.* **13,** 121–200 (1980).

102. Eloy JO, Claro de Souza M, Petrilli R, Barcellos JPA, Lee RJ, Marchetti JM. Liposomes as carriers of hydrophilic small molecule drugs: strategies to enhance encapsulation and delivery. *Colloids Surf. B. Biointerfaces* **123,** 345–63 (2014).

103. Jesorka, A. & Orwar, O. Liposomes: technologies and analytical applications. *Annu. Rev. Anal. Chem. (Palo Alto. Calif).* **1,** 801–32 (2008).

104. Gregoriadis, G. *Liposome technology Volume 2, Entrapment of drugs and other materials into liposomes*. (Informa Healthcare, 2007).

105. Colletier, J.-P., Chaize, B., Winterhalter, M. & Fournier, D. Protein encapsulation in liposomes: efficiency depends on interactions between protein and phospholipid bilayer. *BMC Biotechnol.* **2,** 9 (2002).

106. Orive G, Hernández RM, Gascón AR, Calafiore R, Chang TMS, Vos P De, Hortelano G, Hunkeler D, Lacík I, Shapiro AMJ, Pedraz JL. Cell encapsulation: promise and progress. *Nat. Med.* **9,** 104–7 (2003).

107. Cho, K., Wang, X., Nie, S., Chen, Z. G. & Shin, D. M. Therapeutic nanoparticles for drug delivery in cancer. *Clin. Cancer Res.* **14,** 1310–6 (2008).

108. Therien, J. B., Zadvornyy, O. A., Posewitz, M. C., Bryant, D. A. & Peters, J. W. Growth of Chlamydomonas reinhardtii in acetate-free medium when co-cultured with alginate-encapsulated, acetate-producing strains of Synechococcus sp. PCC 7002. *Biotechnol. Biofuels* **7,** 154 (2014).

109. Nassif N, Roux C, Coradin T, Rager M-N, Bouvet OMM, Livage J. A sol–gel matrix to preserve the viability of encapsulated bacteria. *J. Mater. Chem.* **13,** 203–208 (2003).

110. Cook, M. T., Tzortzis, G., Charalampopoulos, D. & Khutoryanskiy, V. V. Microencapsulation of probiotics for gastrointestinal delivery. *J. Control. Release* **162,** 56–67 (2012).

111. Zengler K, Toledo G, Rappe M, Elkins J, Mathur EJ, Short JM, Keller M. Cultivating the uncultured. *Proc. Natl. Acad. Sci. U. S. A.* **99,** 15681–6 (2002).

112. Desimone MF, Marzi MC De, Copello GJ, Fernández MM, Malchiodi EL, Diaz LE. Efficient preservation in a silicon oxide matrix of Escherichia coli, producer of recombinant proteins. *Appl. Microbiol. Biotechnol.* **68,** 747–52 (2005).

113. Lasic, D. Novel applications of liposomes. *Trends Biotechnol.* **16,** 307–321 (1998).

114. Matthay, K. K., Heath, T. D. & Papahadjopoulos, D. Specific enhancement of drug delivery to AKR lymphoma by antibody-targeted small unilamellar vesicles. *Cancer Res.* **44,** 1880–6 (1984).

115. Pardridge, W. M. Blood-brain barrier drug targeting: the future of brain drug development. *Mol. Interv.* **3,** 90–105, 51 (2003).

116. Kulkarni, P. R., Yadav, J. D. & Vaidya, K. A. Liposomes: a novel drug delivery system. *Int J Curr Pharm Res* **3,** 10–18 (2011).

117. Tan, Y.-C., Hettiarachchi, K., Siu, M., Pan, Y.-R. & Lee, A. P. Controlled microfluidic encapsulation of cells, proteins, and microbeads in lipid vesicles. *J. Am. Chem. Soc.* **128,** 5656–8 (2006).

118. van Swaay, D. & deMello, A. Microfluidic methods for forming liposomes. *Lab Chip* **13,** 752 (2013).

119. Teh, S.-Y., Khnouf, R., Fan, H. & Lee, A. P. Stable, biocompatible lipid vesicle generation by solvent extraction-based droplet microfluidics. *Biomicrofluidics* **5,** 44113–4411312 (2011).

120. Nishimura K, Matsuura T, Nishimura K, Sunami T, Suzuki H, Yomo T. Cell-free protein synthesis inside giant unilamellar vesicles analyzed by flow cytometry. *Langmuir* **28,** 8426–32 (2012).

121. Pautot, S., Frisken, B. J. & Weitz, D. A. Production of Unilamellar Vesicles Using an Inverted Emulsion. *Langmuir* **19,** 2870–2879 (2003).

122. Imura, T., Yanagishita, H., Ikegami, T., Negishi, H. & Kitamoto, D. Drastic Improvements in Trapping Efficiency and Dispersibility for Phosphatidylcholine Liposomes in the Presence of Divalent Metal Ions. *J. Oleo Sci.* **52,** 673–679 (2003).

123. Uludag, H. & Sefton, M. V. Microencapsulated human hepatoma (HepG2) cells: in vitro growth and protein release. *J. Biomed. Mater. Res.* **27,** 1213–24 (1993).

124. Mokarram, R. R., Mortazavi, S. A., Najafi, M. B. H. & Shahidi, F. The influence of multi stage alginate coating on survivability of potential probiotic bacteria in simulated gastric and intestinal juice. *Food Res. Int.* **42,** 1040–1045 (2009).

125. Capela, P., Hay, T. K. C. & Shah, N. P. Effect of homogenisation on bead size and survival of encapsulated probiotic bacteria. *Food Res. Int.* **40,** 1261–1269 (2007).

126. Chen, C.-C. & Su, Y.-C. An autonomous CO 2 discharge and electrolyte agitation scheme for portable microbial fuel cells. *J. Micromechanics Microengineering* **17,** S265–S273 (2007).

127. Walde, P., Cosentino, K., Engel, H. & Stano, P. Giant vesicles: preparations and applications. *Chembiochem* **11,** 848–65 (2010).

128. Batada, N. N., Shepp, L. A. & Siegmund, D. O. Stochastic model of protein-protein interaction: why signaling proteins need to be colocalized. *Proc. Natl. Acad. Sci. U. S. A.* **101,** 6445–9 (2004).

129. Smith, H. O., Hutchison, C. A., Pfannkoch, C. & Venter, J. C. Generating a synthetic genome by whole genome assembly: phiX174 bacteriophage from synthetic oligonucleotides. *Proc. Natl. Acad. Sci. U. S. A.* **100,** 15440–5 (2003).

130. Gibson DG, Glass JI, Lartigue C, Noskov VN, Chuang R-Y, Algire MA, Benders GA, Montague MG, Ma L, Moodie MM, Merryman C, Vashee S, Krishnakumar R, Assad-Garcia N, Andrews-Pfannkoch C, Denisova EA, Young L, Qi Z-Q, Segall-Shapiro TH, Calvey CH, Parmar PP, Hutchison CA, Smith HO, Venter JC. Creation of a bacterial cell controlled by a chemically synthesized genome. *Science (80-.).* **329,** 52–56 (2010).

131. Noireaux, V., Bar-Ziv, R., Godefroy, J., Salman, H. & Libchaber, A. Toward an artificial cell based on gene expression in vesicles. *Phys. Biol. 2 P1 Phys. Biol* **2,** 1–8 (2005).

132. Shin J, Noireaux V, He M, Kim D, Kigawa T, Choi C, Yokoyama S, Kim D, Swartz J, Sitaraman K, Esposito D, Klarmann G, Grice S Le, Hartley J, Chatterjee D, Kim T, Oh I, Keum J, Kwon Y, Byun J, Lee K, Choi C, Kim D, Kim H, Kim D, Michel-Reydellet N, Calhoun K, Swartz J, Michel-Reydellet N. Efficient cell-free expression with the endogenous E. Coli RNA polymerase and sigma factor 70. *J. Biol. Eng.* **4,** 8 (2010).

133. de Boer, H. A., Comstock, L. J. & Vasser, M. The tac promoter: a functional hybrid derived from the trp and lac promoters. *Proc. Natl. Acad. Sci. U. S. A.* **80,** 21–5 (1983).

134. Olins, P. O., Devine, C. S., Rangwala, S. H. & Kavka, K. S. The T7 phage gene 10 leader RNA, a ribosome-binding site that dramatically enhances the expression of foreign genes in Escherichia coli. *Gene* **73,** 227–235 (1988).

135. Klein, R. ., Moore, M. . & Smith, M. . Selective diffusion of neutral amino acids across lipid bilayers. *Biochim. Biophys. Acta - Biomembr.* **233,** 420–433 (1971).

136. Alvarez, J. D., Chen, D., Storer, E. & Sehgal, A. Non-cyclic and developmental stage-specific expression of circadian clock proteins during murine spermatogenesis. *Biol. Reprod.* **69,** 81–91 (2003).

137. Pilz, R. B. & Casteel, D. E. Regulation of gene expression by cyclic GMP. *Circ. Res.* **93,** 1034–46 (2003).

138. Cole, S. E., Levorse, J. M., Tilghman, S. M. & Vogt, T. F. Clock Regulatory Elements Control Cyclic Expression of Lunatic fringe during Somitogenesis. *Dev. Cell* **3,** 75–84 (2002).

139. Shin Y, Davis JH, Brau RR, Martin A, Kenniston JA, Baker TA, Sauer RT, Lang MJ. Single-molecule denaturation and degradation of proteins by the AAA+ ClpXP protease. *Proc. Natl. Acad. Sci. U. S. A.* **106,** 19340–5 (2009).

140. Maglica, Ž., Kolygo, K. & Weber-Ban, E. Optimal Efficiency of ClpAP and ClpXP Chaperone-Proteases Is Achieved by Architectural Symmetry. *Structure* **17,** 508–516 (2009).

141. Baker, T. A. & Sauer, R. T. ClpXP, an ATP-powered unfolding and protein-degradation machine. *Biochim. Biophys. Acta* **1823,** 15–28 (2012).

142. Stricker J, Cookson S, Bennett MR, Mather WH, Tsimring LS, Hasty J A fast, robust and tunable synthetic gene oscillator. *Nature* **456,** 516–9 (2008).

143. Niederholtmeyer H, Sun ZZ, Hori Y, Yeung E, Verpoorte A, Murray RM, Maerkl SJ Rapid cell-free forward engineering of novel genetic ring oscillators. *Elife* **4,** (2015).

144. Budin, I. & Devaraj, N. K. Membrane assembly driven by a biomimetic coupling reaction. *J. Am. Chem. Soc.* **134,** 751–3 (2012).

145. Stoyanov, J. V, Hobman, J. L. & Brown, N. L. CueR (YbbI) of Escherichia coli is a MerR family regulator controlling expression of the copper exporter CopA. *Mol. Microbiol.* **39,** 502–11 (2001).

146. Collman, J. P., Devaraj, N. K. & Chidsey, C. E. D. 'Clicking' Functionality onto Electrode Surfaces. *Langmuir* **20,** 1051–1053 (2004).

147. Saliba A-E, Vonkova I, Ceschia S, Findlay GM, Maeda K, Tischer C, Deghou S, Noort V van, Bork P, Pawson T, Ellenberg J, Gavin A-C. A quantitative liposome microarray to systematically characterize protein-lipid interactions. *Nat. Methods* **11,** 47–50 (2014).

148. Zhao, H. & Lappalainen, P. A simple guide to biochemical approaches for analyzing protein-lipid interactions. *Mol. Biol. Cell* **23,** 2823–30 (2012).

149. Hodnik, V. & Anderluh, G. Capture of intact liposomes on biacore sensor chips for protein-membrane interaction studies. *Methods Mol. Biol.* **627,** 201–211 (2010).

150. Di Paolo, G. & De Camilli, P. Phosphoinositides in cell regulation and membrane dynamics. *Nature* **443,** 651–657 (2006).

151. Kraft, J. C., Freeling, J. P., Wang, Z. & Ho, R. J. Y. Emerging research and clinical development trends of liposome and lipid nanoparticle drug delivery systems. *J. Pharm. Sci.* **103,** 29–52 (2014).

152. Lombard, J., López-García, P. & Moreira, D. The early evolution of lipid membranes and the three domains of life. *Nat. Rev. Microbiol.* **10,** 507–15 (2012).

153. Luisi, P. L., Walde, P. & Oberholzer, T. Lipid vesicles as possible intermediates in the origin of life. *Curr. Opin. Colloid Interface Sci.* **4,** 33–39 (1999).

154. Deamer, D. W. The first living systems: a bioenergetic perspective. *Microbiol. Mol. Biol. Rev.* **61,** 239–61 (1997).

155. Rivas, G., Vogel, S. K. & Schwille, P. Reconstitution of cytoskeletal protein assemblies for large-scale membrane transformation. *Curr. Opin. Chem. Biol.* **22,** 18–26 (2014).

156. Sott K, Lobovkina T, Lizana L, Tokarz M, Bauer B, Konkoli Z, Orwar O Controlling enzymatic reactions by geometry in a biomimetic nanoscale network. *Nano Lett.* **6,** 209–14 (2006).

157. Karlsson M, Davidson M, Karlsson R, Karlsson A, Bergenholtz J, Konkoli Z, Jesorka A, Lobovkina T, Hurtig J, Voinova M, Orwar O. Biomimetic nanoscale reactors and networks. *Annu. Rev. Phys. Chem.* **55,** 613–49 (2004).

158. Moscho, A., Orwar, O., Chiu, D. T., Modi, B. P. & Zare, R. N. Rapid preparation of giant unilamellar vesicles. *Proc. Natl. Acad. Sci. U. S. A.* **93,** 11443–7 (1996).

159. Shindou, H., Hishikawa, D., Harayama, T., Yuki, K. & Shimizu, T. Recent progress on acyl CoA: lysophospholipid acyltransferase research. *J. Lipid Res.* **50 Suppl,** S46–S51 (2009).

160. Shindou, H. & Shimizu, T. Acyl-CoA:lysophospholipid acyltransferases. *J. Biol. Chem.* **284,** 1–5 (2009).

161. Wick, R. & Luisi, P. L. Enzyme-containing liposomes can endogenously produce membrane-constituting lipids. *Chem. Biol.* **3,** 277–85 (1996).

162. Deamer, D. W. & Boatman, D. E. An enzymatically driven membrane reconstitution from solubilized components. *J. Cell Biol.* **84,** 461–7 (1980).

163. Takakura K, Yamamoto T, Kurihara K, Toyota T, Ohnuma K, Sugawara T, Walde P, Ichikawa S, Vriezema DM, Argones MC, Elemans JAAW, Cornelissen JJLM, Rowan AE, Nolte RJM, Kian T, Ho RJY, Soussan E, Cassel S, Blanzat M, Rico-Lattes I, Zepik HH, Walde P, Ishikawa T, Suzuki K, Toyota T, Takakura K, Sugawara T, Okahata Y, Kunitake T Spontaneous transformation from micelles to vesicles associated with sequential conversions of comprising amphiphiles within assemblies. *Chem. Commun.* **50,** 2190 (2014).

164. Minkenberg CB, Li F, van Rijn P, Florusse L, Boekhoven J, Stuart MCA, Koper GJM, Eelkema R, van Esch JH Responsive Vesicles from Dynamic Covalent Surfactants. *Angew. Chemie Int. Ed.* **50,** 3421–3424 (2011).

165. Blain, J. C. & Szostak, J. W. Progress toward synthetic cells. *Annu. Rev. Biochem.* **83,** 615–40 (2014).

166. Budin, I. & Szostak, J. W. Expanding Roles for Diverse Physical Phenomena During the Origin of Life. *Annu. Rev. Biophys.* **39,** 245–263 (2010).

167. Martin, W. & Russell, M. J. On the origin of biochemistry at an alkaline hydrothermal vent. *Philos. Trans. R. Soc. Lond. B. Biol. Sci.* **362,** 1887–925 (2007).

168. Dawson, P. E., Muir, T. W., Clark-Lewis, I. & Kent, S. B. Synthesis of proteins by native chemical ligation. *Science* **266,** 776–9 (1994).

169. Wieland, T., Bokelmann, E., Bauer, L., Lang, H. U. & Lau, H. Über Peptidsynthesen. 8. Mitteilung Bildung von S-haltigen Peptiden durch intramolekulare Wanderung von Aminoacylresten. *Justus Liebigs Ann. Chem.* **583,** 129–149 (1953).

170. Dirksen, A. & Dawson, P. E. Expanding the scope of chemoselective peptide ligations in chemical biology. *Curr. Opin. Chem. Biol.* **12,** 760–6 (2008).

171. Clark, R. J. & Craik, D. J. Native chemical ligation applied to the synthesis and bioengineering of circular peptides and proteins. *Biopolymers* **94,** 414–22 (2010).

172. Hackenberger, C. P. R. & Schwarzer, D. Chemoselective ligation and modification strategies for peptides and proteins. *Angew. Chem. Int. Ed. Engl.* **47,** 10030–74 (2008).

173. Johnson, E. C. B. & Kent, S. B. H. Insights into the mechanism and catalysis of the native chemical ligation reaction. *J. Am. Chem. Soc.* **128,** 6640–6 (2006).

174. Kent, S. Novel forms of chemical protein diversity -- in nature and in the laboratory. *Curr. Opin. Biotechnol.* **15,** 607–14 (2004).

175. Shin Y, Winans KA, Backes BJ, Kent SBH, Ellman JA, Bertozzi CR. Fmoc-Based Synthesis of Peptide- $^{\alpha}$ Thioesters: Application to the Total Chemical Synthesis of a Glycoprotein by Native Chemical Ligation. *J. Am. Chem. Soc.* **121,** 11684–11689 (1999).

176. Wilcoxen, K. M., Leman, L. J., Weinberger, D. A., Huang, Z.-Z. & Ghadiri, M. R. Biomimetic catalysis of intermodular aminoacyl transfer. *J. Am. Chem. Soc.* **129,** 748–9 (2007).

177. Raibaut, L., Ollivier, N. & Melnyk, O. Sequential native peptide ligation strategies for total chemical protein synthesis. *Chem. Soc. Rev.* **41,** 7001–15 (2012).

178. McGrath, N. A. & Raines, R. T. Chemoselectivity in chemical biology: acyl transfer reactions with sulfur and selenium. *Acc. Chem. Res.* **44,** 752–61 (2011).

179. Kent, S. B. H. Total chemical synthesis of proteins. *Chem. Soc. Rev.* **38,** 338–51 (2009).

180. Dawson, P. E. & Kent, S. B. Synthesis of native proteins by chemical ligation. *Annu. Rev. Biochem.* **69,** 923–60 (2000).

181. Vázquez, O. & Seitz, O. Templated native chemical ligation: peptide chemistry beyond protein synthesis. *J. Pept. Sci.* **20,** 78–86 (2014).

182. Reinhardt U, Lotze J, Zernia S, Mörl K, Beck-Sickinger AG, Seitz O. Peptide-Templated Acyl Transfer: A Chemical Method for the Labeling of Membrane Proteins on Live Cells. *Angew. Chemie Int. Ed.* **53,** 10237–10241 (2014).

183. Roloff A, Seitz O, Gartner ZJ, Tse BN, Grubina R, Doyon JB, Snyder TM, Liu DR, Hansen MH, Blakskjær P, Petersen LK, Hansen TH, Højfeldt JW, Gothelf K V., Hansen NJ V., Georghiou G, Kleiner RE, Pulkoski-Gross M, Liu DR, Seeliger MA, Kleiner RE, Dumelin CE, Liu DR, Jacobsen MF, Cló E, Mokhir A, Gothelf K V., Arian D, Cló E. Bioorthogonal reactions challenged: DNA templated native chemical ligation during PCR. *Chem. Sci.* **4,** 432–436 (2013).

184. Roloff, A. & Seitz, O. The role of reactivity in DNA templated native chemical PNA ligation during PCR. *Bioorg. Med. Chem.* **21,** 3458–64 (2013).

185. Roloff, A. & Seitz, O. Reducing product inhibition in nucleic acid-templated ligation reactions: DNA-templated cycligation. *Chembiochem* **14,** 2322–8 (2013).

186. Jung JP, Sprangers AJ, Byce JR, Su J, Squirrell JM, Messersmith PB, Eliceiri KW, Ogle BM. ECM-incorporated hydrogels cross-linked via native chemical ligation to engineer stem cell microenvironments. *Biomacromolecules* **14,** 3102–11 (2013).

187. Canalle, L. A., Löwik, D. W. P. M. & van Hest, J. C. M. Polypeptide-polymer bioconjugates. *Chem. Soc. Rev.* **39,** 329–53 (2010).

188. Chafekar SM, Malda H, Merkx M, Meijer EW, Viertl D, Lashuel HA, Baas F, Scheper W. Branched KLVFF tetramers strongly potentiate inhibition of beta-amyloid aggregation. *Chembiochem* **8,** 1857–64 (2007).

189. Reulen SWA, Brusselaars WWT, Langereis S, Mulder WJM, Breurken M, Merkx M. Protein−Liposome Conjugates Using Cysteine-Lipids And Native Chemical Ligation. *Bioconjug. Chem.* **18,** 590–596 (2007).

190. Grogan, M. J., Kaizuka, Y., Conrad, R. M., Groves, J. T. & Bertozzi, C. R. Synthesis of lipidated green fluorescent protein and its incorporation in supported lipid bilayers. *J. Am. Chem. Soc.* **127,** 14383–7 (2005).

191. Dose, C. & Seitz, O. Convergent synthesis of peptide nucleic acids by native chemical ligation. *Org. Lett.* **7,** 4365–8 (2005).

192. Stafford, R. E., Fanni, T. & Dennis, E. A. Interfacial properties and critical micelle concentration of lysophospholipids. *Biochemistry* **28,** 5113–20 (1989).

193. Kramer, J. K., Blackwell, B. A., Dugan, M. E. & Sauer, F. D. Identification of a new sphingolipid 3-O-acyl-D-erythro-sphingomyelin in newborn pig and infant plasma. *Biochim. Biophys. Acta* **1303,** 47–55 (1996).

194. Van Blitterswijk, W. J., Van Hoeven, R. P. & Van Der Meer, B. W. Lipid structural order parameters (reciprocal of fluidity) in biomembranes derived from steady-state fluorescence polarization measurements. *Biochim. Biophys. Acta - Biomembr.* **644,** 323–332 (1981).

195. Litman, B. J., Lewis, E. N. & Levin, I. W. Packing characteristics of highly unsaturated bilayer lipids: Raman spectroscopic studies of multilamellar phosphatidylcholine dispersions. *Biochemistry* **30,** 313–9 (1991).

196. Mashiach E, Sela S, Weinstein T, Cohen HI, Shasha SM, Kristal B Mesna: a novel renoprotective antioxidant in ischaemic acute renal failure. *Nephrol. Dial. Transplant* **16,** 542–51 (2001).

197. Almén, M. S., Nordström, K. J. V, Fredriksson, R. & Schiöth, H. B. Mapping the human membrane proteome: a majority of the human membrane proteins can be classified according to function and evolutionary origin. *BMC Biol.* **7,** 50 (2009).

198. Gamper, N. & Shapiro, M. S. Regulation of ion transport proteins by membrane phosphoinositides. *Nat. Rev. Neurosci.* **8,** 921–34 (2007).

199. Maître, J.-L. & Heisenberg, C.-P. Three Functions of Cadherins in Cell Adhesion. *Curr. Biol.* **23,** R626–R633 (2013).

200. Campbell, I. D. & Humphries, M. J. Integrin Structure, Activation, and Interactions. *Cold Spring Harb. Perspect. Biol.* **3,** a004994–a004994 (2011).

201. Overington, J. P., Al-Lazikani, B. & Hopkins, A. L. How many drug targets are there? *Nat. Rev. Drug Discov.* **5,** 993–6 (2006).

202. Hotamisligil, G. S. Inflammation and metabolic disorders. *Nature* **444,** 860–7 (2006).

203. Selkoe, D. J. Alzheimer's Disease: Genes, Proteins, and Therapy. *Physiol Rev* **81,** 741–766 (2001).

204. Nichols, C. G., Singh, G. K. & Grange, D. K. KATP channels and cardiovascular disease: suddenly a syndrome. *Circ. Res.* **112,** 1059–72 (2013).

205. Rigaud, J. L., Pitard, B. & Levy, D. Reconstitution of membrane proteins into liposomes: application to energy-transducing membrane proteins. *Biochim. Biophys. Acta* **1231,** 223–46 (1995).

206. Seddon, A. M., Curnow, P. & Booth, P. J. Membrane proteins, lipids and detergents: not just a soap opera. *Biochim. Biophys. Acta* **1666,** 105–17 (2004).

207. Baker, M. Making membrane proteins for structures: a trillion tiny tweaks. *Nat. Methods* **7,** 429–34 (2010).

208. Jewett, J. C. & Bertozzi, C. R. Cu-free click cycloaddition reactions in chemical biology. *Chem. Soc. Rev.* **39,** 1272–9 (2010).

209. Hardy MD, Yang J, Selimkhanov J, Cole CM, Tsimring LS, Devaraj NK. Self-reproducing catalyst drives repeated phospholipid synthesis and membrane growth. *Proc. Natl. Acad. Sci.* **112,** 8187–8192 (2015).

210. Brea, R. J., Cole, C. M. & Devaraj, N. K. In Situ Vesicle Formation by Native Chemical Ligation. *Angew. Chemie Int. Ed.* **53,** 14102–14105 (2014).

211. Hein, J. E. & Fokin, V. V. Copper-catalyzed azide-alkyne cycloaddition (CuAAC) and beyond: new reactivity of copper(I) acetylides. *Chem. Soc. Rev.* **39,** 1302–15 (2010).

212. Tornøe, C. W., Christensen, C. & Meldal, M. Peptidotriazoles on solid phase: [1,2,3]-triazoles by regiospecific copper(i)-catalyzed 1,3-dipolar cycloadditions of terminal alkynes to azides. *J. Org. Chem.* **67,** 3057–64 (2002).

213. Rostovtsev, V. V, Green, L. G., Fokin, V. V & Sharpless, K. B. A stepwise huisgen cycloaddition process: copper(I)-catalyzed regioselective "ligation" of azides and terminal alkynes. *Angew. Chem. Int. Ed. Engl.* **41,** 2596–9 (2002).

214. Yoshikawa, S., Muramoto, K., Shinzawa-Itoh, K. & Mochizuki, M. Structural studies on bovine heart cytochrome c oxidase. *Biochim. Biophys. Acta - Bioenerg.* **1817,** 579–589 (2012).

215. Yoshikawa, S., Muramoto, K. & Shinzawa-Itoh, K. The O2 reduction and proton pumping gate mechanism of bovine heart cytochrome c oxidase. *Biochim. Biophys. Acta - Bioenerg.* **1807,** 1279–1286 (2011).

216. Vik, S. & Capaldi, R. Lipid requirements for cytochrome c oxidase activity. *Biochemistry* **16,** 5755–5759 (1977).

217. Smith, L. & Conrad, H. A study of the kinetics of the oxidation of cytochrome c by cytochrome c oxidase. *Arch. Biochem. Biophys.* **63,** 403–413 (1956).

218. Rosevear, P., VanAken, T., Baxter, J. & Ferguson-Miller, S. Alkyl glycoside detergents: a simpler synthesis and their effects on kinetic and physical properties of cytochrome c oxidase. *Biochemistry* **19,** 4108–4115 (1980).

219. Rigaud JL, Mosser G, Lacapere JJ, Olofsson A, Levy D, Ranck JL. Bio-Beads: an efficient strategy for two-dimensional crystallization of membrane proteins. *J. Struct. Biol.* **118,** 226–35 (1997).

220. Straubinger, R. M., Papahadjopoulos, D. & Hong, K. Endocytosis and intracellular fate of liposomes using pyranine as a probe. *Biochemistry* **29,**

4929–4939 (1990).

221. Doshi R, Ali A, Shi W, Freeman E V, Fagg LA, Veen HW van Molecular disruption of the power stroke in the ATP-binding cassette transport protein MsbA. *J. Biol. Chem.* **288,** 6801–13 (2013).

222. Eckford, P. D. W. & Sharom, F. J. Functional characterization of Escherichia coli MsbA: interaction with nucleotides and substrates. *J. Biol. Chem.* **283,** 12840–50 (2008).

223. Haubertin, D. Y., Madaoui, H., Sanson, A., Guérois, R. & Orlowski, S. Molecular dynamics simulations of E. coli MsbA transmembrane domain: formation of a semipore structure. *Biophys. J.* **91,** 2517–31 (2006).

224. Antoine, S., Pinet, C. & Coulombe, A. Are B-type Ca2+ channels of cardiac myocytes akin to the passive ion channel in the plasma membrane Ca2+ pump? *J. Membr. Biol.* **179,** 37–50 (2001).

225. Pinet, C., Antoine, S., Filoteo, A. G., Penniston, J. T. & Coulombe, A. Reincorporated plasma membrane Ca2+-ATPase can mediate B-Type Ca2+ channels observed in native membrane of human red blood cells. *J. Membr. Biol.* **187,** 185–201 (2002).

226. Zacharias, D. A. & Kappen, C. Developmental expression of the four plasma membrane calcium ATPase (Pmca) genes in the mouse. *Biochim. Biophys. Acta* **1428,** 397–405 (1999).

227. Strehler, E. E. & Zacharias, D. A. Role of Alternative Splicing in Generating Isoform Diversity Among Plasma Membrane Calcium Pumps. *Physiol Rev* **81,** 21–50 (2001).

228. Tate, C. G. Overexpression of mammalian integral membrane proteins for structural studies. *FEBS Lett.* **504,** 94–8 (2001).

229. Chicka, M. C. & Strehler, E. E. Alternative splicing of the first intracellular loop of plasma membrane Ca2+-ATPase isoform 2 alters its membrane targeting. *J. Biol. Chem.* **278,** 18464–70 (2003).

230. Fang, G.-M., Cui, H.-K., Zheng, J.-S. & Liu, L. Chemoselective ligation of peptide phenyl esters with N-terminal cysteines. *Chembiochem* **11,** 1061–5 (2010).

231. Khan, M. S., Dosoky, N. S. & Williams, J. D. Engineering lipid bilayer membranes for protein studies. *Int. J. Mol. Sci.* **14,** 21561–97 (2013).

232. Ries, R. S., Choi, H., Blunck, R., Bezanilla, F. & Heath, J. R. Black Lipid Membranes: Visualizing the Structure, Dynamics, and Substrate Dependence of Membranes. *J. Phys. Chem. B* **108,** 16040–16049 (2004).

233. Capone, R., Blake, S., Restrepo, M. R., Yang, J. & Mayer, M. Designing nanosensors based on charged derivatives of gramicidin A. *J. Am. Chem. Soc.* **129,** 9737–45 (2007).

234. Blake, S., Mayer, T., Mayer, M. & Yang, J. Monitoring chemical reactions by using ion-channel-forming peptides. *Chembiochem* **7,** 433–5 (2006).

235. Hille, B. *Ion Channels of Excitable Membranes*. (Sinauer Associates, inc., 2001).

236. Majd S, Yusko EC, Billeh YN, Macrae MX, Yang J, Mayer M. Applications of biological pores in nanomedicine, sensing, and nanoelectronics. *Curr. Opin. Biotechnol.* **21,** 439–76 (2010).

237. Montal, M. & Mueller, P. Formation of bimolecular membranes from lipid monolayers and a study of their electrical properties. *Proc. Natl. Acad. Sci. U. S. A.* **69,** 3561–6 (1972).

238. Lefevre, T., Coraboeuf, E., Ghazi, A. & Coulombe, A. Divalent cation channels activated by phenothiazines in membrane of rat ventricular myocytes. *J. Membr. Biol.* **147,** 147–58 (1995).

239. The MA pET19b plasmid was generously donated by Dr. Geoffrey Changc (University of California, San Diego).

240. The EGFP-hPMCA2z/b plasmid was donated by Prof. Emanuel E. Strehler (Mayo Clinic College of Medicine, Rochester).

241. HYNES, R. Integrins: A family of cell surface receptors. *Cell* **48,** 549–554 (1987).

242. Beck, J., Garcia, R., Heiss, G., Vokonas, P. S. & Offenbacher, and S. Periodontal Disease and Cardiovascular Disease. (2010).

243. Carpenter, E. P., Beis, K., Cameron, A. D. & Iwata, S. Overcoming the challenges of membrane protein crystallography. *Curr. Opin. Struct. Biol.* **18,** 581–6 (2008).

244. Luche, S., Santoni, V. & Rabilloud, T. Evaluation of nonionic and zwitterionic detergents as membrane protein solubilizers in two-dimensional

electrophoresis. *Proteomics* **3,** 249–53 (2003).